Palestine Polytechnic University

Deanship of Graduate Studies and Scientific Research

Master of Architecture – Sustainable Design

Assessing the Effect of Façade Materials, Urban canyon, and Orientation on Outdoor Thermal Comfort in a Mediterranean City: A Case Study of Hebron, Palestine

Raghad Nader Zatary

Supervisors

Prof .Rabee M .Reffat

Dr. Abdel-Rahman Halawani

Thesis submitted in partial fulfillment of requirements of the degree Master of Architecture-Sustainable Design

Jan, 2026

The undersigned hereby certify that they have read, examined and recommended to the Deanship of Graduate Studies and Scientific Research at Palestine Polytechnic University:

Assessing the Effect of Façade Materials, Urban Canyon, and Orientation on Outdoor Thermal Comfort in a Mediterranean City: A Case Study of Hebron, Palestine

Raghad N Zatary

In partial fulfillment of the requirements for the degree of Master in Architecture- Sustainable Design.

Graduate Advisory Committee:

Prof. Rabee M. Reffat …….,……..

(Supervisor), University (University of Nottingham Ningbo China)

Signature:——  Date: 10/05/2026

Dr. Abdelarhamn Halawani ……, ……..

(Co-supervisor), University (Palestine Polytechnic University)

Signature:———————————— Date: 10/05/2026

Dr. Bader Al-Atawneh …….,……..

(Internal committee member), University (Palestine Polytechnic University).

Signature:———————————— Date: 10/05/2026

Dr. Sameh Monna……,……..

(External committee member), University (Al-Najah University).

Signature: 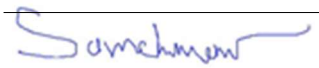 Date: 10/05/2026

Thesis Approved by:

Dr. Mahmood Al Haddad

Dean of Graduate Studies & Scientific Research

Palestine Polytechnic University

Signature:……...……

Date:…..……...……

Assessing the Effect of Façade Materials, Urban Canyon, and Orientation on Outdoor Thermal Comfort in a Mediterranean City: A Case Study of Hebron, Palestine

Raghad N Zatary

Abstract

Outdoor thermal comfort is one of the most significant challenges in cities within a Mediterranean climate, as it significantly impacts the health and well-being of residents and the quality of the urban environment, many variables influence outdoor thermal comfort. In this context, the study aims to investigate the combined effect of facade materials, street orientation, and urban canyon on outdoor thermal comfort indicators in the commercial center of Hebron.

A mixed-method approach was adopted, combining field measurements of air temperature, relative humidity, and wind speed with ENVI-met V5.6.1 simulations, following calibration and validation procedures. Three streets with different orientations and canyon configurations were analyzed, and nine façade material scenarios were evaluated based on their thermo-physical properties. Thermal performance was evaluated using comfort indices (PET and UTCI) in summer and winter, using statistical methods to test the significance of differences between certain scenarios and identify the most influential factors.

The results indicate that facade materials and urban canyon configurations together significantly affect thermal comfort levels. According to the statistical analysis, material alone affects outdoor thermal comfort. The best street orientations are north-south and northwest-southeast, while the worst orientation is east-west. The best value for urban canyons ranges from 1 to 2. The study highlights the importance of integrating material properties with urban configuration to improve outdoor thermal conditions in Mediterranean commercial streets and provides evidence-based insights to support climate-responsive urban design.

Keywords: outdoor thermal comfort/performance, urban canyon, building façade, orientation, statistical analysis, Envi met

تقييم تأثير مواد الواجهة والوادي الحضري والتوجيه على الراحة الحرارية الخارجية في مدينة البحر الأبيض المتوسط: دراسة حالة الخليل، فلسطين

رغد نادر الزعتري

المستخلص Abstract (Arabic)

تشكّل الراحة الحرارية الخارجية أحد أبرز التحديات في المدن ذات المناخ المتوسطي، لما لها من تأثير كبير على صحة ورفاهية السكان وجودة البيئة الحضرية. هناك العديد من المتغيرات التي تؤثر على الراحة الحرارية الخارجية ،وفي هذا السياق، تهدف هذه الدراسة إلى تحليل الأثر المشترك لمواد الواجهات، وتوجّه الشوارع، والوادي الحضري على مؤشرات الراحة الحرارية الخارجية في المركز التجاري لمدينة الخليل.

اعتمدت الدراسة على منهجية مزدوجة جمعت بين القياسات الميدانية لدرجة الحرارة، والرطوبة النسبية، وسرعة الرياح والمحاكاة باستخدام برنامج ENVI-met V5.6.1 بعد إجراء معايرة وتحقق لضمان دقته. وتم تحليل ثلاثة شوارع ذات اتجاهات وتكوينات مختلفة للمباني، كما تم تقييم تسعة سيناريوهات لمواد الواجهات بناءً على خصائصها الحرارية والفيزيائية. وقُيّم الأداء الحراري باستخدام مؤشرات الراحة الحرارية (PET وUTCI) في الصيف والشتاء، باستخدام أساليب إحصائية لاختبار دلالة الفروق بين سيناريوهات محددة وتحديد العوامل الأكثر تأثيرًا.

أظهرت النتائج أن مواد الواجهات وتكوين الوادي الحضري تؤثر بشكل كبير على مستويات الراحة الحرارية. ووفقًا للتحليل الإحصائي، تؤثر المادة وحدها على الراحة الحرارية الخارجية. أفضل اتجاهات الشوارع هي الشمال-الجنوب والشمال الغربي-الجنوب الشرقي، بينما أسوأها هو الشرق-الغرب. تتراوح أفضل قيمة للشوارع الحضرية بين ١ و٢. تُبرز هذه الدراسة أهمية دمج خصائص المواد مع التصميم الحضري لتحسين الظروف الحرارية الخارجية في الشوارع التجارية المتوسطية، وتقدم رؤى قائمة على الأدلة لدعم التصميم الحضري المُراعي للمناخ.

الكلمات المفتاحية: الراحة/الأداء الحراري الخارجي, الوادي الحضري , مواد المباني , التوجيه, التحليل الاحصائي,برنامج محاكاة

Declaration

I declare that the Master Thesis entitled" Assessing the Effect of Façade Materials, Urban Canyon, and Orientation on Outdoor Thermal Comfort in a Mediterranean City: A Case Study of Hebron, Palestine" is my own original work, and herby certify that unless stated, all work contained within this thesis is my own independent research and has not been submitted for the award of any other degree at any institution, except where due acknowledgement is made in the text.

Student Name…Raghad Nader Zatary

Signature:———————————— Date:————————————

Dedication

I dedicate this work to my husband, who has walked every step of this journey with me without any complaining and always pushes me to reach and achieve my goals.

To my father, my source of strength and my enduring idol, and to my mother, my warm place who cared for me and my small family.

To my little angel, my daughter Safa', who has been a source of inspiration and strength for me. I hope to be a good idol and a source of pride for you.

To the souls of those who sacrificed their blood so that we may live in dignity

To my professor Rabee Reffat, who taught me the value of critical thinking, the power of the pen and the value of things, even they were small.

Thank you

Acknowledgement

Firstly, I would like to express my gratitude to the Department of Architecture at Palestine Polytechnic University (PPU) for providing me with the opportunity to complete the master's degree.

Foremost, I would like to express my appreciation to my supervisors, Prof. Rabee M. Reffat and Dr. Abed Alrahman Halawani, for their support, wise guidance, help, and continuous encouragement in developing this master’s dissertation.

I’d also like to recognize Dr. Ramzi Al-Qawasmi and Mr. Wael Awad, who allowed me to complete the simulations through the university server.

I want to acknowledge my family and parents for their unwavering love and encouragement, and for their endless patience and kindness.

Finally, many thanks to everyone who has contributed to this work.

Table of Contents

List of Abbreviations

ACP	Aluminum Composite Panel
ANOVA	Analysis of Variance
ASHRAE	American Society of Heating, Refrigerating and Air-conditioning Engineers
BMI	Body Mass Index
d	Index of agreement
DI	Discomfort Index
E	East
EPW	Energy Plus Weather File
Eq	Equation
ET	Effective Temperature
H/W	Height-to-Width ratio
HI	Heat Index
HSI	Heat Stress Index
HW	Heavy Weight
MAE	Mean Absolute Error
MEMI	Munich Energy-balance Model for Individuals
MRT	Mean Radiant Temperature
N	North
NWCT	New Wind Chill Equivalent Temperature
OTC	Outdoor Thermal Comfort
PET	Physiological Equivalent Temperature
PMV	Predicted Mean Vote
PPD	The predicted percentage of dissatisfied
R^2	the coefficient of determination
RH	Relative Humidity
RMSE	Root Mean Square Error
S	South
Ta	Temperature
Ts	Surface temperature
Tukey HSD	Honestly Significant Difference
UA	Urban Albedo
UCA	Urban Canyon Albedo
UHI	Urban Heat Islands
UHII	UHI Intensity
UTCI	Universal thermal climate index
W	West
WBGT	Wet Bulb Globe Temperature Index
WCI	Wind Chill Index
WCT	Wind Chill equivalent Temperatures
Ws	Wind speed

List of Figures

List of Tables

Chapter 1: Introduction

1.1 Preface

Achieving thermal comfort in open urban spaces is one of the most significant challenges in cities with Mediterranean climates, as thermal comfort is directly linked to the health and productivity of residents and the quality of the built environment (Nazarian, Acero and Norford, 2019). With rapid urbanization increasing building density and declining vegetation cover in urban areas, the urban heat island effect (UHI) has become one of the most significant challenges facing cities with Mediterranean climates, such as Hebron. This phenomenon leads to higher surface temperatures, reduced air quality, and decreased outdoor thermal comfort, negatively impacting human activity and energy consumption in buildings (Lopez-Cabeza *et al.*, 2022; Tabatabaei and Fayaz, 2023). This phenomenon is influenced by several architectural and material factors, most notably the street shape (height-to-width ratio, H/W), its orientation, and the thermal and optical properties of facade materials(Chatzidimitriou and Yannas, 2017).

Design interventions, such as enhancing vegetation or employing reflective materials, can alleviate the effects of urban heat islands and enhance thermal comfort, rendering public places more habitable and appealing in warmer regions (Djamila and Moussadek, 2024). Within this context, research on building envelope systems has primarily focused on two complementary objectives: reducing the intensity of the urban heat island in the outdoor environment and achieving comfortable indoor temperatures that enhance thermal comfort quality (Wonorahardjo *et al.*, 2022). Consequently, Outdoor thermal comfort has become an emerging and essential field of research, gaining increasing importance for its direct role in improving the quality of urban life and supporting sustainable urban planning strategies (Achour-Younsi and Kharrat, 2016).

In this context, several studies have focused on the impact of facade materials on the external climate (Abrahem, Hassan and Khamees, 2020), using ENVI-met simulations in Baghdad's hot, dry climate, found that variations in facade materials lead to significant differences in MRT and PMV indices, and that materials with high mass tend to store heat during the day and release it at night. Further supporting this, (Wonorahardjo *et al.*, 2022) emphasized the role of façade thermal mass and wall composition in regulating heat storage and delayed heat release, significantly influencing outdoor thermal conditions. In addition, (Salvati *et al.*, 2022) demonstrated that façade radiative properties, particularly albedo, can alter the radiative balance within urban canyons, sometimes increasing MRT despite reducing surface

temperatures, depending on street geometry. These findings suggest that the effect of façade design on outdoor thermal comfort is complex and context-dependent, highlighting the need for further investigation into conventional façade materials and their interaction with urban canyon.

At the local level, several Palestinian studies have examined building materials mainly from the perspective of energy efficiency and indoor thermal performance., such as Nasereddin(2022) study, which analyzed the exterior walls of residential buildings in Hebron and demonstrated the importance of insulation in reducing energy consumption; and (Idkaidek, 2021) study, which compared the thermal performance of different façade cladding materials in commercial buildings. Although these studies improved understanding of building energy performance, they did not address the influence of façade materials on outdoor thermal comfort at the street scale. More recently (Atawneh and Alqadi, 2025) proposed climate adaptation strategies such as façade greening and urban afforestation to improve pedestrian thermal conditions. However, both locally and globally, most studies tend to examine urban geometry, street orientation, or façade materials separately.

Despite this progress, specialized studies on outdoor thermal comfort in Mediterranean urban environments remain limited, particularly those that integrate facade material properties with urban canyon. While some studies have examined surface properties such as albedo or emissivity e.g (Rosso *et al.*, 2018; Lopez-Cabeza *et al.*, 2022), Most research has focused on horizontal surfaces or internal thermal performance (Faragallah and Ragheb, 2022), necessitating a comprehensive study that links material properties with urban canyon to explain the variation in outdoor thermal comfort indicators in Hebron.

1.2 Problem Statement

Although the building envelope is the element most in contact with the urban climate, most previous studies have focused on the internal thermal performance of buildings, while the impact of facade materials on external thermal comfort has remained under-researched, particularly in commercially driven and high-density cities. Local studies such as (Hushlamoun, 2020; Idkaidek, 2021; Nasereddin, 2022), have shown interest in the internal thermal performance of walls and facades of buildings in Hebron, but they have not addressed pedestrian thermal comfort or the impact of facade materials on the surrounding climate. In contrast, regional and international research (Abrahem, Hassan and Khamees, 2020;

Wonorahardjo *et al.*, 2022; Tabatabaei and Fayaz, 2023) has shown that the properties of exterior materials directly affect external thermal comfort indices (PET and UTCI), but most of this research was conducted in climates other than the semi-arid Mediterranean climate.

In the Palestinian context, this problem is exacerbated by the widespread use of modern materials such as aluminum and steel for aesthetic purposes without prior thermal or environmental assessment. In Hebron, a city typical of commercial areas with a dry, hot Mediterranean climate in summer, the proliferation of these materials, coupled with the lack of green spaces and water features, has contributed to reduced thermal comfort levels in the streets and increased the likelihood of heat island formation.

Therefore, the research problem addressed in this study is: The lack of a quantitative scientific evaluation of the performance of different facade materials within the diverse urban street environments of Hebron, and how these materials perform with orientation characteristics, height-to-width ratios, and their combined impact on external thermal comfort indicators (PET, UTCI).

1.3 Research Questions

The main research question of this study is "What is the influence of façade material properties and urban configuration on outdoor thermal performance in commercial streets?"

The sub-questions are:

1. What is the level of the effect of materials for the facades and other variables on the outdoor thermal level?
2. Which materials and configurations achieve the best thermal comfort during summer and winter conditions in Hebron?
3. Which canyon aspect ratios perform best under summer/winter conditions?
4. How do façade materials interact with other urban factors, like street orientation and urban geometry, in affecting outdoor thermal performance?

1.4 Research Hypothesis

The study assumes that facade material type and its structural composition significantly influence external thermal comfort indicators, and that this effect is associated with urban variables such as orientation and aspect ratio. The research hypotheses of this study include:

RH-01: There is no statistically significant difference in outdoor thermal comfort (PET, UTCI) between different façade material compositions under identical canyon configurations.

RH-02: Street orientation and H/W ratio have no significant interaction with façade material type in determining outdoor thermal comfort levels.

RH-03: Façade material type significantly influences air temperature, humidity, and PET/UTCI indices, with either positive or negative effects.

RH-04: The combination of material, orientation, and canyon geometry has a measurable effect on outdoor thermal comfort indicators.

1.5 Research Aim and Objectives

The main aim of this research is to investigate the combined effect of façade materials, urban geometry, and street orientation on outdoor thermal performance in the commercial city center of Hebron, Palestine.

To achieve the main aim, several objectives are proposed, including:

1. Investigate the effect of façade materials and cladding compositions on microclimatic variables (air temperature, wind speed, relative humidity) and thermal comfort indices (PET and UTCI).
2. Examine the interaction between façade materials and urban geometry parameters, including canyon aspect ratio (H/W) and orientation.
3. Identify optimal physical and urban canyon geometry to improve thermal comfort in commercial streets.
4. Provide design recommendations applicable to similar environments.

1.6 Research Significance

This study addresses a critical research gap in the local and regional context of Palestine, where façade design is rarely evaluated from a microclimatic perspective. By integrating field measurements with ENVI-met simulations, the research contributes to understanding the link between building material properties, urban geometry, and thermal performance in real urban settings. The research results are supporting sustainable urban design and planning decisions.

1.7 Research Scope and limitations

The scope of the study includes the following:

1. The city of Hebron in Palestine. The climate zone of Hebron is Mediterranean: hot in summer and rainy in winter
2. The commercial area city center Hebron, urban open spaces.
3. The study focuses to two streets with different orientations.
4. The study addresses on the impact of facades overlooking the street and excluding side facades.

There are some limitations that I encountered during the research process:

1. Time constraints limited the number of scenarios and materials studied.
2. Lack of previous studies relevant to the topic in the local context.
3. Lack of measuring devices (thermal camera) to confirm simulation results from experimental results.
4. Limited accurate climate data for the studied area.

These limitations contribute to focusing the study on the factors that are most influential in the local context, with the recognition that generalizing the results requires further studies in different urban settings.

1.8 Thesis structure

In addition to Chapter 1 that presents the research problem, objectives, questions, hypotheses, and structure, the thesis content include:

Chapter 2: Theoretical Framework and Literature Review - Reviews existing literature and theories on outdoor thermal comfort, façade materials, and urban geometry.

Chapter 3: Methodology and Case Study—Describes the adopted methods, study area, data collection, data analysis, simulation setup, and calibration process.

Chapter 4: Results and Discussion—Presents and interprets simulation outcomes, statistical analyses, and comparative evaluations.

Chapter 5: Conclusions and Recommendations—Summarizes the main findings, contributions, conclusions, future work and design implications for future urban development.

chapter 1 Introduction

- Defines the study context, research gap, questions, hypotheses, scope, and structure.

Chapter 2 literature review-Theoretical study

- Reviews concepts of outdoor thermal comfort (PET, UTCI)
- Analyzes studies on material properties, orientation, H/W
- Identifies research gaps and theoretical models

Chapter 3 (Methodology,Case study)

- Describes research design and data collection-
- Explains study area (Hebron) and ENVI-met simulation setup-
- Details calibration, validation, and statistical analysis

Chapter 4 Results and discusion

- Presents measured and simulated data
- Compares material, orientation, and canyon configurations -
- Interprets results using statistical tests (ANOVA, MLR) -
- Discusses findings with reference to previous studies

Chapter 5 Conclusion and Recommendation

- Summarizes main findings
- Highlights theoretical and practical contributions-
- Provides design guidelines for planners and architects
- Suggests future research directions

Figure 1-1 Research strucure outline

Chapter 2: Urban Geometry, Façade Materials, and Outdoor Thermal Comfort: Theoretical Framework and Literature Review

2.1 Introduction

The concept of Outdoor Thermal Comfort (OTC) is a central focus in built environment studies, given its direct role in determining urban quality of life, patterns of public space use, and environmental sustainability in cities. With increasing urban density, climate change, and the rise in heat waves, urban streets—especially commercial streets—have become among the most thermally stressed spaces, negatively impacting pedestrian behavior, social activities, and public health.

Urban climate research focuses on understanding the complex relationship between microclimatic variables, the geometric characteristics of urban streets, and the thermal properties of facade materials as an interconnected system that controls the level of thermal comfort for pedestrians. The urban configuration of the street (such as height-to-width ratio and street orientation), along with the properties of facade materials (such as thermal conductivity, thermal mass, and reflectivity), play a pivotal role in modifying solar radiation, natural ventilation, and thermal energy balance within the urban valley. In this context, this study falls within the field of research linking urban development, material properties, and outdoor thermal comfort, focusing on Hebron as a case study representing Mediterranean-climate cities with a dense commercial fabric. In the Palestinian context, urban development patterns and high building density have often resulted in narrow streets with restricted ventilation and unfavorable thermal conditions.

Accordingly, this chapter establishes the theoretical foundation for the study by explaining the key concepts related to outdoor thermal comfort and the main factors influencing the urban microclimate. It also reviews relevant previous studies addressing urban geometry, façade materials, and environmental mitigation strategies in order to identify the research gap that motivates the present investigation.

2.2 Concept and Definition of Outdoor Thermal Comfort

Thermal comfort is generally defined as the mental state in which a person feels satisfied with their surrounding thermal conditions, a definition adopted by the American Society of Heating, Refrigerating and Air-Conditioning Engineers (ASHRAE). It is a key factor influencing the use of public spaces, the health of residents, and the quality of life in cities (Abd Elraouf *et al.*, 2022; Spaces and Liu, 2023).However, when applied to outdoor spaces, this concept takes on more complex dimensions compared to indoor environments, due to the constant change in

climatic factors and the impact of direct solar radiation, wind patterns, and prolonged exposure to weather conditions.

The literature indicates that outdoor thermal comfort depends on the body's thermal energy balance, which is influenced by climatic factors such as air temperature, relative humidity, wind speed, and average radiant temperature, in addition to human and behavioral factors such as physical activity and clothing (Abdollahzadeh and Biloria, 2021). It is also defined as a state of feeling but not perceived by any of the five basic senses(Spaces and Liu, 2023).

Comfortable outdoor spaces encourage individuals to use them and increase movement, physical activity, and social interaction. This, in turn, impacts individuals' psychological well-being and health. Consequently, increased use of outdoor spaces reduces the use of air conditioning within buildings, thereby reducing energy consumption, which is in line with the Sustainable Development Goals (Abd Elraouf *et al.*, 2022).

Outdoor thermal comfort differs from indoor thermal comfort, as individuals accept a wider range of thermal conditions outdoors than indoors(Ata Chokhachian *et al.*, 2017). Distinguishing between indoor and outdoor thermal comfort is a crucial issue in urban research, as indicators and criteria originally developed to assess indoor environments (such as PMV/PPD) have proven limited when applied to outdoor spaces. This is due to the significant role played by solar radiation, shading, natural ventilation, and adaptive user behavior in shaping the thermal perception of streets and squares. Outdoor spaces in hot, humid climates recorded higher thermal acceptance rates (CERs), although the so-called "neutral temperature" was not necessarily higher. The greater influence of air movement, direct radiation and shading, radiative cooling at night, as well as user behavior, clothing, and physical activity must be considered. Therefore, thermal environment design should differentiate indoors from outdoors and exploit the natural potential of open spaces to enhance thermal comfort and expand its thermal range during the transitional and summer seasons.

Accordingly, it has become necessary to adopt assessment concepts and tools that take into account the dynamic nature of the external environment and link the physical characteristics of the urban street with the behavior of users, which paves the way for the use of advanced thermal indices such as PET and UTCI, which will be discussed later in this chapter.

2.3 Factors Influencing Outdoor Thermal Comfort: A Conceptual Classification

Thermal comfort in outdoor spaces is the product of a complex interplay between a range of environmental, urban, user-related, and socio-cultural factors, making its assessment more complex than that of indoor environments. Research on outdoor thermal comfort emphasizes that these factors should not be considered in isolation but rather as part of an integrated urban system influencing the pedestrian-level microclimate. (Abd Elraouf *et al.*, 2022; Spaces and Liu, 2023)

2.3.1 Environmental and Microclimatic Factors

Air temperature is one of the most influential microclimatic factors on individuals' thermal perception. Thermal comfort also depends on other climatic factors, such as radiant temperature and wind speed. Wind speed plays an important role in achieving thermal comfort. Its influence varies depending on climatic conditions and urban context. (Abd Elraouf *et al.*, 2022; Djamila and Moussadek, 2024) It's worth noting that air movement at speeds exceeding 1.5 m/s has a significant impact on the thermal perception of outdoor space users. Relative humidity (RH) also affects the human body's thermal energy balance (Abdollahzadeh and Biloria, 2021; Abd Elraouf *et al.*, 2022).

2.3.2 Physiological factors

Due to individual differences, people may experience different thermal sensations even in the same outdoor thermal environment(Spaces and Liu, 2023). Therefore, physiological factors play a role in determining outdoor thermal comfort. These factors refer to the biological and physical processes occurring within the human body that influence how an individual perceives and responds to environmental thermal conditions. These factors operate through heat exchange mechanisms between the human body and its surroundings (Porwal, 2025).

Several studies have shown that personal factors, including age, gender, clothing insulation (Clo), and physical activity level (metabolic rate), directly influence individuals' responses to external climatic conditions. The results showed that older adults are more susceptible to heat stress due to their reduced physiological ability to regulate temperature. Women's responses differ from those of men, especially in cold environments(Aghamolaei *et al.*, 2023) ,studies show that women are more sensitive to heat, despite studies indicating their higher physiological tolerance. This discrepancy is attributed to psychological and social factors(Djamila and Moussadek, 2024). Seasonal clothing choices also affect thermal balance,

as the need for insulation increases as temperatures drop; this differs between genders, increases with age, and has a significant impact on heating energy consumption(Aghamolaei *et al.*, 2023; Djamila and Moussadek, 2024)." For example, a western outfit has a thermal insulation value of 0.3 CLO while a North African traditional loose dress in bright colors CLO value of up to 0.5"(Abd ElHamied, 2018) . Furthermore, physical activity levels are associated with increased internal heat production, which is reflected in feelings of thermal comfort or discomfort. These individual differences emphasize the importance of integrating environmental and human dimensions when assessing outdoor thermal comfort in urban spaces(Aghamolaei *et al.*, 2023). Body mass index (BMI) affects thermal comfort. Higher BMIs typically result in a higher percentage of body fat, which acts as an insulator and retains heat, potentially leading to discomfort in hot weather. Studies suggest that the effect of weight and skin color on outdoor thermal comfort is limited and variable. Those with a higher BMI tend to have lower thermal sensation, while some research has shown that skin color may affect thermal sensation to varying degrees, with darker skin tones being more sensitive. However, the evidence remains inconclusive and requires further research (Spaces and Liu, 2023; Porwal, 2025).

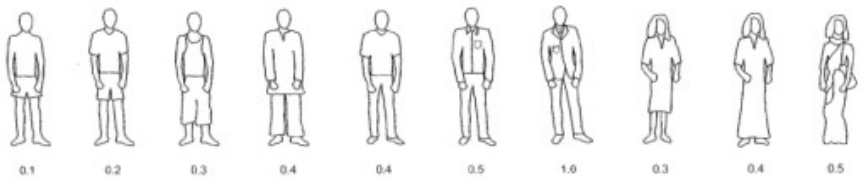

Figure 2-1 Clothing insulation value for diffrent outfits (Abd ElHamied, 2018)

2.3.3 Urban design and Physical factors

Urban design and physical characteristics of the built environment are among the most influential factors affecting outdoor thermal comfort and are the most amenable to design intervention. These factors include urban street geometry, street orientation, height-to-width ratio (H/W), sky visibility factor (SVF), and the properties of facade and surrounding surface materials. Therefore, understanding the relationship between built environment components and climate parameters is essential for designing more comfortable urban streets that are effective in mitigating climate stress in cities (Shishegar, 2013; Abd Elraouf *et al.,* 2022) .

The geometric configuration of the street directly affects the amount of solar radiation reaching pedestrian level and the patterns of natural ventilation within the urban valley, which in turn

affects air temperature and MRT. The H/W contribute to increase daytime shading, but they can simultaneously reduce nighttime heat loss and increase the intensity of the urban heat island effect(Hu *et al.*, 2020).

Conversely, facade materials play a crucial role in modifying the thermal load within a street through their radiative and thermal properties, such as reflectivity, emissivity, thermal mass, and U-value (Djamila and Moussadek, 2024). Studies indicate that high-reflectivity materials may reduce surface temperatures but can also increase the thermal conductivity due to increased reflected radiation in narrow streets, sometimes leading to reduced thermal comfort for pedestrians(Salvati *et al.*, 2022).

2.3.4 Psychological and socio-cultural factor

Outdoor thermal comfort is influenced not only by climatic and physical conditions but also by psychological and socio-cultural factors, such as preconceived expectations, prior climatic experience, cultural background, and patterns of social behavior. An individual's thermal history contributes to their tolerance to climatic conditions, while expectations based on previous experiences and cultural norms influence perceptions of comfort and satisfaction. A sense of control is also a pivotal psychological factor that enhances individuals' ability to adapt to thermal conditions (Porwal, 2025). psychological factors influence temperature perception and preferences, as individuals adapt to their environmental climate and their expectations change depending on the season or mood, with them feeling warmer or cooler based on their feelings and psychological conditions (Spaces and Liu, 2023).

Studies indicate that assessing outdoor thermal comfort requires a comprehensive understanding of sociocultural factors. Sociocultural factors, such as cultural background, religion, lifestyle, and economic and educational levels, are key determinants in shaping individuals' perceptions and interactions with the outdoor thermal environment. Cultural background plays a fundamental role in shaping individuals' responses to thermal environments through their norms and perceptions of heat. Social context is a significant factor influencing comfort perceptions, as social interactions and collective environments foster a sense of belonging and mitigate heat-related discomfort. These factors influence behavioral preferences related to sun exposure, clothing, and activities, which in turn impact their level of sensitivity and tolerance to climate conditions. Studies have shown that individuals from higher socioeconomic backgrounds tend to exhibit greater sensitivity to heat conditions. Although there have been attempts to develop assessment models that take these variables into account,

the lack of scientific consensus points to the need for further research to develop more comprehensive and accurate assessment frameworks (Spaces and Liu, 2023; Porwal, 2025) .

The study suggests that cultural and religious contexts influence individuals' thermal behavior, with women exhibiting a higher tolerance for heat due to their commitment to modest dress and avoidance of crowded spaces with men. The results confirm that thermal adaptation is influenced more by culturally associated customs and behaviors than by actual thermal comfort (Djamila and Moussadek, 2024) .

However, given that this study relies on quantitative analysis and environmental simulation to assess outdoor thermal comfort, psychological and socio-cultural factors were kept within the terms of reference, with a focus on measurable physical and urban factors, such as street geometry and facade material properties. Psycho-social factors are viewed here as an explanatory framework supporting the findings, rather than as direct analytical variables.

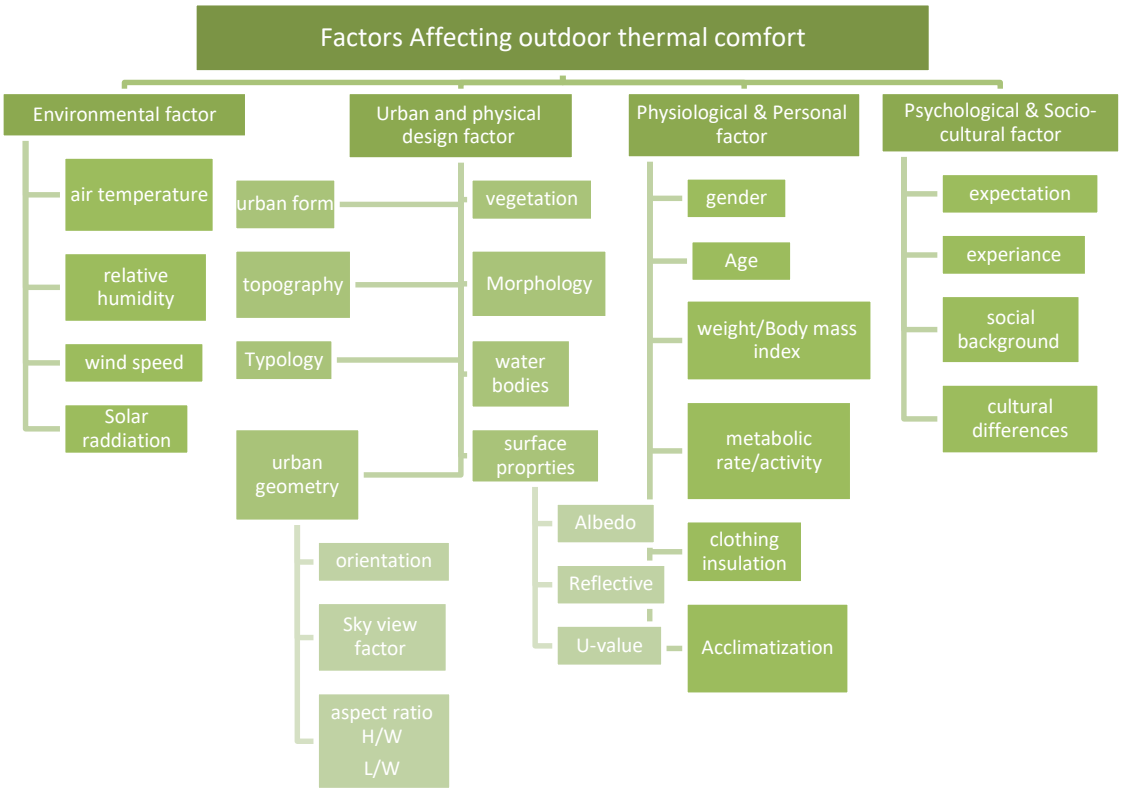

Figure 2-2 Factors affecting thermal comfort in urban spaces (author)

2.4 Urban Geometry and Street Configuration

Urban street geometry plays a pivotal role in shaping the microclimate within open urban spaces, particularly densely populated commercial streets. The literature suggests that the urban

street is not merely a passageway for movement, but a microclimate system whose geometric characteristics govern the distribution of solar radiation, natural ventilation, and heat loss or retention, directly impacting the thermal comfort level for pedestrians (Shishegar, 2013) .The concept of an urban street canyon is used to describe the space formed between two rows of buildings facing each other, where the climatic behavior is determined by a complex interplay of geometric variables, most notably street orientation, height-to-width ratio (H/W), sky view factor (SVF) , length-to-width ratio (L/W). Numerous studies have confirmed that these variables do not operate independently but rather interact to determine the intensity of thermal stress and the ventilation characteristics within the street (Shishegar, 2013).

Most academic studies agree that the height-to-width ratio (H/W) and street orientation are among the most influential urban factors in modifying the local climate within urban valleys, given their direct impact on regulating solar radiation and facilitating ventilation, which has clear implications for thermal comfort levels at the pedestrian level (Abd Elraouf *et al.*, 2022).

2.4.1 Street Orientation

Street orientation significantly affects the daily and seasonal distribution of solar radiation, particularly on vertical surfaces, although it has little impact on the total amount of radiation. Therefore, street design for efficient ventilation and optimal solar energy utilization is essential for improving the local climate and reducing building energy consumption(Shishegar, 2013).

Studies show that north-south streets provide the best outdoor thermal comfort for pedestrians, while east-west orientations are the least favorable (Abdollahzadeh and Biloria, 2021).

2.4.2 Aspect Ratio (H/W) and Canyon Geometry

The geometry of urban canyons is defined by their height-to-width ratio (H/W), which is used to classify urban street forms. An urban canyon is typically classified as a shallow canyon when $H/W < 0.5$, which exposes street surfaces to higher levels of solar radiation. A uniform canyon occurs when $H/W \approx 1$, while deep canyons ($H/W \geq 2$) provide greater daytime shading but may restrict ventilation. Canyon length (L) is an integral factor in its characterization, as the L/H ratio is used to classify canyons as short (L/H = 3), medium (L/H = 5), or long (L/H = 7), providing a precise framework for analyzing the geometric configuration of urban streets and their impact on the local climate (Shishegar, 2013; Hu *et al.*, 2020). The (H/W) affects the amount of solar energy received by street surfaces, including facades, roofs, and floors (Shishegar, 2013).

Urban street canyons are also classified based on their geometric characteristics into symmetric and asymmetric forms based on building height similarity and into complex geometries—such as intersections, overpasses, underpasses, and noise barriers—capturing structural diversity relevant to advanced urban applications(Hu *et al.*, 2020) .Urban renewal projects often result in varying building heights, creating asymmetrical urban configurations within urban canyons, which directly impact ventilation patterns, heat transfer, and outdoor air quality (Li *et al.*, 2020).

2.4.3 Sky View Factor and Shading Mechanisms

The sky visibility index (SVI) is a dimensionless indicator that reflects the percentage of sky visible from a given point, and it is closely related to both H/W and building heights (Ata Chokhachian *et al.*, 2017). Studies indicate that a lower SVI leads to lower daytime temperatures and a relatively higher nighttime temperature due to heat retention (Spaces and Liu, 2023). A higher H/W ratio reduces SVF, which limits long wave radiation loss and increases the urban heat island (UHI) intensity(Ata Chokhachian *et al.*, 2017).

Sky View Factor (SVF) is a key factor influencing the effectiveness of high-albedo materials; the higher the SVF and the greater the percentage of visible sky, the more effective these materials are in improving pedestrian thermal comfort (Lopez-Cabeza *et al.*, 2022).
Street valley geometry and orientation directly impact urban climate by regulating airflow, controlling solar radiation, influencing outdoor and indoor thermal comfort, and building energy consumption. The design challenge lies in reconciling contrasting seasonal climatic requirements, such as shading in the summer and solar exposure in the winter, which are linked to compactness and openness to the sky. The height-to-width ratio (H/W) and street orientation are among the most prominent parameters influencing local climate, yet there remains a need to provide accurate, scientifically based quantitative data to guide the design of climate-efficient urban streets (Shishegar, 2013).

This analysis demonstrates that urban engineering forms the dominant framework for the thermal environment within a street, but it does not operate in isolation from the thermal properties of facade surfaces. Therefore, the next section of the chapter moves on to analyze the role of facade materials and their thermal properties in modifying thermal comfort within urban streets.

2.5 Façade Materials and Thermo-Physical Properties Affecting OTC

Non-geometrical configurations refer to the set of material and surface characteristics that affect the outdoor thermal environment without altering the physical geometry of the urban canyon. These parameters determine how building envelopes absorb, store, reflect, and release heat, thereby influencing the surrounding microclimate and the level of outdoor thermal comfort (OTC). While geometric parameters such as height-to-width ratio and orientation control solar access and shading, non-geometrical factors govern the thermal behavior of façades and their interaction with the environment through radiation and conduction processes. This category mainly includes two essential components: surface properties and thermo-physical properties of building materials.

2.5.1 Surface Radiative Properties (Albedo, Emissivity)

The thermal properties of building materials are crucial in influencing how walls and facades respond to the external climate and in determining thermal comfort levels in urban areas. The radiative properties of materials are among the most important factors determining the amount of solar energy absorbed or reflected by a surface (Djamila and Moussadek, 2024). Albedo expresses the surface's ability to reflect solar radiation, and its values range from 0 to 1, with darker surfaces absorbing more radiation and lighter surfaces reflecting more (Lopez-Cabeza *et al.*, 2022). Absorptivity also contributes to determining the percentage of radiation absorbed, dark-colored or low-reflectance materials absorb more heat, contributing to higher daytime surface temperatures. while emissivity determines the surface's ability to re-radiate long-wavelength heat, which is an important factor for the effectiveness of nighttime cooling (Tripathy, 2006).

2.5.2 Thermo-physical Properties of Façade Materials (Conductivity, Thermal Mass, Thermal Inertia)

In addition to radiative properties, thermo physical properties influence how a material responds to daily temperature variations. These properties include thermal conductivity (k), specific heat capacity (Cp), and density (ρ), thermal mass and thermal inertia (Balaji, Mani and Venkatarama Reddy, 2013; Hong *et al.*, 2022) .These values reflect the material's ability to store heat during the day and release it later, which may improve thermal stability or exacerbate nighttime heating depending on the urban context(Wonorahardjo *et al.*, 2022) .The thermal inertia of a building facade material represents its ability to store heat, and can significantly affect the range of temperature variation of its surface (Hong *et al.*, 2022).

Time lag represents the delay between the peak of the external temperature and the corresponding temperature peak on the inner surface.
U-value is used as a general indicator for measuring the rate of heat transfer across a wall layer assembly(Tripathy, 2006) .In general, the literature suggests that a lower U-value implies a lower conductivity transition, which may reduce the heating of the facade and adjacent air during peak hours. However, the results are not always linear; materials with a high thermal mass may store and release significant heat at night, increasing nighttime heat stress in densely populated streets (Tripathy, 2006; Johra, 2019).

2.5.3 Heat Transfer Mechanisms in Urban Streets

The effect of facades on thermal comfort is mediated through three main heat transfer pathways: conduction within the wall layers, the rate of conduction depends on the thermal conductivity and thickness of the material, convection between the surface and the surrounding air depending on wind speed and radiation between surfaces and the sky, and between opposite surfaces within the urban valley (Tripathy, 2006), the thermo physical properties of the façade material and the insulation layer that has been added to the façade wall have a significant impact on heat transfer behavior (Wonorahardjo *et al.*, 2022).

High albedo generally reduces surface temperatures but may increase MRT and PET values in narrow urban spaces due to multiple radiation reflections. Therefore, it is recommended to use low and medium albedo walls (0.1- 0.4) with high albedo floors (>0.7) to achieve a better balance between heat reduction and improved thermal comfort. In addition, it is necessary to combine albedo with other strategies such as shading and green facades. (Lopez-Cabeza *et al.*, 2022; Salvati *et al.*, 2022)

It is worth noting that (Ata Chokhachian *et al.*, 2017) study focused on the external surface properties of facades, such as reflectivity and emissivity, along with street orientation and W/W, to analyze their direct impact on the urban climate, whereas this thesis addresses the wall as an integrated thermal mass with all its layers (stone, concrete, insulation, etc.). This methodological difference expands the scope of the analysis and allows for a deeper understanding of the impact of the entire material composition of the wall on external thermal comfort.

2.6 Thermal Comfort Indices Used in Outdoor Studies (PET & UTCI)

Due to the complexity of factors influencing outdoor thermal comfort, it is no longer possible to characterize human thermal sensation based solely on a climatic variable, such as air temperature. Therefore, composite thermal comfort indices have been developed, combining climatic variables with human physiological characteristics to provide a more comprehensive assessment of comfort or thermal stress in outdoor environments (Spaces and Liu, 2023) .Over one hundred thermal indices have been developed to assess hot and cold environments; however, many of them were designed primarily for indoor environments or rely on static assumptions that do not account for the dynamic nature of outdoor spaces, particularly urban streets exposed to direct solar radiation and constant wind variations as shown in Table 2-1 (Walls, Parker and Walliss, 2015) .In this context, the Physiologically Equivalent Temperature (PET) and Universal Thermal Climate Index (UTCI) have emerged as two of the most widely used and reliable indicators in outdoor thermal comfort studies.

Table 2-1 Parameters related to commonly used thermal comfort evaluation indices.(Spaces and Liu, 2023)

index	Ta	Rh	Ws	Average radiant temperature	Skin moisture	Core temperature	Clothing thermal resistance	Human metabolic
HIS	•			•				•
WBGT	•	•	•	•				
DI	•	•						
HI	•	•						
WCI	•		•					
WCT	•		•					
NWCT	•	•	•			•		
ET	•	•	•					
ET*	•	•	•		•	•		•
SET*	•	•	•		•	•	•	•
OUT_SET*	•	•	•	•	•	•	•	•
PMV	•	•	•	•			•	•
PET	•	•	•	•	•	•	•	•
UTCI	•	•	•	•	•	•	•	•

2.6.1 Physiological Equivalent Temperature

The PET index is one of the most commonly used indicators in urban studies, particularly in temperate and Mediterranean climates. It was developed based on the Human Body Energy Balance (MEMI) model, integrating air temperature, wind speed, relative humidity, and mean radiant temperature (MRT), assuming standard reference conditions for clothing and physical activity (Matzarakis, Mayer and Iziomon, 1999) .PET is distinguished by being expressed in degrees Celsius (°C), making it easier for urban planners and decision-makers to interpret compared to other, and more complex indicators. German technical guidelines (VDI 3787) recommend PET as a standard tool for assessing the thermal component of urban climate. The

literature indicates that PET is particularly well-suited for analyzing spatial differences within cities, such as comparing streets with different orientations or geometric configurations (Matzarakis, Mayer and Iziomon, 1999) (Błazejczyk *et al.*, 2013; Walls, Parker and Walliss, 2015).

However, some studies suggest that PET may show limited sensitivity in highly variable environments or in situations where climatic conditions exceed the range of moderate thermal comfort, thus calling for its support with more comprehensive indicators in certain climatic contexts.

2.6.2 Universal Thermal Climate Index

The UTCI was developed by an international committee of the International Society of Biometeorology with the aim of creating a global index capable of assessing heat stress across different climates and seasons. The UTCI is based on an advanced Fiala multi-node physiological model, which takes into account the dynamic interactions between the human body and its surrounding environment (Błazejczyk *et al.*, 2013; Walls, Parker and Walliss, 2015).

The UTCI is defined as the air temperature under reference conditions (still air, 50% relative humidity, and complete shade) that elicits the same physiological response as actual climatic conditions. This index is unique in its ability to classify heat stress within clear ranges, from "severe heat stress" to "no heat stress," making it an effective tool for comparing different locations and climates (Walls, Parker and Walliss, 2015).

Studies have shown that UTCI is more flexible than PET in representing thermal responses under extreme conditions; however, its interpretation may be less straightforward for non-experts compared to PET, due to its reliance on a more complex physiological model (Evgenia, Mela and Tseliou, 2024).

2.6.3 Comparison and Rationale for Using PET and UTCI

The Physiological Equivalent Temperature (PET) and the Universal Thermal Climate Index (UTCI) are among the most widely used indices in outdoor thermal comfort research. Both indices are based on the human energy balance concept; however, they differ in their underlying models and level of physiological complexity.

The literature suggests that using PET and UTCI together provides a more integrated picture of outdoor thermal comfort, with PET enabling accurate and easy-to-interpret spatial analysis, while UTCI provides a more comprehensive physiological assessment of thermal stress across varying climatic conditions (Błazejczyk *et al.*, 2013; Walls, Parker and Walliss, 2015).

In the context of urban streets with a Mediterranean climate, numerous studies have demonstrated that combining these two indices helps capture the differences arising from street geometry, facade materials, and levels of shading and ventilation.

2.7 Urban Heat Island Effect and Its Relation to Outdoor Thermal Comfort

The urban heat island (UHI) phenomenon is one of the most prominent environmental challenges associated with rapid urbanization, where temperatures are higher in urban areas compared to surrounding rural areas. This phenomenon is directly linked to a decline in outdoor thermal comfort, particularly in densely populated urban streets, due to heat accumulation and retention within the built environment(Abdollahzadeh and Biloria, 2021; Ornam, Wonorahardjo and Triyadi, 2024).

An urban island is described as a dome of warm, stagnant air covering dense urban areas(Najah, Abdullah and Abdulkareem, 2023).

2.7.1 Causes of Urban Heat Island in Street Canyons

The causes of urban heat islands are numerous, but the literature agrees that the shift from natural surfaces to build surfaces with high heat capacity and low reflectivity is the primary factor exacerbating this phenomenon. Materials such as asphalt and concrete absorb large amounts of solar radiation during the day and release it slowly at night, leading to higher nighttime temperatures and reduced effectiveness of natural cooling(Mohajerani, Bakaric and Jeffrey-Bailey, 2017; Piselli et al., 2018; Ornam, Wonorahardjo and Triyadi, 2024).

In the context of urban streets, this phenomenon is exacerbated by the urban engineering of the urban valley, where high height-to-width ratios (H/W) and a low sky visibility factor (SVF) limit the loss of long-wavelength heat to the night sky, and contribute to the trapping of radiation within the urban space(Rosso *et al.*, 2018).

2.7.2 Relationship between UHI and Outdoor Thermal Comfort

Mitigating the urban heat island effect is an important measure to improve outdoor air temperature (OTC). As the UHI increases, the outdoor ambient temperature rises, heat waves

become more frequent, heat stroke becomes more common, and OTC decreases. In addition, air flow rate plays a crucial role in convective and evaporative heat transfer, which in turn affects thermal comfort. This study highlights the relationship between the severity of the heat island and the deterioration of outdoor thermal comfort conditions. Therefore, understanding this relationship is essential to guide sustainable urban planning strategies and improve the quality of life in urban areas(Ren *et al.*, 2023). Human activities, such as traffic and air conditioning systems, also add artificial heat loads that increase the intensity of the heat island effect, especially in busy commercial streets(Mohajerani, Bakaric and Jeffrey-Bailey, 2017).

2.7.3 Mitigation Strategies and Their Implications for OTC

Several methods can mitigate the impact of the heat island phenomenon in cities. Among these methods used to reduce solar radiation absorption and lower surface temperatures is the use of reflective materials, such as white roofs and highly reflective pavements. Vegetation coverage, whether through green roofs or tree planting, is also a prominent natural means of mitigating this phenomenon.

Shading, whether using natural elements such as trees or through the creation of canopies and architectural structures, is a direct means of reducing the heat load in urban spaces. It reduces the amount of direct solar radiation and radiant temperatures, improving thermal comfort for pedestrians and reducing the need for cooling within adjacent buildings. Advanced solutions also include the use of thermally smart materials, such as modular composite materials (PCMs) and thermochromic materials, in addition to improving natural ventilation patterns and redesigning urban blocks to enhance air circulation. The integrated alignment of these strategies within the framework of sustainable urban design is one of the most effective ways to reduce the effects of heat islands and achieve a more comfortable, healthier, and energy-efficient urban environment (Akbari *et al.*, 2016).

One proposed strategy to mitigate the urban heat island phenomenon is to use interior courtyards as urban cooling islands. Interior courtyards are a traditional architectural element that contributes to a moderate local climate, enhancing thermal comfort and reducing cooling energy consumption in buildings (Lopez-Cabeza *et al.*, 2022).

2.7.4 Urban Heat Island and Outdoor Thermal Comfort in the Palestinian Context

In the Palestinian context, the effects of the urban heat island are compounded by unplanned urban growth, land scarcity, and geopolitical constraints that have limited horizontal expansion and led to denser urban fabric within cities. These factors have contributed to a decline in green spaces and an increased reliance on manufactured materials, further intensifying the UHI in Palestinian cities (Shaheen, 2013).

Local studies, such as (Abadla, 2020) one in Tulkarm, have shown that urban areas experienced higher temperatures and lower wind speeds compared to surrounding areas, leading to increased levels of heat stress, particularly during the summer. These findings underscore that improving outdoor thermal comfort in Palestinian cities requires a comprehensive approach that combines urban planning improvements and the selection of appropriate facade materials, rather than relying on piecemeal solutions.

This section explains that the urban heat island phenomenon represents the broader climatic framework within which street characteristics and facade materials interact to determine the level of outdoor thermal comfort. The final section then provides an analytical summary of previous studies and identifies the research gap that this study aims to address.

2.8 Previous studies:

This section systematically reviews previous studies that addressed the influence of urban configuration, facade materials, and microclimatic variables on outdoor thermal comfort to identify relevant research trends and scientific gaps. The review included studies from the period 2007–2025 in hot, dry, humid, and Mediterranean climates, providing a comparative basis with the Mediterranean context of Hebron.

The review is organized according to key themes, including urban variables (orientation, aspect ratio, SVF), material and surface characteristics, green elements and shading strategies, and microclimatic variables. The chapter concludes by presenting the optimal values for these factors, highlighting research gaps that provide the framework for the current study.

2.8.1 Studies on urban geometry

Although this study focuses on a specific set of variables—facade materials, street orientation, and height-to-width ratio (urban configuration)—this part reviews additional variables that influence outdoor thermal comfort. The review aims to situate the study's variables within its

broader research framework and to pave the way for future studies in urban commercial contexts.

To enhance clarity and avoid unnecessary repetition, a synthesized comparative review of previous studies, focusing on objectives, methodologies, key findings, and limitations. Detailed numerical outputs and scenario-level results reported in original studies are therefore reproduced in references.

Ali-Toudert and Mayer conducted a numerical study using the ENVI-met 3.0 model to evaluate the effect of the geometric configuration of urban canyons on thermal comfort in a hot, dry climate (Ghardaia, Algeria). The study analyzed the influence of street orientation, aspect ratio (H/W = 1 and 2), symmetry, galleries, architectural overhangs, and vegetation. The results indicated that east–west (E–W) oriented streets recorded the highest PET values (up to 67°C) and were most exposed to heat stress compared to N–S, NE–SW, and NW–SE orientations, which recorded shorter and less intense periods of thermal discomfort. Galleries significantly reduced the duration and intensity of thermal discomfort, especially in E–W streets at H/W = 2, while architectural overhangs were more effective in N–S and NW–SE streets. Asymmetric configurations also improved ventilation and nighttime cooling, although they were less efficient during the day. As for trees, they reduced the PET index by up to 24°C under dense canopies, with limited local impact. The study concluded that a thoughtful combination of design elements, orientation, and aspect ratio achieves a significant improvement in thermal comfort on urban streets.(Ali-Toudert and Mayer, 2007)

A study conducted in Singapore using numerical simulations demonstrated that street design has a direct impact on outdoor thermal comfort. The results indicated that streets oriented northwest to southeast (NW–SE) with a height-to-width ratio (H/W = 3) provide more favorable thermal conditions for pedestrians, making this urban configuration recommended for improving thermal comfort levels in urban environments with hot, humid climates.(Aboelata, 2020)

Unlike other studies that focused on the pedestrian level, (Tablada and Nouri, 2021) examined thermal comfort conditions on open balconies within urban canyons in Barcelona. The results showed that orientation and height were crucial factors, with balconies at 6–9 m being most comfortable, while northern balconies on east–west streets, and balconies above 12 m,

experienced elevated levels of thermal stress. This expands the analysis from horizontal (pedestrian) to vertical (building) thermal comfort.

Qaid and Ossen (2014) studied the effect of asymmetric height-to-width ratios (H1/W–H2/W) in urban streets on microclimates in a hot and humid environment, simulating a northeast-southwest-oriented Putrajaya Boulevard in Malaysia using the ENVI-met model. The study focused on six urban canyon scenarios with varying ratios as shown in Figure 2-3, Figure 2-4. The study found that asymmetric configurations significantly enhance outdoor thermal comfort by reducing solar radiation, improving ventilation, and altering temperature distribution. A configuration of 2–0.8 (taller buildings on the northwest side) reduced air temperature by up to 4.7°C and surface temperatures by 10–14°C. The authors recommended asymmetrical street design as an effective strategy to balance shading and airflow in tropical climates.(Qaid and Ossen, 2014)

The sky view factor (SVF) is important in determining street exposure to solar radiation; however, it is insufficient to explain climatic differences without considering street orientation and the location of tall buildings. The study confirmed that similar SVF values in certain scenarios (such as 2–0.8 and 0.8–2) can produce different climatic conditions, depending on the location and shade of buildings.(Qaid and Ossen, 2014)

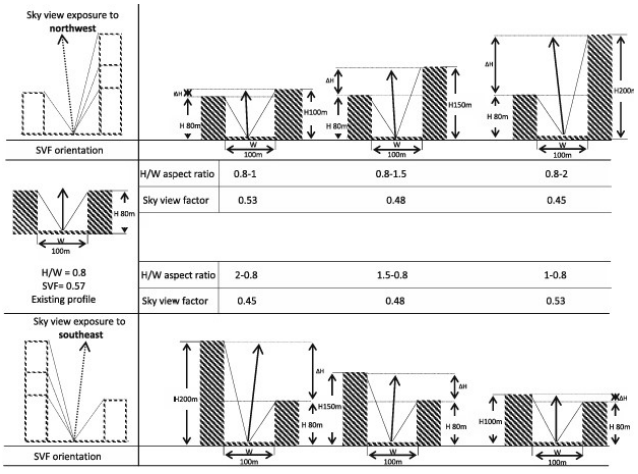

Figure 2-3 Asymmetric H/W ratios in urban canyons(NE-SW orientation) as reported in a study Orientation(Qaid and Ossen, 2014)

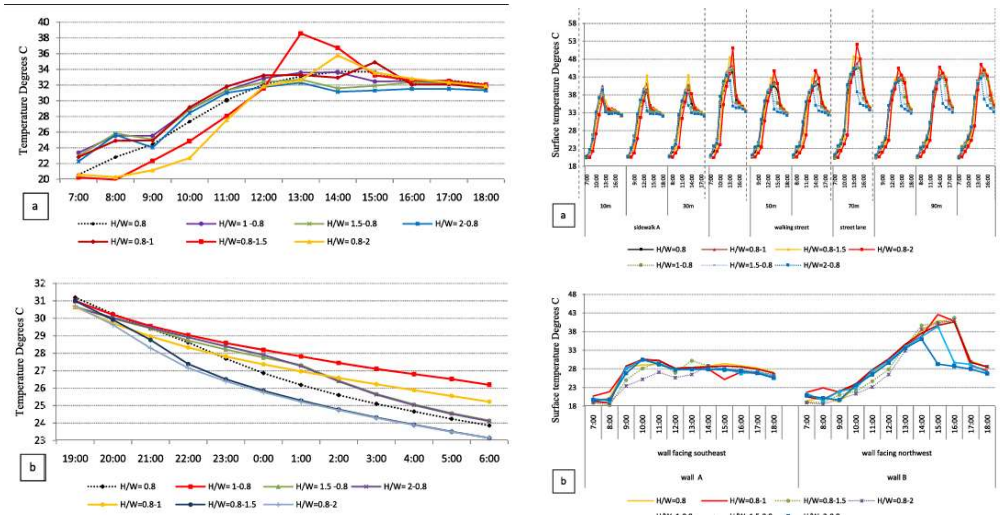

Figure 2-4 left(Variations in air temperature during the day (a) and at night (b))-Right(Ground surface temperatures (a) and wall temperatures (b) during the day)(Qaid and Ossen, 2014)

Table 2-2 Previous Study for urban geometry

Ref	Aim	Climatic season	METHODOLOGY	Key Findings	Limitations
(Abd Elraouf et al., 2022)	To assess the impact of urban geometry on outdoor thermal comfort	Hot-Humid-Summer (July)	Field measurements + Simulation (ENVI-met v4.4.5 + Rayman)	The H/W ratio is the most influential factor on thermal comfort (PET difference ≈ 5.8°C). Optimal performance is achieved when H/W = 2.5 with an N–S and NW–SE orientation. The orientation has a greater impact than the building style.	The study is limited to a hot-humid climate and a single city, and relies solely on simulation, without analyzing the impact of materials, vegetation, or human behavior.
(Abdollahzadeh and Biloria, 2021)	Analyze and improve outdoor thermal comfort by simulating the influence of street orientation, H/W ratio, building type, and landscaping.	Humid Subtropical - Summer	Simulation(ENVI-met V4.4.5 + Biomet V2.0)	Street orientation had the greatest impact (≈46.42%) on improving thermal comfort, followed by the water/water ratio (≈30.59%), while wind speed was the most significant climatic factor affecting this coastal area. Tree insertion also reduced PET, but its effect was less pronounced.	The results are based on simulation modeling of specific urban conditions in Sydney, and may not be generalizable to different urban climates or satellites without field verification or broader seasonal analysis.
(Qaid and Ossen, 2014)	Evaluating the impact of asymmetric ratios (H1/W – H2/W), with the aim of improving shading and ventilation and reducing heat island in hot and humid areas.	Hot humid/summer day & night	Field measurements + Simulation(ENVI-met V3.1 Beta)	2–0.8 reduced air temp by 4.7°C and surface temp by 10–14°C; taller NW buildings improve afternoon shading; SVF alone insufficient to predict thermal performance; asymmetry enhances microclimate adaptation in hot–humid contexts.	The results are based on ENVI-met modeling at a single location and may not be generalizable to all urban examples or other climates without broader field verification or inclusion of other factors such as materials and vegetation surfaces.

Ref	Aim	Climatic season	METHODOLOGY	Key Findings	Limitations
(Ali-Toudert and Mayer, 2007)	To evaluate the effect of geometrical street design features on outdoor thermal comfort	Hot-dry (Ghardaia, Algeria) – Summer (01 August)	Simulation(ENVI-met 3.0)	Design elements have a limited impact on air temperature but a strong effect on thermal perception. Increased skylight exposure increases thermal stress, with the east-west orientation being the worst. Shading through galleries, projecting facades, and vegetation reduces discomfort.	The results are based on modeling of specific conditions and climates, and may not be generalizable to all cities or climates.
(Chatzidimitriou and Yannas, 2017)	Evaluate impact of street geometry, shading, and vegetation on PET across seasons	Mediterranean – summer & winter	Field measurements + simulations(ENVI-met v4 + Rayman)	The head-to-wheat ratio has a strong effect on shading and radiant temperature. Deep valleys improve comfort in summer. Street orientation is a crucial factor, as comfort is reduced on directions directly exposed to the sun, especially east-west.	The results are based on simulations of specific scenarios and a particular climate, and do not include the influence of materials, vegetation, or human behavior.
(Elkhayat et al., 2024)	Assess effect of aspect ratio (H/W) and orientation on outdoor thermal comfort in two contrasting climates in Egypt	Aswan (hot desert, summer) Alexandria (hot-humid, summer)	Field data (validation) + simulations (ENVI-met V4.0 + Rayman V3.1)	It showed that deep urban formations and high H/W ratios reduce solar radiation and radiant temperature and improve thermal comfort in summer, and that street orientation is a crucial factor in determining the level of thermal stress.	The study is confined to a hot desert climate and theoretical engineering scenarios, and does not incorporate the impact of materials, vegetation cover, or extensive field verification, which limits the generalizability of the results to other urban and climatic contexts.
(Achour-Younsi and Kharrat, 2016)	Analysis of the impact of urban canyon engineering (street surrounded by buildings) on outdoor thermal comfort in the city of Tunis.	Mediterranean subtropical – summer	SIMULATION(ENVI-met (3D microclimate model)	The heat/water ratio strongly influences shading and radiant temperature. Deep valleys improve thermal comfort in summer. Street orientation is a crucial factor, with increased heat suffering in sunnier directions.	The study is limited to one city and a specific climate, relies more on simulation than extensive measurements, and does not incorporate the effect of materials or vegetation cover in detail.
(Jareemit and Srivanit, 2019)	Assess the effect of street canyon orientation, aspect ratio, and length on wind velocity and pedestrian ventilation potential	Hot-humid (Bangkok, Thailand) – annual	Simulation + validation(ENVI-met v4)	The shape and orientation of a valley greatly influence wind speed. More open valleys allow for better ventilation, while deep, enclosed valleys reduce wind speed. A street oriented in line with the prevailing wind provides optimal ventilation.	The study focuses on suburbs in Bangkok and a hot-humid climate only, and relies on simulation without a comprehensive integration of the effect of materials or direct thermal comfort (such as PET or UTCI).

Ref	Aim	Climatic season	METHODOLOGY	Key Findings	Limitations
(Tablada and Nouri, 2021)	To assess thermal comfort conditions in open balconies in relation to street orientation and height	Mediterranean – Summer	Simulation(Rayman pro)	The street layout clearly affects the degree of solar exposure and ventilation on balconies. Deeper streets and less sun-exposed directions improve thermal comfort, while direct sun exposure increases heat stress.	The study is confined to a Mediterranean climate and specific design cases, and relies primarily on simulation without extensive coverage of the impact of materials, human behavior, or long-term field measurements.
(Taleghani et al., 2015)	Evaluation of the impact of urban forms (single, linear, courtyard) on outdoor thermal comfort in a temperate climate	Temperate (Netherlands) – Summer	Simulation + Field Validation (ENVI-met 3.1 + Rayman 1.2)	The shape of the urban fabric clearly affects shading and ventilation. More compact forms improve shading but may impair ventilation, while open forms improve wind with increased solar exposure.	The study is limited to a temperate climate and specific design cases, and does not focus on the impact of materials, human behavior, or extreme climatic variations.

2.8.2 Studies on façade materials

A study by (Abrahem, Hassan and Khamees, 2020) examined the effect of façade materials on outdoor thermal comfort in residential areas of Baghdad using ENVI-met. Six common materials were analyzed based on air temperature, MRT, wind speed, humidity, and PMV. The results showed that façade materials significantly affect thermal comfort in high-rise buildings, while their impact is limited in low-rise cases. Thermo-stone with granite finish achieved the best performance, whereas burnt brick showed the lowest.

(Wonorahardjo *et al.*, 2022) demonstrated that the behavior of walls in radiating heat inward and outward varies depending on the facade system. The results indicated that a conventional brick wall acts as a thermal mass that stores a significant amount of solar energy during the day and releases it later, with the heat emitted outward being twice as much as the heat emitted inward, which explains its contribution to the urban heat island effect (UHI). In contrast, the use of natural insulation materials (such as newspapers and corn husks) reduced the heat emitted to the outside by approximately 2°C, while lowering the indoor air temperature by more than 1°C. The addition of aluminum composite panels (ACPs) with insulation and air gaps improved the indoor thermal performance but increased the ambient air temperature by approximately +4°C during the daytime heating period. These results highlight the importance

of balancing indoor thermal comfort with minimizing the external impact on the urban climate when selecting facade systems.

The study of (Vassiliades, Savvides and Buonomano, 2022) investigates the effect of active solar energy systems on existing facades of buildings on thermal comfort in public spaces in two coastal cities of Naples, Italy, and Thessaloniki, Greece, using physiological equivalent temperature. Thermal conditions are simulated at street level by Envi-MET. The study compared the thermal conditions in public places before and after the integration of solar energy systems in the facades of buildings for a typical example of the urban system for each city. Simulation results show that the negative effects of solar energy systems on the public space temperature and thermal comfort at the level of the pedestrian street are limited.

Studies (Lopez-Cabeza *et al.*, 2022; Salvati *et al.*, 2022)indicate that high albedo reduces surface temperatures but may increase MRT and PET values in narrow urban spaces due to multiple radiation reflections. Therefore, it is recommended to use low and medium albedo walls (0.1- 0.4) with high albedo floors (>0.7) to achieve a better balance between heat reduction and improved thermal comfort. In addition, it is necessary to combine albedo with other strategies such as shading and green facades.

It is worth noting that (Ata Chokhachian *et al.*, 2017) study focused on the external surface properties of facades, such as reflectivity and emissivity, along with street orientation and W/W, to analyze their direct impact on the urban climate, whereas this thesis addresses the wall as an integrated thermal mass with all its layers (stone, concrete, insulation, etc.). This methodological difference expands the scope of the analysis and allows for a deeper understanding of the impact of the entire material composition of the wall on external thermal comfort.

In the context of facade cladding, the literature presents examples such as aluminum composite panels (ACP/Alucobond) as common architectural solutions, but they may yield varying results depending on the layering configuration (presence of air gap/insulation) and the properties of the internal core. Some studies suggest alternatives such as WPC to improve the material's thermal performance (Mahmood Mussa and Wasmi M. Salih, 2020).

Table 2-3 Previous studies for material variables

Ref-year of publication	Aim	Climatic season	Methodology	Key Findings	Limitations
(Abrahem, Hassan and Khamees, 2020)	Evaluation of the effect of facade materials of mass residential buildings (high-rise and low-rise) on external thermal comfort in a hot, dry climate	Hot and dry – Baghdad/summer (21July)	simulation (ENVI-met V4.4.4)	Facade materials significantly affect radiant temperature and thermal perception. Materials with high reflectivity or appropriate thermal mass improve outdoor comfort compared to darker or highly absorbent materials.	The study is limited to a hot-dry climate and specific housing conditions, relies more on simulation than long-term measurements, and does not deeply incorporate the impact of vegetation cover or human behavior.
(Rosso *et al.*, 2018)	Evaluating the impact of innovative materials on thermal comfort in historic urban canyons	Mediterranean climate-Summer	Field measurement-simulation(ENVI-met)	Innovative materials with enhanced reflectivity or emissivity reduce radiant temperature and improve thermal perception, while their effect on air temperature is limited.	The study is limited to specific historical sites and climates, relies on simulation without extensive field investigation, and does not study the interaction with urban engineering in depth.
(Tabatabaei and Fayaz, 2023)	Assess effect of façade materials and coatings on UHI mitigation & outdoor thermal comfort	Hot semi-arid (Shiraz, Iran) – Summer	Field measurement + simulation(ENVI-met 4.4.5)	Highly reflective coatings and light-colored materials reduce surface temperature and radiant temperature and improve thermal comfort, while their effect on air temperature is relatively less.	The study is limited to a hot, semi-arid climate and specific design cases, and relies on simulation without extensive field verification, and does not incorporate the effect of vegetation cover or human behavior.
(Wonorahardjo *et al.*, 2022)	Assess effect of different façade systems on indoor comfort and outdoor UHI	Tropical (Indonesia) – Summer (dry season)	Field measurements + Laboratory experiments(Experimental (no simulation software)	Facade systems with better thermal properties (higher reflectivity, adequate insulation or thermal mass) reduce surface temperature and radiant temperature and improve thermal feel, with a limited effect on air temperature.	The experiment is confined to a single location and a limited number of systems, does not represent all urban or climatic contexts, and does not comprehensively study the interaction of the facade with street .architecture

Ref-year of publication	Aim	Climatic season	Methodology	Key Findings	Limitations
(Salvati *et al.*, 2022)	Assess impact of reflective materials on UCA, outdoor thermal comfort, and indoor environment	Temperate (London, UK) – summer heatwave (July 2019)	Field measurements + Physical 1:10 scale model + simulations (ENVI-met v4.4.6+ Energy Plus)	Reflective materials raise the albedo and reduce surface temperature and radiant temperature, improving outdoor comfort and reducing indoor heat load, while their effect on air temperature is limited.	The study focuses on specific conditions and climates, and does not adequately incorporate the impact of complex urban engineering, human behavior, or vegetation cover.
(Lopez-Cabeza *et al.*, 2022)	Assess influence of surface albedo on microclimate and thermal comfort in small courtyards	Mediterranean (Csa) – hot summer	Field monitoring (2017, 2018) + ENVI-met validation & simulations(ENVI-met v4.4.5 (validated with in-situ data, BioMet for PET))	High albedo reduces surface temperature and radiant temperature and improves daytime thermal comfort, but may increase unpleasant reflections in some cases.	The study focuses on courtyards, a single season, and a Mediterranean climate. It relies on simulation without extensive field verification and does not include streets or the open urban fabric.
(Faragallah and Ragheb, 2022)	Evaluate effect of cool paving on UHI mitigation and pedestrian thermal comfort	Mediterranean – Summer (Alexandria, Egypt)	Simulation + validation (ENVI-met + meteorological station)(ENVI-met 4.0)	Cold paving materials reduce surface temperature and radiant temperature and improve thermal feel, while their effect on air temperature is limited.	The study is limited to specific cases and climates, relies on simulation without extensive field verification, and does not fully integrate the impact of facades or vegetation cover.
(Yuan, Farnham and Emura, 2021)	Assess effect of DHR, SR, RR façade reflections on outdoor thermal environment and indoor loads	humid subtropical climate-summer	Simulation(CFD (STREAM))	Mirror-reflective surfaces strongly alter the radiation distribution and may increase local thermal stress, while diffuse reflection is thermally safer. The effect of reflective properties is greater on radiation and Tmrt than on air temperature.	The study is based on CFD modeling of specific theoretical cases and does not include extensive field verification or interaction with complex urban architecture or user behavior.

However, it is noted that there is little research in the existing literature concerning the potential impacts of façade materials on outdoor environments, accounting for the UHI effect.

2.8.3 Studies on vegetation and shading

The Sri Lanka study indicated that shading in deep canyons (high H/W) is the primary strategy for reducing air temperature and improving thermal comfort, as it reduces the exposure of surfaces and pedestrians to direct sunlight (Aboelata, 2020).

Tall street trees alter wind movement and impair ventilation within urban canyons, leading to increased concentrations of air pollutants (Cui *et al.*, 2022) . 100% vegetation coverage of the facades showed a maximum decrease in air temperature (Ta) of 1°C and an average of 0.3°C (Cui *et al.*, 2022). Vertical trees have less impact on wind speed than traditional trees, which may help avoid negative impacts on street air quality (Cui *et al.*, 2022).

Vertical vegetation systems (VGS) provide their greatest thermal benefits at the pedestrian level, while their impact is significantly reduced when placed above 6 meters above ground level. VGS systems help reduce the temperature of building exterior surfaces by reducing their exposure to direct solar radiation (Cui *et al.*, 2022).

The study emphasizes the importance of preserving green spaces, as converting them into buildings and streets negatively impacts the local climate, environment, and urban structure. It also highlights the role of building forms, especially plazas, in increasing the heat island phenomenon in hot and dry climates due to the loss of vegetation to urban expansion (Tawfeeq Najah, Fakhri Khalaf Abdullah and Ameen Abdulkareem, 2023).

The study, which examined the impact of converting urban green spaces (GUSs) in Baghdad, emphasizes the importance of these spaces in improving thermal comfort in a hot, dry climate. The results showed that converting these spaces into solid buildings led to a significapnt increase in temperatures and deterioration in thermal comfort conditions. The study also highlighted the impact of urban configuration and courtyard shape on the local climate. Urban configurations with semi-open courtyards (U-shaped) showed better environmental performance than closed courtyards or open configurations, due to more effective shade distribution, improved air circulation, and connections to planted areas. These results highlight the importance of integrating climate-adaptive urban design with the preservation of green spaces to achieve a more sustainable and comfortable urban environment.
The implementation of open green spaces should be integrated with architectural design considerations, such as building form, height, and choice of materials and colors, to ensure

sustainable environmental design principles are met and thermal comfort is enhanced (Najah, Abdullah and Abdulkareem, 2023).

(Oquendo-Di Cosola *et al.*, 2023) conducted a field evaluation of the impact of green walls on outdoor thermal comfort in a continental Mediterranean climate. The study was conducted on two facades (south and west) of the itdUPM building in Madrid during the summer and winter of 2021–2022. Air temperature, relative humidity, and solar radiation data were recorded at four distances from the wall (0.25–1.00 m) using high-resolution sensors at a sampling rate of 10 minutes. The results, using a one-way analysis of variance (ANOVA), showed a significant temperature decrease on the south facade of 0.63°C in summer and 0.54°C in winter, while the west facade recorded a slight increase in summer (+0.56°C) and insignificant differences in winter. The distance from the wall also showed a limited effect (≤0.6°C), and the facade orientation was the most influential factor. The study concluded that green walls can improve the microclimate at the pedestrian level in the summer, especially on southern facades, while their impact is reduced in the winter. It is recommended that additional variables such as wind speed and vegetation types be studied.

(Piselli *et al.*, 2018) .conducted a comprehensive study in the Italian city of Perugia (Mediterranean climate) to evaluate strategies for mitigating urban heat islands and improving thermal comfort in an open urban transit area containing a train and bus station. The methodology combined continuous field monitoring of local climate characteristics, surveys of 367 pedestrians to assess their perceptions of thermal comfort, air quality, and noise, and numerical modeling using ENVI-met V4 software for five design scenarios including increased green spaces, the application of cool, highly reflective materials, and the installation of photovoltaic elements, as well as a combined scenario combining these interventions. The results showed that the increased vegetation scenario and the combined intervention scenario achieved the greatest improvement in the local climate, reducing air temperature by up to 1°C, the mean radiant temperature (MRT) by more than 20°C, and improving the PET index by up to 15°C in summer, with no significant negative effects in winter. The surveys also showed a clear congruence between pedestrian preferences (increased green space) and quantitative modeling results, underscoring the importance of incorporating nature-based environmental solutions to improve urban thermal comfort and enhance the attractiveness of the urban landscape.

Table 2-4 Previous studdies for vegetation

Ref-year of publication	Aim	Climatic season	Methodology	Key Findings	Limitations
(Chen *et al.*, 2020)	Quantify integrated impact of trees & aspect ratios on thermal/wind environment	Subtropical hot-humid (Guangzhou, China) – Autumn	Scaled outdoor experiment (SOMUCH platform, 1:15) Experimental (scaled outdoor), not simulation	Trees reduce radiation and radiant temperature, improve thermal comfort, and their effect is amplified in deep valleys. The interaction between heat/water and afforestation is more significant than the effect of each factor individually.	The experiments are scaled down and do not represent the full complexity of real cities, nor do they include the diversity of materials, patterns of human use, or different climates.
(Cui *et al.*, 2022)	Evaluating the impact of vertical vegetation arrangements on pedestrian thermal comfort and air quality (PM10)	sub-tropical maritime climate-summer	Field measurement-simulation(ENVI-met V4.4)	Green facades reduce radiation and radiant temperature and improve thermal perception, and their effect is more pronounced in deep valleys compared to shallow ones.	The study focuses on a specific type of street (deep) and certain greening systems, relies on a limited number of scenarios, and does not incorporate the impact of other materials, human behavior, or diverse climates.
(Aboelata, 2020)	Identify optimal vegetation ratio in different street orientations (H/W 1:1) to mitigate UHI and reduce building energy	Hot arid (Cairo, summer)	Field measurements (24h validation) + ENVI-met simulations(ENVI-met v4.3.2 + Design Builder)	Tree planting reduces radiant temperature and improves thermal comfort in all directions, and is most effective in directions with the most sun exposure.	The study focuses on only one H/W ratio (1:1), and does not study the effect of other ratios or the plant's interaction with different materials and interfaces.

Table 2-5 Matrix of optimal variables for outdoor thermal comfort

Factor/sub variable	Optimal range	Climate context
Urban geometry(H/W)	0.5-2.5	Hot-arid / Mediterranean
Urban geometry(orientation)	NS/NW-SE	Mediterranean / Semi-arid
Urban geometry(SVF)	0.3-0.6	Mixed climates
Material properties(Albedo)	0.3-0.5	Hot-arid / Urban canyons
Vegetation & Shading (Tree Canopy Coverage)	30-50%	Hot-dry / Mediterranean

2.8.4 Thermal comfort indicators

Based on the theoretical comparison of thermal indices presented in Section 2.6.3, this section focuses on the selection of appropriate indices for the current study.

Therefore, this study relies on **PET and UTCI** as the two primary indices for assessing outdoor thermal comfort, consistent with the nature of the variables studied, the environmental simulation tools used, and the analytical research objectives.

Studies varied in their choice of thermal indicators used to assess comfort. Previous studies have used different indices to analyze outdoor thermal comfort. (Abd Elraouf *et al.*, 2022) used the PET index for its ability to represent climate impacts on humans in urban environments, while (Zhou *et al.*, 2022) preferred the UTCI index for its accuracy and comprehensiveness in accordance with recent European recommendations (Favero, Luparelli and Carlucci, 2023) .Recommended combining the PET and UTCI to achieve a more comprehensive assessment. Overall, the UTCI is the most widely used in recent studies, while the PET remains the most widely used due to its ease of application and comparability.

(Zare *et al.*, 2018) compared the UTCI with several thermal indices and environmental parameters in a dry climate over a year, showing a strong correlation with PET (r=0.96) and dry matter temperature (r=0.89) and a negative correlation with relative humidity (r=-0.67), while the UTCI thermal sensation was closest to the WBGT during most months of the year, confirming its effectiveness as a comprehensive index for assessing heat stress in outdoor environments.

Despite this consistency, the two indices differ in their methodological basis. PET is derived from the human energy balance model (MEMI) and is particularly suitable for analyzing the effects of radiation, shading, and material properties within urban spaces. In contrast, UTCI is based on a multi-node thermophysiological model, providing a more detailed representation of human thermal response and showing higher sensitivity to microclimatic variations, especially wind speed and humidity.

Therefore, the combined use of PET and UTCI in this study enhances the robustness of the analysis by allowing cross-validation of results and providing a more comprehensive understanding of outdoor thermal comfort under varying urban conditions. This is particularly important in the context of this research, where façade materials, urban canyon geometry, and street orientation interact to influence both radiative and convective heat exchange processes.

Given that PET and UTCI rely on the equations of the human body's heat balance and are widely used in urban climate studies, they were chosen in this study as the primary indicators for measuring and interpreting thermal comfort in outdoor spaces.

In a field study conducted in Rome, (Salata *et al.*, 2016) determined the thermal comfort range of residents to be between 21.1 and 29.2°C using the PET index, with neutral values of 26.9°C in the summer and 24.9°C in the winter. The results showed that thermal preference was approximately two degrees lower than the neutral values, confirming the effect of seasonal adaptation in the Mediterranean climate. These results suggest that comfort ranges may vary between climatic environments, making it necessary to conduct local comparisons with other studies in the region, reinforcing the need to employ multiple indices to capture these variations more accurately.

2.9 Simulation tools and Methods used in previous studies

Many previous studies have relied on numerical simulation models to analyze the performance of urban environments in terms of outdoor thermal comfort. The ENVI-met model is one of the most widely used models, due to its ability to simulate the precise interactions between air, surfaces, and vegetation at a three-dimensional urban scale.

For example, (Cui *et al.*, 2022) used ENVI-met V4.4 to simulate the impact of vertical vegetation cover (VGS) arrangements on thermal comfort indices such as air temperature (Ta), mean radiant temperature (MRT), and PET index, as well as fine pollutant (PM10) concentrations within deep urban canyons. The model's accuracy was verified through field measurements, with results showing high agreement between measured and simulated values, reflecting the reliability of ENVI-met in assessing microclimatic changes resulting from green facade designs.

While (Chatzidimitriou and Yannas, 2017) used ENVI-met v4 to simulate the effect of urban aspect ratio and canyon orientation on the local climate, calibrating the results with field measurements, and Rayman to calculate PET and UTCI thermal comfort indices based on observational and mean radiant temperature (Tmrt) data.

ENVI-met is more comprehensive than Rayman and ANSYS, allowing simulation of all elements of the urban environment, calculating microclimate indicators such as air temperature, humidity, radiation, wind, and the thermal comfort coefficient (PMV), while Rayman is limited to calculate thermal comfort indices such as PET and UTCI based on meteorological inputs, and ANSYS does not support outdoor comfort analysis (Najah, Abdullah and Abdulkareem, 2023).

In (Yuan, Farnham and Emura, 2021) study, numerical analysis (CFD) was used to compare the effects of three directional reflectance properties of building facades (diffuse high reflectance (DHR), specular high reflectance (SR), and retro reflective high reflectance (RR)) on the outdoor thermal climate and indoor cooling loads in an urban canyon in Osaka. The results showed that the differences in Ta, WBGT, and SET* between the materials were limited (<0.35°C), while the SR and RR facades reduced the mean radiant temperature (MRT) by up to 1.4°C compared to DHR and contributed to a 9.2–18.2% reduction in inward heat flux, thereby reducing cooling loads.

2.10 Research Gap

Previous studies indicate that external thermal comfort is influenced by a complex interplay between urban engineering, facade materials, green elements, and climatic variables. There is general agreement that street orientation and height-to-width ratio (H/W) are among the most important factors controlling solar exposure, shade, and ventilation, while facade materials exert influence through their radiative and thermal properties, such as reflectivity, thermal mass, and insulation value. Vegetation and shading also play a significant role in reducing thermal stress, particularly during peak summer periods.

However, the literature reveals considerable variation in the optimal values for these factors depending on climate, season, and urban fabric, indicating the lack of universally applicable solutions. Furthermore, many studies have addressed these factors in isolation, rarely examining their combined effect or considering the wall as an integrated stratified system that influences both external and internal climate. Additionally, most studies are concentrated in tropical or temperate climates, while Mediterranean environments, particularly the dense commercial streets of the Middle East, are underrepresented.

Accordingly, this study fills a research gap by analyzing the combined effect of facade materials as a stratification system, street orientation, and H/W ratio on external thermal comfort in commercial streets in the Mediterranean climate city of Hebron, combining field measurements and simulations using ENVI-met to obtain calibrated results that are appropriate for the local context.

2.11 Summary

Previous studies have shown that street orientation and aspect ratio (H/W) directly affect radiation distribution and ventilation, and consequently, thermal comfort indices such as PET

and UTCI. They have also shown that material properties (reflectivity, conductivity, and thermal mass) influence surface and air temperature and that vegetation and shading are among the most effective means of improving thermal comfort. Most studies have used numerical simulation models such as ENVI-met and Rayman, but these need to be supported by field measurements to verify accuracy.

Most previous studies have focused on discrete variables such as vegetation cover, orientation, or reflectivity, without comprehensively integrating physical, geometric, and microclimatic factors. The majority of research has also been limited to residential environments or open spaces, with a clear lack of research on commercial canyons.

The literature also lacks studies that combine field measurements and simulations (ENVI-met), as well as seasonal analysis of comfort indices such as PET and UTCI.

Accordingly, this thesis seeks to address these gaps through an integrated analysis that links facade materials, street orientation, and height-to-width ratios in the Palestinian urban context. The review results show that most studies focused on the effects of orientation, urban composition, or vegetation cover separately, with little research integrating facade material properties, height-to-width ratios, and street orientation in commercial urban contexts. Furthermore, none of the previous studies addressed the local characteristics of building materials in Palestinian cities or their impact on outdoor thermal comfort.

Hence, the importance of this study, which seeks to fill this gap through an integrated analysis that combines material, composition, and orientation in a real urban environment (the commercial center of Hebron), while leveraging the results of previous studies to determine optimal values and improve the quality of outdoor spaces in a moderate climate.

The findings and analysis in Chapter Three indicate that comprehending the interplay among materials, urban composition, and microclimatic variables necessitates a research methodology that integrates field measurements, numerical simulations, and comparative analysis.

Chapter Four presents the study methodology developed to address research gaps, outlining the steps of experimental model design, field calibration, and analysis of thermal comfort indices (PET and UTCI) using the ENVI-met model within the commercial street environment of Hebron.

Chapter 3: Methodology and Case Study

3.1 Preface

This chapter presents the methodological framework adopted to examine the influence of façade materials, street orientation, and urban canyon geometry (H/W ratio) on outdoor thermal comfort in the commercial center of Hebron, Palestine. The chapter is structured into three main sections: a preface, the research design stage, and a concluding summary. It follows a quantitative, simulation-based approach supported by empirical field measurements to ensure accuracy and reliability. The characteristics of the study area are introduced within the methodology itself, as it's physical, climatic, and geometric attributes directly inform model parameterization, material assignment, and the development of simulation scenarios.

The first section outlines the overall research approach and research type, describes the study context, and explains the data collection procedures, including on-site microclimate measurements. The second section details the ENVI-met V5.6.1 model configuration, the simulation workflow, and the calibration and validation processes using statistical indicators such as RMSE, MAE, Pearson's correlation coefficient (R), and the Index of Agreement (d). The final section presents the analytical framework used to assess the effects of façade materials, street orientation, and canyon geometry on outdoor thermal comfort. This encompasses the extraction and analysis of air temperature, relative humidity, wind speed, and thermal comfort indices (PET and UTCI) at various spatial locations and at five temporal intervals during the daytime as shown in Figure 3-1.

Overall, the methodological structure is designed to systematically capture the interaction between material properties, urban canyon configuration, and microclimatic behavior to determine their combined impact on outdoor thermal comfort in commercial urban environments. Therefore, selecting an appropriate and rigorous methodological approach is essential to achieving the objectives of this study.

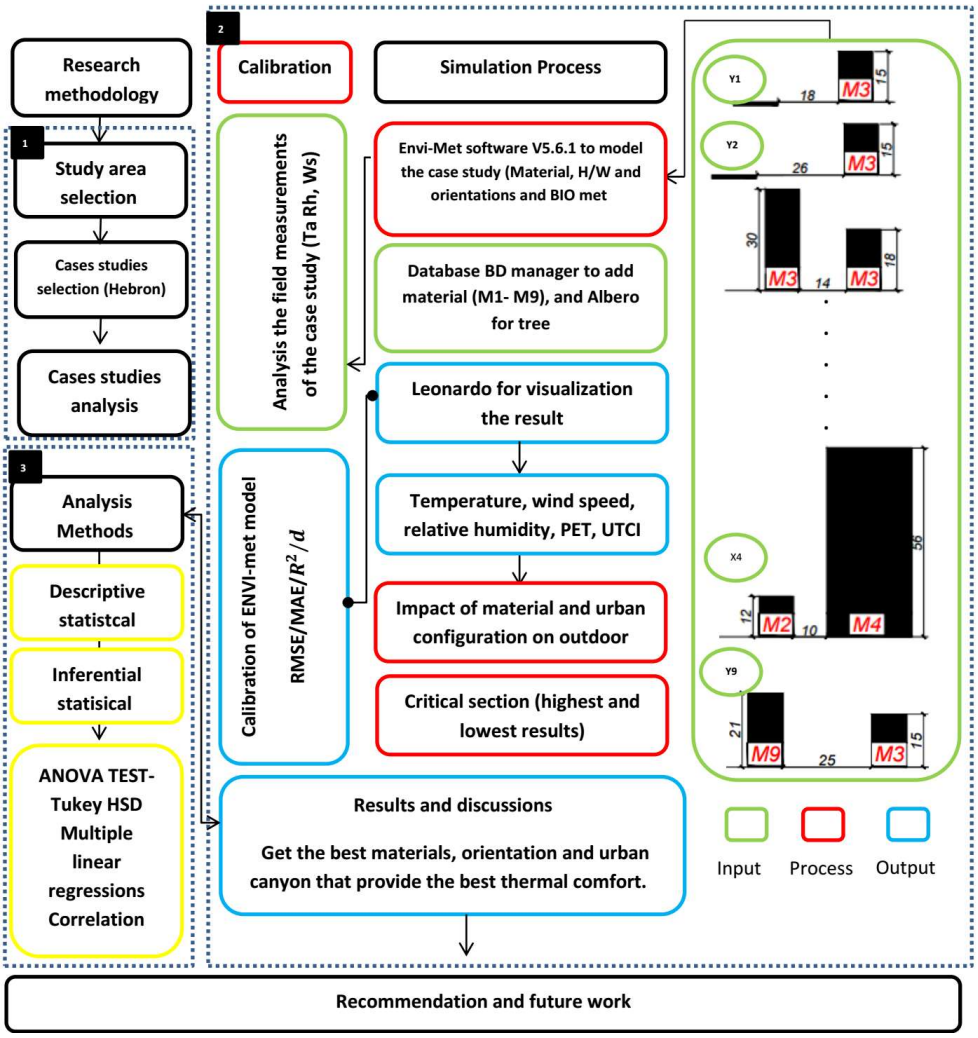

Figure 3-1 Methodlogy strucutre

3.2 Research approach and type

This study utilizes a quantitative approach. Quantitative components constitute the core of the study and include field measurements, numerical simulations using ENVI-met (v6.5.1), and statistical analysis.

The study begins with field measurements and ENVI-met simulations for two streets to investigate the effects of façade materials and urban canyon configurations on outdoor thermal comfort. This involves collecting data on air temperature, wind speed, relative humidity, PET, and UTCI, which are analyzed using descriptive and inferential statistical methods, including ANOVA–Tukey HSD, regression, and correlation, to identify trends and relationships.

Methodologically, the study adopts an inductive and exploratory orientation. Rather than testing predefined hypotheses, the analysis derives patterns directly from measured and simulated environmental data. This inductive approach is well suited to urban microclimate

research, where interactions among material properties, canyon geometry, and street orientation are complex and require observation-driven interpretation

Within this research strategy, microclimate simulation forms a central methodological component. ENVI-met was selected as the primary simulation tool because it is a three-dimensional, non-hydrostatic urban climate model capable of resolving airflow, radiation exchange, surface-air interactions, and vegetation processes at a micro scale resolution (Huttner, 2012). This feature makes it easier to examine how facade materials and urban configuration influence local climates. Several simulation models, such as ENVI-met, OTC Model, SOLWEIG Model, TownScope, Rayman, Ecotect, etc., are used to assess human thermal comfort in outdoor spaces (Faragallah and Ragheb, 2022).However, a review of literature in this field shows that 77% of studies carried out in the last five years selected ENVI-met software because it is a reliable tool that gives accurate data on current meteorological conditions, particularly for summertime calculations (Abdollahzadeh and Biloria, 2021; Yilmaz, Kurt and Gölcü, 2023). In addition to producing the statistical findings of parameters, ENVI-met displays high-resolution 2D and 3D visuals. So in this study, the ENVI-met tool V 5.6.1 has been used to extract these effective meteorological factors, including temperature, humidity, and wind speed. After that, Biomet (V5.6.1) is used in the study to calculate PET and UTCI to analyze the effect of material and urban configuration on OTC.

3.3 Study area description and selection criteria:

Selecting an appropriate study area is a critical step in outdoor thermal performance research, as urban morphology, street geometry, and façade materials strongly influence local microclimatic conditions. Therefore, this section describes the spatial context of the study and explains the criteria used to select the study location and the analyzed streets. The selection was based on methodological considerations, including the representativeness of the urban commercial fabric, the diversity of street orientations and urban canyons, and the accessibility required for field measurements and model calibration. The following subsections present the rationale for selecting Hebron as the study area and the criteria used to define and analyze the selected cases.

3.3.1 Study area selection Criteria

The study context was selected within Palestine after evaluating three major cities: Ramallah, Bethlehem, and Hebron (Appendix B). Analysis of commercial streets and building patterns in

these cities revealed a clear similarity in the materials used, building heights, and street orientations and widths. Accordingly, Hebron was chosen as the study area due to its geographical proximity to the researcher, which facilitated easy access and the necessary frequency of field visits, particularly during the calibration phase, which required measurements at multiple times of day. it is a commercial capital with significant trade from neighboring areas and has urbanization problems., and the limited number of studies addressing outdoor thermal comfort in commercial areas further solidified the selection of Hebron as a suitable case study.

The selection of Hebron consequently facilitated the acquisition of reliable data, precise calibration, and the generation of contextually meaningful simulation outputs.

3.3.2 The study area

The study was conducted in Hebron, which is situated at an elevation of 950 meters above sea level in the southern part of Palestine's West Bank, 30 kilometers (19 miles) south of Jerusalem, as shown on the map of Palestine (Figure 3-2) with a latitude of 31° 31' 43.7844" N) and a longitude of 35° 5' 54.528" E (Latlong, 2025). It is the commercial capital of the West Bank, (HRC, 2024) and is classified under the Csa Hot-summer Mediterranean climate according to the Köppen–Geiger system. The Mediterranean climate of Hebron is described by short, cool winters and long, hot, dry summers (Al-Salaymeh, Al-Khatib and Arafat, 2011) .Hebron has a moderate climate, with average annual temperatures ranging from 15 to 16° (with an average of 7° in the winter and 21° in the summer). On average, 502 mm of precipitation falls each year. (HRC, 2024)

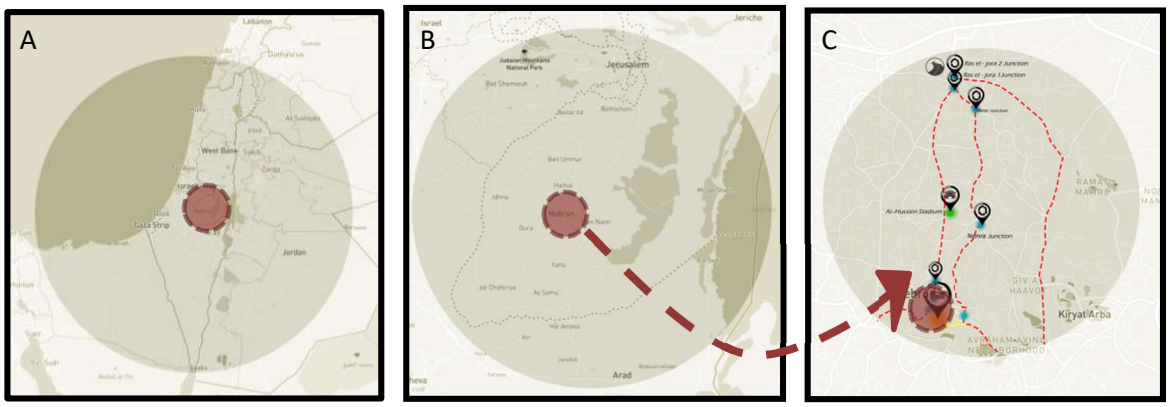

Figure 3-2 Palestine map showing Hebron in the middle (A), Hebron city (B), study area location in Hebron(C) (mapbox, 2024)

Recent climatic records (PCBS, 2024) indicate a maximum annual temperature of 22.6 °C, a minimum of 13.9 °C, and an annual mean of 17.8 °C. The average relative humidity is approximately 65%, and annual wind speeds exceed 5 m/h. August is the warmest month in Hebron, with highs of 29°C and lows of 18°C on average. And January is the coldest month of the year in Hebron, with average high temperatures of 11°C and lows of 3°C. (Weather-Spark, 2024)

Hebron's wind patterns change throughout the seasons; westerly and northwesterly winds predominate. From May to September, they average over 3.2 m/s, with a peak speed of 3.6 m/s in July. On the other hand, from December to February, wind speeds drop to about 2.9 m/s. Wind speeds are moderate in the following months. (Weather-Spark, 2024) Relative humidity also varies seasonally, with slightly more humid conditions between July and September (Weather-Spark, 2024).

This section's weather data helps establish the study's limiting factor, which is the typical weather conditions of the Mediterranean. The preceding figures display the climatic profile of Hebron City, which includes temperature, relative humidity, wind direction, and wind speed. The Envi-met program was used to create a simulation model based on this data.

3.3.3 Cases Selection Criteria

To ensure that the selected instances reflect typical typologies in the city and that various cases are selected, the case studies were chosen using several criteria derived from the initial survey. The most important of which are:

The first criterion focused on building type and land use, where the study intentionally concentrated on the commercial core of Hebron. This focus excluded residential and mixed-use areas to ensure that the analysis reflects outdoor thermal conditions in dense commercial environments, which typically experience higher pedestrian activity, reduced vegetation cover, and more pronounced heat retention.

The second criterion involved street function, orientation, and construction period. Preference was given to commercial streets that accommodate pedestrian movement—particularly those frequently used during special occasions and public events—due to their relevance to assessing pedestrian comfort. Within these streets, segments with different orientations were intentionally selected to capture variations in solar exposure and shading patterns. No buildings were excluded based on construction period; therefore, both old and newly constructed

buildings were included to ensure that the selected cases reflect the full morphological and material diversity present in the commercial district.

The third criterion ensured variation in key physical and material variables, including façade materials, building heights, and street widths. To achieve this, each street was divided into smaller segments, typically 10–15 meters in length, allowing the selection of individual cases where differences in material composition or canyon geometry were clearly distinguishable. In several segments, the presence of new cladding materials on one side of the street, contrasted with traditional stone on the opposite side, provided a valuable opportunity to analyze the impact of material heterogeneity within the same canyon. Where materials were similar, variations in the height-to-width (H/W) ratio or façade configuration provided additional differentiation for case selection.

Based on these criteria, three primary commercial streets were selected for analysis as shown in Figure 3-3: the street between Al-Manara Roundabout and Ibn Rushed Roundabout (yellow line), Wadi Al-Tuffah (Weddad Street), and Al-Haymoni Street (Red line).

These streets were then divided into detailed sections, resulting in 21 segments along Weddad Street and 12 segments along Ibn Rushed Street, each representing a distinct case with specific geometric and material characteristics that support the objectives of the study.

The analysis of each selected street segment was based on a set of standardized criteria, including: the analysis of the building and the street in terms of the direction of the main facade, the number of floors, the height of the building, the width of the street, the components of the wall and the external cladding of each building located along the street, the type of trees present, and the materials used for the street and sidewalk.

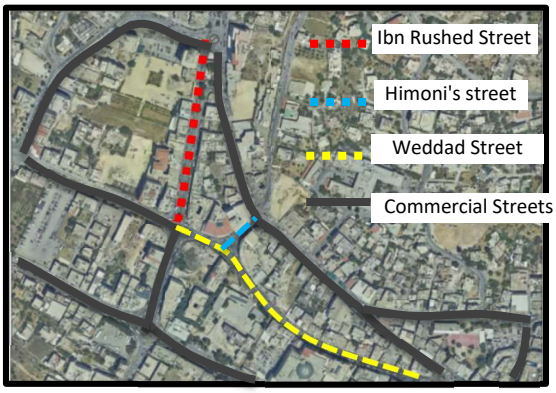

Figure 3-3 Hebron streets in commercial area (Case study- Red: Ibn rushed street, Blue: Himoni's street, Yellow: Weddad street) (Hebron municipality, 2023)

3.3.4 Description of the Case Study

The case study area is located within the commercial center of Hebron. Based on field surveys and preliminary observations, three streets were selected for detailed analysis: Wadi Al-Tuffah (Weddad Street), Al-Haymoni Street, and Ibn Rushed Street. These streets collectively represent typical urban canyon conditions in Hebron, with variations in orientation, building heights, and façade materials. Their characteristics make them suitable for examining how different urban configurations influence outdoor thermal comfort.

1. Weddad Street

Wadi Al-Tuffah Street (Weddad Street), which is regarded as one of the most significant modern commercial streets with NW-SE orientation. It features both old and linear commercial buildings, along with shopping center like the Hebron Center, which was the first commercial mall on the street. Ismaeleyeh Mall and Crown Mall has recently appeared with isolated and stacked units block. The length of the street, as per to the selected analysis area, is approximately 416 meters, and the width varied between 8m and 20m. Pedestrians primarily use this street, with a slight presence of cars. On special occasions, the entire street becomes pedestrian-only. Most of the commercial buildings on the street consist of one to six floors, with an average height of 6 meters for the ground floor, with the exception of the old buildings, which range between 3 and 4 meters. The mall system has expanded from 6 floors to 17 floors, like Crown Mall, which has a portion situated underground so the urban canyon ranges between 0.5 and exceeds 2. The building materials primarily consisted of stone and concrete, each with varying thicknesses. Modern materials and cladding, such as aluminum composite panels, curtain wall and transparent glass, were incorporated in high proportions, particularly in the lower floors. The street primarily relied on asphalt and cement bricks pavements. The trees were spread at almost fixed distances, of the Mila azedarach type, in addition to the cypress and willows in the courtyard of the Weddad School and other types of trees that were mentioned in detail with their numbers.

2. Himoni's street

Al-Haymoni Street is a secondary connector that links to Weddad Street and follows a northeast–southwest (NE–SW) orientation, with partial east–west (EW) alignment. The analyzed section measures approximately 55 meters in length and 10–12 meters in width. Building heights exceed three floors, resulting in H/W values between 0.5 and 2.1.

Some of the buildings were of mixed commercial and administrative use, including offices and clinics. The materials used for the buildings were stone and concrete, in addition to the external cladding. The percentage of glass was less. There were no trees present.

Figure 3-4 Photo for Weddad Street, Himoni's and Ibn rushed street shows the buildings and the urban canyon.

3. Ibn Rushed Street

The segment between Ibn Rushed Roundabout and Al-Manara Roundabout represents a major commercial corridor with continuous pedestrian activity. The street measures approximately 250 meters in length, with widths ranging from 12 to 20 meters, and expanding to 36 meters near the branching intersection. The shops take a linear system without any commercial centers. Building heights vary substantially—from 6 meters to 44 meters—reflecting a combination of old commercial shops and multi-story administrative and commercial buildings. The resulting canyon ratios range between 0.4 and 1.2. Façade materials consist primarily of stone and reinforced concrete, with extensive use of double-glazed curtain walls in prominent buildings such as the City Center and the Golden Tower. Modern aluminum composite panels (ACP) have been used in recent façade renovations along the street. The median area, which divides the street in two, features a ficus tree. The distance between the ficus trees is approximately 6 meters. The trees in Ibn Rushed Square are diverse, such as willow, jacaranda, ficus, Olea europaea, ligustrum, and Washingtonia palm, and as for the pavements, there were no trees planted.

The internal facades confined to the street were studied, while the side facades were not studied because the buildings are adjacent (zero setback ratio). There were other commercial streets in the area, but they were not directly pedestrianized. Some had the same orientation, and some streets with different orientations did not have a large variety of building materials and urban canyon, so they were excluded from the study.

The study region has increased construction density and reduced setback lengths between structures. The varied combinations of orientations, materials, and configurations rendered the

chosen research area an exemplary case for evaluating the influence of urban design on outdoor thermal comfort.

3.4 Data collection method

Primary and secondary data-gathering methods are the two primary categories into which data collection techniques fall. For a particular goal, researchers employ various methods to acquire primary data. Therefore, compared to secondary data types, primary data has better validity, dependability, objectivity, and authenticity. Although one may conduct research using secondary data, obtaining a trustworthy conclusion requires the inclusion of primary data as well (Taherdoost, 2022) .

In this study, data were collected on the case studies through a physical survey that included site observations and a walk among the selected samples to document building heights, street widths, façade configurations, pavement materials, and the distribution and type of vegetation, for constructing an accurate ENVI-met base model. in addition to interviews with the Hebron Municipality and engineering offices specialized in commercial buildings to obtain all Secondary data related to the selected streets, such as aerial photographs, construction details, materials used for the horizontal and vertical surfaces of the street itself, buildings, and types of trees used, and Document review survey study at public records on " the guidelines for energy-efficient building design " from the Palestinian Engineers Association and the Hebron Municipality.

The primary goal of the street observation is to gather all the parameters that can be input into the Envi-met to produce a real base model that can be evaluated. The characteristics that impact thermal comfort include the building height, wall, pavement, and street materials.

3.5 Simulation setup

The ENVI-met microclimate model (version 5.6.1) was used to simulate the thermal behavior of the selected street canyons in Hebron. The simulation setup included creating a detailed 3D digital model, defining grid resolution and domain size, assigning material and vegetation properties, configuring boundary conditions, and preparing climatic forcing files. This setup ensured an accurate representation of the physical urban environment and its interaction with meteorological conditions.

3.5.1 3D Model Construction

A detailed three-dimensional representation of Weddad Street and Ibn Rushed Street was constructed using ENVI-met Spaces based on the field survey, municipal documents, and architectural observations. The model included accurate building footprints, heights, façade compositions, street widths, sidewalk dimensions, vegetation elements, and pavement materials.

After gathering and organizing the necessary data, we create a unique database for each street. Any materials or trees that are missing from the database manager of the program or need to be changed to fit the study area are added. There are more than three layers in the study, but ENVI-met only defines three. To solve this problem, the external and internal materials layers are defined as they are. Furthermore, the rest of the materials between these two layers are defined as if they were a new material, and their new thermal properties are calculated as shown in Table B-1. These are shown in Appendix A,which show the wall layers used in both streets.

Trees were added using ENVI-Met's Albero tool. Missing species were generated with custom parameters (height, crown diameter, LAD profiles) as shown in Figure 3-5. Tree modeling was limited to representation but excluded from comparative result analysis to isolate the effects of façade materials and canyon geometry.

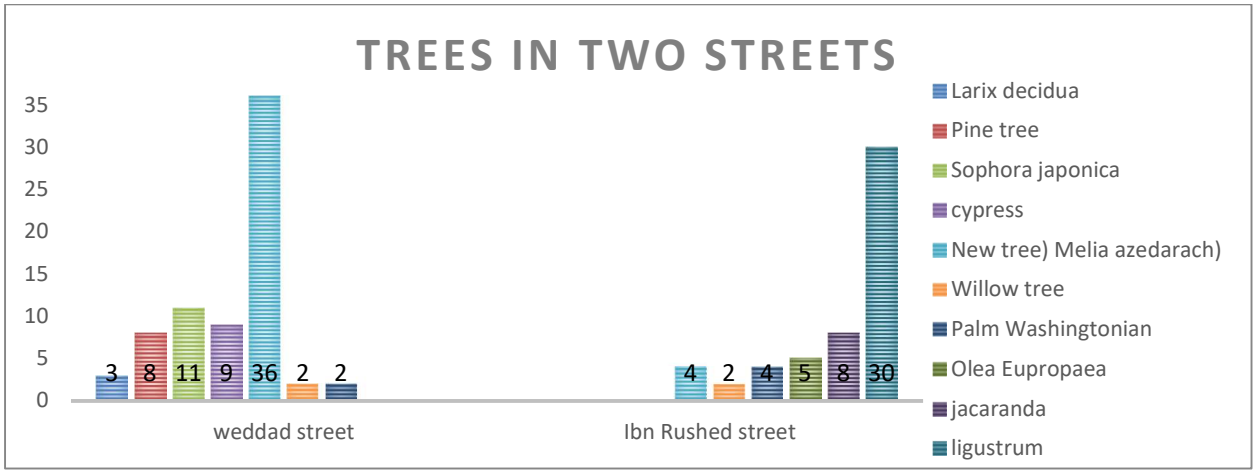

Figure 3-5 Tree Type used in streets

3.5.2 Domain Size and Grid Resolution

After building the database, a 3D computer model was created for every street using the actual building information and building materials obtained during the fieldwork (mapping the case studies). Based on the street dimension, the size of the ENVI-met net for Weddad and Ibn

rushed streets was 210 × 120 × 30, 60×170×30 for the X, Y, and Z dimensions, and respectively. To optimize the resolution of the micro-scale thermal indices in the target region, the grid cells were set to a small size with a grid cell size of dx=2 m, dy=2 m, and dz=2 m. The analysis of this study focused on the horizontal dimensions of x and y at the pedestrian-height microclimate and outdoor thermal comfort indices. Vertical grids were subjected to a telescoping technique to provide enough distance between the top model boundary and the highest object in the domain. With a 10% extension factor, telescoping began at a height of 15 meters for Weddad Street and a 10% extension factor after a height of 13 meters for Ibn Rushed Street. The heights of the buildings and trees were obtained from estimated field measurements. The Weddad model was rotated out of the grid north by 45° to set the actual direction of the site. The height of the contour at the highest point was 7 meters. Table 3-1 shows all this data

3.5.3 Boundary Conditions

Boundary conditions were defined using Hebron's local climatic characteristics: In this study, the indoor air temperature of all simulated buildings was fixed at a constant set-point throughout the simulation period (Building indoor temperature: 23 C). Maintaining a uniform indoor temperature as a boundary condition ensured that any variation in outdoor air temperature, wind speed, or thermal comfort indices was solely attributed to the thermal properties of the wall assemblies (e.g., U-value, thermal mass, reflectivity). Although this assumption does not fully represent real operational conditions, it was necessary to establish a controlled environment for comparative analysis across all scenarios. It should be noted that ENVI-met imposes a limitation on the maximum input wind speed (≤ 5 m/s) due to model stability requirements. This constraint was considered during the preparation of the forcing file and influenced the selection of the simulation date.

Table 3-1 the input parameters for the ENVI-met program

Model location **City** **Latitude** **longitude**	Palestine Hebron 31.5326°N 350998E	
Software and version	Envi-met V 5.6.1	
Street geometry	Weddad street &himonies	Model Dimensions: x-Grids 210 / y-Grids 120 / z-Grids 30 Size of grid cell in meter, dx = 2 / dy = 2 / dz = 2 Model rotation out of grid north: 45/telescoping factor 10% after 15m height/dz not split into 5 sub cells/ DEM highest point 7m
	Ibn rushed street	Model Dimensions: x-Grids 60 / y-Grids 170 / z-Grids 30 Size of grid cell in meter, dx = 2 / dy = 2 / dz = 2 Model rotation out

Computation domain		of grid north: 9/ telescoping factor 10% after 13m height/dz not split into 5 sub cells/DEM highest point 7m 420m*240m(Weddad) 120m*340m (Ibn rushed)
Simulation data	time	22/6-21/12 at (8am/10am/12pm/2pm/4pm)
	Lateral boundaries setup	Full forcing; 30 min time steps at the inflow
	Indoor conditions	Constant, 23 °C
	Data output	60 min interval

Figure 3-6 shows the model of Weddad Street and the Figure 3-7 shows Ibn Rushed Street model.

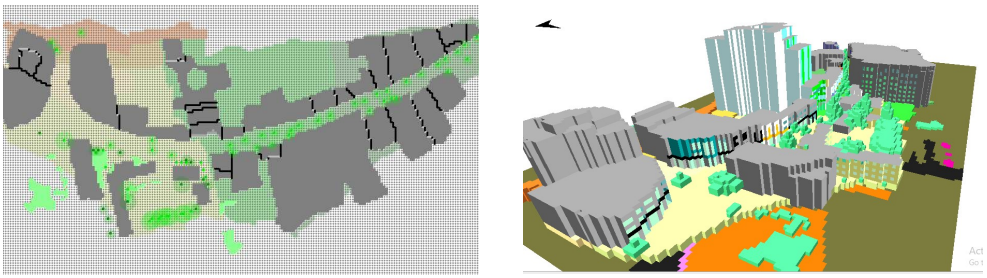

Figure 3-6 Weddad street model

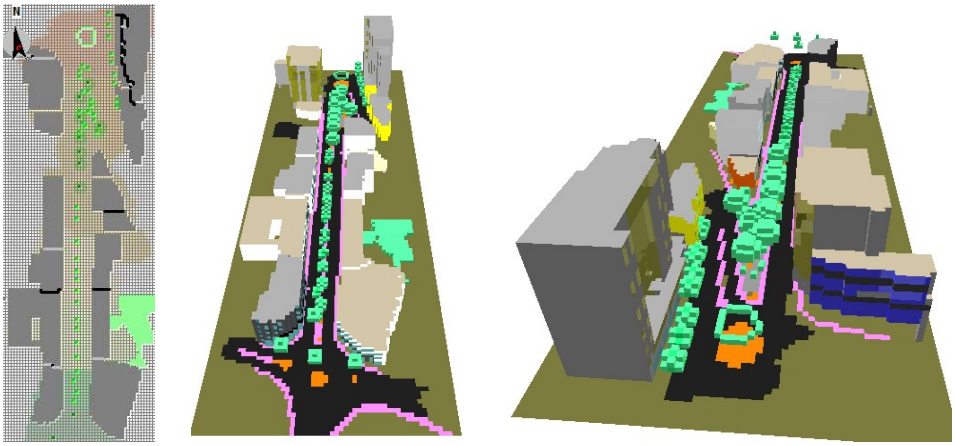

Figure 3-7 Ibn rushed street model

3.5.4 Simulation Period and Peak-Hour Selection

The study times were determined during the day based on peak hours, which are 8 am, 10 am, 12 pm, 2 pm, and 4 pm, which are the start and end times of work for employees, workers, and students and the movement of shop owners, shoppers, and commuters to and from the city. These periods document changes in temperature during the day and how they affect thermal comfort.

3.5.5 Forcing File Preparation

Hourly climatic data were imported using an ENVI-met forcing file (.EWP) extracted from Ladybug Tools (ladybug tools, 2024) for the Hebron climate. The forcing file included: Hourly air temperature, Relative humidity, solar radiation, Long wave radiation, Wind speed and direction. The simulation was conducted on June 22 instead of June 21 (summer solstice). This adjustment was necessary due to a limitation in ENVI-met, which does not allow wind speed inputs exceeding 5 m/s within the forcing file. The recorded wind speed on June 21 exceeded this threshold; therefore, June 22 was selected as the closest representative day with similar climatic conditions while remaining within the acceptable wind speed range, and in the winter, December 21, the winter solstice. The simulation was carried out in summer and winter, starting at 5 am and continuing for 12 hours.

3.5.6 Receptor Points

Strategic sensor/receptor's locations were chosen to cover open spaces and zones surrounding building facades. So, three sensors were placed in each section to study the program's outputs in three pedestrian locations: the right of the building (left of the street), the left of the building (right of the street), and the middle of the street between the two buildings. To assess the level of comfort for users of outdoor spaces, results are obtained for a standing person at 1.4 meters above the ground. Figure 3-8. These sensors were applied to all sections selected for study on both streets. These receptor points provided the basis for subsequent PET and UTCI calculations.

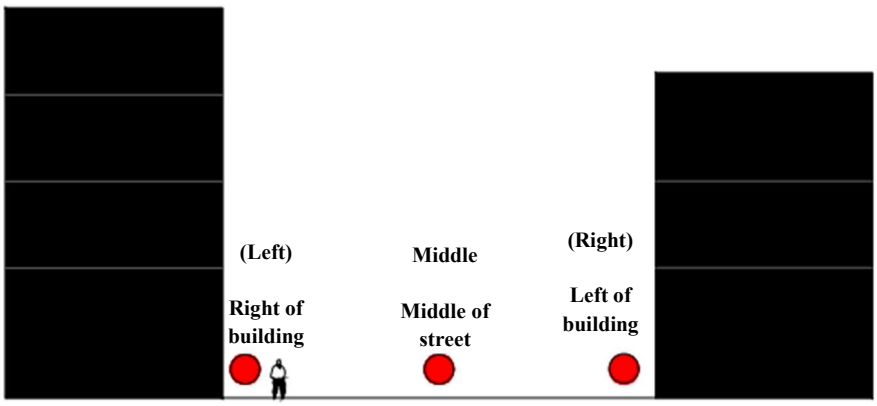

Figure 3-8 Three sensor/receptors location

3.5.7 Material properties and ground surface

Material properties were assigned based on municipal records and field observations. Ground surfaces were matched to real conditions: From the model database, ground materials (including street lanes, walking streets, and sidewalks) were selected to match current

conditions. Granite concrete pavement, basalt brick roads in walking streets, and asphalt in the street lanes were among the ground materials. Wall materials included various combinations of stone, reinforced concrete, insulation, hollow block, aluminum composite panels, curtain wall glazing, and transparent glass. The complete dataset is presented in Table 3-2. Figure B-7 shows the material that used in two streets.

Surface optical properties, such as albedo, also influence the urban microclimate. In ENVI-met, albedo values are mainly defined for horizontal surfaces through soil profiles, while façade surfaces follow the default optical properties of the material database; therefore, albedo was not treated as an independent variable in this study.

Table 3-2 Wall construction for case study

Material name	Section in wall	Wall component			u-value
M1	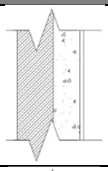	25cm stone	20cm reinforced concrete	2cm plaster	2.189
M2	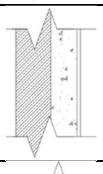	20cm stone	15cm reinforced concrete	2cm plaster	2.504
M3	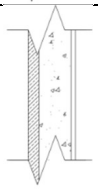	5cm stone	15cm reinforced concrete	2cm plaster	3.205
M4	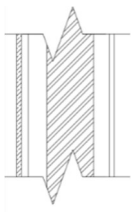	2cm stone	3cm stone mortar 0.8cm steel 20cm hollow block 4cm polyurethane 10cm hollow block =0.378cm for M4}	2cm plaster	0.47
M5	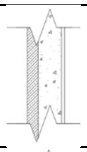	7cm stone	15cm reinforced concrete	2cm plaster	3.087
M6	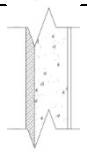	5cm stone	20cm reinforced concrete	2cm plaster	2.94

Material name	Section in wall	Wall component			u-value
M7	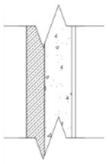	10cm stone	15cm reinforced concrete		2.934
M8'	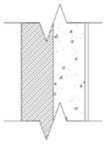	20cm stone	20cm reinforced concrete		2.33
M9	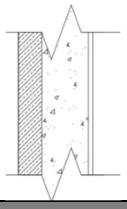	10cm stone			2.7
Cladding					
Cladding 1		0.4 aluminum	0.35m for M2	2cm plaster	2.504
Cladding 3/Cll 1			0.22m for M5		3.087
Cladding 2		0.5 aluminum	0.2m for M3		3.205
Cladding 4			0.25m for M6		2.94
Cladding 5		0.4 aluminum	0.25m for M7		2.93
Cladding 6			0.35m for M2		2.504
Cladding 7			0.45m for M1		2.193
Cladding 8			0.378m for M4		0.46
Q-Noor cladding			40cm (Q-Noor material)		2.341
Double green glass		6mm green glass	12mm air	6 mm green glass	
Double blue glass		6mm blue glass		6mm blue glass	
Cll2		0.3aluminum	25cm for M7	2cm plaster	2.93
Cll3		0.2 aluminum	25cm for M7		2.93
Cll4		0.3 aluminum	25cm for M6		2.943
Cll9		0.3 aluminum	30cm for M9		2.705

Note: Most of the claddings in the table are used simply on the sides of shops or as part of the shop name and their effect was simple except in section X8 on Weddad Street where the Alucobond material covered most of the facade of the floors above the ground floor level. Also in Ibn Rushed Street at section Y8, cladding 9 was used and in Y3, cladding 7 was used.

3.6 Calibration process

Model calibration ensured that ENVI-met outputs represented Hebron's microclimatic conditions accurately. Calibration relied on measured environmental data collected from a single reference location within the study area.

3.6.1 Field Data Used for Calibration and procedure

To evaluate the outside thermal environmental conditions of the sites and to calibrate the accuracy of the model, field measurements of environmental factors were conducted. The following environmental factors were measured: humidity, air temperature, and air velocity. The accuracy of urban microclimate modeling has been studied in the past, as in (Gusson and

Duarte, 2016; Ayyad and Sharples, 2019; Koletsis *et al.*, 2022).Additionally, this study used a similar methodology.

An urban-scale simulation of the commercial streets of Hebron City was used to study the effect of building materials and cladding on external thermal comfort and their relationship to other variables. For calibration, microclimate measurements were carried out in the streets on November 1, 2024, at eight different points for two streets at three different times: 7-8 a.m., 2-3 p.m., and between four and five p.m. in (Figure 3-9 For verification, the data was collected on June 13, 2025, at 11:30 p.m. in two sections for three points in the same section (right, middle, and left).Figure 3-10 .These measurements formed the empirical baseline for calibration.

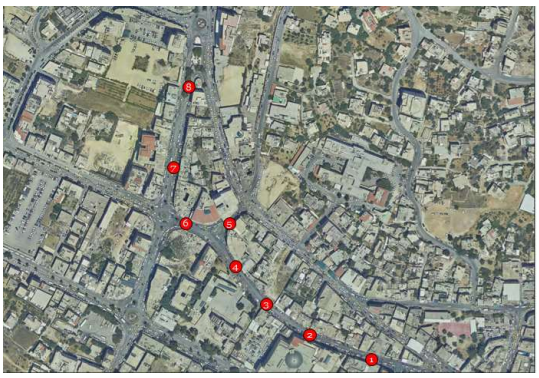

Figure 3-9 Location of 8 points that Ta, Rh and wind speed was measured

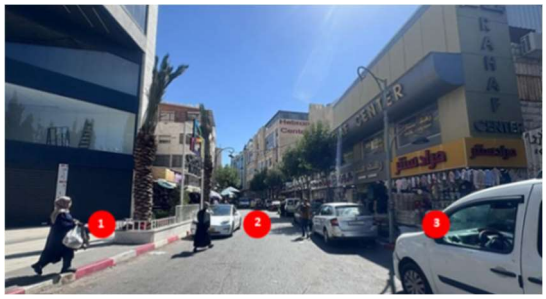

Figure 3-10 Example of Location of 3 points for verifaction

To collect data, UNI-T A37 Digital Carbon Dioxide was used to measure temperature (Ta °C), a wireless weather station was used to measure the temperature and humidity (RH %), and a DT-619 CFM/CMM Thermo-Anemometer was used to measure wind speed (m/s), as shown in

Figure 3-11 at a height of 1.4 m.

Figure 3-11calibration tools(a- UNI-T A37 Digital Carbon Dioxide, b- wireless weather station ,c- DT-619 CFM/CMM Thermo-Anemometer)

Simulated values from ENVI-met were compared against the measured dataset. The goal was to minimize model–measurement error to ensure accurate representation of canyon microclimates in both summer and winter scenarios. The simulation process had two stages. In the first, a given day was selected from each monitoring campaign for the comparison of monitoring and simulation data to validate and calibrate the software. Once it was calibrated, it was used to analyze different configurations of outdoor thermal comfort in open spaces. The correctness of the software was evaluated by comparing the generated simulations with the field measurements.

3.6.2 Calibration process analysis

The accuracy of the model was evaluated using standard statistical indicators, including the Root Mean Square Error (RMSE), Mean Absolute Error (MAE), Coefficient of Determination (R^2), Index of Agreement (d), and Pearson Correlation Coefficient (R). These indicators quantify the level of agreement between measured and simulated values and ensure the validity of the ENVI-met model for subsequent scenario analyses.Table 3-3 show he summary of statistical indicators.

Table 3-3 summary of the accepted values for calibration in study

Metric	Acceptable Value
MAE	Within 10–15% of average measured values
RMSE	Within 10–15% of average measured values
Index of Agreement (d)	0.8 or higher; 0.9+ is excellent
Coefficient of Determination (R^2)	0.8 or higher; 0.9+ is excellent

3.7 Simulation scenarios

A set of cases (sections) will be analyzed in each street based on the existing situation to study the effect of variables on external thermal comfort. Table 3-4 it discusses the cases gathered from a site survey for three streets. It shows details about the city and materials, including how

the streets are arranged, their width, the height and distance between buildings, and the types of materials used for the walls, like limestone, Alucobond, and reinforced concrete, and their composition, such as stone, mortar, hollow block, and insulation.

3.7.1 Section-Based Definition of Scenarios

There were 21 sections in Weddad Street and 12 sections in Ibn Rushed Street, summer and winter, for five times and variables and 3 locations for each section, with a total of 4950 readings, as shown in Appendix . This approach enabled the evaluation of microclimatic variation within the same street, and not only between streets.

Table 3-4 Simulation Senarios

<table>
<tr>
<td>Weddad street (NW-SE)and himonies street(NE-SW,EW)(Y1/15-Y25-Z1/85-Z2/75) case/sections
Right(R),Left(L)
Number of floors
Orientation of facades
Urban canyon</td>
<td colspan="3"> 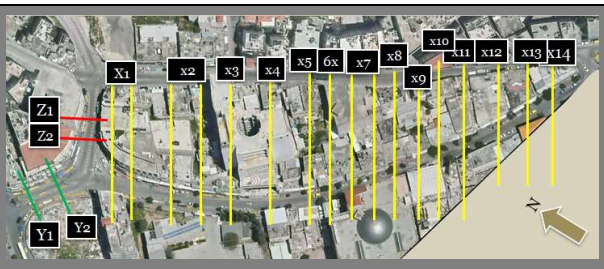
</td>
</tr>
<tr>
<td>1- Single-sided canyon (Y1-15)
 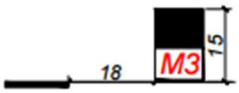

R-4FLOORS,SW
Canyon:C0,C3(0.8-0)</td>
<td>2- Single-sided canyon (Y2-25)
 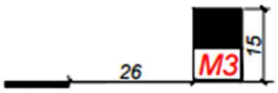

R-5FLOORS,SW
Canyon:C0,C2</td>
<td>3- Asymmetrical canyon (H/W: deep on one side, moderate on the other) (Z1-85)/80
 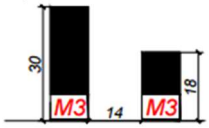

R-4floors,NW
L-10floors,SE
Canyon C12,C7</td>
</tr>
<tr>
<td>4- Asymmetrical canyon (Moderate canyon)(Z2-75)
 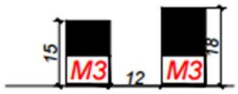

Vegetation area
R-4floors, NW
L-4floors,SE
Canyon C7,C8</td>
<td>5- Symmetrical canyon (Shallow canyon)(X1-35)
 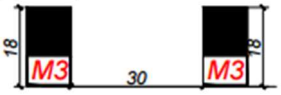

R-5floors,W
L-4floors,E
Canyon:C2,C2</td>
<td>6- Symmetrical canyon- Moderate canyon (X1-45)
 

R-5floors,W
L-4floors,E
Canyon:C5,C5</td>
</tr>
<tr>
<td>7- Asymmetrical canyon-Shallow & Moderate canyon (X2-55/65)
 

R-3floors,W
L-3floors,NE
Canyon:C2,C3</td>
<td>8- Single-sided canyon- Shallow canyon (X3-75)
 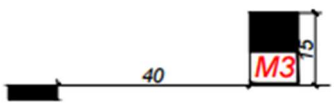

R-3floors,W
Canyon:C0,C1</td>
<td>9- Asymmetrical canyon(H/W: deep on one side, moderate on the other) (X4-95)
 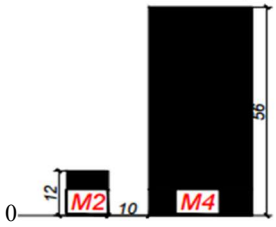
</td>
</tr>
</table>

Weddad street (NW-SE)and himonies street(NE-SW,EW)(Y1/15-Y25-Z1/85-Z2/75) case/sections Right(R),Left(L) Number of floors Orientation of facades Urban canyon	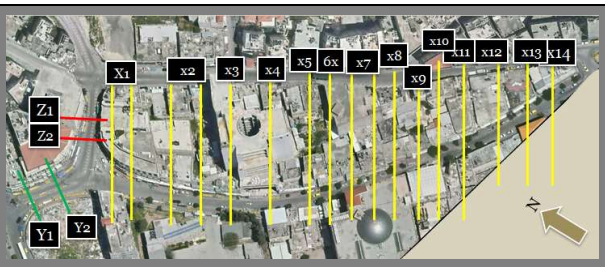	
		R-10floors,SW L-2floors,NE Canyon:C6,C16
10- canyon- Shallow canyon (X5-105) 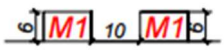 Vegetation area R-1floor,SW L-1floor,NE Canyon:C2,C2	11- Asymmetrical canyon - Moderate canyon (X6-115) 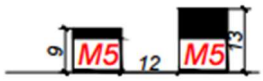 R-3floors,SW L-2floors,NE Canyon:C3,C5	12- Asymmetrical canyon (H/W: deep on one side, moderate on the other) (X7-120/130) 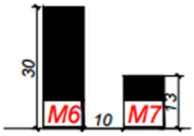 R-3floors,SW L-6floors,NE Canyon:C7,C14
13- Asymmetrical canyon (H/W: deep on one side, moderate on the other) (X8-140) 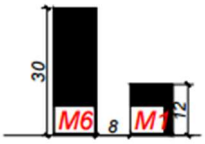 R-2floors,SW L-6floors,NE Canyon:C15,C8	14- Asymmetrical canyon (H/W: deep on one side, moderate on the other) (X9-145) 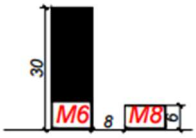 R-1floor,SW L-7floors,NE Canyon:C15,C3	15- Symmetrical canyon- Moderate canyon (X10-155) 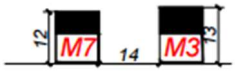 R-3floors,SW L-3floors,NE Canyon:C4,C4
16- Asymmetrical canyon-Moderate canyon (X11-165)  R-5floors,SW L-3floors,NE Canyon:C10,C11	17- Asymmetrical canyon - Moderate & shallow canyon (X12-175) 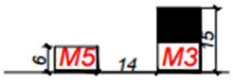 R-3floors,SW L-1floor,NE Canyon:C1,C5	18- Asymmetrical canyon -(H/W: deep on one side, moderate on the other) (X13-185) 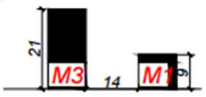 R-2floors,SW L-5floors,NE Canyon:C12,C4
19- Single-sided canyon - Moderate canyon (X14-195) 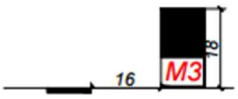 R-5floors,SW Canyon:C0,C5		

Ibn Rushed street(NS) sections		
1- Asymmetrical canyon- Moderate canyon (Y1-140) 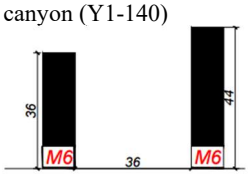 R-11flooors,W L-11floors,E Canyon:C5,C6	2- Asymmetrical canyon – Shallow & Moderate canyon (Y2-125) 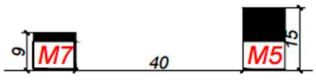 R-3floors,W L-2floors,E Canyon:C11,C1	3- Single-sided canyon- Shallow canyon (Y3-110) 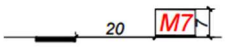 R-1floor,W Canyon:C0,C1
4- Asymmetrical canyon - Moderate canyon (Y4-1000) 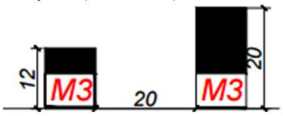 R-6floors,W L-3floors,E Canyon:C2,C5	5- Symmetrical canyon- Moderate canyon (Y5-90١١ تعديل الارتفاع من ٩ ل 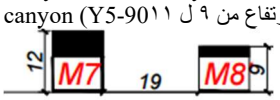 R-1floor,W L-3floors,E Canyon:C2,C2	6- Asymmetrical canyon- Moderate canyon (Y6-80/70) 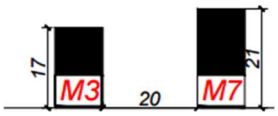 R-6floors,W L-4floors,E Canyon:C4,C5
7- Asymmetrical canyon- Moderate canyon (Y7-60/50)  R-3floors,W L-4floors,E Canyon:C3,C4	9- Asymmetrical canyon- Moderate canyon (Y8-40/30) 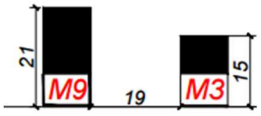 R-4floors,W L-6floors,E Canyon:C5/6,C3	10- Asymmetrical canyon -Moderate canyon (Y9-20) 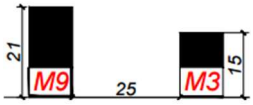 R-4floors,W L-6floors,E Canyon:C3,C2
Where C0=0,C1=0.2,C2=0.4,C3=0.6,C4=0.8,C5=0.9,C6=1.1,C7=1.2,C8=1.3,C9=1.5,C10=1.6,C11=1.8,C12=1.9,C13=2.1,C14=3,C15=3.8,C16=5.6		

Each material pair creates its own microclimatic condition. Material differences between the two sides affect MRT and air temperature differently across the canyon. The street center experiences the combined effect of both façades.

3.7.2 Human Parameters (BIO-met)

Table 3-5 shows the simulation and input data for thermal comfort calculation in BIO met; human parameters used were 35 years old, height (170 cm), and clothing insulation (clo) and metabolic activity (met) were varied according to the season to reflect real-world differences in thermal insulation and activity levels. For the summer scenario, light clothing was assumed, with an outdoor insulation value of 0.5 clo. For the winter scenario, warmer clothing was assumed with 0.9 clo. From Leonardo Tools, the output data is extracted, such as temperature,

wind speed, relative humidity, PET, and UTCI as heat maps. The results were extracted for the two streets.

Thermal comfort assessment in this study was conducted using both PET and UTCI indices to ensure a comprehensive evaluation of outdoor thermal conditions. The use of these two indices allows for capturing both simplified human energy balance responses (PET) and advanced thermophysiological responses (UTCI), thereby improving the reliability and robustness of the simulation outputs. This dual-index approach is particularly suitable for ENVI-met-based studies, where multiple microclimatic variables such as air temperature, wind speed, humidity, and mean radiant temperature interact simultaneously.

Table 3-5 BIOmet Input data for PET and UTCI output

Biomet input data	Clothing insulation	(0.5 clo summer, 0.9clo winter clothes)/speed 1.21-1.34m/s
	Activity	walking
	Body position	standing
Personal data	Height	1.7m
	Weight	75kg
	Age	35 years old
	Sex	male

After identifying the research gap from previous studies, the study area and case studies were selected and analyzed. The ENVI-met model is validated by simultaneously comparing the simulation results with the field observations from the same case study. Simulation of the two streets by ENVI-Met v. 5.6.1: This stage was implemented by using 3 tools:

a) ENVI-MET is utilized for modeling and simulation processes.
b) The LEONARDO tool is used to obtain environmental parameters such as Ta, Ws, and Rh, exporting maps during specific hours,
c) Biomet tools are utilized for calculating PET and UTCI based on the previous environmental parameters and studying the effects of urban canyons and materials to determine the best and worst results.

3.8 Analysis Framework:

This section presents the analytical framework used to interpret the simulation outputs and measured data. The analysis focuses on examining the relationship between the independent variables—façade materials, street orientation, and urban canyon aspect ratio—and their influence on microclimatic parameters and outdoor thermal comfort indices. The framework

combines descriptive analysis of ENVI-met outputs with statistical methods to evaluate the significance of differences between scenarios and to identify the most influential variables affecting outdoor thermal comfort.

3.8.1 Simulation and data process analysis

After calibrating the program to ensure the model's accuracy, the results were extracted from the model using the Leonardo tool in five hours at three points for each section. The data was arranged in a table initially according to Appendix , which shows the results on the right of the building (left), the left of the building (right), and the middle of the street in all the sections that were approved for each street in summer and winter and included the following indicators (temperature, wind speed, humidity, PET, and UTCI).

After organizing and classifying the data, we statistically analyzed the results for each street using Excel sheet. The first phase included descriptive analysis, which covered two stages of analysis. The first stage extrapolated the data expressed by the curves for each indicator individually, and coloring map for PET and UTCI, and the second stage linked these indicators together. The second phase was inferential statistical analysis using Anova-Tukey HSD test, multiple linear regression tests and correlation coefficients such as (Luo *et al.*, 2024),and (Bao *et al.*, 2023) studies. This comprehensive approach provides a deeper understanding of the results, linking indicators and variables and their impact on each other.

3.8.1.1 Descriptive statistics

Descriptive statistics and comparative figures were used to examine trends in microclimatic variables and thermal indices across materials, orientations, locations, and seasons. The descriptive analysis found the highest and lowest values of the indicators, as well as the mean and standard deviation for each street, regardless of where it was located, to the right or left of the building or in the middle street, and at five different times of the year (summer and winter), as shown in the next section (results). For each indicator, the curve was divided into the right (left) of the building, its left (right), and the middle of the street, after naming each side of the section according to the material, orientation of the facade, and urban canyon. For instance, we assigned the names M1-SW-C1 .The horizontal axis was fixed to represent the materials, and the vertical axis to represent the temperatures, humidity, wind speed, PET, and UTCI during the five hours. First, the comparison was general between the two streets; then it was specific to each street and each orientation individually. The extracted curves connected to maps and

color tables that displayed the results of the two streets simultaneously to identify the PET and UTC I indicators. Table 3-6, categorized by global thermal comfort indicators, display the results of the two streets simultaneously. The same analysis methodology used in the research (Elkhayat *et al.*, 2024) was followed.

In this study, the classification of thermal comfort is based on the standard PET thresholds proposed by Matzarakis and Mayer (1996), where the neutral thermal sensation is defined within the range of 18°C to 23°C (Matzarakis, Mayer and Iziomon, 1999). This global classification allows consistency and comparability with other international research. However, it is important to acknowledge that studies in Mediterranean climates have suggested slightly higher neutral PET thresholds. For example, (Labdaoui *et al.*, 2021) identified a neutral PET range between 20°C and 26°C in the city of Annaba, Algeria. Although this broader range may better reflect local thermal perception in Mediterranean environments, the global classification was retained in this study to ensure methodological alignment with similar works.

Table 3-6 Human thermal sensation for PET and UTCI internal heat production: 80 W, heat transfer resistance of the clothing: 0.9 clo(Matzarakis, Mayer and Iziomon, 1999; Jo *et al.*, 2023)

Thermal perception	PET(C°)	UTCI(C°)	Grade of physiological Stress
Very cold	<4	<-40	Extreme cold stress
		-27~-40	Very Strong cold stress
Cold	4–8	-13~-27	Strong cold stress
Cool	8–13	0~-13	Moderate cold stress
Slightly cool	13–18	9~0	Slight cold stress
Comfortable	18–23	9~26	No thermal stress
Slightly warm	23–29		Slight heat stress
Warm	29–35	26~32	Moderate heat stress
Hot	35–41	32~38	Strong heat stress
Very hot	>41	38~46	Very Strong heat stress
		>46	Extreme heat stress

3.8.1.2 Inferential Statistical Analysis Methods

To test the significance of the differences and relationships among the variables under study, inferential statistical analysis methods were employed. These methods allow us to apply the results from our sample to the larger population and help us understand how wall material, orientation, and urban canyon layout affect outdoor thermal comfort. A one-way analysis of variance (ANOVA) was used to see if there were important differences in thermal comfort indicators (like air temperature, PET, and UTCI) based on different types of wall materials. After that, use the Tukey HSD test to identify groups that differ significantly between them. Also, multiple linear regression (MLR) analysis was used to see how important factors (like U-value, urban canyon, and orientation) connect to thermal comfort results. Figure 3-12 , this

model helps to identify the most influential variables affecting outdoor thermal comfort and assess the strength and direction of these effects. Detailed formulas and computation steps are included in Appendix C.

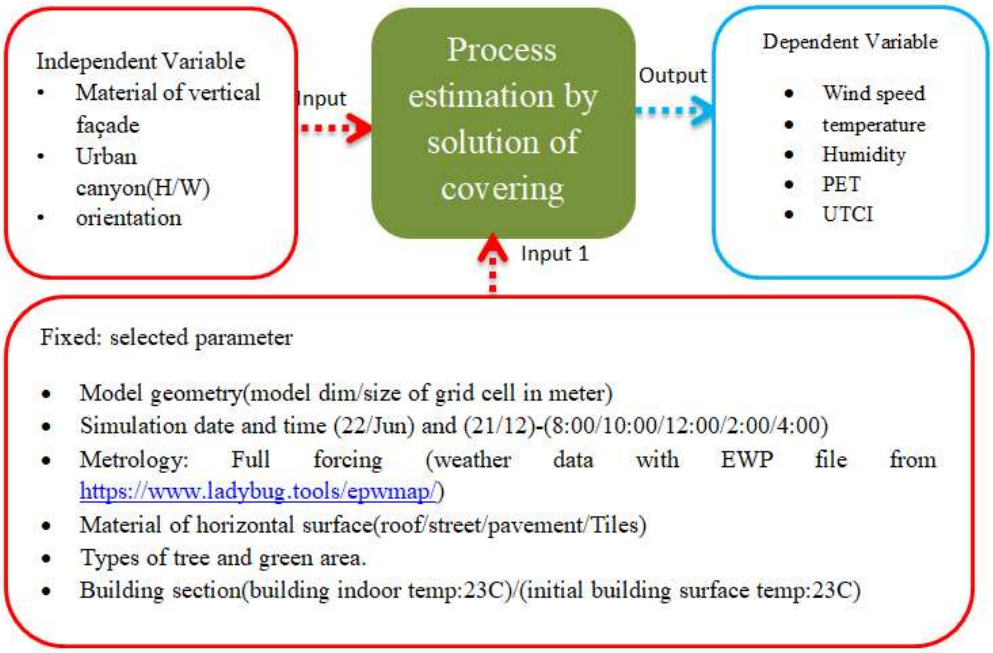

Figure 3-12 Independent and dependent variables

3.9 Summary

This chapter explains the research methodology used to evaluate the impact of urban materials, urban street and orientation on outdoor thermal comfort in open commercial areas. In the literature review phase, data were collected through field surveys, observations, field measurements, and personal interviews. The criteria used to select the study area and analyze the case studies were also explained. It describes how the simulation works and the software used to input data about building materials and trees that the program doesn't recognize, including the set and changing input factors and the calibration step that involves comparing field data with simulation results. Finally, it explains how the results of the study and calibration were analyzed using four statistical parameters to check if the model was accurate, along with descriptive and inferential statistical analysis to look at the data and give recommendations and general conclusions at the end of the study as shown in Figure 3-13. This stage was essential for clarifying the influence of urban configuration and materials on outdoor thermal comfort through the results chapter

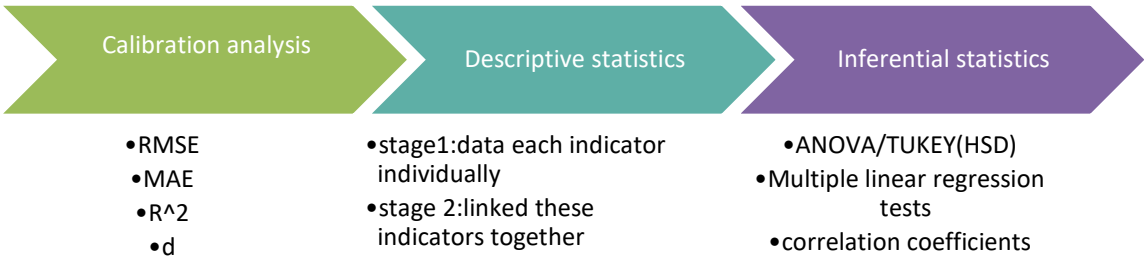

Figure 3-13 Framework for analyse output data

Chapter 4: Results and Discussion

4.1 Preface

This chapter aims to present and analyze the performance of façade materials and to relate their effects to other variables influencing outdoor thermal comfort during summer and winter conditions. The analysis is based on calibrated ENVI-met simulations, which provide reliable microclimatic outputs for temperature, wind speed, humidity and thermal comfort indices. While previous studies have typically examined material properties, street orientation, or canyon geometry independently, this research evaluates their combined influence to identify which variables exert the strongest effect under Mediterranean climatic conditions. The results demonstrate that variations in façade materials, street orientation, and height-to-width (H/W) ratios produce measurable differences in air temperature, humidity, wind speed, PET, and UTCI. These impacts become more pronounced at specific times of day and in certain orientations, particularly when materials with distinct thermal behaviors interact with urban canyon constraints.

Statistical analyses—including ANOVA, Tukey HSD, correlation analysis and multiple linear regressions—further validate these relationships and quantify the significance of each factor. To enhance clarity, the analysis is presented in an aggregated comparative form, whereas detailed numerical results for each point (right, middle, and left) and for all materials, and ENVI-met maps are provided in the appendices.

The chapter begins with model calibration and verification, followed by the comparative analysis of microclimatic variables and thermal comfort indicators for both seasons, winter results are presented concisely and complementarily to highlight seasonal variations without repetition. The findings are then discussed in relation to previous studies to highlight areas of agreement, divergence, and local specificity.

4.2 Model Calibration and verification (ENVI –Met V5.6.1)

To obtain useful findings, model correctness is essential. Therefore, calibration is crucial for determining the model's accuracy, errors, and limitations. Ultimately, this process enhances the model's reliability and builds confidence in its applicability to real-world situations. The model’s simulation has been validated through a comparison between the observed current site measures and the predicted study results. The field measurements that monitored Ta, Ws, and RH were used for calibrating the ENVI-met model; these parameters could also provide the OTC. Ta readings were taken in the middle of the street and on the right and left sides to ensure

the difference in measured and simulation values for the same section at different points, verifying the model.

4.2.1 Calibration (Air temperature, relative humidity, and wind speed)

Both simulated data produced using ENVI-met and empirical measurements are included in (Table D1-1) in appendix D, for temperature, relative humidity, and wind speed. In several published studies, the temperature was a significant climatic element that was used to validate model performance, and Figure 4-1, Figure 4-2, and Figure 4-3 show the simulation and measured values of air temperature, relative humidity, and wind speed at monitoring points. The simulated temperatures were between 19.5 and 30.4, while the measured temperatures were between 17.8 and 27.5, as shown in the figure (Figure 4-1). Temperatures in Envi-MET values are generally higher than the observed ones by an average difference of 3.2 °C at all points, Relative humidity was overestimated by ENVI-met, deviating by around 15% from the field data, Relative humidity with an average difference of 6.4 % for all points except (1, 2, and 3 from 2-3 pm), and 0.31 m/s for several points, in Figure 4-3 . There are many of reasons for these variations. External Influences include Things like parked vehicles and concrete wall that were present in the outdoor area could have caused temperature changes that the simulation did not take into consideration.

Model input data: The telescoping adopted to reduce the simulation time may have affected the value of the results as well. Grid size may affect the accuracy of ENVI-met outputs.

The tendency of the ENVI-met simulations to yield higher values of air temperature, wind speed, and relative humidity compared to field measurements can be partly explained by the constant indoor air temperature applied in all scenarios. This constant boundary condition likely maintained a steady heat flux through façades, elevating simulated outdoor temperatures. Additionally, the absence of small-scale urban obstructions in the model setup allowed higher wind speeds, which enhanced evapotranspiration and slightly increased simulated RH.

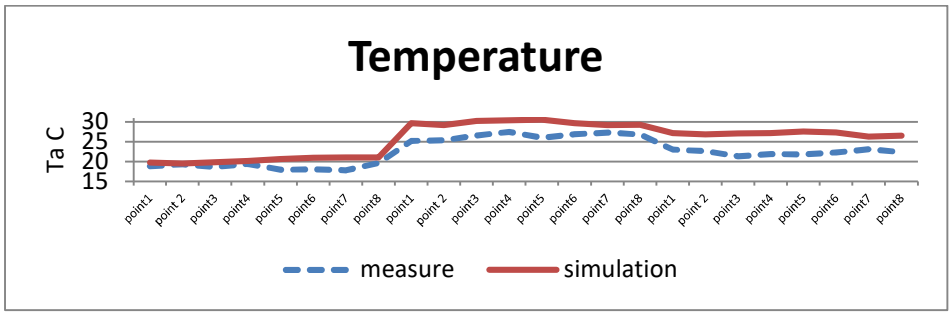

Figure 4-1 Air temprature measured and simulation

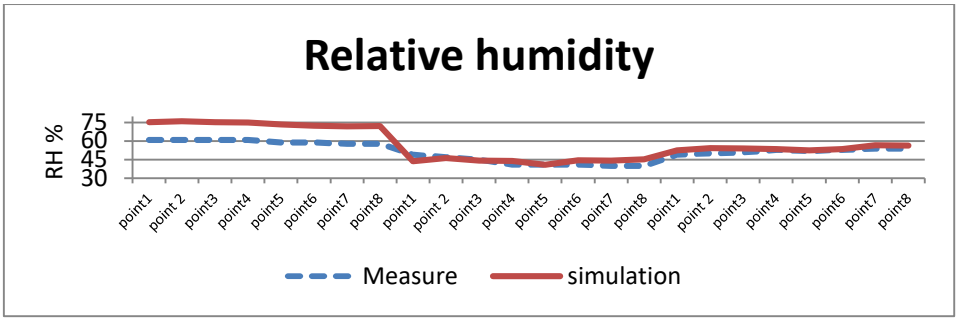

Figure 4-2 Relative humidity measered and simulation

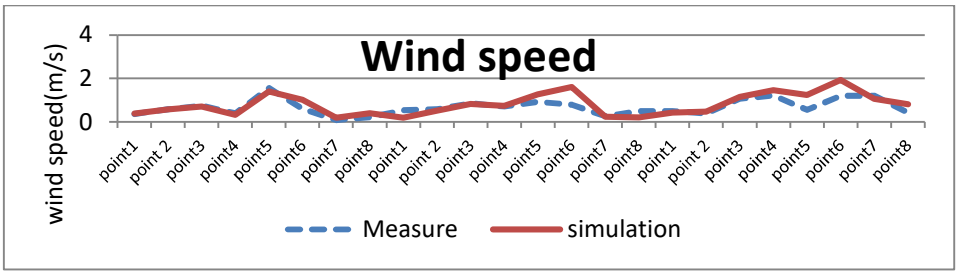

Figure 4-3 Wind speed measured and simulation

The statistical validation of the outcomes of the ENVI-met model was accomplished by the four quantitative measurements, the coefficient of determination (r2), Willmott's index of agreement (d), Mean Absolute Error (MAE), and Root Mean Squared Error (RMSE) (Faragallah and Ragheb, 2022).

Table 4-1 shows the four error calculations that have been calculated for each of the three output parameters. The air temperature R2 in the current research is equal to 0.86, suggesting a significant correlation between the simulated and observed values. The d value is 0.79, indicating a sufficient degree of consistency between the simulated and measured values. The RMSE and MAE metrics were evaluated as very good (less than 15%), with values of 3.58°C and 3.22°C, respectively. In addition, the measurements of the relative humidity and wind speed exist (R2 and d) within the normal range, as shown in Table 4-1 The RMSE and MAE of RH were high, indicating possible errors in ENVI-met simulations. These could be due to the failure of ENVI-met to successfully simulate the solar and/or the moisture brought by the wind (Koletsis *et al.*, 2022) . Relative humidity had low validation evaluations, although it should be noted that people's perceptions of air humidity are unclear; therefore, this should have a minor impact on people's thermal perception (Koletsis *et al.*, 2022).

While there are significant individual variances in wind speed, the predicted values and the actual values are quite comparable. In this instance, Envi-MET's results remain valid despite the extremely poor correlation displayed by the model validation techniques in Table 4-1. The

challenge of attempting to test Envi-MET with a parameter that fluctuates quickly, like the wind, is demonstrated by this example. This mismatch may arise from ENVI-met inability to incorporate real-time wind speed and direction(Koletsis *et al.*, 2022) .Detailed scatter plots (Figure D1-1 , Figure D1-2 , Figure D1-3) Were relocated to the appendix to avoid redundancy; shows the scatter plot of the data above the 1:1 line in Ta and Rh, indicating a persistent positive bias. However, the scatter plot for wind speed shows that part of the data falls below the line, indicating a negative effect. Although the positive correlation is clear, there is an overestimation of the values. All statistical indicators are summarized in Table 4-1.

Table 4-1 summery of the error normas for the calibration(7-5pm) (RMSE), correlation coefficient, Pearson's correlation coefficient(R), Index of Agreement (d), (MAE) (https://agrimetsoft.com/calculators,2024)

indicators	01/11/2024				
	RMSE	R^2	d	MAE	Pearson's correlation coefficient(R)
Ta air	3.58	0.86	0.79	3.22	0.928
Humidity	8.565	0.875	0.821	6.38	0.935
Wind speed	0.322	0.629	0.843	0.222	0.793

4.2.2 Verification (Air temperature)

Table D1-1 in appendix D-1 shows the simulation and measured data; Field temperature measurements were conducted in two sections of the street to compare values within each section between the right, left, and center sides at 11:30 am. This procedure was performed to verify that the field differences were consistent with the simulation results, which, for the most part, showed a clear convergence between the three sides. The air temperature R2 in the current research is 0.994 and 0.74, indicating a correlation between the simulated and observed values. The d-value is 0.12 and 0.24, suggesting a poor consistency between the simulated and measured values. In contrast, the RMSE and MAE metrics were assessed as very good (less than 15%), with values of 1.189°C, 1.031°C and 1.147°C,0.91°C respectively. Table 4-2

Table 4-2 Summery of the error normas for the verifaction point

13/6/2025 (11:30 am)				
Indicators(temperature)	RMSE	R2	d	MAE
Section 1	1.189	0.994	0.12	1.147
Section 2	1.031	0.74	0.24	0.91

The results of this study show general agreement with previous research on the accuracy of the ENVI-met model after calibration, with differences related to climatic conditions and methodology. (Gusson and Duarte, 2016) in a subtropical climate recorded an RMSE for

temperature between 1.6–1.9°C and d between 0.85–0.92, while (Ayyad and Sharples, 2019) in a hot-dry climate achieved an RMSE of 2.45–2.60°C and d ≈ 0.89, and (Koletsis *et al.*, 2022) in a Mediterranean climate showed an RMSE of 2.0°C and d = 0.8, with lower performance for humidity and wind, which was reflected in thermal comfort indicators.

The study and (Koletsis *et al.*, 2022) showed that any deviation in Ta could raise the PET and UTCI values by about 1–2°C when other variables are held constant, which strengthens the reliance on simulation results in analyzing the effect of materials, orientation, and urban composition on thermal comfort.

Based on (Ayyad and Sharples, 2019), the temperature and humidity results were strongly correlated. However, the correlation was weak for wind speed and the individual differences were large. However, the Envi-MET results were valid and were relied upon for the study's analysis. This study concludes that the ENVI-met V5.6.1 tool is a reliable tool for analyzing thermal conditions in open areas.

Finally, in all comparisons of the study, a difference between field measurements and simulation results is considered acceptable for model calibration; it is useful in PET and UTCI analysis. The results indicate that although the model has acceptable accuracy, especially for temperature and humidity, there is a persistent overestimation of temperature and an underestimation of wind speed—both of which are essential factors affecting thermal comfort indices.

Because PET and UTCI are composite indices derived from air temperature, wind speed, and humidity, any calibration discrepancies in these variables can propagate into the thermal comfort outcomes. PET is especially sensitive to air temperature and wind speed, while UTCI gives additional weight to humidity under warm and humid conditions. In this study, a temperature deviation of approximately 3–3.5°C may result in a PET shift of 3–5°C and a UTCI shift of about 2.5–4°C, particularly during hot afternoon periods. Likewise, the underestimation of wind speed by nearly 0.3 m/s reduces convective cooling, consequently elevating PET and UTCI values. As such, the simulated thermal comfort indicators should be interpreted within a ±3–4°C uncertainty margin, especially in summer conditions and locations with limited ventilation. Following the satisfactory calibration and validation of the ENVI-met model, the analysis proceeds to examine the general microclimatic behavior of the study streets. This section provides a descriptive overview of air temperature, relative humidity, and wind speed patterns prior to discussing thermal comfort indices, allowing the baseline climatic characteristics of each street to be clearly identified.

4.3 General Microclimate Behavior of the Study Streets (summer)

This section provides an overall description of the summer microclimatic behavior of the three study streets based on ENVI-met simulation outputs (Figure 4-4). The aim is to characterize the thermal behavior of each street at the macro level—before conducting detailed variable-specific analysis—by examining typical daily patterns of temperature, humidity, and wind.

4.3.1 Weddad Street – General Overview

Weddad Street (NW–SE) exhibits the most balanced microclimatic performance among the three streets due to its oblique orientation, which distributes solar exposure more gradually throughout the day. Morning hours show slightly higher temperatures on the NE-facing side, while the opposite SW side remains shaded. As the sun shifts, this pattern inverts, producing a small temperature gradient that typically does not exceed 1–1. 5°C.Wind flow is relatively stable, with the street acting as a partial ventilation channel aligned with the prevailing afternoon winds. The middle of the street consistently receives higher wind speeds than either side. Despite the improved wind penetration along the street, the change in direction angle led to an uneven distribution of wind and the emergence of areas with zero wind speed. Humidity follows an inverse pattern with temperature—higher in the morning (≈55–58%) and lowest at midday (≈31–34 %.) Overall, Weddad Street maintains the most moderate thermal conditions due to distributed shading, partial wind alignment, and reduced stagnation zones.

4.3.2 Haymoni Street – General Overview

Haymoni Street, characterized by combined EW and NE–SW orientations, demonstrates the poorest overall microclimatic performance during the summer season among the three studied streets. The E–W sections experience the most intense heat exposure, registering the highest temperatures among all streets due to prolonged direct solar incidence during morning and midday hours, especially the left and the middle regions suffered from higher temperatures than the right throughout the day, NE–SW orientation, the temperature rises on the southeast side in the morning due to solar exposure, then shifts in the afternoon to the northwest side, showing the effect of orientation on daily temperature variation. Wind speeds in the NE–SW sections are relatively higher during morning hours, while the E–W segments remain poorly ventilated, especially at midday. Humidity shows higher morning values (≈59%) and significant drops at noon due to elevated temperatures (≈27–30%). Overall, Haymoni Street demonstrates the least favorable microclimatic performance due to its geometric exposure to solar radiation and weaker ventilation.

4.3.3 Ibn Rushed Street – General Overview

Ibn Rushed Street (N–S) shows a pronounced thermal contrast between its two sides. The east-facing side is warmer in the morning, while the west-facing side becomes significantly hotter in the afternoon; with differences reaching up to 2°C. Midday temperatures in the middle street remain high due to the limited shading and prolonged exposure to direct solar radiation. Wind speeds remain modest throughout the day due to the misalignment between the street axis and predominant wind direction, though intersections and open nodes enhance ventilation locally, a slight variation in the distribution of winds was observed laterally, with the speed being higher in the middle of the street and lower near the facades as a result of the buildings obstructing the movement of air. The entrances to Ibn Rushed Street recorded lower temperatures and better ventilation than the center, which improved thermal comfort relatively, although the street remained generally hot due to sun exposure and weak winds. Humidity follows the expected inverse pattern with temperature, decreasing substantially during peak solar hours. Overall, Ibn Rushed Street exhibits stronger thermal fluctuations than Weddad Street but performs better than Himonies Street due to occasional cross-ventilation at key segments.(Detailed hourly values and side-by-side comparisons for Weddad, Haymoni and Ibn Rushed Streets are provided in Appendix D-2)

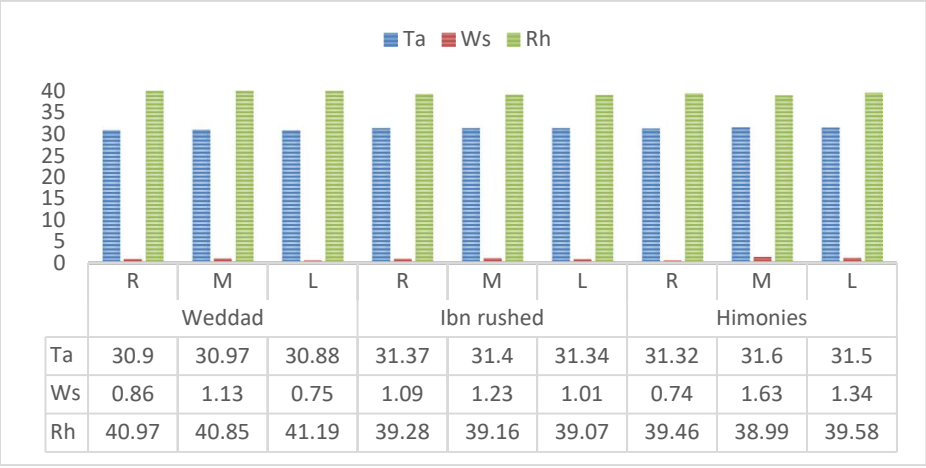

	Weddad			Ibn rushed			Himonies		
	R	M	L	R	M	L	R	M	L
Ta	30.9	30.97	30.88	31.37	31.4	31.34	31.32	31.6	31.5
Ws	0.86	1.13	0.75	1.09	1.23	1.01	0.74	1.63	1.34
Rh	40.97	40.85	41.19	39.28	39.16	39.07	39.46	38.99	39.58

Figure 4-4 Average results (Ta,Ws, and Rh) for three streets

4.4 Microclimate analysis in summer (Ta, Rh, Ws)

This section presents a descriptive analysis of the microclimatic conditions (air temperature, wind speed, and relative humidity), comparing the right, middle, and left canyon points in each street, along the three study streets during a representative summer day (22 June), in order to clarify the combined effect of street orientation and canyon geometry (H/W) on the local

microclimate. To maintain clarity, the results are presented in an aggregated comparative form, while detailed numerical outputs are available in the appendices.

4.4.1 Air Temperature in summer - Comparative Analysis

The three streets exhibit a broadly similar diurnal temperature pattern, with mild conditions in the early morning (8:00–10:00), followed by a rapid rise towards midday and peak values between 12:00 and 14:00. However, clear differences emerge between orientations and between the right, left, and middle of the street due to orientation and canyon geometry.

a) Comparison between the three streets (Weddad - Ibn Rushed - Al-Haymoni)

In all streets, the sun-exposed façades in the morning (typically east- or southeast-facing) record higher temperatures than the shaded side, while this pattern reverses in the afternoon when the sun moves towards the west. The street centers, which remain more exposed to direct solar radiation, usually approach or slightly exceed the maximum values recorded on the sunny façades at noon. Weddad Street (NW–SE) shows relatively moderate temperature levels during the day compared with Ibn Rushed (N–S) and Haymoni (NE–SW and EW). Although some points on Ibn Rushed are slightly cooler than Weddad at 8:00–10:00, the overall daytime average is lower along Weddad, especially at peak hours. The difference in mean Ta between Weddad and Ibn Rushed is typically around 0.5 °C, reaching about 1 °C when compared with Haymoni Street, particularly at 12:00 as shown in Table 4-3Error! Reference source not found.. Haymoni, especially in its EW segments, systematically shows the highest temperatures on all sides and at most times of the day.

b) Comparison between Right-Middle-Left

Within each street, spatial differences across the section are limited but noticeable; the middle of the street was typically warmer than both sides during midday. On Weddad Street, the temperature difference between right, left, and middle can reach about 1.5 °C in some locations, whereas in Ibn Rushed the cross-sectional difference usually remains below 1°C, except in a few sections where it exceeds 2°C between the center and the left side at 12:00–14:00 as shown in appendix E. The temperature variation on Weddad Street was limited (1–2.5°C) along a street to one side, while it exceeded 3°C on Ibn Rushed Street, especially on the left side of the buildings at 12 noon. The standard deviation values were generally lower in Ibn Rushed than in Weddad see TableD2-3 and Table D2-4, which indicates more homogeneous temperature

distribution along its length, despite the overall higher heat load. Overall, the NW–SE orientation of Weddad Street provides a more balanced alternation of sun and shade along the day, limiting excessive heating of any single façade, while the EW alignment in Haymoni amplifies pre-noon and midday solar gains and leads to consistently higher Ta.

4.4.2 Relative humidity in summer- Comparative Analysis

Relative humidity across the three streets follows a clear inverse pattern to air temperature, with the highest values observed in the early morning and the lowest occurring during midday and early afternoon. Morning values ranged between 52–60%, decreasing sharply at noon to approximately 27–34% across all streets. The lowest humidity corresponded to the highest temperature periods (12:00–14:00). When comparing streets, Weddad Street consistently recorded the highest RH levels at most times and sections, followed by Ibn Rushed, while Al-Haymoni exhibited the lowest RH during the afternoon peak. The differences between streets typically ranged between 2–4% for similar times and positions. Within each street, the differences between right, middle and left sides were generally modest (about 1.5–2%), and standard deviations were mostly low, especially in the morning, indicating relatively homogeneous humidity distributions compared with temperature. Shaded façades consistently showed slightly higher RH than sun-exposed façades, reflecting reduced evaporative drying. The middle of the street usually records intermediate values matching its exposure conditions.

Differences between right–middle–left segments remain small (<2%), confirming that RH is more sensitive to macroclimatic heating than to local street geometry. The middle of the canyon tends to experience the sharpest RH decline during midday when solar penetration and heat accumulation are highest. This effect is more pronounced in streets with lower H/W ratios or wider sections that allow more direct sunlight to reach the canyon floor.

4.4.3 Wind speed in summer- Comparative Analysis

Wind speed during summer exhibits considerable variation driven by canyon geometry, orientation, and alignment with prevailing winds. Wind speed is highest in the middle of all streets and lowest near façades. The differences between the streets are especially prominent during the afternoon, when wind flow intensifies and interacts with canyon morphology. The maximum values typically occur at 16:00, when large-scale atmospheric circulation is strongest, with peak speeds of about 4.7 m/s in Ibn Rushed, 4.2 m/s in Weddad, and around 3.9 m/s in Haymoni (see Table D2-1).

a) Comparison between the three streets (Weddad - Ibn Rushed - Al-Haymoni)

Ibn Rushed Street shows relatively regular airflow along its length, with moderate variations between the right and left sides (usually less than 1.5 m/s) and a gradual increase from morning to afternoon. Ventilation was slightly enhanced near intersections, where openings into the surrounding network facilitated air entry. However, its N–S orientation is not fully aligned with the prevailing winds, so overall speeds remain moderate. Weddad Street, in contrast, exhibits more pronounced spatial variability. Some sections show sharp peaks in the middle and right side, while adjacent segments on the left experience almost stagnant conditions (<0.5 m/s). These patterns reflect local geometrical effects that create acceleration in some zones and thermal stagnation in others.

Haymoni Street demonstrates a clear contrast between its two orientations. In the NE–SW sections, wind speeds are relatively favorable in the morning but drop significantly during peak heating hours. In the EW sections, the alignment with the prevailing wind enables better ventilation throughout the day, with the largest differences between center and sides sometimes exceeding 2.8 m/s. detailed wind speed tables, hour-by-hour values, and ENVI-met wind maps for each sectional location are presented in Appendix D-2

b) Right–Middle–Left Spatial Differences

Within streets, right–middle–left comparisons indicate that the middle section of the canyon typically has the highest wind speeds. Along all the streets, the middle of the canyon typically records the lowest wind speeds, especially in deeper or more enclosed segments, due to increased friction and reduced sky openness. Higher speeds appear near canyon edges where lateral ventilation is more effective. However, the extent of these differences varies strongly by street geometry. Weddad Street, for example, experiences abrupt changes in wind speed between adjacent segments due to changes in alignment and localized sheltering. Ibn Rushed, in contrast, shows more gradual variation, with smaller differences between sides. Haymoni Street exhibits the largest side-to-side differences, especially in its NE–SW segment.

Table 4-3 Summury of Avegrage results for streets in summer

Average of summer results in three points(sides R , M ,L) at (8,10,12,2,4)										
Parameters	time	Weddad			Ibn rushed			Himonies		
		R	M	L	R	M	L	R	M	L
Ta	8	25.48	25.61	25.73	26.06	26.2	26.25	26.27	26.52	26.45
	10	28.73	28.92	28.9	28.93	29.29	29.63	29.07	29.72	29.62
	12	32.72	32.81	32.58	33.49	33.45	33.41	32.8	33.26	33.23
	2	34.34	34.32	34.33	34.85	34.69	34.23	34.91	34.91	34.72

Average of summer results in three points(sides R , M ,L) at (8,10,12,2,4)										
	4	33.22	33.18	33.07	33.48	33.36	33.19	33.57	33.6	33.56
	Average	30.9	30.97	30.88	31.37	31.4	31.34	31.32	31.6	31.5
Differences		-0.46	-0.43	-0.42	-0.43	-0.63	-0.59	0.04	-0.20	-0.17
		Weddad vs. Ibn rushed			Weddad Vs. Himonies			Ibn rushed vs. Himonies		
Wind speed	8	0.64	0.79	0.45	0.46	0.6	0.59	1.01	1.69	1.32
	10	0.7	0.88	0.54	0.41	0.54	0.46	0.86	1.48	1.16
	12	0.85	1.1	0.71	0.87	0.99	0.79	0.85	1.7	1.35
	2	0.9	1.24	0.87	1.58	1.73	1.42	0.43	1.39	1.18
	4	1.19	1.65	1.16	2.15	2.31	1.78	0.54	1.9	1.7
	Average	0.86	1.13	0.75	1.09	1.23	1.01	0.74	1.63	1.34
Differences		-0.24	-0.10	-0.26	0.12	-0.50	-0.60	0.36	-0.40	-0.33
		Weddad vs. Ibn rushed			Weddad Vs. Himonies			Ibn rushed vs. Himonies		
RH	8	56.22	55.88	55.61	53.79	53.31	52.89	55.45	55.57	56.65
	10	48.15	47.85	48.21	45.92	45.11	44.23	45.46	43.8	44.79
	12	35.93	35.92	36.72	33.56	33.57	33.44	34.02	33.19	33.53
	2	29.75	29.77	30.26	28.87	29.15	29.85	28.4	28.45	28.86
	4	34.78	34.85	35.14	34.28	34.67	34.95	33.99	33.92	34.08
	Average	40.97	40.85	41.19	39.28	39.16	39.07	39.46	38.99	39.58
Differences		1.68	1.69	2.12	1.50	1.87	1.61	-0.18	0.18	-0.51
		Weddad vs. Ibn rushed			Weddad Vs. Himonies			Ibn rushed vs. Himonies		

4.4.4 Integrated Summer Microclimate

Considering air temperature, wind speed, and relative humidity together, Weddad Street offers the most favorable microclimatic conditions for pedestrians on the simulated summer day. It combines relatively lower Ta, slightly higher RH, and acceptable but not excessive wind speeds, resulting in a more moderate thermal sensation. Ibn Rushed Street presents a hotter and drier environment, with higher temperatures, lower humidity, and stronger winds. This combination increases heat stress in exposed periods despite the potential cooling effect of ventilation. Haymoni Street, especially its EW segments, shows the least favorable behavior, with systematically higher Ta and low RH, and only moderate improvements in wind speed.

In summary, the NW–SE orientation of Weddad allows a more balanced distribution of sun and shade and aligns reasonably with the prevailing winds, producing a relatively comfortable microclimate. By contrast, the N–S orientation of Ibn Rushed and the mixed NE–SW/EW configuration of Haymoni create harsher conditions during hot periods, particularly when combined with shallow, highly exposed canyon geometries.

Table 4-4 Summury of Microclimte condiction results for streets in summer

Parameter	Note	Better for comfort
Temperature	Weddad Street is approximately 0.5°C cooler at all locations compared to Ibn Rushed and Al-Haymoni.	Weddad
Humidity	Higher on Weddad Street, especially on the left (an important factor in mitigating perceived heat).	Weddad
Wind speed	Slightly stronger on Ibn Rushed, but not enough to offset the temperature and humidity differences.	Ibn Rushed

4.4.5 Material Influence on Microclimatic Variables

The absence of a direct effect of facade materials on air temperature (Ta), relative humidity (RH), and wind speed (Ws) in in-street comparisons does not imply that these materials are ineffective. Rather, it is due to methodological factors. The effects of urban geometry—particularly street orientation and height-to-width ratio (H/W)—were significantly greater, producing thermal differences of 1–3 °C, compared to the material effect, which did not exceed 0.5 °C. Furthermore, no controlled cases were available combining the same geometry with different materials that could be compared with a clear difference, thus preventing the direct isolation of the material effect. Additionally, the effect of thermal properties of materials, such as thermal mass and conductivity, accumulates over time and is more pronounced in surface temperatures than in instantaneous air temperatures, which are governed by shadows and wind patterns. Therefore, the material effect is only apparent in controlled statistical analyses (ANOVA and regression), where materials with lower U-values were shown to contribute to lower PET and UTCI indices. Therefore, the absence of a material effect in raw comparisons is a methodological issue and not evidence of the absence of its physical effect.

4.4.6 Effect of H/W on Ta, Ws, Rh

This section evaluates the influence of height-to-width ratio (H/W) and façade orientation on the microclimatic conditions of the three streets. Unlike Sections 4.4.1-4.4.2-4.4.3, which focused on general climatic patterns, the present section isolates the geometric effect using "within-street" comparisons for identical materials. Full numerical tables and case-by-case comparisons are provided in Appendix D-2 (Table 4-5) – example for right side Weddad street (Table 4-6) - example for right side Ibn rushed street, while the text below presents a synthesized interpretation based on the most representative patterns. Analysis at the time of highest variability (12:00) reveals that temperature differences of 1–2.5 °C can occur between locations with the same façade material but different height-to-width (H/W) ratios and orientations.

a) Air temperature (Ta):

Air temperature exhibited a clear but orientation-dependent sensitivity to changes in H/W. In most SW- and NE-facing façades, increasing H/W resulted in lower temperatures during peak hours (12:00–14:00), as deeper canyons provided extended shading and reduced exposure to direct radiation. This effect was most evident in Weddad Street, where increasing H/W from 1.1 to approximately 1.8 lowered the temperature by up to 2.5°C for the same material. Generally, Ta reduces by enhancing shading, especially for sections with H/W between about

1.5 and 2.0, which show markedly better performance than very shallow canyons (H/W ≈ 0.6–1.1). However, this relationship is not strictly linear. In west-oriented segments, a low H/W combined with good exposure to prevailing winds can occasionally compensate for the lack of shade, leading to lower temperatures than in some deeper sections. This reveals the importance of the combined effect of orientation, H/W, and local airflow, rather than H/W alone. A similar pattern appears in Ibn Rushed Street: for the west-facing façades, wider canyons (H/W ≈ 0.6) tend to be cooler at midday, as they allow more effective ventilation, whereas narrowing the canyon to H/W ≈ 1.1–1.2 increases Ta by limiting air exchange and trapping reflected radiation. On the east side, the behavior can invert: higher H/W may reduce Ta by providing earlier shading during the critical morning hours, especially when the façade material has poor thermal insulation and is highly sensitive to direct solar gains. The temperature in the middle of the streets reflects the integrated effect of both sides. Sections where both façades have high H/W and/or favorable NE orientations, combined with moderately insulating materials, tend to show the lowest mid-street temperatures. Conversely, combinations of low H/W, a west or southwest orientation, and highly conductive materials result in the highest Ta at the street center. Overall, the results confirm that optimal canyon ratios lie in a moderate range (approximately H/W ≈ 1.5–2.0), but their effectiveness depends strongly on orientation and material properties. Very shallow or very deep canyons can both perform poorly under certain solar and wind conditions.

b) Wind speed (Ws):

Wind speed showed the highest sensitivity to H/W among the three variables. In all streets, lower H/W (0.6–0.8) generally improved ventilation by widening the canyon opening and allowing airflow to penetrate more effectively. This was evident in both Weddad and Ibn Rushed, where low H/W sections exhibited façade-level speeds between 1.5 and 3 m/s, compared to <1 m/s in deeper sections. However, the relationship was not purely linear. Several exceptions appeared: Medium H/W (≈1.1–1.2) occasionally produced peak speeds due to localized Venturi effects, particularly where the street converged geometrically or aligned with the prevailing wind. High H/W (≥1.8–2) consistently produced the lowest speeds across all orientations due to canyon blockage and limited vertical mixing. Large variations occurred in sections near intersections, open squares, or street bends—indicating that local geometry can override the pure H/W effect. Overall, ventilation in the studied canyons depended jointly on H/W, street orientation relative to prevailing wind, and the precise geometric configuration of each segment.

c) Relative humidity (Rh):

At the canyon scale, the impact of H/W on RH is weaker and more subtle than its effect on Ta or Ws. In Weddad, deeper canyons (higher H/W) tend to retain slightly more humidity at midday by reducing ventilation and evaporation, but the differences rarely exceed 1–2%. In contrast, in some west- or east-oriented segments, increasing H/W can reduce RH when enhanced solar exposure and heat retention dominate over shading benefits. In cases using insulating materials (e.g., M7 or M9), the influence of H/W on RH was negligible because wall temperatures remained comparatively stable. Overall, the results support previous research indicating that relative humidity in urban canyons is primarily controlled by the large-scale climate and temperature field, while the effect of H/W is secondary and usually limited to small differences between scenarios. While the microclimatic variables (Ta, RH, and Ws) provide essential information about the outdoor environment, they do not fully capture human thermal perception. Therefore, the following section evaluates outdoor thermal comfort using PET and UTCI indices, which integrate radiative, convective, and physiological factors to reflect pedestrian thermal stress more comprehensively.

Table 4-5 M1,M2,M3,M7 temperature,wind apeed,relative humidity results in Weddad street in right side in summer

layout	Case	H/W	Façade orientation	Ta12pm	Ws 4pm	RH 12pm
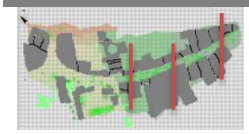	X8-M1a-SW-C15	3.8	SW	31.97	0.3	37.4%
	X5-M1b-SW-C3	0.6	SW	33.25	1.55	35.6%
	X13-M1c-SW-C13	2.1	SW	32.19	0.88	36.1%
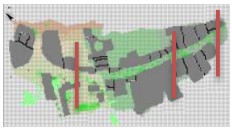	X2/55-M2a-W-C3	0.6	W	33.87	2.13	33.8%
	X2/55-M2b-W-C3	0.6	W	33.62	2.51	34.6%
	X9-M2c-SW-C15	3.8	SW	32.09	0.65	37.1%
	X14-M2d-SW-C0	0	SW	32.29	0.41	36.1%
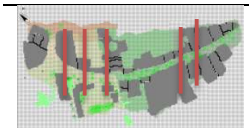	X1/35-M3e-W-C3	0.6	W	33.37	0.11	32.93%
	X1/45-M3f-W-C6	1.1	W	34.3	3.16	32.4%
	X3-M3g-W-C0	0	W	33.1	2.62	35.6%
	X10-M3h-SW-C5	0.9	SW	31.88	0.72	37.4%
	X11-M3i-SW-C11	1.8	SW	31.72	0.62	37.3%
	X12-M3j-SW-C2	0.4	SW	32.2	0.31	36.2%
	X7/120-M7a-SW-C14	3.0	SW	32.56	1.21	37.1%

layout	Case	H/W	Façade orientation	Ta12pm	Ws 4pm	RH 12pm
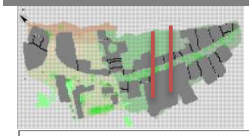	X7/130-M7b-SW-C15	3.8	SW	32.06	0.55	37.6%

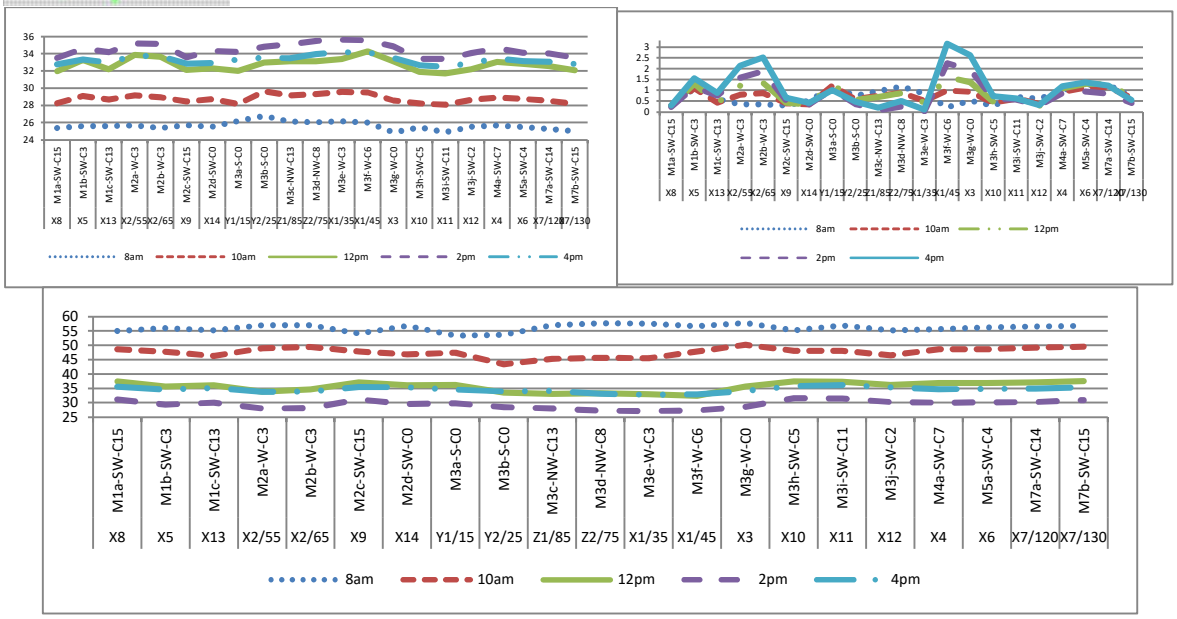

Figure 4-5 a) temperature b) wind speed c) Humidity in Weddad (summer)

Table 4-6 M3, M7 temperature, wind apeed,relative humidity results in Ibn rushed street for right side in summer

layout	case	H/W	Façade orientation	Ta 12pm	Ws 4	Rh 10
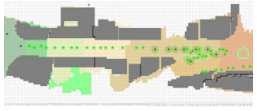	Y4-M3a-W-C3	0.6	W	32.7	3.05	48.46
	Y7/60-M3b-W-C4	0.8	W	33.68	2.26	43.95
	Y7/50-M3c-W-C4	0.8	W	33.9	2.24	43.99
	Y8/40M3d-W-C6	1.1	W	33.93	0.72	44.79
	Y8/30-M3e-W-C7	1.2	W	34.25	1.8	46
	Y9-M3f-W-C4	0.8	W	33.92	1.65	45.04
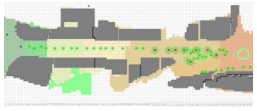	Y3-M7a-W-C0	0	W	33.23	1.86	47.78
	Y6/80-M7b-W-C5	0.9	W	33.16	1.73	45.94
	Y6/70-M7c-W-C5	0.9	W	33.12	2.32	45.71

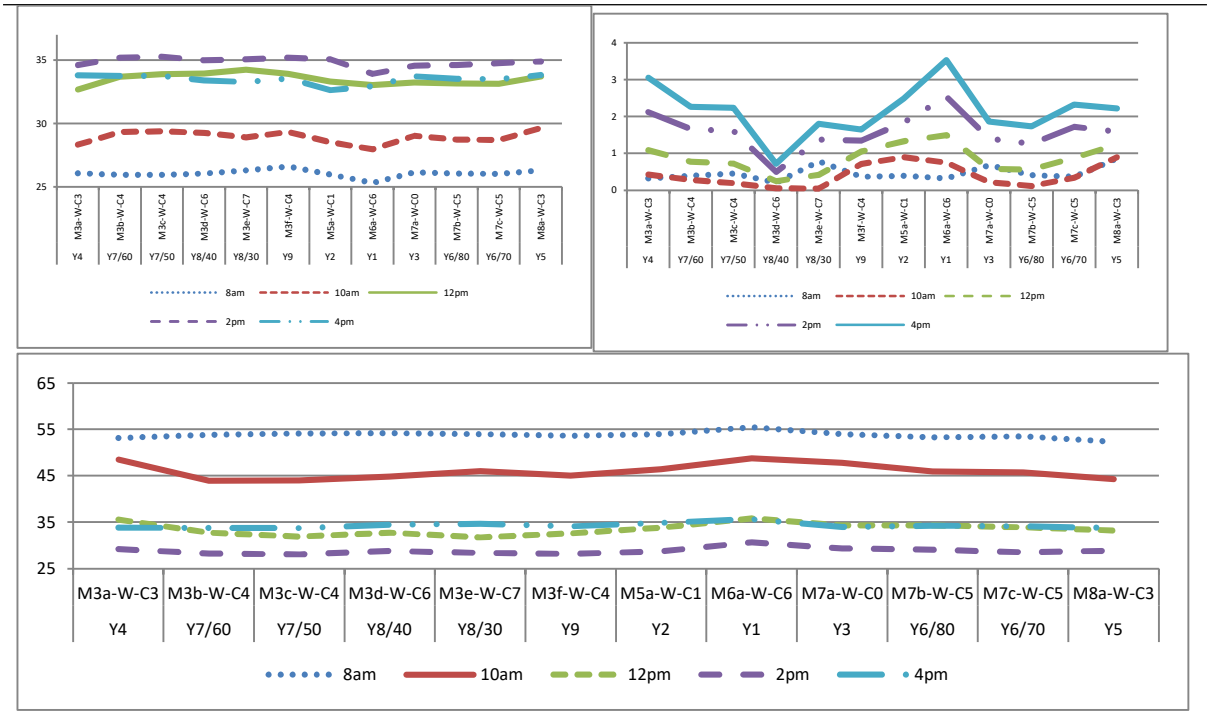

Figure 4-6 a) temperature b) wind speed c) Humidity in Ibn rushed (summer)

4.5 Outdoor Thermal Comfort analysis (PET and UTCI) in summer

Thermal comfort during summer was evaluated using PET and UTCI indices. Because these indices are more sensitive to combined environmental effects, the influence of canyon geometry and orientation becomes much more pronounced and material effects begin to emerge more clearly compared to microclimatic variables alone. All thermal comfort descriptions in this section follow the PET classifications introduced earlier in Table 3-6, where terms such as "warm," "hot," or "very hot" refer to predefined stress categories. PET and UTCI results in summer reveal clear patterns driven primarily by street orientation, canyon geometry (H/W), shading distribution, and—in more subtle ways—by façade material properties.

4.5.1 PET Results in summer

a) Overall comparison between streets

In general, all investigated streets exhibited high thermal stress during the summer reference day, particularly between 12:00 and 16:00, reflecting the severity of the local hot-summer Mediterranean conditions. However, the severity and spatial distribution of heat stress varied among streets due to differences in orientation, shading dynamics, and ventilation potential. Among the studied cases, Weddad Street (NW–SE) exhibited relatively lower PET values, followed by Ibn Rushed Street (N–S), while Al-Haymoni Street (E–W) showed the highest PET levels (see Table E-7, Table E-8). These findings confirm that street orientation plays a

decisive role in modulating outdoor thermal stress, even when all scenarios remain outside the neutral comfort range.

b) Street-specific patterns (brief overview)

Weddad Street (NW–SE) shows strong diurnal variability. At peak hours (12:00–14:00), PET frequently exceeds the very hot category in exposed locations, especially in center sections and southwest-facing façades. Morning and late-afternoon periods, however, record substantially lower PET values on the shaded right and left sides, falling into the warm or hot categories. This alternating pattern results from the NW–SE alignment, which distributes sunlight unevenly across the day and allows partial recovery on one side as the other heats up.

Ibn Rushed Street (N–S) behaves differently. Despite the theoretical advantage of reduced façade exposure in an N–S orientation, PET in the middle of the street becomes extremely high during peak hours, often surpassing 45°C and entering the very hot category. The lack of effective shading in the canyon center and the restricted longitudinal ventilation result in strong heat trapping. Side façades show asymmetric patterns: the east-facing side warms rapidly in the morning, whereas the west-facing side peaks sharply in the afternoon, producing large temporal contrasts. Overall, Ibn Rushed Street was thermally less comfortable than Weddad Street during peak hours, particularly in the middle of the street. The findings highlight the critical role of street orientation and spatial configuration in shaping the intensity and distribution of outdoor thermal stress, emphasizing the need for targeted design interventions—especially in central street zones—to mitigate heat accumulation and improve pedestrian comfort.

c) Right–Middle–Left distribution

Across all streets, the middle of the street consistently recorded the highest PET values during peak hours, frequently exceeding the very hot category. This pattern reflects heat accumulation resulting from direct solar exposure, reflected radiation from opposing façades, and reduced convective cooling within the canyon. In contrast, the right and left sides generally showed lower PET values, although their performance varied depending on façade orientation and the timing of solar exposure.

The street sides generally performed better than the center; however, their relative performance depended on façade orientation and shading timing. In Weddad Street, the right and left sides alternated between shaded and exposed conditions, leading to noticeable temporal differences

in PET, In general, the worst thermal conditions occurred in the street center, followed by the right side, while the left side offered comparatively better conditions during certain periods due to favorable shade timing. In Ibn Rushed Street, the sides showed less variation, while the middle consistently remained the most thermally stressed zone.

4.5.2 UTCI Results in summer

In order to complement the PET-based assessment, UTCI is analyzed in parallel. Although both indices indicate similar thermal trends, UTCI exhibits a higher sensitivity to humidity and wind speed, offering additional insight into physiological heat stress under summer conditions.

a) Overall comparison between streets

The UTCI analysis indicates that all studied streets fall within thermally stressful categories during summer, with most values classified as strong to very strong heat stress after 10:00 AM. Despite this general trend, noticeable differences were observed between streets as a result of orientation, and ventilation efficiency. Among the three streets, Weddad Street (NW–SE) exhibited comparatively lower UTCI values, followed by Ibn Rushed Street (N–S), while Al-Haymoni Street (E–W) showed the highest physiological heat stress (Table E-9, Table E-10).

b) Street-specific patterns (brief overview)

In Weddad Street, UTCI values varied considerably across the street and throughout the day. This variability is associated with the NW–SE orientation, which creates alternating patterns of solar exposure and shading between the morning and afternoon. Consequently, some locations experienced temporary reductions in physiological heat stress, particularly on the shaded façades during early and late hours. In contrast, Ibn Rushed Street exhibited a more consistent and severe UTCI pattern, especially in the middle of the street. Although the north–south orientation reduces direct solar exposure on façades, the street center remained highly stressed due to reflected radiation, limited shading at pedestrian level, and weak longitudinal ventilation, leading to sustained heat accumulation during peak hours.

c) Right–Middle–Left distribution

For both streets, the middle zone consistently recorded the highest UTCI values, often exceeding 40°C between 12:00 and 14:00, indicating very strong heat stress. The street sides generally showed lower UTCI values than the center; however, their relative performance varied by orientation and time of day. In Weddad Street, UTCI values on the sides fluctuated

noticeably due to shifting shadow patterns, while in Ibn Rushed Street, both sides showed a more uniform thermal response, with a pronounced late-afternoon increase on the west-facing façade.

4.5.3 Integrated Interpretation (PET & UTCI)

The slight differences observed between PET and UTCI results can be attributed to the differences in their underlying models. While PET primarily reflects human energy balance under simplified assumptions, UTCI provides a more detailed thermos physiological response and demonstrates higher sensitivity to variations in wind speed and humidity. Despite these differences, both indices confirm the same core thermal behavior: Street orientation is the primary determinant of heat stress. Canyon geometry (H/W) has a strong but nonlinear influence—beneficial at moderate ratios, harmful at extremes. Façade materials exert a secondary but detectable effect, especially when combined with unfavorable orientations or shallow geometries. Street centers consistently experience the worst thermal conditions. Weddad Street provides the most thermally diverse and occasionally favorable zones. Ibn Rushed Street suffers from intense heat buildup and limited ventilation. These findings emphasize that material selection alone cannot improve outdoor comfort unless paired with optimized canyon geometry and shading conditions.

4.5.4 Effect of H/W and Façade Materials on PET and UTCI (summer)

This section examines the combined influence of urban canyon geometry (H/W ratio) and façade material properties on outdoor thermal comfort indices (PET and UTCI) during summer conditions. The analysis focuses on peak thermal stress periods (12:00–14:00), when differences between scenarios are most pronounced, and considers the interaction between geometry, orientation, and material performance rather than isolating each parameter independently.

a) Effect of H/W on PET and UTCI

Across all studied streets, variations in the H/W ratio produced clearer and more consistent effects on PET and UTCI than changes in façade material alone. In general, moderate to high H/W ratios (~H/W=1.5-2.0) contributed to lower PET and UTCI values during peak hours by enhancing self-shading and reducing mean radiant temperature. Wide canyons (H/W ≈ 0–0.8) and very confined configurations (H/W ≈ 0.6–1.1) allow direct solar penetration during peak hours, leading to high PET and UTCI despite good ventilation. However, this effect was

strongly orientation-dependent. In west-facing and southwest-facing configurations, increasing H/W often intensified heat stress due to reduced ventilation and enhanced radiative trapping, whereas in east-facing configurations, higher H/W ratios tended to improve thermal conditions by limiting direct solar exposure during morning and midday hours. These findings indicate that H/W should not be interpreted as a universal mitigation parameter; instead, its effectiveness depends on its interaction with solar path and airflow patterns. Consequently, similar H/W ratios may yield opposite thermal responses under different orientations.

Table 4-7 M1,M2,M3,M7 PET and UTCI results for right side in weddad street in summer

	Case	H/W	Façade orientation	PET 2pm	UTCI 2pm
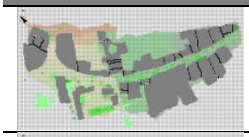	M1a-SW-C15	3.8	SW	37.07	33.58
	M1b-SW-C3	0.8	SW	47	39.85
	M1c-SW-C13	2.1	SW	44.71	37.5
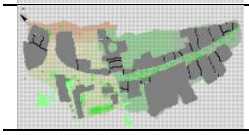	M2a-W-C3	0.8	W	46.9	40.54
	M2b-W-C3	0.8	W	46.1	39.61
	M2c-SW-C15	3.8	SW	37.08	33.76
	M2d-SW-C0	0	SW	42.4	37.54
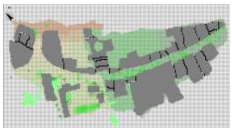	M3e-W-C3	0.6	W	52.5	40.8
	M3f-W-C6	1.1	W	46	39.66
	M3g-W-C0	0	W	45.14	39.28
	M3h-SW-C5	0.9	SW	35.74	33.14
	M3i-SW-C11	1.8	SW	40.97	36.11
	M3j-SW-C2	0.4	SW	46.77	39.38
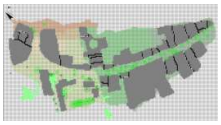	M7a-SW-C14	3.0	SW	40.8	39.72
	M7b-SW-C15	3.8	SW	35.85	32.91

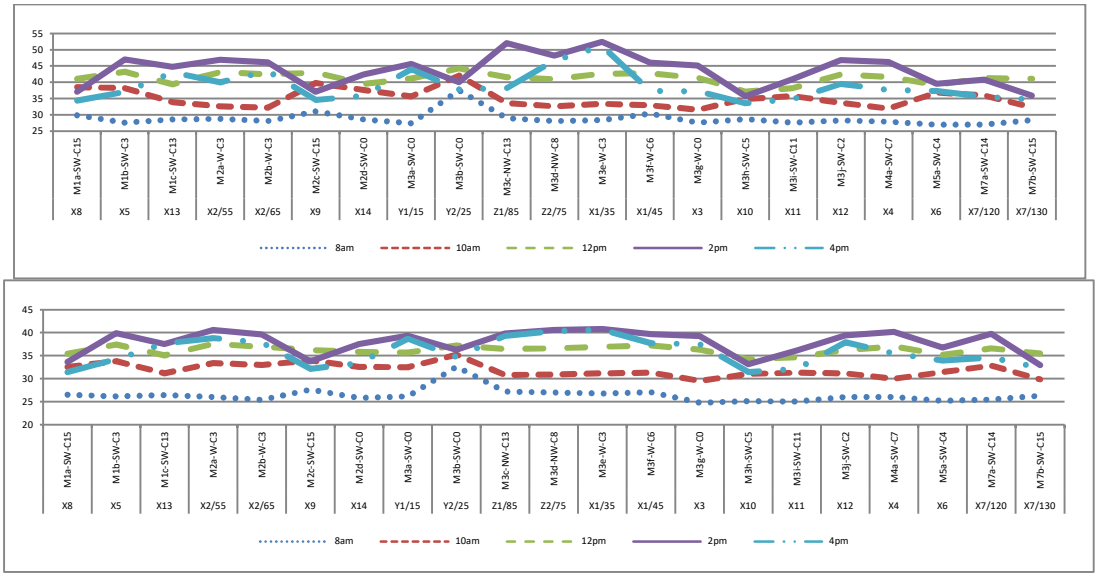

Figure 4-7 a)PET b) UTCI in Weddad (summer)

b) Effect of material on PET and UTCI

When comparing scenarios with similar H/W ratios and orientations, façade material properties—particularly thermal transmittance (U-value)—exerted a secondary but measurable influence on PET and UTCI. Materials with lower U-values generally exhibited more stable thermal performance, resulting in reduced sensitivity to geometric changes. In contrast, materials with higher U-values showed greater fluctuations in PET and UTCI under the same urban configuration, especially during peak hours. Nevertheless, the descriptive analysis revealed that the effect of material alone was often masked by concurrent variations in H/W, orientation, and street openness. This limitation explains why material-induced differences were not consistently apparent in the microclimatic analysis (Ta, RH, Ws) and why a purely descriptive comparison was insufficient to isolate the material effect. To overcome the limitations of descriptive analysis and the non-uniform distribution of scenarios across streets, statistical methods were employed to quantify the individual and combined effects of façade material, H/W ratio, and orientation on PET and UTCI.

High-conductivity materials (e.g., M3) amplify PET under shallow or west-facing configurations. Materials with moderate to low U-values (e.g., M7) exhibit greater stability, showing smaller PET and UTCI fluctuations when H/W or orientation changes. In some cases, increased H/W reduces PET by up to 5–10°C for materials with poor insulation—highlighting the strong interaction between geometry and wall inertia. After examining the extreme thermal conditions observed during the summer season, the analysis shifts to winter in order to assess how the same urban configurations perform under milder climatic conditions. This seasonal contrast helps to clarify whether the identified patterns persist or reverse under reduced solar intensity.

4.6 Microclimatic analysis (Ta, Rh, Ws) and thermal comfort analysis (PET, UTCI) in winter

Winter microclimatic conditions on December 21 show a generally stable and homogeneous pattern across street sides compared to summer. Air temperature increased gradually from morning toward early afternoon, while relative humidity decreased inversely, and wind speed remained low-to-moderate with slightly higher values in the street center. The spatial contrasts between right/left/center were smaller than in summer, indicating reduced radiative forcing and a more uniform pedestrian-level environment. Detailed statistics (means and standard deviations for Ta, RH, and Ws across all points and street sides) are reported in Appendix D-3 to avoid repetition.

4.6.1 Temperature, wind speed, relative humidity in winter

Ta: Across the winter day, Ta follows a typical diurnal increase from morning toward early afternoon, followed by a decline toward 4:00 PM. Compared to summer, peak air temperatures are lower and the thermal contrasts between sections are generally less pronounced. However, orientation-driven asymmetry remains visible, particularly in Ibn Rushed Street, where the east–west façades receive solar exposure in alternating halves of the day. This leads to a stronger side-to-side temperature contrast during transitional hours (10:00 AM and 2:00 PM), when one façade becomes sunlit while the opposite façade remains shaded. In contrast, Weddad Street demonstrates a relatively smoother distribution of Ta between the right, left, and middle zones, consistent with its oblique NW–SE alignment, which tends to distribute solar access more gradually across the canyon.

Ws: Winter wind speed patterns remain primarily controlled by street openness and local exposure rather than thermal buoyancy. In general, the street center maintains higher Ws than façade-adjacent points. Differences between Weddad and Ibn Rushed are mainly attributed to the degree of alignment with prevailing wind directions and to the presence of junctions and open nodes that locally accelerate the flow. As in summer, entrances and intersection-adjacent sections tend to exhibit higher Ws than enclosed core segments; however, the thermal significance of ventilation is generally lower in winter due to reduced heat load, although it remains important for explaining localized PET/UTCI variations.

RH: Relative humidity shows an inverse trend relative to temperature: higher values occur during the cooler morning and late afternoon periods, while RH decreases during midday when air temperature increases. Spatial RH differences across street sides are generally modest, yet they still reflect shading and ventilation interactions: shaded and less ventilated zones tend to retain higher RH, whereas sunlit or more ventilated zones exhibit comparatively lower RH due to enhanced drying.

While summer results showed clear thermal variations between different urban materials and valleys, winter is characterized by lower solar convection, which reduces the intensity of the differences. However, the results were analyzed for the same variables for seasonal comparison.

4.6.2 PET and UTCI result in winter

a) General winter PET and UTCI patterns

The winter PET and UTCI results demonstrate that both streets shift toward lower heat-stress categories relative to summer, with most time periods remaining within comfort to slightly warm conditions. The indices increase from morning to midday/early afternoon and then decline toward 4:00 PM, reflecting the daily radiation cycle. In general, Weddad Street exhibits greater spatial consistency between sides, while Ibn Rushed Street shows stronger side-to-side contrasts during transitional hours due to its east–west façade exposure pattern. Full PET/UTCI numerical outputs are provided in Appendix D-4

b) Right–Middle–Left distribution

Weddad Street presents a moderate and stable winter thermal profile. In the morning (8:00 AM), PET and UTCI remain within a comfortable/slightly cool band, indicating minimal thermal stress. As solar radiation increases toward 10:00 AM and noon, both indices rise gradually, but the three sides remain relatively close, On Weddad Street, the differences between the sides are limited; the right (southwest) side is slightly warmer due to solar exposure, while the values in the middle and left remain similar and relatively cooler thanks to partial shading and air movement, reflecting balanced shade distribution in the NW–SE-oriented canyon. Peak values occur around midday to 2:00 PM, after which the indices decline toward the afternoon (4:00 PM) and return to the comfort range. This behavior indicates that Weddad's geometry and orientation support winter thermal moderation without producing sharp local overheating.

In contrast, Ibn Rushed Street showed stronger spatial variability in winter thermal comfort indices. PET and UTCI values fluctuated more noticeably between the east- and west-facing facades, particularly during the late morning and early afternoon. On Ibn Rushed Street, the contrast between the sides is more pronounced; the left (eastern) side is hotter in the morning, and the sides converge at noon with the left remaining hotter, while the right (western) side becomes hotter in the afternoon as the eastern side's temperature decreases due to the shade. This behavior reflects the street's north–south orientation, which exposes opposite facades to direct solar radiation at different times of the day. Although winter conditions generally reduced heat stress, some locations on Ibn Rushed Street still experienced locally elevated PET and UTCI values during peak radiation periods.

c) Effect of H/W on PET and UTCI –winter

The winter influence of the height-to-width ratio (H/W) can be summarized as a radiation-access tradeoff. In several configurations, lower H/W (more open sections) allows greater solar penetration and increases PET/UTCI during peak hours, improving perceived warmth. Conversely, higher H/W (deeper canyons) increases shading and tends to reduce PET/UTCI, which may enhance comfort if overheating occurs but may also reduce beneficial winter warming. The effect of the H/W ratio on the PET index in winter shows a clear difference between the two streets. On Weddad Street, high ratios lead to a decrease in PET due to shading, while open sections (H/W ≈ 0–0.8) register the highest values due to solar exposure, and deep grooves (H/W ≥ 2) remain within a relatively comfortable range. On Ibn Rushed Street, however, the relationship is more complex. Medium ratios (H/W ≈ 1.0–1.1) may register the highest PET, especially on western facades, while open or deep sections sometimes allow for a decrease in values depending on the orientation, making radiation retention a crucial factor on some facades. However, the relationship is not strictly linear, as local openings, junction effects, and façade material behavior can amplify or dampen the geometric effect. Therefore, winter comfort in Hebron's urban canyons is best interpreted through the combined interaction of orientation, H/W, and local openness, with detailed examples documented in Appendix D-4.

Overall, winter results demonstrate that thermal comfort in Hebron's urban streets is governed by a balance between solar access and shading. While deep canyons are advantageous in summer, moderate canyon proportions appear more suitable in winter to avoid excessive shading and to maintain comfortable pedestrian conditions. The separate analysis of summer and winter conditions highlights notable differences in thermal behavior. To better understand these variations, a direct seasonal comparison is conducted in the following section, focusing on the combined effects of orientation, canyon geometry, and façade materials on PET and UTCI.

4.6.3 Seasonal Comparison: Summer vs. winter

Seasonal comparison confirms that the performance of urban geometry and façade configurations in Hebron is not constant across the year. Summer conditions are dominated by high solar gains and stronger heat stress, leading to elevated PET and UTCI values and larger side-to-side differences. Winter conditions show reduced forcing and generally lower indices,

with more spatial homogeneity, although orientation-driven asymmetry still appears in streets with east–west façade exposure.

In Weddad Street, in the summer, PET values ranged between approximately 27 and 52°C, registering high heat stress, while in the winter, readings dropped to a moderate range between 14 and 40°C. The PET index on Ibn Rushed Street recorded high values (27–50 °C) in the summer, especially in the westward direction, while in the winter it decreased to (16–40 °C) with a comfortable average (20–26 °C), with the eastward direction remaining more moderate. The UTCI temperature index results showed clear seasonal variations on Weddad and Ibn Rushed streets. High values were recorded in summer (Weddad: 25–41°C, Ibn Rushed: 26–41°C), reflecting high heat stress, especially on the southwest/west side. Values decreased in winter to a more moderate range (Weddad: 12–31°C, Ibn Rushed: 11–30°C), with shaded areas, particularly the northeast, remaining more comfortable.

Across both streets, PET and UTCI exhibit a strong reduction from summer to winter, particularly during peak hours (12:00–2:00 PM). This demonstrates the decisive influence of seasonal solar altitude and radiation intensity on pedestrian thermal sensation. Although winter values are lower, the orientation effect remains visible. Weddad Street maintains relatively balanced conditions between sides in both seasons, whereas Ibn Rushed Street continues to show side-to-side contrasts due to the alternating exposure of east and west façades across the day. Thus, orientation is a robust determinant of spatial thermal variability year-round.

In summer, higher H/W commonly improves comfort through increased shading and reduced radiant load, while in winter; the same shading can reduce beneficial solar access and lower PET/UTCI, particularly in deep canyons. Across both streets: Moderate H/W ratios (approximately 1.0–1.5 on Weddad and 0.8–1.0 on Ibn Rushed) provide the best compromise between summer shading and winter solar access. Very shallow or very deep configurations tend to be seasonally biased: either optimized for summer at the expense of winter comfort, or vice versa. This seasonal tradeoff indicates that “optimal” canyon geometry in Hebron should aim for balanced ratios rather than extreme openness or extreme depth, and design recommendations must consider year-round comfort rather than summer-only optimization.

This seasonal evidence supports the design implication that comfort-oriented urban strategies in Hebron should combine: (i) orientation-aware shading control, (ii) moderate canyon proportions, and (iii) façade material selection that reduces summer heat burden without

eliminating winter solar benefits. These implications are discussed in detail in the subsequent discussion and recommendations chapters.

Table 4-8 Seasonal comparison between Weddad Street and Ibn Rushed Street for the PET index in summer and winter

season	Weddad street(NW-SE)	Ibn rushed street(NS)	Results
Summer	PET ≈ 41–44 °C	PET ≈ 43–47 °C	Weddad is more comfortable in the summer (less hot)
Winter	PET ≈ 24–28 °C	PET ≈ 30–34 °C	Ibn Rushed is warmer in winter (less cold)

4.6.4 Seasonal Role of Façade Materials

Seasonal analysis confirms that: Material properties alone do not radically change local air temperature, humidity, or wind, but they do modulate PET and UTCI, especially under extreme orientations and at critical H/W values. High-U materials (like M3) are more sensitive to canyon geometry and orientation, amplifying both summer and winter extremes (e.g., very hot west façades, warm winter afternoons). Better-insulated materials (e.g., M7, M9) provide more stable thermal responses across seasons, especially when combined with moderate canyon depths. Therefore, optimal façade design must be considered jointly with orientation and H/W. Material improvements without geometric optimization will have a limited impact on outdoor comfort.

In addition to thermal characteristics such as U-value and thermal mass, façade surfaces also possess optical properties that influence the urban radiation balance. One of these properties is albedo. Materials with higher albedo reflect a larger fraction of incoming solar radiation, which may influence the radiation conditions within the street canyon and consequently affect outdoor thermal comfort. Although albedo was not analyzed as an independent variable in this study, its influence is implicitly accounted for by the selected façade materials and their surface characteristics.

4.7 Inferential statistical results

Descriptive analysis provided an initial understanding of the influence of façade materials, street orientation, and canyon geometry (H/W) on microclimatic variables and outdoor thermal comfort indices. To examine whether these observed differences were statistically significant, inferential statistical methods were applied, including one-way ANOVA with Tukey's HSD post-hoc tests, Pearson correlation analysis, and multiple linear regression (MLR).

The inferential analysis focused primarily on the summer period, where thermal stress variations were more pronounced, while winter results were interpreted mainly through descriptive analysis with limited regression verification. Detailed statistical outputs are presented in Appendix D - , and this section summarizes the key significant findings.

4.7.1 ANOVA / Tukey (HSD)-summer

ANOVA and Tukey HSD were applied to eight experimental groups (Cases 1–8) designed with the same orientation and H/W ratio but differing in wall materials and internal layer compositions. ENVI-met outputs were collected for three summer days (23, 24, and 27 June) plus the five-time steps from 22 June. For each case, microclimatic variables (Ta, Ws, Rh) and thermal indices (PET, UTCI) were extracted at five hours (8:00, 10:00, 12:00, 14:00, and 16:00), resulting in repeated measurements per material under quasi-identical boundary conditions.

ANOVA was performed for each hour separately and for each variable. When the p-value is greater than 0.05, Tukey HSD was used to identify which pairs of wall systems differed significantly. In cases with only two materials (e.g., Cases 5 and 8), ANOVA is mathematically equivalent to an independent-samples t-test, and Tukey is not required.

In general, the results of Anova test for air temperature (Ta), p-values were > 0.05 at all hours in all groups. Temperature differences between materials were not statistically significant when orientation and H/W were held constant. Consequently, post-hoc tests for Ta were not applicable. For relative humidity (RH), most ANOVA results were non-significant, with some exceptions (notably in Cases 4 and 6 at specific afternoon hours), where changes in wall composition led to small but statistically significant differences in humidity. For wind speed (Ws), UTCI, and especially PET, significant differences emerged between materials in several cases, confirming that wall systems can affect the dynamic microclimate and thermal comfort even when Ta differences are small.

Tukey's HSD indicated that configurations located near intersections, open squares, or wider segments (low H/W) recorded significantly higher Ws compared to deeper or more enclosed locations, even when the nominal H/W was similar. Tukey's HSD for PET and UTCI consistently showed that walls with higher thermal mass and more balanced compositions (e.g., walls similar to M7, M8, M9, or thicker concrete cores such as M2d, M6a, M9b) achieved significantly lower PET values (≈ 2–4°C reduction) compared with more conductive or lighter configurations (e.g., M2c, M3a–M3f, M1 with less favorable layer distribution).

Below is a concise synthesis of the eight cases (see Table 4-9 and Table D6-1 for full numerical details):

Case1- SW orientation, same H/W, materials M1a, M2c, M7b

ANOVA showed no significant differences in Ta between materials (all p-values > 0.05), but wind speed differed significantly at 8:00, 10:00, and 16:00. Tukey HSD indicated that M7b generally produced higher wind speeds and more favorable ventilation compared to M1a and M2c.For UTCI and PET, significant differences were found at 8:00 and 10:00. M7b consistently recorded the lowest PET and UTCI values in the morning, while M2c was the worst performer. This indicates that M7b (10 cm stone + 15 cm concrete, moderate thermal mass) is thermally more balanced for SW streets in the early hours, reducing heat stress without excessive heat storage. The M7b interface has moderate thermal inertia—it doesn't store heat as well as the thicker M1, and doesn't heat up as quickly as the thinner M2.

Case2- SW orientation, same H/W, materials M2d, M3a, M3b

Ta and RH showed no significant differences, but wind speed differed significantly at 12:00, 14:00, and 16:00. Based on the Tukey test, it was found that there is a statistically significant difference between M3a and M2d, as well as between M3a and M3b. Tukey showed that M3a often coincided with higher wind speeds (and less favorable comfort) during hot periods. For UTCI and PET, ANOVA revealed significant differences at several hours, especially in the morning and early afternoon. Tukey indicated that M2d-SW-C0 systematically recorded lower PET and UTCI values (≈ 3.5–4°C less PET) than M3a and M3b. The better performance of M2d is explained by its higher thermal inertia (greater concrete thickness and lower U-value) under SW exposure.

Case 3- W orientation, same H/W, high-mass vs. lighter walls (e.g. M8a-W-C3)

Wind speed showed significant differences at all hours. ANOVA for UTCI and PET was significant at almost all times except around noon for PET. Tukey HSD indicated that M8a-W-C3 (20 cm stone + 20 cm concrete) achieved the lowest PET values among the materials. This advantage is attributed to the high thermal inertia resulting from the large mass of the wall, which reduced the surface temperature during peak periods and helped improve thermal comfort on the western facades.

Case 4- W orientation, same outer material, different inner thickness (M3 vs. M6)

Wind speed and RH showed significant differences at several hours, especially in the afternoon. For UTCI, a significant difference was found at 16:00, where M3f recorded UTCI values approximately 9–10°C higher than M6a and M3d. For PET, ANOVA was significant at all hours except 12:00, with the largest differences at 14:00. Tukey confirmed that M6a recorded lower PET values and better performance than M3 variants. Although external stone thickness was constant (5 cm), increasing concrete thickness in M6 improved thermal inertia and reduced thermal stress on west-oriented façades. This superior performance can be attributed to its lower U-value, which limits heat transfer and heat storage. While the reflective façade may increase solar reflection, its overall effect is outweighed by the reduction in heat gain, resulting in improved thermal comfort conditions.

Case5- Open W orientation, M7a vs. M3g

Wind speed differed significantly only at 8:00. For UTCI, differences were significant at most hours from 8:00 to 16:00. There are only two groups, so no additional Tukey test is necessary. While PET differences were not statistically significant, At 2 p.m., the difference approaches the significance threshold ($p \approx 0.08$). Although not always significant for PET, M7a-W-C0 tended to record slightly lower PET than M3g during peak hours, confirming the relative advantage of intermediate mass over lighter, more conductive walls in open western streets.

Case 6- E orientation, multiple materials including M3c and M9b

Wind speed differences were significant at 12:00, 14:00, and 16:00, with M3c showing significant contrasts with other materials. RH also differed significantly at 10:00 and 12:00 for some material pairs; A Tukey HSD test result for hour 10 showed that no pair exceeded the 0.05 threshold. However, for hour 12, several pairs appeared. For UTCI, only 16:00 showed a statistically significant ANOVA, and Tukey did not detect strongly significant pairwise differences despite notable numerical gaps (up to ~5°C) between M9b-E-C3 and less insulating materials. For PET, ANOVA showed statistically significant differences at all hours except 10:00. Tukey HSD indicated that M9b-E-C3 (20 cm stone + 20 cm concrete) consistently recorded the lowest PET values, especially during the afternoon, confirming the high thermal inertia and stable surface temperature on the eastern facades.

Case 7- NE orientation, four locations/materials (including M1 and M6d)

ANOVA results showed significant differences in wind speed at all hours, with the strongest contrasts at 16:00. UTCI and PET also exhibited statistically significant differences at all hours,

particularly in the morning (8:00–10:00) and around peak radiation (12:00–14:00 for PET).Tukey HSD showed a clear contrast between M1 (25 cm stone + 20 cm concrete) and M6d (5 cm stone + 20 cm concrete). Surprisingly, M6d provided better outdoor PET and UTCI values than the thicker M1 and high thermal inertia. This suggests that in the external environment, very thick stone can store excessive heat and re-radiate it towards pedestrians, while a thinner stone layer with sufficient concrete behind it can maintain lower external surface temperatures.

Case 8- NE orientation, two materials M3f vs. M6e

ANOVA results for wind speed at 10:00 and 12:00 and for PET/UTCI from 8:00 to 12:00 showed statistically significant differences between the two façades. During the afternoon (14:00 and 16:00), differences diminished and became non-significant.

Overall, M6e-NE-C5 was thermally superior, with lower PET values and more stable behavior due to increased concrete thickness and higher thermal inertia, while M3f responded more rapidly to solar radiation and reached higher surface temperatures.

Overall conclusion from ANOVA–Tukey:

Under constant orientation and canyon ratio (H/W), wall material and composition significantly affect PET and UTCI, even when Ta and RH remain statistically similar. High-mass or well-insulated configurations (M2d, M7b, M8a, M6, M9b, M6d, M6e) consistently outperform lighter or more conductive walls (M2c, M3 variants, M1) in terms of thermal comfort. The effect of material is strongest in southwest and northeast orientations during critical hours (morning for NE, afternoon for SW), where direct solar exposure is highest.

Table 4-9 P-value for one way ANOVA-test

		P-value							
parameter	time	Case1	Case 2	Case 3	Case 4	Case 5	Case 6	Case 7	Case 8
Ta	8 am	0.481	0.178	0.69	0.91	0.31	0.98	0.3	0.8
	10 am	0.63	0.424	0.901	0.21	0.95	0.98	0.54	0.58
	12 pm	0.89	0.588	0.88	0.37	0.67	0.986	0.6	0.71
	2 pm	0.95	0.799	0.46	0.18	0.33	0.84	0.67	0.49
	4 pm	0.99	0.885	0.59	0.2	0.38	0.78	0.91	0.91
Wind speed	8 am	0.0009	0.48	0.0019	0.02	0.027	0.0509	2.45E-05	0.79
	10 am	0.028	0.073	0.0168	0.007	0.19	0.21	0.03	0.003
	12 pm	0.05046	0.00087	0.0021	0.001	0.28	0.015	0.0029	0.035
	2 pm	0.107	0.00099	1.89E-06	3.09E-05	0.098	5.81E-06	0.0003	0.12
	4 pm	0.00097	0.00041	2.02E-10	1.19E-07	0.52	3.27E-09	1E-10	0.88
Rh	8 am	0.86	0.57	0.82	0.82	0.44	0.86	0.99	0.97
	10 am	0.65	0.16	0.41	0.26	0.4	0.043	0.9	0.59

		P-value							
parameter	time	Case1	Case 2	Case 3	Case 4	Case 5	Case 6	Case 7	Case 8
	12 pm	0.72	0.32	0.41	0.37	0.39	0.0102	0.34	0.59
	2 pm	0.97	0.88	0.07	0.01	0.109	0.65	0.26	0.2
	4 pm	0.99	0.95	0.122	0.011	0.106	0.191	0.91	0.77
	8 am	1.7E-07	4.15E-06	3.71E-08	0.01	0.32	0.01	5.04E-08	0.12
	10 am	3.46E-07	0.00015	3.69E-07	0.003	0.65	0.14	0.0026	0.0004
PET	12 pm	0.055	0.0061	0.128	0.065	0.94	0.001	8.81E-06	0.004
	2 pm	0.2	0.002	0.011	0.00048	0.076	0.00011	4.94E-06	0.08
	4 pm	0.705	0.0004	0.0052	0.02	0.62	0.00015	0.00082	0.076
	8 am	0.00022	7.71E-07	7.99E-05	0.86	0.00096	0.064	8.69E-08	0.0002
	10 am	1.35E-06	0.0093	0.000818	0.14	0.017	0.76	1.21E-05	0.01
UTCI	12 pm	0.52	0.337	0.19	0.2	0.55	0.63	0.0072	0.0356
	2 pm	0.64	0.12	0.03	0.059	0.25	0.08	0.0054	0.24
	4 pm	0.55	0.0145	0.017	0.0028	0.23	0.03	0.0056	0.28

P-value < 0.05 (Green), P-value> 0.05 (gray)

4.7.2 Correlation U-value, H/W vs. Ta, Rh, Ws, PET, UTCI -summer

Pearson correlation analysis was used to quantify the relationships between U-value (thermal transmittance), H/W, and both microclimatic variables (Ta, Ws, RH) and thermal comfort indices (PET, UTCI) for four façade orientations (E, W, SW, NE) and five hours (8:00, 10:00, 12:00, 14:00, 16:00). The main findings (see Table 4-10) can be summarized as follows:

Ta: In the NE orientation, a strong negative correlation was found between U-value and Ta at 8:00 ($r \approx -0.73$), indicating that, within the tested configurations, changes in U-value were systematically associated with changes in early-morning air temperature near the façade. In the SW orientation, H/W showed a moderately strong negative correlation with Ta around 14:00 ($r \approx -0.63$), confirming that deeper canyons in SW help reduce afternoon air temperature at the pedestrian level.

Rh: In the W orientation, Rh showed a significant positive correlation with H/W between 10:00 and 14:00 ($r \approx 0.56–0.63$), suggesting that narrower, deeper canyons retain more moisture (higher Rh), consistent with reduced ventilation and higher shading. In the NE orientation, correlations between Rh and U-value were positive but not always statistically significant.

Ws: In the NE orientation, U-value exhibited a strong and significant negative correlation with Ws throughout most of the day (r=-0.72 to −0.78), indicating that, in this specific urban configuration, façade thermal properties interacted with local airflow patterns. Correlations between H/W and Ws in other orientations were weaker or not statistically significant, reflecting the dominant role of large-scale wind direction and local openings/intersections.

PET and UTCI: For PET, both U-value in the SW orientation and H/W in the NE orientation showed significant negative correlations at 14:00 (e.g., $r \approx -0.77$ for U-value in SW and $r \approx$

−0.57 for H/W in NE), indicating that façade properties and canyon depth both contribute to reducing heat load during critical afternoon hours. For UTCI, a strong negative correlation was observed between U-value and UTCI in the NE orientation at 14:00 ($r \approx -0.82$), while H/W in SW and W orientations also showed significant negative correlations with UTCI at selected hours, confirming that urban geometry and material properties jointly shape perceived thermal stress.

Overall, the correlation analysis supports the hypothesis that material thermal properties (U-value) and canyon ratio (H/W) have orientation- and time-dependent effects on microclimate and thermal comfort. Their influence is strongest during critical solar exposure periods.

Table 4-10 Correlation matrix between U-value,H/W and microclimte conditions and thermal comfort

SUMMER Correlation/Note: * represent p-value <0.05									
orientation Independent	time	E		W		SW		NE	
		u-value	H/W	u-value	H/W	u-value	H/W	u-value	H/W
temp	8	-0.093	-0.467	0.14	0.311	0.026	-0.513	-0.73*	-0.084
	10	0.315	-0.028	-0.082	0.074	-0.236	-0.457	-0.61*	0.084
	12	-0.031	-0.158	0.018	0.461	-0.42	-0.363	-0.50*	0.099
	2	-0.13	-0.39	0.168	0.049	-0.35	-0.63*	-0.61*	0.034
	4	-0.145	-0.399	-0.065	-0.071	-0.323	-0.466	-0.62*	-0.01
wind	8	-0.63*	-0.499	-0.176	-0.305	-0.032	-0.334	-0.72*	-0.035
	10	-0.385	-0.198	-0.378	-0.303	-0.036	-0.226	-0.77*	-0.113
	12	-0.127	-0.1	-0.33	-0.164	-0.111	-0.196	-0.76*	-0.14
	2	0.131	0	-0.162	-0.021	-0.199	-0.267	-0.77*	-0.165
	4	0.178	-0.028	-0.153	-0.005	-0.285	-0.166	-0.77*	-0.156
humid	8	0.173	0.046	-0.004	-0.210	-0.086	0.174	-0.357	-0.059
	10	-0.14	-0.024	-0.202	-0.379	-0.215	0.557*	0.271	-0.045
	12	0.042	0.067	-0.242	-0.450	-0.089	0.627*	0.693	0.06
	2	0.121	0.347	-0.158	-0.028	0.092	0.621*	0.626	0.017
	4	0.17	0.408	-0.018	0.1627	0.176	0.43	0.63	0.028
PET	8	0.088	-0.373	-0.425	0.082	0.13	-0.077	0.372	0.39
	10	-0.032	0.103	-0.368	0.035	0.272	-0.091	0.1	0.41
	12	0.064	-0.341	-0.079	0.161	-0.18	0.008	-0.301	-0.207
	2	-0.499	-0.442	0.122	0.147	-0.337	-0.57*	-0.77*	-0.235
	4	-0.469	-0.425	-0.078	-0.248	-0.018	-0.452	-0.49*	-0.14
UTCI	8	0.35	-0.25	-0.208	-0.297	0.082	-0.129	0.327	0.339
	10	0.49	0.12	-0.53*	-0.28	0.224	-0.146	-0.405	0.176
	12	-0.12	-0.25	0.217	0.471	-0.38	-0.176	-0.55*	-0.164
	2	-0.48	-0.64*	0.308	0.142	-0.284	-0.54*	-0.82*	-0.173
	4	-0.41	-0.56*	-0.017	-0.50*	-0.045	-0.49*	-0.48*	-0.11

4.7.3 Multiple linear regressions (summer and winter)

Multiple linear regression (MLR) was used to model the combined effect of U-value and H/W on each dependent variable (Ta, Ws, RH, PET, UTCI), separately for each orientation (E, W, SW, NE) and each time step (8:00, 10:00, 12:00, 14:00, 16:00) as shown in Table 4-11. The objective was to quantify how much variance in microclimate and thermal indices can be

explained by these two key design variables and how this varies with orientation and time of day.

- MLR in summer:

Ta: In W and E orientations, most models were not statistically significant ($p > 0.05$), with adjusted R^2 generally below 0.10, this confirms that temperature variability in these orientations is dominated by background climate and solar trajectory rather than by U-value and H/W alone. U-value and H/W did not explain temperature variance consistently, except for a few borderline cases (e.g. canyon approaching significance at 12:00 in W, the period when the western facade begins to receive direct solar radiation, which may explain its relative sensitivity to street configuration at this time. and 8:00 in E, Due to exposure to sunlight in the morning).

In the SW orientation, the model became statistically significant at 14:00 ($p \approx 0.006$, adjusted $R^2 \approx 0.53$ At this hour, both U-value and H/W had significant negative coefficients, indicating that higher canyon ratios and better thermal performance of walls jointly lowered the outdoor temperature during peak radiation and explained more than half of the afternoon temperature variance on south-facing façades. The regression equation at 14:00 indicates that a one-unit increase in U-value reduces Ta by about 0.28°C, and a one-unit increase in H/W reduces Ta by about 0.22°C (as parameterized in the Table D6-2).

In the NE orientation, the model was significant at several hours (especially 8:00 and 10:00, adjusted R^2 up to 0.48 as shown in Table D6-2), with U-value showing a consistently significant negative effect, while H/W remained weak and non-significant. However, its coefficients were positive, suggesting a potential (but uncertain) relationship between increased building height and decreased radiative cooling in the morning. This confirms that NE façades are primarily sensitive to material properties during morning hours. In the Table D6-2, the canyon coefficients were replaced, but their effect remains weak. In order to confirm, a simple regression analysis was performed between the u-value and the temperature in the northeast direction. The results were shown in the Table D7-1, and the results were close.

Ws: In E, W, SW orientations, MLR models for wind speed were generally weak and non-significant, indicating that U-value and H/W alone cannot explain the complex wind behavior in these orientations, emphasizing that wind is primarily controlled by larger-scale flow and openings.

In the NE orientation, however, the model was statistically significant at all hours ($p < 0.005$), with U-value showing a strong, significant negative effect and H/W remaining insignificant. This suggests that, in NE layouts of this specific urban configuration, variations in wall systems co-vary with local flow patterns, whereas canyon geometry alone does not.

Rh: In E and W orientations, MLR models for RH were not significant at any hour ($p > 0.05$), and neither U-value nor H/W explained humidity variation. This points to the dominance of larger-scale climatic controls over local geometry and material properties for RH in these orientations.

In the SW orientation, the full model was not significant at 8:00 or 10:00, but became near-significant around midday. Canyon (H/W) became a significant predictor at 12:00 and 14:00 ($p \approx 0.02$), with adjusted R^2 values around 0.28–0.31. A simple regression using H/W only (Table D7-3) confirmed that H/W alone explains a substantial portion of RH variation between 10:00 and 14:00, with weaker effects at 8:00 and 16:00.

In the NE orientation, U-value became a significant predictor for RH during the hottest hours (12:00–16:00), with R^2 values up to ~0.47 when using simple linear regression between U-value and RH. H/W remained non-significant. Therefore, the simple linear regression in the Table D7-3 shows that the model is statistically significant from 12 to 4 pm.

PET and UTCI:

For E and W orientations, MLR models for PET were non-significant at all hours. U-value and H/W did not explain PET variation in these orientations, suggesting that other factors (wind patterns, detailed shading from irregular geometries) dominate. In the SW orientation, the PET model was significant only at 14:00 (adjusted $R^2 \approx 0.41$). Canyon was statistically significant ($p \approx 0.012$), while U-value was close to significance ($p \approx 0.07$). Simple regression analysis confirmed that H/W is the main driver of PET reduction at 14:00 in SW façades. The linear regression equation for the SW orientation, increasing the u-value and H/W ratio, reduces PET by 2.34°C and 1.77°C, respectively, indicating that higher u-values and greater urban openness enhance outdoor cooling at this time. In the NE orientation, the PET model was statistically significant at 14:00 ($p < 0.01$, adjusted $R^2 \approx 0.54$), with U-value as the only significant predictor, while canyon remained non-significant. This again highlights the role of material properties for NE façades. Since canyon is the only independent variable that affects PET, a simple linear regression analysis was performed as shown in Table D7-4.

In the E orientation, the UTCI model was significant only at 14:00 (adjusted $R^2 \approx 0.31$). Canyon had a statistically significant negative effect, while U-value was not significant. Simple regression confirmed that H/W is the dominant predictor of UTCI at this time. The multiple linear regression equation shows that each one-unit increase in u-value causes a decrease in UTCI of 2.33°C and each one-unit increase in canyon leads to a decrease in UTCI of 3.6°C, a statistically significant effect ($p = 0.046$). In the W orientation, the full model was not significant at most hours; however, U-value alone became significant at 10:00 and canyon alone at 16:00 (as shown by simple regressions in Appendix D), indicating that the relative importance of material vs. geometry shifts during the day. In the southwest (SW) orientation, the regression model was statistically significant only at 2 PM ($p < 0.05$, adjusted $R^2 = 0.31$). At this time, the canyon ratio was significant, while the u-value remained insignificant, confirming that canyon geometry plays the primary role in influencing UTCI. Simple regression analysis further highlighted the dominance of the canyon effect at this hour. In the NE orientation, the UTCI model was strongly significant at 14:00 (adjusted $R^2 \approx 0.61$, $p < 0.001$), with U-value as the main predictor. This confirms that NE façades are particularly sensitive to wall thermal performance in terms of perceived thermal stress.

Table 4-11 MLR P-VALUE results for independent variables (u-value, H/W) in summer

SUMMER p-value (P-value <0.05 green, P-value >0.05 pink)									
orientation	time	E		W		SW		NE	
Independent		u-value	H/W	u-value	H/W	u-value	H/W	u-value	H/W
temp	8	0.73	0.105	0.73	0.26	0.86	0.07	0.001	0.59
	10	0.23	0.57	0.72	0.74	0.25	0.08	0.0052	0.239
	12	0.9	0.6	0.79	0.069	0.07	0.1	0.028	0.318
	2	0.94	0.21	0.54	0.94	0.04	0.004	0.008	0.366
	4	0.97	0.205	0.84	0.82	0.13	0.053	0.008	0.484
The u-value and the H/W affect the temperature when the facade orientation is SW at 2 pm, But The u-value affect the temperature from 8 to 4pm in the NE orientation									
wind	8	0.053	0.23	0.62	0.28	0.78	0.25	0.0013	0.43
	10	0.25	0.84	0.18	0.32	0.81	0.44	0.0005	0.64
	12	0.75	0.85	0.24	0.67	0.64	0.48	0.00056	0.76
	2	0.64	0.85	0.55	0.97	0.413	0.31	0.00048	0.86
	4	0.5	0.73	0.56	0.93	0.29	0.47	0.00053	0.83
The u-value has an effect on wind speed only in the NE orientation from 8 to 4 pm without any effect of the urban canyon.									
humid	8	0.58	0.94	0.9	0.42	0.83	0.59	0.17	0.9
	10	0.64	0.9	0.57	0.17	0.59	0.054	0.27	0.65
	12	0.95	0.85	0.48	0.09	0.99	0.023	0.002	0.55
	2	0.96	0.27	0.56	0.99	0.44	0.017	0.007	0.49
	4	0.9 5	0.205	0.86	0.53	0.37	0.107	0.007	0.52
The u-value affects the humidity after 12 pm and until 4 pm in the NE orientation, while the urban canyon affects the humidity in the SW orientation from 10 am to 2 pm.									

PET	8	0.37	0.13	0.082	0.51	0.69	0.84	0.24	0.21
	10	0.8	0.68	0.14	0.69	0.38	0.85	0.99	0.12
	12	0.46	0.17	0.68	0.51	0.55	0.95	0.32	0.59
	2	0.17	0.29	0.71	0.63	0.07	0.012	0.00062	0.79
	4	0.21	0.31	0.89	0.37	0.76	0.11	0.057	0.94

There is no significant effect of the u-value and the urban canyon on PET in a tangible way, only a scattered change at different orientation and different times.

UTCI	8	0.08	0.12	0.53	0.31	0.83	0.69	0.31	0.29
	10	0.09	0.78	0.04	0.39	0.49	0.69	0.066	0.23
	12	0.94	0.45	0.56	0.07	0.15	0.4	0.03	0.9
	2	0.26	0.04	0.27	0.72	0.14	0.02	0.0001	0.85
	4	0.4	0.09	0.76	0.044	0.66	0.08	0.06	0.96

There is no significant effect of the u-value and the urban canyon on UTCI in a tangible way, only a scattered change at different orientation and different times.

Overall conclusion for summer MLR:

- SW orientation: most sensitive to the combined effect of U-value and H/W, especially at 14:00.
- NE orientation: predominantly controlled by U-value (material) for Ta, RH, PET, and UTCI.
- E and W orientations: less responsive to U-value and H/W in the MLR framework, except for a few specific hours and variables.

- MLR in winter:

  Winter MLR results (see "Table D6-3) showed that the influence of U-value and H/W on microclimatic variables was generally limited, with most models not reaching statistical significance ($p > 0.05$) and low explanatory power compared to summer.

  H/W had the clearest effect in SW façades, particularly on afternoon temperature and relative humidity. In the NE orientation, U-value affected wind speed (adjusted $R^2 = 0.65$, $p < 0.001$ see Table D6-4) during most of the day and had a more noticeable impact on PET and UTCI at 12:00 and 14:00.

  However, overall thermal differences between scenarios in winter remained small and most PET and UTCI values fell within comfort or mild heat stress ranges.

  For this reason, detailed regression coefficients and equations are presented in the appendix only, while the main text emphasizes the conceptual conclusion:

  - In summer, the combined effect of material thermal properties (U-value) and canyon geometry (H/W) is strongest in SW and NE orientations, particularly around 14:00.

- In winter, their influence is weaker and often secondary to global climatic conditions, with H/W and orientation playing a more visible role than material properties.

Building on the statistical outcomes, the following discussion interprets the results in the context of previous studies and the specific climatic characteristics of Hebron, highlighting the theoretical and practical implications of the findings.

4.8 Discussion

This section synthesizes the results and interprets them in light of existing literature, focusing on underlying mechanisms rather than reiterating numerical outcomes. The discussion clarifies how street orientation, urban canyon geometry, and façade materials interact to influence outdoor thermal comfort, highlighting seasonal differences and positioning the findings within the relevant body of literature on Mediterranean urban environments.

4.8.1 Hierarchy of Influencing Factors on Outdoor Thermal Comfort

The findings indicate that outdoor thermal comfort, within the context of dense commercial streets in Hebron, is primarily governed by radiative exposure controlled by street orientation, followed by urban canyon geometry (H/W ratios ranging from 0 to 5.6), while façade material properties play a secondary and conditional role.. This hierarchy is specifically valid for urban canyon configurations where shading patterns and solar access vary significantly due to orientation and aspect ratio. The limited and inconsistent effect of façade materials observed in the descriptive microclimatic analysis, particularly for air temperature and relative humidity. This observation is consistent with previous studies conducted in Mediterranean and hot-humid climates, which reported that orientation and shading patterns exert a stronger influence on thermal comfort than façade thermal properties alone (Chatzidimitriou and Yannas, 2017; Abd Elraouf *et al.*, 2022). However, the present study further demonstrates that material effects become statistically significant when evaluated in combination with geometric and directional variables, supporting the argument that materials influence thermal comfort indirectly rather than independently, as also suggested by (Piselli *et al.*, 2018).

Importantly, this hierarchy may shift under extreme material scenarios. For instance, in cases where façade surfaces are predominantly composed of high-reflectivity or low-thermal-mass materials (e.g., extensive glazing systems), material properties can significantly alter mean

radiant temperature (MRT) and local thermal perception. Under such conditions, materials may transition from a secondary to a more dominant factor influencing outdoor thermal comfort.

4.8.2 Orientation as a Regulator of Thermal Stress

Street orientation emerged as a critical factor that can amplify or mitigate thermal stress, regardless of material selection. East–west oriented streets consistently exhibited the highest PET and UTCI values due to prolonged solar exposure and limited ventilation, while northwest–southeast and north–south orientations provided more moderate conditions through balanced shade distribution. These results align with findings reported by (Chatzidimitriou and Yannas, 2017; Abd Elraouf *et al.*, 2022) , who identified NW–SE and NS orientations as thermally favorable in Mediterranean and hot-humid contexts. However, they contrast with the conclusions of (Abdollahzadeh and Biloria, 2021), who reported poor performance for NW–SE orientations in a humid subtropical climate. This discrepancy highlights the importance of climatic context and confirms that orientation effectiveness is climate-specific rather than universal.

4.8.3 Urban Canyon Geometry and Seasonal Trade-offs

The relationship between the height-to-width ratio (H/W) and thermal comfort was found to be non-linear and strongly dependent on orientation and season. While increasing H/W generally reduced PET and UTCI values in summer by enhancing shading and reducing mean radiant temperature, this effect weakened or reversed in orientations with restricted ventilation or prolonged afternoon solar exposure. In winter, the relationship was partially reversed. Deeper canyons restricted solar access and resulted in lower PET and UTCI values, potentially reducing thermal comfort during colder periods. Wider streets, on the other hand, benefited from increased solar penetration and improved winter warmth. These findings highlight the importance of adopting intermediate H/W ratios that balance summer shading with winter solar access.

Similar trends were reported by (Achour-Younsi and Kharrat, 2016; Chatzidimitriou and Yannas, 2017), who emphasized the cooling role of deep canyons in Mediterranean climates. However, the present results show that excessive depth may limit airflow and reduce cooling efficiency, producing context-specific exceptions. This supports recent studies arguing that H/W should be optimized in relation to ventilation potential rather than maximized indiscriminately (Elkhayat *et al.*, 2024).

4.8.4 Material–Geometry Interaction and Conditional Material Effects

Façade materials influenced outdoor thermal comfort primarily through their interaction with orientation and urban geometry rather than through their intrinsic thermal properties alone. Insulating materials reduced thermal sensitivity under moderate conditions but were insufficient to offset unfavorable orientation or excessive solar exposure during peak summer periods. Poorly insulated materials exhibited stronger sensitivity to solar radiation, making them more dependent on geometric shading strategies such as increased H/W ratios. Conversely, better-insulated materials demonstrated more stable thermal behavior, reducing—but not eliminating—the impact of orientation and canyon geometry.

These results indicate that material optimization alone cannot ensure outdoor thermal comfort and must be integrated within a broader urban design framework that considers street orientation, canyon proportions, and ventilation potential.

4.8.5 Spatial Interaction between Street Sides and the Urban Center

The analysis revealed that the thermal conditions at the center of the street are strongly influenced by the combined characteristics of both facing façades. Even when one side exhibits favorable orientation or material properties, adverse conditions on the opposite side can significantly elevate thermal stress in the middle of the urban space. This finding underscores the limitation of unilateral design interventions and highlights the importance of integrated façade treatment on both sides of the street. Achieving thermal comfort in the pedestrian zone requires coordinated consideration of materials, orientation, and geometry across the entire street section rather than isolated improvements on individual façades.

4.8.6 Seasonal Interpretation of Inferential Results (summer vs. winter)

The inferential statistical analysis confirmed that the significance of individual variables varies between summer and winter. Orientation and H/W ratio exerted stronger influence during summer due to intense solar radiation, while material-related effects became more pronounced during winter and transitional periods. This seasonal variability reinforces the necessity of interpreting statistical outcomes within their climatic context. Design strategies that are statistically effective in summer may not yield the same benefits in winter, highlighting the importance of seasonal balance when formulating urban thermal comfort guidelines.

These findings highlight the importance of adopting an integrated and seasonally responsive urban design approach, where orientation, canyon geometry, and façade materials are

considered collectively. Practical design recommendations derived from these results are presented in the following chapter.

4.8.7 Study limitations

Despite the comprehensive scope and rigorous methodology adopted in this study, several limitations should be acknowledged. Recognizing these limitations is essential for accurately interpreting the results and defining the boundaries within which the findings can be generalized.

First, this study primarily relied on ENVI-met simulations to assess outdoor microclimatic conditions and thermal comfort. Although the model was carefully calibrated and validated using field measurements, numerical simulations inherently involve simplifications of complex urban environments. In particular, the representation of wind speed in dense urban canyons remains a known limitation of microscale climate models. Moreover, ENVI-met restricts the maximum allowable wind speed input to 5 m/s, which prevents the simulation of extreme wind conditions. This constraint influenced the selection of the simulation date, as days with higher recorded wind speeds (e.g., June 21) were excluded, and the closest representative day (June 22) was used instead. Therefore, the findings should be interpreted within the operational limits of the model rather than as absolute representations of extreme climatic conditions. Nevertheless, this limitation does not affect the comparative analysis between different scenarios, which remains the core objective of this research.

Second, the study is limited in its use of façade performance indicators, particularly the use of U-value instead of Solar Reflectance Index (SRI). The U-value governs heat transfer through the entire wall assembly, including conduction, thermal storage, and delayed heat release, making it a system-level indicator that captures the dynamic thermal behavior of multi-layered façades. It is an assembly property. In contrast, SRI is a surface-level metric that primarily describes shortwave solar reflectance and surface temperature reduction. It governs the surface energy balance: how much incoming solar radiation is reflected vs. absorbed as heat at the very surface. It determines peak surface temperature and the intensity of radiant heat re-emitted towards the street (mean radiant temperature - Tmrt). It is a surface property. While SRI is useful for evaluating cool surface strategies, it does not account for thermal mass, time lag, or heat storage capacity.

Given that this study focuses on the combined effect of façade materials, urban canyon, and orientation on outdoor thermal comfort, the wall assembly (layers of stone, concrete, insulation, cladding) behavior is more relevant than surface reflectivity alone.

The research investigates how different material configurations (e.g., variations in thickness, density, and insulation) influence heat storage and release over time, particularly during peak stress conditions (e.g., 2:00 PM). A material can have a high SRI (reflective) but very low thermal mass (e.g., a thin aluminum panel). Conversely, a material with a low SRI (dark stone) can have very high thermal mass. U-value, derived from the entire assembly (density, specific heat, conductivity, thickness), is the correct metric to capture this time-dependent thermal storage and release behavior. SRI cannot capture this.

In this thesis, wall composition plays a key role, as different internal layer configurations (e.g., 5 cm vs. 25 cm stone, with or without insulation) directly affect the U-value while often maintaining the same external surface and SRI. Therefore, SRI cannot distinguish between walls with identical cladding but different thermal mass, whereas U-value captures these differences effectively. This is evidenced by the results (e.g., M3 vs. M6 in Case 4), where variations in internal composition led to different outdoor thermal comfort levels, confirming that U-value is the more relevant explanatory variable.

Additionally, in the context of Hebron, where traditional construction is dominated by multi-layer stone and concrete systems, U-value aligns more closely with local building practice and energy efficiency standards (e.g., the Palestinian Energy Efficiency Guideline, Reference Facility, 2004), making it more suitable for interpretation and application. SRI is a more niche metric for specialized "cool roof/wall" products, which are not the dominant material palette in Hebron's existing commercial center. ENVI-met also requires detailed wall layer properties (thickness, density, thermal conductivity, and specific heat) to simulate heat conduction and storage, which are governed by U-value and thermal inertia. Although surface albedo (related to SRI) is also included as an independent input, dynamic heat exchange between the façade and the outdoor environment is primarily controlled by conductive and storage properties. This is particularly relevant during peak heat stress periods (e.g., 2:00 PM), when stored heat is released, making U-value more influential than surface albedo alone.

Third, the spatial scope of the study was limited to selected commercial streets in the city center of Hebron. While these streets represent typical dense commercial urban canyons in Mediterranean cities, the results may not be directly transferable to other urban typologies such as residential neighborhoods, suburban areas, or industrial zones. Consequently, the applicability of the findings should be considered within contexts that share similar urban morphology, land-use patterns, and climatic conditions.

Fourth,the temporal scope of the analysis focused on representative summer and winter periods. Transitional seasons such as spring and autumn were not examined, despite their potential influence on outdoor thermal comfort conditions. As a result, seasonal variability outside peak summer and winter conditions was not fully captured.

Fifth,the assessment of outdoor thermal comfort was based on widely recognized bioclimatic indices (PET and UTCI), which quantify physiological thermal stress but do not account for subjective human perception. Factors such as individual adaptation, behavioral responses, cultural expectations, and psychological comfort were not incorporated into the analysis. Therefore, the calculated comfort levels represent objective thermal conditions rather than perceived comfort experienced by pedestrians.

Sixth, a key methodological limitation relates to the calibration approach. The study used air temperature (Ta) for model calibration instead of Mean Radiant Temperature (Tmrt). This decision was based on both practical and scientific considerations. The Mean Radiant Temperature (Tmrt) is not measured by a single sensor. It is calculated from a shortwave and longwave radiation fluxes from six directions (or from a globe thermometer with assumptions). Alternatively, it is modeled from surface temperatures, solar geometry, and view factors. In field conditions, accurate Tmrt measurement requires specialized, expensive equipment (e.g., net radiometers, pyranometers, or ISO-compliant globe thermometers with known diameter and emissivity). There is a lack of measuring devices (thermal camera)" . In this study, available instruments (e.g., UNI-T A37 CO_2 meter, wireless weather station, and anemometer) allowed reliable measurement of air temperature, relative humidity, and wind speed, but not radiation fluxes required for direct Tmrt measurement.

Furthermore, Measuring Tmrt in a narrow urban canyon with moving pedestrians, parked cars, and variable shading would require: A six directional radiation sensor at 1.4 m height, with a clear view of all surrounding surfaces; Simultaneous measurement of surface temperatures of walls, ground, and sky; and Correction for sensor response time and emissivity. None of this was possible with the available study resources. Attempting to calibrate Tmrt using incomplete or indirect measurements would introduce greater uncertainty than relying on a well-validated air temperature baseline. This research chose the honest, scientifically sound path: calibrate what can be measured reliably.

This thesis aims to compare relative differences in outdoor thermal comfort (PET, UTCI) between façade materials, orientations, and H/W ratios – not to forecast absolute Tmrt values with high precision. For comparative analysis, systematic biases cancel out. Calibrating Ta ensures that the baseline climate (diurnal cycle, magnitude of heating) matches local

observations. Once Ta is validated, the differences in Tmrt and PET between scenarios are driven by the independent variables (material U value, orientation, H/W). Those differences remain valid even if absolute Tmrt has a small offset. The thesis's verification (Section 4.2.2) also compared Ta between right, middle, and left sides within the same section – a spatial consistency check that directly supports the reliability of canyon scale thermal patterns, which are the foundation of Tmrt.

ENVI-met computes Tmrt from: Direct, diffuse, and reflected shortwave radiation; Longwave radiation exchange between surfaces and the sky; and Surface temperatures of walls, ground, and vegetation. If the model correctly simulates air temperature (which governs convective heat exchange and longwave emission from the air), wind speed (affecting surface convection), and solar geometry (predefined), then Tmrt will be realistic. Calibrating Ta ensures that the energy balance of the canyon is fundamentally correct. Errors in Tmrt are typically caused by incorrect surface albedo, emissivity, or shading geometry – not by an uncalibrated Ta. This study carefully assigned material properties (Table 3-2, Appendix B) and vegetation, so Tmrt errors are minimized without needing direct Tmrt calibration. The calibration results for Ta fall within literature benchmarks, and the spatial verification further supports model reliability. Therefore, the absence of Tmrt calibration does not compromise the validity of the thesis findings.

Finally, the study focused on outdoor thermal comfort and did not explicitly examine the interaction between outdoor microclimate and indoor energy performance. Although façade materials influence both environments, the indoor implications of the selected material configurations were beyond the scope of the present research.

Despite these limitations, the study provides robust and internally valid insights into the combined effects of façade materials, street orientation, and urban canyon geometry on outdoor thermal comfort. Rather than undermining the findings, these limitations define a clear contextual framework for their interpretation and highlight opportunities for future research aimed at expanding and refining the results.

4.9 Summary

This chapter presented an integrated analysis of the simulated and measured microclimatic conditions in selected commercial streets in Hebron, focusing on the combined effects of façade materials, street orientation, and urban canyon geometry (H/W) on outdoor thermal comfort during summer and winter conditions. The results demonstrated that variations in

façade materials, urban form, and orientation produce measurable differences in air temperature, wind speed, relative humidity, and consequently in thermal comfort indices (PET and UTCI).

The findings confirmed that street orientation and canyon geometry exert a stronger and more consistent influence on microclimatic behavior than material properties alone, particularly during peak thermal periods. While façade materials with lower thermal conductivity and favorable surface properties contributed to moderating thermal stress, their effectiveness was highly dependent on the surrounding urban configuration and solar exposure. Deep urban canyons enhanced shading and reduced thermal stress in summer, whereas more open configurations promoted thermal comfort in winter by allowing greater solar access.

A clear spatial contrast was observed between the three street sections (right, left, and center), with the thermal conditions in the street center being strongly governed by the combined characteristics of both facing façades. This interaction highlights the importance of treating the street as an integrated thermal system rather than as isolated building elements. Seasonal analysis further revealed that strategies effective in reducing heat stress during summer may have the opposite effect in winter, emphasizing the need for seasonally balanced design approaches in Mediterranean climates.

Statistical analyses supported these observations, showing that the height-to-width ratio and façade thermal properties were the most influential variables affecting air temperature and wind speed, while relative humidity was less sensitive to geometric variation. The inferential results confirmed that material performance cannot be evaluated independently from urban form and orientation, reinforcing conclusions reported in previous Mediterranean and hot-climate studies.

Overall, this chapter demonstrates that achieving improved outdoor thermal comfort in Hebron's commercial streets requires an integrated design approach that considers façade materials, street orientation, and urban canyon geometry simultaneously. These findings provide the analytical foundation for the final chapter, which synthesizes the study's contributions and translates them into practical design recommendations and broader conclusions.

Chapter 5: Conclusion and Recommendations

5.1 Preface

This chapter presents a synthesized conclusion of the research outcomes and highlights the main scientific and practical contributions of the study. It also provides evidence-based recommendations directed at urban planners, architects, engineers, and policy makers, followed by proposed directions for future research.

The study investigated the combined influence of façade materials, street orientation, and urban canyon geometry on outdoor thermal comfort in Hebron's commercial core—an area with dense urban fabric and high pedestrian activity. Using calibrated ENVI-met v5.6.1 simulations supported by field measurements, the research evaluated microclimatic factors (air temperature, relative humidity, and wind speed) and thermal comfort indices (PET and UTCI) during summer and winter conditions.

Rather than treating urban parameters as isolated variables, this study demonstrated that outdoor thermal comfort in commercial streets is governed by the synergistic interaction between material properties, urban geometry, and orientation. This integrated perspective constitutes the central conceptual outcome of the research.

5.2 Summary of key findings

The results of the study revealed several consistent patterns that explain how urban form and materiality shape the thermal environment experienced by pedestrians in Hebron’s commercial streets , particularly Weddad and Ibn Rushed streets:

Street orientation showed a statistically significant influence on outdoor thermal comfort ($p < 0.05$), where north–south (N–S) and northwest–southeast (NW–SE) orientations provided the best thermal performance, while east–west (E–W) orientation recorded the highest thermal stress levels. This is consistent with the simulation and statistical results, which indicate increased solar exposure duration in E–W streets, particularly during peak hours (12:00–14:00).

Urban canyon aspect ratio (H/W) demonstrated an optimal performance range between 1 and 2, as confirmed by the statistical analysis. Within this range, a balance between solar shading and airflow was achieved. Lower ratios resulted in excessive solar exposure, while higher ratios reduced ventilation efficiency.

Façade materials had a direct and measurable effect on outdoor thermal comfort, where materials with lower thermal transmittance (low U-value) significantly improved thermal conditions.The statistical analysis confirmed that material alone has a significant effect on PET

and UTCI values ($p < 0.05$), indicating that façade composition is not only a secondary factor but a primary driver of thermal performance.

The interaction between façade materials and urban geometry was clearly observed, where the effectiveness of materials increased under optimal canyon configurations (H/W = 1–2) , particularly in Weddad Street scenarios. This confirms that material performance is context-dependent, rather than absolute.

Seasonal variations influence the magnitude of these effects, with summer conditions showing stronger sensitivity to geometry and materials, while winter conditions remain largely within acceptable comfort ranges.

Optimal thermal performance is not achieved through a single parameter, but through the integration of appropriate orientation, moderate H/W ratios, and thermally efficient façade materials.

5.3 Conclusion

Based on the analyzed results, the following general conclusions can be drawn:

1. Validity of ENVI-met Calibration

The calibrated ENVI-met model demonstrated satisfactory reliability in simulating the outdoor microclimate of Hebron. Air temperature and relative humidity showed agreement with field measurements, while wind speed exhibited acceptable deviations consistent with known limitations of micro scale models in complex urban settings. These deviations did not compromise the reliability of PET and UTCI outputs, confirming the model's suitability for evaluating outdoor thermal comfort in Mediterranean attaching contexts.

2. Effect of Street Orientation

Street orientation emerged as a dominant factor influencing outdoor thermal comfort due to its control over solar exposure and shading patterns, with a strongly season-dependent impact. In summer, Streets oriented along the NW–SE axis consistently exhibited more favorable thermal conditions due to balanced solar exposure and improved ventilation potential. In contrast, E–W oriented streets experienced prolonged direct solar radiation and reduced airflow, leading to higher air temperatures and increased heat stress. In winter, the pattern reverses, as E–W orientations enhance solar access and improve thermal conditions, whereas N–S orientations may limit solar gain and reduce comfort. These findings confirm that orientation acts as a primary regulator that amplifies or mitigates the effects of materials and geometry.

Overall, no single orientation is optimal year-round, highlighting the need for a seasonally adaptive design approach integrated with geometry and material strategies.

3. Impact of Canyon Geometry (H/W)

Canyon geometry (H/W ratio) significantly influences thermal comfort by controlling shading, solar access, and ventilation, with a clear seasonal trade-off. Increasing the height-to-width (H/W) ratio enhanced shading and reduced air temperature, particularly during midday and afternoon periods in summer. However, excessively deep canyons were associated with reduced wind speed, limiting convective cooling. In winter, these same configurations limit solar penetration, leading to lower temperatures and reduced comfort, while lower H/W ratios enhance solar access. An intermediate H/W range (≈1–2) offers a balanced solution, ensuring shading in summer and solar access in winter. Thus, canyon design should follow a context-sensitive, seasonally responsive approach rather than fixed geometric values.

4. Influence of Façade Materials

Façade materials with lower U-values (below 2.5 $W/m^2 \cdot K$) and higher thermal inertia demonstrated superior performance in mitigating heat stress. These materials reduced air temperature by up to 2 °C and PET values by approximately 3–4 °C during summer conditions. In winter, materials with higher thermal mass can enhance comfort by storing and releasing heat. Materials with extreme reflectivity, while reducing surface temperature, showed potential to increase radiant heat exposure at the pedestrian level, highlighting the importance of achieving a balance between optical and thermal properties.

Therefore, façade materials should be applied within an integrated design framework, balancing summer heat mitigation with winter thermal benefits.

5. Integrated Effects of Urban Parameters

The most favorable microclimatic and thermal comfort conditions were achieved when thermally massive façades, NW–SE oriented streets, and moderate H/W ratios were combined. This integrated configuration minimized heat accumulation, reduced thermal stress, and improved pedestrian comfort throughout the day. The findings confirm that urban thermal comfort cannot be optimized through isolated design decisions but rather through coordinated and context-sensitive urban strategies.

Therefore, outdoor thermal comfort in Mediterranean climates is governed by a seasonal trade-off, requiring an integrated and adaptive design approach.

5.4 Contribution:

This section outlines the research's main contributions to both scientific and practical understanding of outdoor thermal comfort in urban streets.

1. Scientific Contribution

This thesis contributes to the existing body of knowledge by developing an integrated analytical framework that links façade material properties, street orientation, and urban canyon geometry to outdoor thermal comfort indices (PET and UTCI) in a Mediterranean context. Unlike studies that focus on single variables, this research demonstrates the compounded and interactive nature of urban parameters and provides empirical evidence from a Middle Eastern Mediterranean city, a context that remains underrepresented in the literature.

2. Practical contribution

At the practical level, the study provides context-based insights derived from the analysis of selected commercial streets in Hebron. Although the research does not aim to develop comprehensive design guidelines, the findings highlight how variations in façade materials, street orientation, and canyon geometry may influence outdoor thermal comfort. These observations can support municipalities, urban planners, and designers in understanding the environmental implications of urban configurations within similar Mediterranean urban contexts.

5.5 Recommendations

Based on the study findings, the following recommendations are proposed:

1. Urban planning level

- Adopt urban canyon H/W ratios between 1.5 and 2.0 for new commercial streets to balance shading and natural ventilation.

- Favor street orientations within the NW–SE to N–S range to reduce excessive solar exposure and improve airflow.
- Rehabilitate existing commercial streets by upgrading façade and pavement materials with thermally efficient alternatives.

- Integrate small-scale open spaces and pocket parks within dense urban fabrics to enhance thermal relief and pedestrian comfort.

2. Engineers and architects

- Select façade materials with moderate reflectivity and adequate thermal mass, avoiding highly reflective surfaces that may increase radiant heat exposure.
- Consider both thermal and optical properties of materials to reduce heat accumulation at the pedestrian level.
- Introduce innovative façade systems such as green walls, cool façades, and hybrid envelope solutions where feasible.
- Adopt design approaches that balance heritage preservation with improved thermal performance in historic urban contexts.

3. Policy and regulatory level

- Require outdoor thermal comfort assessments for new commercial developments using indices such as PET and UTCI.
- Develop local building and urban design codes tailored to the Palestinian and Mediterranean climate, incorporating orientation, geometry, and material considerations.
- Encourage sustainable urban solutions through financial incentives, tax exemptions, or regulatory support for projects that demonstrably reduce thermal stress.

5.6 Future Studies

Building upon the identified limitations of this study, several directions for future research are proposed to expand the scope, validity, and applicability of the findings.

- Future studies should combine numerical simulations with extended long-term field measurements to further enhance model calibration, particularly with respect to wind speed and humidity in dense urban canyons. The integration of high-resolution meteorological data and advanced sensing techniques would improve the accuracy of microclimatic simulations and strengthen confidence in thermal comfort assessments.
- To address the spatial limitations of the present research, future investigations should examine a wider range of urban typologies, including residential, mixed-use, and industrial neighborhoods. Comparative studies across different Palestinian cities—such

as Ramallah, Nablus, and Gaza—would allow for the evaluation of how variations in urban morphology, socio-economic conditions, and climatic exposure influence outdoor thermal comfort.

- Future research should also extend the temporal coverage of analysis to include transitional seasons, such as spring and autumn. Long-term simulations and measurements covering the full annual cycle would provide a more comprehensive understanding of seasonal thermal comfort dynamics and support year-round urban design strategies.
- In order to complement objective thermal comfort indices, future studies should incorporate subjective thermal perception surveys and behavioral observations. Examining the relationship between calculated indices (PET and UTCI) and perceived comfort would offer valuable insights into local thermal adaptation, cultural expectations, and pedestrian behavior in Mediterranean cities.
- Further research is recommended to explore the interaction between outdoor thermal comfort and indoor energy performance. Integrated studies assessing how façade material properties simultaneously influence outdoor microclimate and building energy demand would support holistic and energy-efficient urban design solutions.
- Finally, future studies should investigate the thermal performance and practical feasibility of emerging materials and innovative façade systems, such as nano-coatings, smart materials, and adaptive envelopes. Pilot projects and real-world implementations in collaboration with municipalities or real estate developers would enable the evaluation of these solutions under actual urban conditions.

References

English references

Abadla, A. (2020) 'Urban Heat Island and Thermal Human Comfort in Tulkarm, West Bank, Palestine', *J. Mater. Environ. Sci*, 2020(8), p. 1361.

Abd ElHamied, R. B. (2018) *Model for Urban Features of Open Spaces and their Interrelationships for Energy Saving and Thermal Comfort in Touristic Resorts Touristic Resorts in Red Sea Governorate , Egypt as a case study Ruwaa Bahgat Abd ElHamied Model for Urban Features of Open Spa*. Assiut University.

Abd Elraouf, R. *et al.* (2022) 'The impact of urban geometry on outdoor thermal comfort in a hot-humid climate', *Building and Environment*, 225(July), p. 109632. doi: 10.1016/j.buildenv.2022.109632.

Abdollahzadeh, N. and Biloria, N. (2021) 'Outdoor thermal comfort: Analyzing the impact of urban configurations on the thermal performance of street canyons in the humid subtropical climate of Sydney', *Frontiers of Architectural Research*, 10(2), pp. 394–409. doi: 10.1016/j.foar.2020.11.006.

Aboelata, A. (2020) 'Vegetation in different street orientations of aspect ratio (H/W 1:1) to mitigate UHI and reduce buildings' energy in arid climate', *Building and Environment*, 172(October 2019). doi: 10.1016/j.buildenv.2020.106712.

Abrahem, S. A., Hassan, S. A. and Khamees, W. A. (2020) 'Impact of Facade Material of Mass Housing on Outdoor Thermal Comfort in Hot-arid Climate', *IOP Conference Series: Materials Science and Engineering*, 881(1). doi: 10.1088/1757-899X/881/1/012006.

Achour-Younsi, S. and Kharrat, F. (2016) 'Outdoor Thermal Comfort: Impact of the Geometry of an Urban Street Canyon in a Mediterranean Subtropical Climate – Case Study Tunis, Tunisia', *Procedia - Social and Behavioral Sciences*, 216(October 2015), pp. 689–700. doi: 10.1016/j.sbspro.2015.12.062.

Aghamolaei, R. *et al.* (2023) 'A comprehensive review of outdoor thermal comfort in urban areas: Effective parameters and approaches', *Energy and Environment*, 34(6), pp. 2204–2227. doi: 10.1177/0958305X221116176.

Akbari, H. *et al.* (2016) 'Local climate change and urban heat island mitigation techniques - The state of the art Local Climate Change and Urban Heat Island Mitigation Techniques – The State of the Art', (January). doi: 10.3846/13923730.2015.1111934.

Al-Salaymeh, A., Al-Khatib, I. A. and Arafat, H. A. (2011) 'Towards Sustainable Water Quality: Management of Rainwater Harvesting Cisterns in Southern Palestine', *Water Resources Management*, 25(6), pp. 1721–1736. doi: 10.1007/s11269-010-9771-0.

Ali-Toudert, F. and Mayer, H. (2007) 'Effects of asymmetry, galleries, overhanging façades and vegetation on thermal comfort in urban street canyons', *Solar Energy*, 81(6), pp. 742–754. doi: 10.1016/j.solener.2006.10.007.

Ata Chokhachian *et al.* (2017) 'How Material Performance of Building Façade Affect Urban Microclimate', *PowerSkin 2017*, (January).

Atawneh, R. and Alqadi, S. (2025) 'Urban Climate Climate change adaptation in cities : Enhancement of pedestrian thermal comfort using afforestation and greening buildings', 61(March).

Ayyad, Y. N. and Sharples, S. (2019) 'Envi-MET validation and sensitivity analysis using field

measurements in a hot arid climate', *IOP Conference Series: Earth and Environmental Science*, 329(1). doi: 10.1088/1755-1315/329/1/012040.

Balaji, N. C., Mani, M. and Venkatarama Reddy, B. V. (2013) 'Thermal performance of the building walls', *Building Simulation Applications*, 2013-Janua(May 2014), pp. 151–159.

Bao, J. *et al.* (2023) 'The Influence of Street Morphology on Thermal Environment Based on ENVI-met Simulation: A Case Study of Hangzhou Core Area, China', *ISPRS International Journal of Geo-Information*, 12(8). doi: 10.3390/ijgi12080303.

Błazejczyk, K. *et al.* (2013) 'An introduction to the Universal thermal climate index (UTCI)', *Geographia Polonica*, 86(1), pp. 5–10. doi: 10.7163/GPol.2013.1.

Chatzidimitriou, A. and Yannas, S. (2017) 'Street canyon design and improvement potential for urban open spaces; the influence of canyon aspect ratio and orientation on microclimate and outdoor comfort', *Sustainable Cities and Society*, 33(June), pp. 85–101. doi: 10.1016/j.scs.2017.05.019.

Chen, T. *et al.* (2020) 'Science of the Total Environment Integrated impacts of tree planting and aspect ratios on thermal environment in street canyons by scaled outdoor experiments', *Science of the Total Environment*, 764, p. 142920. doi: 10.1016/j.scitotenv.2020.142920.

Cui, D. *et al.* (2022) 'Effects of different vertical façade greenery systems on pedestrian thermal comfort in deep street canyons', *Urban Forestry and Urban Greening*, 72(January), p. 127582. doi: 10.1016/j.ufug.2022.127582.

Djamila, D. and Moussadek, B. (2024) 'Factors Affecting Microclimate and Thermal Comfort in Outdoor Spaces : a literature review', 3(1), pp. 48–63.

Elkhayat, K. *et al.* (2024) 'Urban geometry as a climate adaptation strategy for enhancing outdoor thermal comfort in a hot desert climate', *Frontiers of Architectural Research*, (xxxx). doi: 10.1016/j.foar.2024.08.004.

Evgenia, T., Mela, A. and Tseliou, A. (2024) 'Thermal Stress in Outdoor Spaces During Mediterranean Heatwaves: A PET and UTCI Analysis of Different Demographics', *Urban Science*, 8(4). doi: 10.3390/urbansci8040193.

Facility, G. E. (2004) *الدليل الارشادي لتصميم المباني الموفرة للطاقة*.

Faragallah, R. N. and Ragheb, R. A. (2022) 'Evaluation of thermal comfort and urban heat island through cool paving materials using ENVI-Met', *Ain Shams Engineering Journal*, 13(3), p. 101609. doi: 10.1016/j.asej.2021.10.004.

Favero, M., Luparelli, A. and Carlucci, S. (2023) 'Analysis of subjective thermal comfort data: A statistical point of view', *Energy and Buildings*, 281, p. 112755. doi: 10.1016/j.enbuild.2022.112755.

Gusson, C. S. and Duarte, D. H. S. (2016) 'Effects of Built Density and Urban Morphology on Urban Microclimate - Calibration of the Model ENVI-met V4 for the Subtropical Sao Paulo, Brazil', *Procedia Engineering*, 169, pp. 2–10. doi: 10.1016/j.proeng.2016.10.001.

Hong, C. *et al.* (2022) 'Cool facades to mitigate urban heat island effects', *Indoor and Built Environment*, 31(10), pp. 2373–2377. doi: 10.1177/1420326X221115369.

Hu, C. B. *et al.* (2020) 'Classification and mapping of urban canyon geometry using Google Street View images and deep multitask learning', *Building and Environment*, 167(May 2019), p. 106424. doi: 10.1016/j.buildenv.2019.106424.

Hushlamoun, S. M. S. (2020) *Enhancing energy performance of highly glazed facades: Case of office buildings in Hebron, Palestine*. Palestine Polytechnic University.

Huttner, S. (2012) ‘Further development and application of the 3D microclimate simulation ENVI-met’, *Mainz: Johannes Gutenberg-Universitat in Mainz*, p. 147.

Idkaidek, S. A. (2021) *Palestine Polytechnic University Deanship of Graduate Studies and Scientific Research Master of Architecture – Sustainable Design A Comparative Thermal-Performance Study of Cladding Systems in Commercial Buildings in Palestine : Samples from Hebron City* Ⅱ. Palestine Polytechnic University.

Jareemit, D. and Srivanit, M. (2019) ‘Effect of Street Canyon Configurations and Orientations on Urban Wind Velocity in Bangkok Suburb Areas’, *IOP Conference Series: Materials Science and Engineering*, 690(1). doi: 10.1088/1757-899X/690/1/012006.

Jo, S. *et al.* (2023) ‘Comparison of the Thermal Environment by Local Climate Zones in Summer: A Case Study in Suwon, Republic of Korea’, *Sustainability (Switzerland)*, 15(3). doi: 10.3390/su15032620.

Johra, H. (2019) ‘Thermophysical Properties of Building Materials : Lecture Notes’.

Koletsis, I. *et al.* (2022) ‘Validation of ENVI-met microscale model with in-situ measurements in warm thermal conditions across Athens area’, *Proceedings of the 17th International Conference on Environmental Science and Technology*, 17(September), pp. 1–4. doi: 10.30955/gnc2021.00261.

Labdaoui, K. *et al.* (2021) ‘Thermal perception in outdoor urban spaces under the Mediterranean climate of Annaba, Algeria’, *Urban Climate*, 39(Cdd), pp. 1–51. doi: 10.1016/j.uclim.2021.100970.

Li, L. *et al.* (2024) ‘The Impact of Coverage Forms of Exterior Vertical Greening Walls on the Thermal Environmental Benefits of Buildings in Hot and Humid Regions’, *Buildings*, 14(12). doi: 10.3390/buildings14123840.

Li, Z. *et al.* (2020) ‘Effects of height-asymmetric street canyon configurations on outdoor air temperature and air quality’, *Building and Environment*, 183, pp. 1–50. doi: 10.1016/j.buildenv.2020.107195.

Lopez-Cabeza, V. P. *et al.* (2022) ‘Albedo influence on the microclimate and thermal comfort of courtyards under Mediterranean hot summer climate conditions’, *Sustainable Cities and Society*, 81(December 2021), p. 103872. doi: 10.1016/j.scs.2022.103872.

Luo, T. *et al.* (2024) ‘Effects Of Urban Tree Species and Morphological Characteristics On the Thermal Environment: A Case Study in Fuzhou, China’, *Papers.Ssrn.Com*, (2023).

Mahmood Mussa, H. and Wasmi M. Salih, T. (2020) ‘Thermal Insulation Performance of Wood-Plastic Composite Panels As Alternative To Alucobond Cladding Sheets for Buildings’, *Journal of Engineering and Sustainable Development*, 24(Special), pp. 425–433. doi: 10.31272/jeasd.conf.1.47.

Matzarakis, A., Mayer, H. and Iziomon, M. G. (1999) ‘Applications of a universal thermal index: Physiological equivalent temperature’, *International Journal of Biometeorology*, 43(2), pp. 76–84. doi: 10.1007/s004840050119.

Mohajerani, A., Bakaric, J. and Jeffrey-Bailey, T. (2017) ‘The urban heat island effect, its causes, and mitigation, with reference to the thermal properties of asphalt concrete’, *Journal of Environmental Management*, 197(February 2018), pp. 522–538. doi: 10.1016/j.jenvman.2017.03.095.

Nasereddin, H. S. (2022) *The Control of Thermal Comfort and Energy Saving Through External Walls in Apartment Buildings in Palestine : The Case of Hebron Haya Sameh Nasereddin*. Palestine Polytechnic University.

Nazarian, N., Acero, J. A. and Norford, L. (2019) ‘Outdoor thermal comfort autonomy: Performance metrics for climate-conscious urban design’, *Building and Environment*, 155(March), pp. 145–160.

doi: 10.1016/j.buildenv.2019.03.028.

Oquendo-Di Cosola, V. *et al.* (2023) 'Assessment of the impact of green walls on urban thermal comfort in a Mediterranean climate', *Energy and Buildings*, 296(April), p. 113375. doi: 10.1016/j.enbuild.2023.113375.

Ornam, K., Wonorahardjo, S. and Triyadi, S. (2024) 'Several façade types for mitigating urban heat island intensity', *Building and Environment*, 248(May 2023), p. 111031. doi: 10.1016/j.buildenv.2023.111031.

Piselli, C. *et al.* (2018) 'Outdoor comfort conditions in urban areas: On citizens' perspective about microclimate mitigation of urban transit areas', *Sustainable Cities and Society*, 39, pp. 16–36. doi: 10.1016/j.scs.2018.02.004.

Porwal, S. (2025) 'Factors Influencing Outdoor Thermal Comfort : A Review Factors Influencing Outdoor Thermal Comfort : A Review', (January). doi: 10.47857/irjms.2025.v06i02.03123.

Qaid, A. and Ossen, D. R. (2014) 'Effect of asymmetrical street aspect ratios on microclimates in hot, humid regions', *International Journal of Biometeorology*, 59(6), pp. 657–677. doi: 10.1007/s00484-014-0878-5.

Ren, J. *et al.* (2023) 'A Review on the Impacts of Urban Heat Islands on Outdoor Thermal Comfort', *Buildings*, 13(6). doi: 10.3390/buildings13061368.

Rosso, F. *et al.* (2018) 'On the impact of innovative materials on outdoor thermal comfort of pedestrians in historical urban canyons', *Renewable Energy*, 118, pp. 825–839. doi: 10.1016/j.renene.2017.11.074.

Salata, F. *et al.* (2016) 'Outdoor thermal comfort in the Mediterranean area . A transversal study in Rome , Italy', *Building and Environment*, 96, pp. 46–61. doi: 10.1016/j.buildenv.2015.11.023.

Salvati, A. *et al.* (2022) 'Impact of reflective materials on urban canyon albedo, outdoor and indoor microclimates', *Building and Environment*, 207(PB), p. 108459. doi: 10.1016/j.buildenv.2021.108459.

Shaheen, L. (2013) 'Rapid Urbanization and the Challenge of Sustainable', *International Journal of Social, Behavioral, Educational, Economic, Business and Industrial Engineering*, 7(3), pp. 643–649.

Shishegar, N. (2013) 'Street Design and Urban Microclimate : Analyzing the Effects of Street Geometry and Orientation on Airflow and Solar Access in Urban Canyons', 1(1). doi: 10.7763/JOCET.2013.V1.13.

Spaces, U. O. and Liu, Z. (2023) 'A Review of Thermal Comfort Evaluation and Improvement in Urban', *Buildings*, 13(12). doi: 10.3390/buildings13123050.

Tabatabaei, S. S. and Fayaz, R. (2023) 'The effect of facade materials and coatings on urban heat island mitigation and outdoor thermal comfort in hot semi-arid climate', *Building and Environment*, 243(August), p. 110701. doi: 10.1016/j.buildenv.2023.110701.

Tablada, A. and Nouri, A. S. (2021) 'Urban Climate Assessing the influence of street configurations on human thermal conditions in open balconies in the Mediterranean climate', 40(October). doi: 10.1016/j.uclim.2021.100975.

Taherdoost, H. (2022) 'Data Collection Methods and Tools for Research ; A Step-by-Step Guide to Choose Data Collection Technique for Academic and Business Research Projects Hamed Taherdoost To cite this version : HAL Id : hal-03741847 Data Collection Methods and Tools for Resea'.

Taleghani, M. *et al.* (2015) 'Outdoor thermal comfort within five different urban forms in the

Netherlands', *Building and Environment*, 83, pp. 65–78. doi: 10.1016/j.buildenv.2014.03.014.

Tawfeeq Najah, F., Fakhri Khalaf Abdullah, S. and Ameen Abdulkareem, T. (2023) 'Urban Land Use Changes: Effect of Green Urban Spaces Transformation on Urban Heat Islands in Baghdad', *Alexandria Engineering Journal*, 66, pp. 555–571. doi: 10.1016/j.aej.2022.11.005.

Tripathy, P. K. (2006) *A practical approach*. second, *World Cement*. second. doi: 10.5408/0022-1368-4.2-2.83.

Uyanık, G. K. and Güler, N. (2013) 'A Study on Multiple Linear Regression Analysis', *Procedia - Social and Behavioral Sciences*, 106, pp. 234–240. doi: 10.1016/j.sbspro.2013.12.027.

Vassiliades, C., Savvides, A. and Buonomano, A. (2022) 'Building integration of active solar energy systems for façades renovation in the urban fabric: Effects on the thermal comfort in outdoor public spaces in Naples and Thessaloniki', *Renewable Energy*, 190, pp. 30–47. doi: 10.1016/j.renene.2022.03.094.

Walls, W., Parker, N. and Walliss, J. (2015) 'Designing with thermal comfort indices in outdoor sites', *Living and Learning: Research for a Better Built Environment*, pp. 1117–1128.

Wonorahardjo, S. *et al.* (2022) 'Effect of different building façade systems on thermal comfort and urban heat island phenomenon: An experimental analysis', *Building and Environment*, 217(January), p. 109063. doi: 10.1016/j.buildenv.2022.109063.

Yilmaz, S., Kurt, A. and Gölcü, M. (2023) 'ENVI-met Simulations of the Effect of Different Landscape Design Scenarios on Pedestrian Thermal Comfort: Haydar Aliyev Street', *Yuzuncu Yil University Journal of Agricultural Sciences*, 33(3), pp. 338–353. doi: 10.29133/yyutbd.1265752.

Yuan, J., Farnham, C. and Emura, K. (2021) 'Effect of different reflection directional characteristics of building facades on outdoor thermal environment and indoor heat loads by CFD analysis', *Urban Climate*, 38(May), p. 100875. doi: 10.1016/j.uclim.2021.100875.

Zare, S. *et al.* (2018) 'Comparing Universal Thermal Climate Index (UTCI) with selected thermal indices/environmental parameters during 12 months of the year', *Weather and Climate Extremes*, 19(December 2017), pp. 49–57. doi: 10.1016/j.wace.2018.01.004.

Zhou, H. *et al.* (2022) 'Outdoor thermal environment on road and its influencing factors in hot, humid weather: A case study in Xuzhou City, China', *Building and Environment*, 207(PB), p. 108460. doi: 10.1016/j.buildenv.2021.108460.

Website references:

1. Mapbox (n.d.) Mapbox. Available at: https://www.mapbox.com/(Accessed: 14 Aug 2025).
2. AgriMetSoft (2019) Correlation coefficient calculator. Available at: https://agrimetsoft.com/calculators/correlation%20coefficient (Accessed: 3 Sep 2024).
3. U-value calculator. Available at: https://www.changeplan.co.uk/u_value_calculator.php(Accessed: 8 Feb 2024)
4. Ubakus (n.d.) R-value calculator. Available at: https://www.ubakus.de/en/r-value-calculator/?(Accessed: 8 Feb 2024)
5. Housing & Rehabilitation Center (n.d.) [Website]. Available at:https://www.hrc.ps/en/node/22(Accessed: 20 March 2025)
6. Palestinian Central Bureau of Statistics (n.d.) [Website]. Available at:https://www.pcbs.gov.ps/site/lang__ar/738/default.aspx(Accessed: 15 March 2025)

7. Ladybug Tools (n.d.) EPW Map. Available at: https://www.ladybug.tools/epwmap/#close(Accessed: 11 March 2024)
8. LatLong (n.d.) Latitude and longitude finder. Available at: https://www.latlong.net/(Accessed: 5 Feb 2025)

Appendices

Appendix A
Literature view

Thermal Inertia: A measure that reflects a material's ability to resist temperature changes over time. It depends on thermal conductivity (k), density (ρ), specific heat capacity (Cp), and other factors.(Balaji, Mani and Venkatarama Reddy, 2013)

UTCI = f (Ta; Tmrt; va; vp) = Ta + Offset (Ta; Tmrt; va; vp)(Błazejczyk *et al.*, 2013)

Table A-1 Analysis of Previous Studies and optimal value for each variables

Ref-year of	Factor	Sub-variable	value	Other variables			Climate zone -season	Data collection	Urban area type	aim	Simulation/Modeling Tool	Measured Parameters	Key Findings			Optimal value
				Orientation	Building Typology	Other variables							Note	Results	Output	
(Abd Elraouf *et al.*, 2022)	Urban Geometry	Aspect Ratio (H/W)	1	NS	Singular	'	Hot-Humid-Summer (July)	Field measurements +	Residential	To assess the impact of urban geometry on outdoor thermal comfort	ENVI-met v4.4.5 + Rayman	Ta, RH, Va, Tmrt, PET	- The higher the H/W, the greater the comfort level -singular typology is preferred for EW oriented streets -Use special plant or artificial shades on E-W streets to compensate for	37.83	PET(°C)	-Best orientation NS , NW–SE, H/W=2.5, Linear building typology. -worst orientation EW
				EW										40.21		
				NE-SW										37.86		
				NW-SE										35.1		
			1.5	NS										35.1		
				EW										37.8		
				NE-SW										36		
				NW-SE										34		
			2.5	NS										34.9		
				EW										35		

Ref-year of	Factor	Sub-variable	value	Other variables			Climate zone -season	Data collection	Urban area type	aim	Simulation/Modeling Tool	Measured Parameters	Key Findings			Optimal value
				Orientation	Building Typology	Other variables							Note	Results	Output	
				NE-SW									high exposure to solar radiation.	33		
				NW-SE										31.5		
			1	NS	Linear									34		
				EW										41.3		
				NE-SW										37.9		
				NW-SE										36		
			1.5	NS										32		
				EW										39		
				NE-SW										37.5		
				NW-SE										34.5		
			2.5	NS										30		
				EW										40		
				NE-SW										34		
				NW-SE										30.5		
			1	NS	Scattered									36.5		
				EW										43.8		
				NE-SW										40.6		
				NW-SE										37.8		
			1.5	NS										35.1		
				EW										40.9		
				NE-SW										38.1		
				NW-SE										36		
			2.5	NS										33		
				EW										38.2		
				NE-SW										35.2		
				NW-SE										33		
			0.5	NS	Courtyard									38.2		
				EW										41.1		
				NE-SW										42.5		
				NW-SE										41		

Ref-year of	Factor	Sub-variable	value	Other variables			Climate zone -season	Data collection	Urban area type	aim	Simulation/Modeling Tool	Measured Parameters	Key Findings			Optimal value
				Orientation	Building Typology	Other variables							Note	Results	Output	
			0.75	NS										36		
				EW										40.8		
				NE-SW										39		
				NW-SE										38		
			1.25	NS										33		
				EW										38		
				NE-SW										35		
				NW-SE										33		
(Abdollahzadeh and Biloria, 2021)	Urban configuration	Orientation, H/W, Building Typology, Tree-planting	1	NS	linear	No tree	Humid Subtropical - Summer	Simulation	Residential	Analyze and improve outdoor thermal comfort by simulating the influence of street orientation, H/W ratio, building type, and landscaping.	ENVI-met V4.4.5 + Biomet V2.0	Ta, wind speed, RH, MRT, PET	Results are applicable to similar climates, taking into account differences in humidity and wind speed. street orientation and aspect ratio have the most impact (46.42% and 30.59% respectively) - **NS** is second best orientation, the worst one is **NW-SE** and **EW** respectively	49.47%	PET frequency	Optimal orientation: NE-SW
			1	NE-SW	linear	No tree								59.76%		
			1	EW	linear	No tree								52.56%Comfortable-18.54%moderate		
			1	NW-SE	linear	No tree								32.02%		
			1	NE-SW	singular	No tree								58.55%		Optimal building typology: linear NW-SE
			1	NE-SW	Linear(NW-SW)	No tree								60.72%		
			0.5	NE-SW	Linear(NW-SE)	No tree								42.14%		Optimal H/W: 1
			1.5	NE-SW	Linear(NW-SE)	No tree								59.7%		
			2	NE-SW	Linear(NW-SE)	No tree								59.04%		

Ref-year of	Factor	Sub-variable	value	Other variables			Climate zone -season	Data collection	Urban area type	aim	Simulation/Modeling Tool	Measured Parameters	Key Findings			Optimal value
				Orientation	Building Typology	Other variables							Note	Results	Output	
			0.5	NE-SW	Linear(NW-SE	Dense 4m								47.93%		Optimal tree pattern: dense 4m
			0.5	NE-SW	Linear(NW-SE	Sparse 8m								45.73%		
(Qaid and Ossen, 2014)	Urban canyon	Asymmetrical Aspect Ratio (H/W)	2-0.8	NE-SW	linear	SVF=0.45	Hot humid/summer day & night	Field measurements + Simulation	Institutional / Governmental Boulevard	Evaluating the impact of asymmetric ratios (H1/W – H2/W), with the aim of improving shading and ventilation and reducing heat island in hot and humid areas.	ENVI-met V3.1 Beta	Ta, Rh, Ws, T-surface-T wall, SVF, Rs	//	At 2 pm Ta=31.3	Ta(°C)	2–0.8 reduced air temp by 4.7°C and surface temp by 10–14°C; taller NW buildings improve afternoon shading; SVF alone insufficient to predict thermal performance; asymmetry enhances microclimate adaptation in hot–humid contexts.
			0.8-2			SVF=0.45								At 2 pm Ta=35.8		
			1.5-0.8			SVF=0.48								At 2 pm Ta=31.8		
			0.8-1.5			SVF=0.48								At 2 pm Ta=36.8		
			1-0.8			SVF=0.53								At 2 pm Ta=33.8		
			0.8-1			SVF=0.53								At 2 pm Ta=33		
			0.8-0.8			SVF=0.57								At 2 pm Ta=33.8		

Ref-year of	Factor	Sub-variable	value	Other variables			Climate zone -season	Data collection	Urban area type	aim	Simulation/Modeling Tool	Measured Parameters	Key Findings			Optimal value
				Orientation	Building Typology	Other variables							Note	Results	Output	
(Ali-Toudert and Mayer, 2007)	Urban canyon	Aspect Ratio (H/W)	H/W=2 with galleries	NS	--	with galleries	Hot-dry (Ghardaia, Algeria) – Summer (01 August)	simulation	--	To evaluate the effect of geometrical street design features on outdoor thermal comfort	ENVI-met 3.0	Ta, PET	E–W orientation most stressful; N–S canyons most comfortable; vegetation lowered PET by up to 24 K; overhangs reduced PET ≈ 4 K; asymmetry allowed better morning and evening comfort.	At 2pm PET=45 in the middle	PET(°C)	Combined use of galleries, overhangs, and trees in N–S orientation
				EW										At 2pm PET=62 in the middle		
				NE-SW										At 2pm PET=56 in the middle		
				NW-SE										At 2pm PET=46 in the middle		
			H1/W=2,H2/W=1	NS		asymmetrical canyon								At 2pm PET=42 in the middle		
				EW										At 2pm PET=62 in the middle		
				NE-SW										At 2pm PET=62 in the middle		
				NW-SE										At 2pm PET=62 in the middle		
			H1/W=2 H3/W=1.5	NS		overhanging facades and including								At 2pm PET=42 in the middle		
				EW										At 2pm PET=42 in the middle		

Ref-year of	Factor	Sub-variable	value	Other variables			Climate zone -season	Data collection	Urban area type	aim	Simulation/Modeling Tool	Measured Parameters	Key Findings			Optimal value
				Orientation	Building Typology	Other variables							Note	Results	Output	
				NE-SW										At 2pm PET=56 in the middle		
				NW-SE										At 2pm PET=44 in the middle		
			H/W= 2	EW		lateral row of								At 2pm PET=42 in the middle		
			H/W =1	NS		large centr al								At 2pm PET=42in the middle		
(Chatzidimitriou and Yannas, 2017)	Urban Geometry(field measurement)	Aspect ration	0.6				Mediterranean – summer & winter	Field measurements + simulations	Mixed use		ENVI-met v4 + Rayman	Ta, RH, Ws, Tg, Ts, PET	-In summer, the orientation effect was 22 K, H/W about 4 K, and trees 10 K, while in winter the values were 4, 7, and 5 K, respectively. -On the N–S axis, the deepest valley was the most comfortable in summer on both sides, while the widest valley was the most suitable in winter on the east		PET	The best summer conditions were found at Site 12 (H/W 3.2, **EW**) on the south side at 32.4°C, and Site 03 (H/W 1.0, **NW–SE**) on the southwest side at 32.9°C. In all the best orientation NW-SE
			0.7													
			1													

Ref-year of	Factor	Sub-variable	value	Other variables			Climate zone -season	Data collection	Urban area type	aim	Simulation/Modeling Tool	Measured Parameters	Key Findings			Optimal value
				Orientation	Building Typology	Other variables							Note	Results	Output	
													side. On the E–W axis, only the south side was relatively comfortable in summer, especially in the deepest valley. -In winter, the most comfortable site was Site 06 (H/W 1.0, **NE–SW**) at 17.6°C, and Site 13 (H/W 3.0, **N–S**) recorded the highest winter temperature of 20.6°C. -Deep furrows (H/W between 1.7 and 3.3) are most efficient in summer, while			
			1.1													
			1.7													

Ref-year of	Factor	Sub-variable	value	Other variables			Climate zone -season	Data collection	Urban area type	aim	Simulation/Modeling Tool	Measured Parameters	Key Findings			Optimal value
				Orientation	Building Typology	Other variables							Note	Results	Output	
													lower ratios (0.5–1.0) may be more suitable in winter depending on the axis and wind direction.			
			2.8													
			3													
			3.2													

Ref-year of	Factor	Sub-variable	value	Other variables			Climate zone -season	Data collection	Urban area type	aim	Simulation/Modeling Tool	Measured Parameters	Key Findings			Optimal value
				Orientation	Building Typology	Other variables							Note	Results	Output	
			3.3													
	Urban geometry(simulation)		0.5	NS		C								~49		The best orientation **NE–SW** with H/W=2 on SW side and suitable for summer and winter. The second best **EW** in S side with 35.9
						E								~48.8		
						W								~38.5		
				EW		C								~48.8		
						N								~48.2		
						S								~37.8		
				NE-SW		C								~48.2		
						NW								~47.5		
						SE								~46.8		
				NW-SE		C								59.5		
						NE								47.5		
						SW								59.8		
			1	NS		C								~38.2		
						E								~47.5		
						W								~37.5		
				EW		C								~47.5		
						N								~46.8		
						S								~37		
				NE-SW		C								~46.8		

Ref-year of	Factor	Sub-variable	value	Other variables			Climate zone -season	Data collection	Urban area type	aim	Simulation/Modeling Tool	Measured Parameters	Key Findings			Optimal value
				Orientation	Building Typology	Other variables							Note	Results	Output	
						NW								~36.5		
						SE								~45		
				NW-SE		C								~46.2		
						NE								~47		
						SW								~58		
			2	NS		C								~37		
						E								~36.1		
						W								~36.2		
				EW		C								~36.8		
						N								~45		
						S								35.9		
				NE-SW		C								36.2		
						NW								35.6		
						SE								~44.8		
				NW-SE		C								46.8		
						NE								46.5		
						SW								46.5		
(Elkhayat *et al.*, 2024)	Urban canyon	Aspect ratio	1	NS	linear	--	Aswan (hot desert, summer)	Field data (validation) +	Street canyons	Assess effect of aspect ratio (H/W) and orientation on outdoor thermal comfort in two contrasting climates in Egypt	ENVI-met V4.0 + Rayman V3.1	Ta, Rh, Ws, PET	-PET values ranged from 26.6–63.1°C in Aswan. -Aswan: Aspect ratio had greater effect. H/W=2.5 reduced PET by 5–7K but still limited comfort hours (<2h). -The intense heat in Aswan lasted about	57.4(12-14h)	PET (Number of uncomfortable	Aswan: best H/W=2.5 + N–S or NE-SW Worst: EW
				EW										60.2(14h)		
				NW-SE										56.2(13-14h)		
				NE-SW										63.1(12-14h)		
			1.5	NS										55.2(14h)		
				EW										59.9(12h)		
				NW-SE										54.6(14h)		

Ref-year of	Factor	Sub-variable	value	Other variables			Climate zone -season	Data collection	Urban area type	aim	Simulation/Modeling Tool	Measured Parameters	Key Findings			Optimal value
				Orientation	Building Typology	Other variables							Note	Results	Output	
				NE-SW									9–12 hours per day, compared to only 1–7 hours in Alexandria, depending on the aspect ratio.	55.7(11h)		
			2	NS										49(12-13h)		
				EW										58.6(12h-8h >50)		
				NW-SE										50.9(14h)		
				NE-SW										54.8(11h)		
			2.5	NS										50.2(13-14h2h comfortable)		
				EW										58.3(12h)		
				NW-SE										50.9(14h-2h comfortable)		
				NE-SW												
			1	NS			Alexandria (hot-humid,						- PET values ranged from 17.8–51.2°C in Alexandria, reflecting the severity of heat stress in the desert climate compared to the coastal climate.	)		Alexandria: H/W=2.5 + NS, NW–SE. Worst: EW, NE-SW H/W=2.5 is the best aspect ratio for all orientation
				EW										43.8(9-10h)		
				NW-SE												
				NE-SW										51.2(10h)		
			1.5	NS												
				EW										43.9(10h)		
				NW-SE												

Ref-year of	Factor	Sub-variable	value	Other variables			Climate zone -season	Data collection	Urban area type	aim	Simulation/Modeling Tool	Measured Parameters	Key Findings			Optimal value
				Orientation	Building Typology	Other variables							Note	Results	Output	
				NE-SW									-Alexandria: Orientation had stronger impact.	45.3(8h)		
			2	NS												
				EW										34.6(8h)		
				NW-SE												
				NE-SW										45.2)8h)		
			2.5	NS												
				EW										43.2(8h)		
				NW-SE												
				NE-SW										45.2(9h)		
(Achour-Younsi and Kharrat, 2016)	Urban configuration	Aspect ratio / fabrics studied	3.51	NS	Medina(compact and dense fabric/The streets are narrow and winding)	SVF low	Mediterranean subtropical –	SIMULATION	--	Analysis of the impact of urban canyon engineering (street surrounded by buildings) on outdoor thermal comfort in the city of Tunis.	ENVI-met (3D microclimate model)	Ta, Rh, Ws, Tmrt, UTCI	Increasing the H/W ratio clearly enhances thermal comfort, with H/W = 4 providing approximately 8.5°C better conditions compared to H/W = 0.25.	23.5	UTCI	The Medina fabric achieves the best levels of outdoor thermal comfort, while the Colonial fabric shows the worst performance.
				EW												
			1.59	NS	Colonial (Relatively tall buildings distributed	SVF medium								30.06		

Ref-year of	Factor	Sub-variable	value	Other variables			Climate zone -season	Data collection	Urban area type	aim	Simulation/Modeling Tool	Measured Parameters	Key Findings			Optimal value
				Orientation	Building Typology	Other variables							Note	Results	Output	
				EW	on a grid of perpendicular streets of medium width.)											
			0.48	NE-SW	Regulated (modern detached)	SVF high								26.58		
				NW-SE												
		Aspect ratio/simulation	0.25	NS	--	SVF=0.23										-H/W=4 is the best orientation -NS best orientation -EW IS the worst orientation
				EW										45.54		
				NE-SW										34.9		
				NW-SE										35		
			1	NS		SVF=0.65										
				EW										39.8		
				NE-SW										35.2		
				NW-SE										38.5		
			4	NS		SVF==0.8										
				EW										32		
				NE-SW										27.5		
				NW-SE										29.8		
(Jaremit and Srivanit, 2019)	Urban canyon	Aspect ratio	0.5	NS		4units	Hot-humid	Simulation +	Suburban residential clusters	Assess the effect of street canyon orientation, aspect ratio, and length on wind velocity	ENVI-met v4	Wind velocity at 1.5 m pedestrian	-Wind speed is highest at the entrance to the valley and gradually decreases towards its end.	0.8-0.9m/s	WS	Orientation: -Streets parallel to the prevailing winds (N-S and NW-SE) achieve the
						5units								0.85-09m/s		
						10units								0.9-1m/s		
				EW		4units								0.25-03m/s		
						5units								0.3-0.35m/s		

Ref-year of	Factor	Sub-variable	value	Other variables			Climate zone -season	Data collection	Urban area type	aim	Simulation/Modeling Tool	Measured Parameters	Key Findings			Optimal value
				Orientation	Building Typology	Other variables							Note	Results	Output	
						10units				and pedestrian ventilation potential			-Wind speed is highest at the entrance to the valley and gradually decreases towards its end. -Wind speed in vertical streets can be improved by increasing open spaces, gradual building setbacks, or widening openings between urban blocks.	0.35-0.4m/s		highest wind speeds (0.7–1 m/s). -Streets perpendicular to the winds (E-W and NE-SW) produce the lowest speeds (0.2–0.4 m/s).
				NE-SW		4units								0.25-0.3m/s		
						5units								0.3-0.35m/s		
						10units								0.35-0.4m/s		
				NW-SE		4units								0.8-0.9m/s		
						5units								0.85-0.9m/s		
						10units								0.9-1m/s		
			0.7	NS		4units								0.7-0.8m/s		
						5units								0.8-0.9m/s		
						10units								0.9-1m/s		
				EW		4units								0.20-0.25m/s		
						5units								0.25-0.3m/s		H/W: -Shallow canyon (small H/W) tends to provide higher wind speeds. -Deep canyon (H/W = 1.1) showed poorer performance, especially with short lengths.
						10units								0.3-0.35m/s		
				NE-SW		4units								0.2-0.25		
						5units								0.25-0.30		
						10units								0.30-0.35		
				NW-SE		4units								0.7-0.8		
						5units								0.8-0.9		
						10units								0.9-1m/s		
			0.9	NS		4units								0.6-0.7m/s		

Ref-year of	Factor	Sub-variable	value	Other variables			Climate zone -season	Data collection	Urban area type	aim	Simulation/Modeling Tool	Measured Parameters	Key Findings			Optimal value
				Orientation	Building Typology	Other variables							Note	Results	Output	
						5units								0.7-0.8m/s		
						10units								.8-0.9m/s		
				EW		4units								0.2		
						5units								0.25		
						10units								0.3		
				NE-SW		4units								0.2		
						5units								0.25		
						10units								0.3		Streets perpendicular to the wind A low H/W (0.5) with a length of 10 units gives the best performance, but is still lower than parallel to the wind. Streets parallel to the wind The best choice is H/W = 1.1 with a length of 10 units or H/W = 0.5 with a short length.
				NW-SE		4units								0.6-0.7		
						5units								0.7-0.8		
						10units								0.8-0.9		
			1.1	NS		4units								0.45-0.55m/s		
						5units								0.55-0.6		
						10units								0.9-1m/s		
				EW		4units								0.2		
						5units								0.25-0.3		
						10units								0.3-0.35m/s		
				NE-SW		4units								0.2-0.25		
						5units								0.25-0.3		
						10units								0.3-0.35		

Ref-year of	Factor	Sub-variable	value	Other variables			Climate zone -season	Data collection	Urban area type	aim	Simulation/Modeling Tool	Measured Parameters	Key Findings			Optimal value
				Orientation	Building Typology	Other variables							Note	Results	Output	
				NW-SE		4units								0.7-0.8		
						5units								0.75-0.85		
						10units								0.9-1m/s		
(Tablada and Nouri, 2021)	Urban geometry	Orientation, Height	6m/9m	NS	linear	Symmetrical canyons H/W = 1 L(left)C (center) R(right)	Mediterranean – Summer	simulation	Residential area	To assess thermal comfort conditions in open balconies in relation to street orientation and height	Rayman pro	PET	-EW street balconies on the north side (south facing) experience high heat stress 43.4% of the time due to direct sun exposure. -Balconies less than 12m high achieved good thermal comfort, with comfortable PET values ranging between 50.4% and 82.5% of the time. -Balconies less than 12 m high on eastern (NS), southeastern (NE–SW), and southern (EW) facades recorded the lowest levels of heat stress, ranging from	E façade (76.5%)-W façade (50-70%)	PET	NS and SE-NW streets provide the best thermal comfort conditions for Balconies -EW street worst orientation
			>12m											E façade (50.4-82.5%)		
			<12m											More than >12m		
			6m-9m	EW										North façade (81.6%)		
			12m											North façade (50.4-82.5%)		
			<12m											More than 12m		
														All height heat stress 43.4%		
			6m-9m	NE-SW										NW façade (82.5%)		
			>12m											NW façade (50.4-82.5)		
			<12m											NW façade(36.1-54.6% thermal stress		

Ref-year of	Factor	Sub-variable	value	Other variables			Climate zone -season	Data collection	Urban area type	aim	Simulation/Modeling Tool	Measured Parameters	Key Findings			Optimal value
				Orientation	Building Typology	Other variables							Note	Results	Output	
			6-12m	NW-SE									13.1% to 21.9% of the time. -NS: Best balconies at 6–9 m on the east facade (~76.5% comfort).	Any façade >50%		
			<12m											More than 12m		
(Taleghani *et al.*, 2015)	Urban typology	Urban form	linear	NS	-	-	Temperate (Netherlands) –	Simulation + Field Validation	Simplified blocks & courtyards	Evaluation of the impact of urban forms (single, linear, courtyard) on outdoor thermal comfort in a temperate climate	ENVI-met 3.1 + RayMan 1.2	Ta, Tmrt, Rh, Ws, PET	Courtyard: Best performance. N–S linear: Acceptable. Singuler and E–W linear: Worst performance.		PET(number of comfortable	Courtyard (PET ≈ 20.8°C, 17h comfort)
				EW										27.2(4h)		
			singular	NS										26.4(2h)		
				EW										23.5(3h)		
			courtyard	-												

Table A-2 Previous studeis and optimal value for material facade

Ref-year of publication	Factor	Sub-variable	value	Other variables				Climate zone -season	Data collection	Urban area type	aim	Simulation/Modeling Tool	Measured Parameters (Ta,	Key Findings			Optimal value
				Orientation	Building height	Building Typology	Other variables							Note	Results	Output	
(Abrahem, Hassan and Khamees, 2020)	Type of building facade material	Finishing material	burnt clay bricks	-	Low-rise	Linear	Fixed urban layout, constant geometry	Hot and dry – Baghdad/summer (21July)	simulation	Residential building	Evaluation of the effect of facade materials of mass residential buildings (high-rise and low-rise) on external thermal comfort in a hot, dry climate	ENVI-met V4.4.4	Ta, MRT, RH (Specific humidity), Wind speed, PMV	-It is important to mention that The colors of all finishing materials analyzed here were light colors. -Burnt clay bricks, hollow concrete blocks with plaster finish, thermo-stone wall with plaster finish, glazed panels, and thermo-stone wall with granite finish, It is the arrangement of facade materials from worst to best.	Ta=32.45,PMV=4.39	Ta, PMV	The worst material was burnt clay brick. For low-rise buildings, glazed panels was the best material, while For high-rise buildings, granite finish (thermo-stone core) was better.
					High-rise										Ta=32.12,PMV=4.27		
			thermo-stone (with a thin layer of white cement rendering finish		Low-rise										Ta=31.86,PMV=4.24		
					High-rise										Ta=31.67,PMV=4.15		
			hollow concrete blocks		Low-rise										Ta=31.74,PMV=4.21		

Ref-year of publication	Factor	Sub-variable	value	Other variables				Climate zone -season	Data collection	Urban area type	aim	Simulation/Modeling Tool	Measured Parameters (Ta,	Key Findings			Optimal value
				Orientation	Building height	Building Typology	Other variables							Note	Results	Output	
					High-rise										Ta=31.54,PMV=4.11		
			glazed panels		Low-rise										Ta=31.55,PMV=4.13		
					High-rise										Ta=31.25,PMV=3.99		
			granite finish (thermo-stone core)		Low-rise										Ta=32.02,PMV=4.26		
					High-rise										Ta=28.23,PMV=3.19		
(Rosso *et al*	Material	envelope (E)and	Case R	NE - SW	Adjacent buildings of	--	**Albedo(**	Mediter	Field measure	Residential	Evaluating the impact of innovative materials on	ENVI-met	Ta, MRT	-H/W ≈ 3.5, no trees, stone façades, narrow	At 2pm Ta=32.6	**Ta**	**Case 7**: - Red IR mortar (vertical)

Ref-year of publication	Factor	Sub-variable	value	Other variables				Climate zone -season	Data collection	Urban area type	aim	Simulation/Modeling Tool	Measured Parameters (Ta,	Key Findings			Optimal value
				Orientation	Building height	Building Typology	Other variables							Note	Results	Output	
			E-marble P-Traditional stone		uniform height (≈18 m)						thermal comfort in historic urban canyons			street, high SVF sensitivity - Worst case is Case 5,6 (IR white mortar facade) due to high reflectivity at narrow facades. - Case 1 is worse than the reference case (excessive heat due to reflection from the interface)	At 2pm Ta=32.75		- Marble (horizontal)
			E-marble P-IR Gray												At 2pm Ta=31.5		
			E-IR red P-Traditional stone												At 2 pm Ta=32.4		
			E-IR red P-IR gray				Gray IR 0.3								At 2 pm Ta=31.125		

Ref-year of publication	Factor	Sub-variable	value	Other variables					Climate zone -season	Data collection	Urban area type	aim	Simulation/Modeling Tool	Measured Parameters (Ta,	Key Findings			Optimal value
				Orientation	Building height	Building Typology	Other variables								Note	Results	Output	
			E-IR white P-Traditional stone				Red IR mortar	0.4								At 2 pm Ta=32.87		
			E-IR white P-IR gray				White IR	0.66								At 2 pm Ta=32.81		
			E-IR red P-marble				Marble	0.59								At 2 pm Ta=31.12		
(Tabatabaei and Fayaz, 2023)	Facade materials &	Material type	Brick cream	In field measurements, traditional materials	Buildin g heights ranged from 3 to 21 meters, with an average	-	Color, texture, density, albedo, emissivity, thermal mass		Hot semi-arid (Shiraz, Iran) – Summer	Field measurement + simulation	Residential/commercial neighborhoods	Assess effect of façade materials and coatings on UHI mitigation & outdoor thermal comfort	ENVI-met 4.4.5	Ta, Ts, Rh, Ws, Tmrt, PET	-The vertical walls consisted of three layers: 11 cm thick bricks, 7 cm thick polystyrene insulation, and an external finishing	17		PET index(rank) simulation results	In both simulation and field measurement, living wall systems had the lowest temperature - BEST: GREEN WALL (in terms
			Brick red													14		
			Cement white													19		

Ref-year of publication	Factor	Sub-variable	value	Other variables				Climate zone -season	Data collection	Urban area type	aim	Simulation/Modeling Tool	Measured Parameters (Ta,	Key Findings			Optimal value
				Orientation	Building height	Building Typology	Other variables							Note	Results	Output	
			travertine white		of three floors (≈11.5 m), and the urban fabric included buildings of one to four floors.									layer of various facade materials. - Light, smooth, and high thermal mass materials are preferred in semi-arid climates. - Very high reflectivity materials (high albedo) such as white may lower Ts but raise PET due to increased Tmrt.	3		of thermal performance and comfort – PET). - An effective and relatively less expensive option: white travertine and white/cream marble. - Worst: brown ceramic, red brick, black granite. - Cream bricks (most commonly used in Shiraz) recorded the third highest temperature and PET values.
			travertine cream												12		
			travertine brown												13		
			Granite black												7		
			Granite gray												5		
			travertine gray												10		
			Ceramic brown												15		
			Ceramic-Cream												18		
			Marble-Cream												2		
			Marble-White												4		
			Aluminum composite - Gray												6		
			Concrete-multicolor												9		
			Porcelain-Cream												16		

Ref-year of publication	Factor	Sub-variable	value	Other variables				Climate zone -season	Data collection	Urban area type	aim	Simulation/Modeling Tool	Measured Parameters (Ta,	Key Findings			Optimal value
				Orientation	Building height	Building Typology	Other variables							Note	Results	Output	
			Porcelain-Gray												8		
			Artificial Stone-Beige												11		
			Living wall(modular-continuous)												1		
(Wonorahardjo *et al.*, 2022)	Façade systems	Material type(field measurement)	Brick wall	E	-	-		Tropical (Indonesia) – Summer (dry season)	Field measurements + Laboratory experiments	Office buildings	Assess effect of different façade systems on indoor comfort and outdoor UHI	Experimental (no simulation software)	Ts (surface temperature), Ta(air temperature)	-Brick facades are less thermally volatile than ACP and low-emissivity glass. -Monitoring shows that low-E glass recorded the highest Ts, while clear glass showed the lowest values on the 2nd building's western facade.	23.8-27.3	Ts (8-12)	- Bricks showed the lowest surface temperature (23.8–27.3°C) due to their high thermal inertia. - Low-E glass and ACP facades recorded the highest surface temperatures.
				W											24.5-27.3		
			Concrete wall(2nd building)	E											28.4-37.7		
				W											24.5-29.1		
			Clear glass(2nd building)	E											30-34		
				W											32.5-34		
			Low-E glass(1st-2nd building)	E											1st building 23.3-29.9 2nd building 32.4-37.6		
				W											1st building 25.1-28.6 2nd building 23.8-33.4		
			ACP	E											26.1-30.4		

Ref-year of publication	Factor	Sub-variable	value	Other variables				Climate zone -season	Data collection	Urban area type	aim	Simulation/Modeling Tool	Measured Parameters (Ta,	Key Findings			Optimal value
				Orientation	Building height	Building Typology	Other variables							Note	Results	Output	
				W											24.7-28.4		
		Material type(laboratory)	Brick+1cm newspaper ins	--			No air gap							- Adding an ACP facade may improve the interior but harm the exterior (increasing ambient air temperature) -	-	-	Brick wall+insulation+5 cm air gap For good indoor thermal comfort ACP +brick +insulation + air gap
			Brick+1cm newspaper ins				5cm air gap										
			Brick+1cm corn mat				No air gap										
			Brick+1cm corn mat				5cm air gap										
			ACP+1cm newspaper ins				3cm air gap										
			ACP+1cm newspaper ins				5cm air gap										

Ref-year of publication	Factor	Sub-variable	value	Other variables				Climate zone -season	Data collection	Urban area type	aim	Simulation/Modeling Tool	Measured Parameters (Ta,	Key Findings			Optimal value
				Orientation	Building height	Building Typology	Other variables							Note	Results	Output	
(Salvati et al., 2022)	Material	Urban albedo & façade/road reflectance	Road: SR=0.6 Road: SR=0.3 Façade: SR=0.6 Façade: SR=0.1 Façade: SR=0.3 Road: SR=0.6 Façade: SR=0.3	NS - E W	building height is 10 m at the eaves and 12 m at the ridge level,	linear (adjacent rows)	canyon aspect ratio between 0.63 and 0.75.	Temperate (London, UK) – summer heatwave (July 2019)	Field measurements + Physical 1:10 scale model + simulations	Residential canyons (3-storey terraced houses)	Assess impact of reflective materials on UCA, outdoor thermal comfort, and indoor environment	ENVI-met v4.4.6+ Energy Plus	Ta, MRT, PET, Radiation fluxes, Indoor Operative Temp	Increasing road albedo improves UHI mitigation but harms pedestrian comfort; indoor results mixed (slight benefit from cool façades in uninsulated, negative effect from cool roads)	-	PET	Best strategy: High road reflectance + Low façade reflectance (bottom part); Vegetated courtyards optimal for comfort

Ref-year of publication	Factor	Sub-variable	value	Other variables				Climate zone -season	Data collection	Urban area type	aim	Simulation/Modeling Tool	Measured Parameters (Ta,	Key Findings			Optimal value
				Orientation	Building height	Building Typology	Other variables							Note	Results	Output	
			Façade: SR=0.1														
(Lopez-Cabeza et al., 2022)	Material	Albedo(walls(w) and floors(F))(X LA: low albedo (under 0.3))(X MA: medium albedo (0.3–0.7))(X HA high albedo (above 0.7))(M W: Windows material, M GF: Green Facade Material)	Previous (State simulation wall: MHA, MMA, MW, pavement: PS)	-	The courtyard measures 5.2 × 6.9 m, with walls at least 5.0 m high	courtyard	aspect ratio of 1 and 0.7	Mediterranean (Csa) – hot summer	Field monitoring (2017, 2018) + ENVI-met validation & simulations	Educational building courtyard, Seville	Assess influence of surface albedo on microclimate and thermal comfort in small courtyards	ENVI-met v4.4.5 (validated with in-situ data, BioMet for PET)	Ta, Surface Temp, MRT, PET	-Results apply to small courtyards with low H/W and high solar exposure; shading/evaporative cooling still needed for comfort - Air temp differences negligible (≤0.2 °C). - Surface temps strongly reduced with high albedo (up to 25 °C cooler). - Wall albedo most influential on MRT & PET (high albedo ↑PET by +5 °C).	69.4	Max-PET	Pavement: high albedo (>0.7). Walls: medium albedo (~0.4).
			FHA(wall: MHA, MGF, MW, pavement: PHA)												69		

Ref-year of publication	Factor	Sub-variable	value	Other variables				Climate zone -season	Data collection	Urban area type	aim	Simulation/Modeling Tool	Measured Parameters (Ta,	Key Findings			Optimal value
				Orientation	Building height	Building Typology	Other variables							Note	Results	Output	
			FLA(wall: MHA, MGF, MW, pavement: PLA)											-In the simulation of wall albedo (W) variation, walls were considered as homogeneous opaque surfaces without windows to isolate only the effect of albedo on thermal performance and external thermal comfort.	69.2		
			FMA(wall: MHA, MGF, MW, pavement: PMA)												69		
			WHA(wall: MHA, pavement: PMA)												69.8		
			WLA(wall: MLA, pavement: PMA)												67.2		
			WMA(wall: MMA, pavement: PMA)												67.2		

Ref-year of publication	Factor	Sub-variable	value	Other variables				Climate zone -season	Data collection	Urban area type	aim	Simulation/Modeling Tool	Measured Parameters (Ta,	Key Findings			Optimal value
				Orientation	Building height	Building Typology	Other variables							Note	Results	Output	
			Best Case simulation(wall: MMA, MGF, MW, pavement: PHA)												66.2		
(Faragallah and Ragheb, 2022)	Paving materials	Ground cover types (Road Material)	Conventional asphalt/ Conventional interlock tiles	NS	Between 6 meters and 36 meters	-	Vegetation & water bodies(no)	Mediterranean – Summer (Alexandria, Egypt)	Simulation + validation (ENVI-met + meteorological station)	Dense urban street canyon (El Mosheir St.)	Evaluate effect of cool paving on UHI mitigation and pedestrian thermal comfort	ENVI-met 4.0	Ta ,Ws ,Rh	The results showed that cool pavements reduced air temperature by up to 3.5°C compared to the current situation, demonstrating their effectiveness as a sustainable strategy to reduce UHI and improve pedestrian thermal comfort.	27.72C 30.38C	Ta (min ,Max)	Basalt(road)+granite (pavement)+greenery + small water
			Conventional asphalt/ Conventional interlock tiles				Vegetation & water bodies(yes								27.58C 30.32C		
			Colored Asphalt/Brick				Vegetation &								27.16 C 29.53 C		
			Colored Asphalt/ Concrete grey color				Vegetation & water								26.89 C 28.52 C		

Ref-year of publication	Factor	Sub-variable	value	Other variables				Climate zone -season	Data collection	Urban area type	aim	Simulation/Modeling Tool	Measured Parameters (Ta,	Key Findings			Optimal value
				Orientation	Building height	Building Typology	Other variables							Note	Results	Output	
			Basalt/ Concrete light color				Vegetation &								25.92 C 27.14 C		
			Basalt/ Granite stones				Vegetation & water bodies(yes)								25.79 C 26.97 C		
(Yuan, Farnham and Emura, 2021)	Façade material	reflection type	DHR Diffuse highly reflective	-	Street width 20 m, H=40 m	block	different heights (0.1 m, 1.0 m, 1.5 m and 2.0 m)	humid subtropical climate-summer	simulation	-	Assess effect of DHR, SR, RR façade reflections on outdoor thermal environment and indoor loads	CFD (STREAM)	Ta, MRT, WBGT, SET*	SR and RR facades reduce MRT (~1.4°C), and cut indoor cooling loads by ~9–18%, but increase downward solar radiation and ground heat flux by 29–39% vs DHR	41.902	MRT (12pm)-1.5m height	SR and RR lower MRT compared to DHR (up to 1.4°C lower at noon).
			SR Specular reflective												40.452		
			RR Retro-reflective												40.879		

Table A-3 Diffrence between PET and UTCI index(Błazejczyk *et al.*, 2013; Walls, Parker and Walliss, 2015; Spaces and Liu, 2023)

Item	PET (Physiologically Equivalent Temperature)	UTCI (Universal Thermal Climate Index)
Physiological basis	Based on the Model of Energy Balance of the Human Body (MEMI)	Based on the Fiala multi-node physiological model
Unit	degree Celsius (°C)	degree Celsius (°C)
Calculation method	4 climate elements + uniform clothing and activity values	Ta, Tmrt, Wind Speed, Humidity + Integrated Dynamic Model
Reference conditions	Standard indoor environment (T_air = T_mrt, RH = 50%, air velocity = 0.1 m/s)	A person walks at 4 km/h, humidity 50%, T_mrt = Ta, wind 0.5 m/s
Main objective	Evaluate the equivalent thermal sensation outside as if it were inside.	Evaluate the equivalent thermal sensation outside as if it were inside.
climate resilience	Useful in temperate and hot climates	Designed to perform across all climates and seasons.
Indicator outputs	Expresses heat comfort or stress in terms of °C	The degree of "thermal stress" is expressed from heat stress to extreme cold.
range of ideal values	18–23°C (thermal comfort)	9–26°C (no heat stress)
spatial/temporal discrimination	Suitable for assessing differences within a city or park.	Suitable for comprehensive climate assessment (local, regional, global)

Appendix B

The study initially examined three major Palestinian cities—Ramallah, Hebron, and Bethlehem—to identify representative commercial street patterns. Field visits focused on street orientation, building height, street width, construction style, and façade materials. Across the three cities, the central commercial districts showed similar urban characteristics, despite differences in topography and minor climatic variations. Therefore, Hebron was selected as the main study area, with the intention that its findings could be extrapolated to comparable urban settings.

1-In Ramallah, commercial streets—such as those around Al-Sasha and Al-Manara—run mainly in N–S, E–W, and NE–SW directions. Buildings typically use stone, concrete, and glass, with occasional ACP cladding, and heights generally below ten floors.

Figure B-1 Photos of Ramallah site visite the streets.

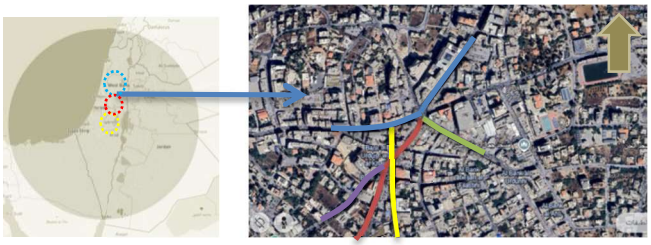

Figure B-2 Ramallah streets

2-In Hebron, street orientations vary (N–S, E–W, and NW–SE), and building heights range widely from around 6 to more than 30 meters. The city shows a transition from traditional stone buildings near Bab al-Zawiya to more modern materials and extensive use of glass and cladding.

Figure B-3 Photo for Hebron site visite streets

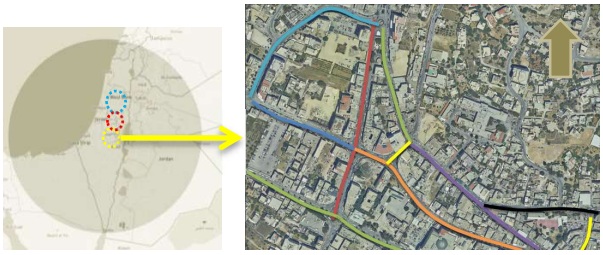

Figure B-4 Hebron streets

3- In Bethlehem, commercial streets around Madbasa Street and Manger Square are mainly oriented NW–SE and NE–SW. The materials transition from modern façades to the traditional forms approaching the Church of the Nativity, with some older façades covered by modern cladding.

Figure B-5 Photo for Bethlehem streets

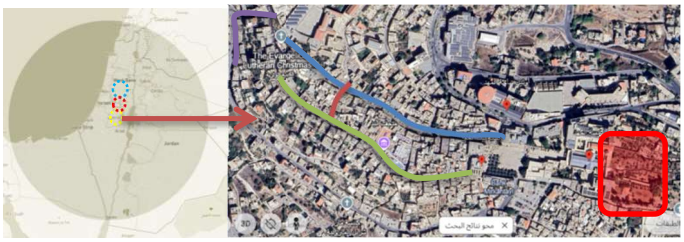

Figure B-6 Bethlehem streets and Church of the Nativity site

Based on the overall similarity of commercial districts and the rich variation of materials and orientations in Hebron, the city was chosen as the primary case study for analyzing façade materials, street orientation, and canyon geometry.

Thermal properties calculations:

The thermal properties of walls with more than three layers of building materials were calculated because the program only recognizes three layers in order to cover all the situations found in the streets, especially as in Crown Mall and facades with external cladding, where the thermal properties differed while the U value remained constant for facades with aluminum composite panels.

Density, thermal conductivity, specific heat, absorption, reflection, and transmittance are calculated using the following equations:

$$\rho total = \frac{\rho 1 * t1 + \rho 2 * t2}{t1 + t2}$$

ρ=density t=thickness

$$Ctotal = \frac{Cvol1 * t1 + Cvol2 * t2}{t1 + t2}$$

C= Specific heat capacity t=thickness

Thermal conductivity

$$Ri = \frac{di}{ki}$$

Where Ri =thermal resistance, di=thickness, Ki=thermal conductivity

K total=d total/R total

R total=R1+R2+R3+…….

Absorbance (α\alphaα): The fraction of incident radiation that is absorbed by the material.
Reflectance (R): The fraction of incident radiation that is reflected by the material (Tripathy, 2006).
Transmittance (T): The fraction of incident radiation that passes through the material.
For opaque materials (like most building walls), transmittance is typically zero, so:
α +R=1

α total≈(α1+α2+α3)/3

R total≈ (R1+R2+R3)/3

Examples:

For M1:

(t1=25cm, t2=20cm)(ρ1=2200, ρ2=2300)(C=1000, C2=1000)(Reflection: R1=0.017, R2=0.068)(Thermal conductivity K1=1.7, K2=1.75)

ρ Total = (2200*25+2300*20)/ (25+20)=2244.4=2244

Specific heat= (1000*25+1000*20)/45=1000

R1=25/1.7, R2=20/1.75

Thermal conductivity= (25+20)/ (R1+R2) =1.72

Absorption = (0.53+0.65)/2=0.59

Reflection = (0.47+0.35)/2=0.41

For M4:

(t1=3cm stone mortar,t2=0.8cmsteel,t3=20cm hollow block,t4=4cm polyurethane,t5=10cm hollow block)

(ρ1=2200, ρ2=1400, ρ3=42, ρ4=1400)(K1=1.4,K2=0.9,K3=0.025,K4=0.9)

(α1=0.73, α2=0.7, α3=0, α40.7)(R1=0.27, R2=0.3,R3=0,R4=0.3)

ρTOTAL= (2200*3) + (1400*20) + (42*4) + (1400*10)/0.378=1290

Specific heat=1000

Thermal conductivity=0.19

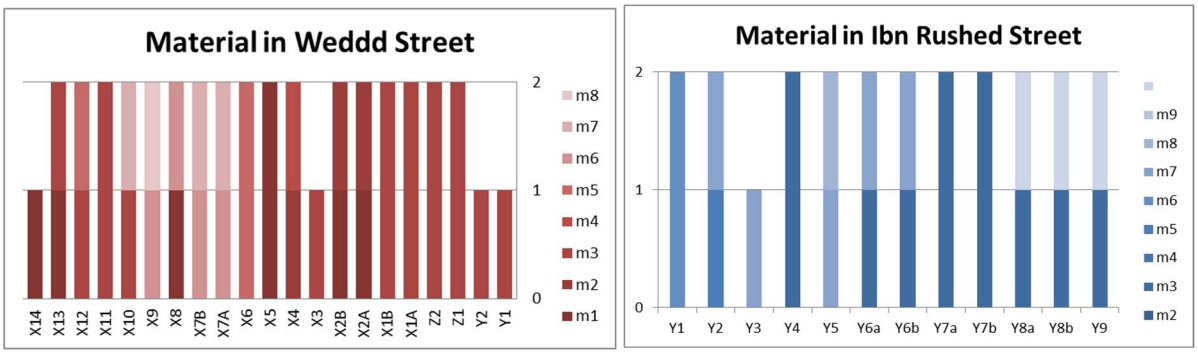

Figure B-7 Material used in two streets

The thermal properties of all materials were calculated and the results are presented in the Table B-1

Table B-1 Thermal proparties of material)Facility, 2004(

material	thickness cm	Density kg/m3	Thermal conductivity	Specific heat	Emissivity	absorption	reflection	Transmission
stone	5/7/10/20/25	2200	1.7	1000	0.9	0.53	0.47	0
stone	3	2200	1.7	1000	0.9	0.62	0.38	0
Reinforced concrete	15/20	2300	1.75	1000	0.91	0.65	0.35	0
plaster	2	1850	0.72	1000	0.93	0.73	0.27	0
Stone mortar	3	2200	1.4	1000	--	0.73	0.27	0
Blue glass	0.6	2500	1.05	750	0.92	0.12	0.26	0.62
Green glass	0.6	2500	1.05	750	0.92	0.18	0.2	0.62
I++(Glass)	0.6	2500	0.5	750				
For M1	45	2244	1.72	1000	0.9	0.59	0.41	0
For M2	35	2240	1.72	1000	0.9	0.59	0.41	0
For M3	20	2275	1.74	1000	0.9	0.6	0.4	0
For M4	37.8	1290	0.19	1000	0.9	0.71	0.29	0
For M5	22	2260	1.73	1000	0.9	0.6	0.4	0
For M6	25	2280	1.74	1000	0.9	0.6	0.4	0
For M7	25	2260	1.73	1000	0.9	0.6	0.4	0
For M8'	35	2250	1.72	1000	0.9	0.59	0.41	0
For M9	30	2267	1.74	1000	0.9	0.59	0.4	0
noor	40	2250	1.72	1000	0.9	0.6	0.4	0
Note: for M1,M2MM3….etc. the thermal properties calculated as shown in Appendices Appendix A								

Appendix C

- Anova - (Tukey HSD):

In this research, the One-Way ANOVA test was used to check whether there are statistically significant differences, especially in the outdoor thermal comfort variable (such as PET index or UTCI) and climate condition (such as temperature, wind speed, and relative humidity) between different groups of an independent variable (such as wall material type).

Table C-1 One way Anova Test variables

One way ANOVA test variable (Tukey HSD)	
Independent variable	Material
Dependent variable	Temperature, wind speed, relative humidity ,PET ,UTCI

-Null hypothesis (H_0): There are no statistically significant differences in the average outdoor thermal comfort values between groups.

- Alternative hypothesis (H_1): There are statistically significant differences in the average outdoor thermal comfort values between groups.

Decision Criteria:

The null hypothesis (H_0) is rejected when the p-value is less than the accepted significance level ($\alpha = 0.05$), indicating a statistically significant difference between

the groups.

If the p-value is greater than 0.05, the null hypothesis is not rejected, and it is assumed that there are no significant differences between the groups, and that the variance is due to random or natural causes.

Decision Criteria	
If the p-value is <0.05	We reject H_0 and accept H_1 ⇒ There is a moral difference
If p-value ≥ 0.05	We do not reject H_0 ⇒ There is no clear moral difference

The F-value in an ANOVA test tells us how strongly the independent variable (such as the type of material) affects the dependent variable (such as temperature).

$$F = \frac{Variance\ within\ groups}{variance\ between\ group}$$

The F-value helps us understand how statistically distinct the groups are.

If the F value is large, it means that the differences between groups are greater than the differences within each group, indicating that there is a potential real effect of the variable we are studying.

If the F value is small (close to or less than 1), it indicates that the differences between groups may be due to randomness, rather than an actual effect.

Although F gives us an idea of the size of the difference, we always need to consider the accompanying P value to determine whether the difference is statistically significant.

Tukey HSD Test

When the H_0 is rejected in an ANOVA test and there are statistically significant differences between groups, the Tukey HSD test (Honestly Significant Difference) is used as a post-hoc comparison tool.

This test aims to determine which pairs of groups differ significantly from each other by comparing the differences between the group means pairwise, taking into account the level of probability error (Type I error).

This test allows for a detailed picture of the differences between the studied cases and is one of the most commonly used after ANOVA due to its accuracy in controlling errors resulting from repeated comparisons.

Calculate the difference between each pair of means after use Anova test and check the result is significance then calculate HSD, and compare the difference between the means with the HSD value.

$$HSD = q\sqrt{\frac{MSE}{n}}$$

Where q: is the studentized range statistic, obtained from a table based on the significance level (α) and degrees of freedom.
MSE: is the Mean Square Error, which is an estimate of the variance within the groups and is typically derived from the ANOVA.
n: is the number of observations per group

If the difference in means is > HSD, the difference is significant.
A p-value is given for each comparison based on the q-distribution.
The test decision for each paired comparison is displayed in the results in a table containing a column labeled "reject."
If the value in this column is "True," it means that the difference between the two materials is statistically significant at the used significance level (usually 0.05). This means that there is sufficient evidence that one material affects thermal comfort differently than the other.
If the value is "False," it means that the difference between the two materials is not significant. Therefore, there is insufficient evidence to suggest that thermal performance differs between them at that specific time. (REF)
To study the effect of wall material on external thermal comfort in isolation from other variables, eight cases were identified that were similar in both facade orientation and facade-to-street ratio (height-to-width ratio H/W), while differing only in the type of wall material used.

These cases were simulated using ENVI-met software over four consecutive summer days: June 22, June 23, June 24, and June 27, to account for daily variations in climatic conditions. Values were recorded at five time intervals throughout the day: 8:00, 10:00, 12:00, 2:00, and 4:00 PM.

To increase the reliability of statistical results resulting from comparing different materials under similar conditions, this temporal and spatial replication was implemented by covering the thermal variations across the day.

- Correlation analysis:

A correlation analysis was conducted to investigate the relationship between thermal conditions (Ta, Ws, Rh, PET, and UTCI) and the independent variables (U-value) and the urban canyon (H/W).

To determine the strength and direction of the relationship The Pearson correlation coefficient (r) was calculated. A positive value of r indicates a direct relationship (as one variable increases, so does the other), while a negative r implies an inverse relationship.

Correlation coefficients were computed separately for different orientations and time intervals (8 am to 4 pm) to observe temporal variation in the relationship strength.

- Linear Regression analysis:

Regression analysis is a statistical method used to estimate the relationships among variables that exhibit a cause-and-effect relationship. The primary objective of univariate regression is to analyze the relationship between a dependent variable and a single independent variable, ultimately formulating a linear equation that represents this relationship. Regression models that feature a single dependent variable and multiple independent variables are referred to as multiple linear regressions. Regression analysis is conducted to ascertain the connection between two or more variables exhibiting a cause-and-effect relationship, and to facilitate predictions regarding the subject based on this relationship. (Uyanık and Güler, 2013) This study employed the model to examine the impact of independent variables such as material facade, orientation, and urban canyon on the dependent variable of thermal environment indicators as shown in Figure 3-12. The standard form of the multiple regression equation is:

$$y=\beta 0+\beta 1x1+\beta 2x2+\cdots\beta i+\varepsilon$$

Where $\beta 0$, $\beta 1,\cdots\beta i$ are partial regression coefficients; ε is the error term; $x1$ and $x2$ are urban canyon configuration; y is Ta, Ws, Rh and thermal comfort PET,UTCI value(dependent variable).

R^2 value: Shows how well your independent variables explain changes in the dependent variable.

P-values: If $p < 0.05$, the variable significantly affects PET.

Regression coefficients (b values): Show the effect of each variable.

Temperature, humidity, wind speed, PET, and UTCI for a given material with a given orientation and urban canyon at a specific hour can be predicted using a multiple linear regression equation. This is easy to analyze with multiple variables.

Coefficient Analysis:

Coefficient sign: If negative, the relationship is inverse, and if positive, the relationship is direct. Coefficient value: Represents the amount of change in the dependent variable when the dependent variable changes by one unit (holding all other variables constant).
The intercept ($\beta 0$) represents the expected value of the dependent variable when all independent variables = 0 (usually of limited meaning in reality but necessary for calculations).

Analyze the results:

- Analyzing the significance of the model as a whole:
  F-test:
  Null hypothesis (H_0): There is no relationship between temperature, wind speed, humidity, PET, UTCI, and the variables u-value, e/W. If the P value (Sig.) associated with $F < 0.05$, the model is statistically significant as a whole.
- Analysis of the significance of independent variables:
  P-value (Sig.) If $P < 0.05$
- Model strength and quality:
  R^2 Explains the proportion of variance in Y that is attributable to X1 and X2.
  Adjusted R^2 is corrected to take into account the number of variables and samples.
  If the difference between R^2 and Adjusted R^2 is large, the model may be over fitting or the number of samples is insufficient.

Multiple linear regression analysis was used to evaluate the influence of U-value and aspect ratio (H/W) as independent variables on a set of dependent variables: air temperature, wind speed, relative humidity, Physiological Thermal Comfort Index (PET), and Universal Comfort Index (UTCI). The analysis was performed using Excel to find predictive relationships between outdoor thermal comfort conditions and urban configuration and building materials.
The study data were systematically grouped and categorized based on facade orientation. Each orientation included in the study was analyzed independently to isolate its effect on local climate and thermal comfort indicators. As a result of this categorization, the sample size for each orientation ranged from 14 to 17 cases, a number considered statistically acceptable for regression analysis when there are a limited number of independent variables. This limitation was taken into account when interpreting the results. In addition,

given the variability of environmental conditions throughout the day, a regression analysis was conducted separately for each hour of measurement (8:00, 10:00, 12:00, 2:00, and 4:00 PM). This study aimed to investigate the temporal variations in the influence of urban and physical characteristics on climate variables.

The importance of the overall model was checked using the F test and by looking at the regression coefficients (B and Beta) for each independent variable one by one. The P-value was used to test the significance of the effect of each variable, with the adjusted R^2 used instead of the simple R^2, given its greater accuracy in small samples and models with limited variables.

The model's adherence to the basic assumptions of regression analysis was verified: linearity between the independent and dependent variables, normal distribution of residuals, and homoscedasticity. These factors were considered to ensure the validity of the statistical model and the accuracy of its results, taking into account limitations related to sample size and data stratification by direction and time.

Appendix D-1

Table D1-1 Data measere and simulation of case study at three diffrent times (TA, RH, and W)

IBN rushed & Wedded street/1/11/2024(7-8am/2-3pm/4-5)								
point	**Time**	**Building name**	**Air temperature (c°)**		**Relative humidity%**		**Wind speed(m/s)**	
			measure	simulation	measure	simulation	measure	simulation
1	7:00am	Al Jab- shoes	18.8	19.7	61	75.3	0.36	0.38
2	7:05am	Hebron center	19.3	19.5	61	76.2	0.59	0.58
3	7:10am	Crown mall	18.7	19.8	61	75.3	0.75	0.7
4	7:15am	library	19.4	20.1	61	74.9	0.39	0.33
5	7:20am	Reyad mall	17.9	20.6	59	73.5	1.56	1.4
6	7:25am	Falafel natsheh	18.0	20.9	59	72.4	0.6	1.02
7	7:30am	Qudsi center	17.8	21.0	58	71.8	0.09	0.19
8	7:35am	Burhan style	19.6	21.0	58	72.2	0.22	0.40
1	1:47pm	Al Jabari shoes	25.2	29.7	49	43.6	0.55	0.19
2	1:50pm	Hebron center	25.4	29.2	47	46.2	0.59	0.52
3	1:53pm	Crown	26.6	30.2	45	44.2	0.85	0.83
4	1:56pm	library	27.5	30.4	41	43.8	0.72	0.73
5	1:58pm	Reyad mall/	26	30.6	41	41.0	0.92	1.27
6	2:00pm	falafel	26.9	29.7	41	44.3	0.8	1.6
7	2:5pm	Qudsi center	27.3	29.2	40	44.2	0.26	0.23
8	2:10pm	Burhan style	26.8	29.3	40	45.1	0.5	0.21
1	4:52pm	Al Jabari shoes	23	27.2	49	52.4	0.5	0.43
2	4:56pm	Hebron center	22.6	26.8	50	54.3	0.39	0.47
3	5:00pm	Crown	21.3	27.04	51	54.1	1.08	1.15
4	5:5pm	library	21.9	27.2	53	53.5	1.22	1.46
5	5:10pm	Reyad mall	21.8	27.6	52	52.4	0.56	1.24
6	5:15pm	falafel	22.3	27.3	53	53.6	1.2	1.94
7	5:20pm	Qudsi center	23.1	26.3	54	56.6	1.2	1.06
8	5:25pm	Burhan style	22.4	26.5	54	56.3	0.42	0.81
verifaction result of two section in the site								
Wedded street (13/6/2025 (11:30 am)								
Temperature/section 1								

Location at measurement point 3	Measured	Simulation
Left(Zamzm)	32.5	31.14
Middle	32.5	31.12
Right(Zeina shop)	31.6	30.9
Temperature/section 2		
Left(Murad kids)	32.7	31.14
Middle	31.9	31.13
Right(Crown mall)	31.2	30.8

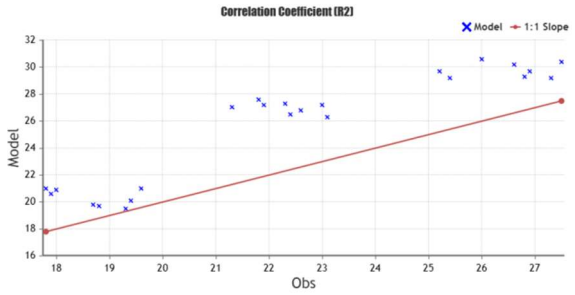

Figure D1-1 Scatter chart of coefficient of determination (R2) comparing the hourly average air temperatures that were simulated and observed.

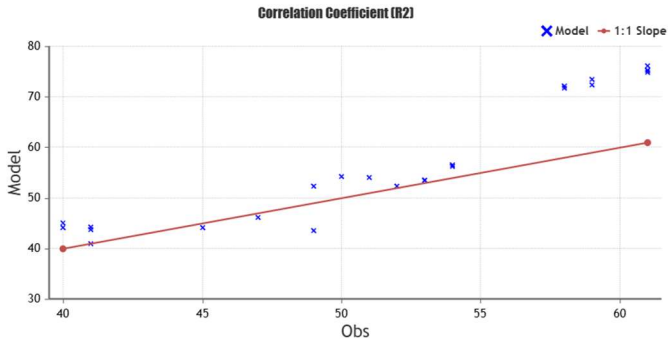

Figure D1-2 Scatter chart of coefficient of determination (R2) comparing the hourly average humidity that were simulated and observed.

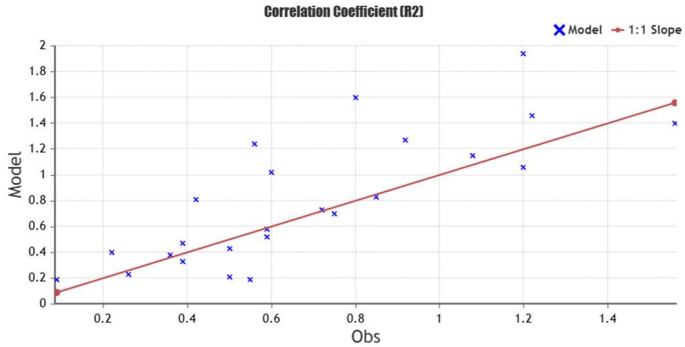

Figure D1-3 Scatter chart of coefficient of determination (R2) comparing the hourly average wind speed that were simulated and observed.

Appendix D-2

This appendix contains the complete numerical results and detailed case-by-case interpretations that support the summary presented in Chapter 4. To avoid overloading the main

text, full tables and fine-grained analyses for each street, side, and canyon configuration are reported here.

Microclimatic Conditions (Temperature, Wind Speed, and Humidity)-summer:

a) Weddad street:

The simulation results showed that Wadded Street exhibited a regular temperature gradient throughout the day, with an average temperature of approximately 25°C at 8:00 AM, gradually rising to around 28°C at 10:00 AM and 32°C at 12:00 PM, before reaching approximately 34°C at 2:00 PM, then dropping slightly to around 33°C at 4:00 PM. Wind speed was low in the morning (approximately 0.5 m/s), but increased significantly during the day, reaching around 2.0 m/s at midday and peaking at 2.3–2.5 m/s at 2:00 PM, with good ventilation continuing into the afternoon. Relative humidity was relatively high in the morning (55–59%), then decreased as the temperature rose, reaching around 31% at 2:00 PM, before increasing slightly in the afternoon (34–36%), with limited variations between sides due to improved ventilation within the street.

b) Ibn rushed street:

The results showed that the average air temperature on Ibn Rushd Street was relatively mild in the morning, reaching approximately 26°C at 8:00, then rising rapidly to about 29.2°C at 10:00 and 33.4°C at 12:00, before peaking at around 34°C at 14:00 and dropping slightly to about 33.5°C at 16:00. Wind speed was low in the morning (≈0.5 m/s), then gradually increased with the rising temperature, reaching about 1.0 m/s at 10:00 and peaking at 1.5 m/s during the heat peak (14:00), particularly in the middle of the street. Relative humidity was relatively high in the morning (53–56%), then decreased significantly with the rising temperature, reaching its lowest point at 14:00 and remaining low in the afternoon (around 34% at 16:00). Slight differences were also observed between the sides depending on solar exposure, with the hotter sides recording lower relative humidity, reflecting the inverse relationship between temperature and humidity during daylight hours.

c) Al Haymoni:

The results showed that the temperature on Al-Himuni Street was around 26°C at 8:00, then rose to about 29°C at 10:00, and reached 33°C at noon, peaking between 34–35°C at 14:00 before dropping to about 33°C at 16:00. The wind speed was highest in the morning hours, recording about 1.3 m/s, and then gradually decreased during the period from 10:00 to 12:00

to range between 1.1–1.3 m/s, with higher values recorded in the middle of the street, especially in the east-west direction. Relative humidity recorded high values in the morning (55–60%), then gradually decreased to about 33% at 12:00, and reached its lowest levels at 14:00 (27–29%), before rising again in the afternoon to about 33–34%, reflecting the inverse relationship between temperature and humidity during the day.

This appendix presents the full numerical outputs from the ENVI-met simulations for the three case-study streets (Weddad, Ibn Rushed, and Al-Haymoni).

Table D2-1 Summury of wind speed results in summer in three streets

Standard	Weddad	Ibn rushed	Himonies
Maximum wind speed (M)	4.21m/s(X1/45) at 4p.m	4.69m/s(Y1)at 4p.m	3.87m/s(Y1/15)4p.m
Distribution uniformity	Irregular (high variability)	relatively regular	relatively regular
Wind speed in (M)	Good in some sections	Very good most of the day	Very good
Wind speed in (R/L)	Varying (some very weak)	Acceptable to good	Acceptable to good

Table D2-2 Two street result in summer 22-Jun

Weddad street and Himonies street Note:Y1/15 -Y2/25 - Z1/85 - Z2/75 are point for Himonies street	Ibn rushed street
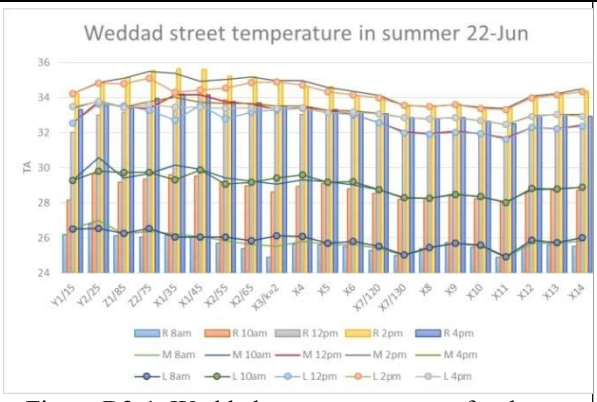	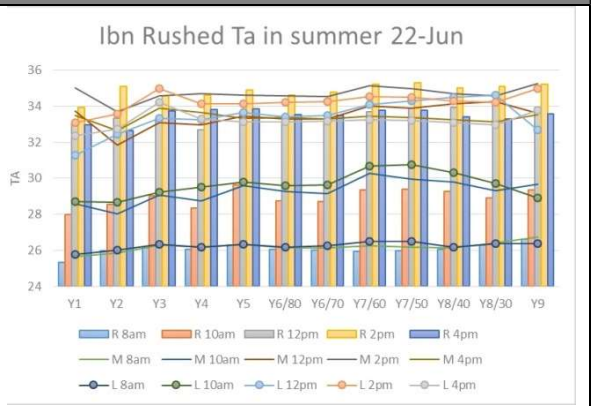
Figure D2-1 Weddad street temperature for three sides in summer	Figure D2-2Ibn rushed Ta summer result for three sides
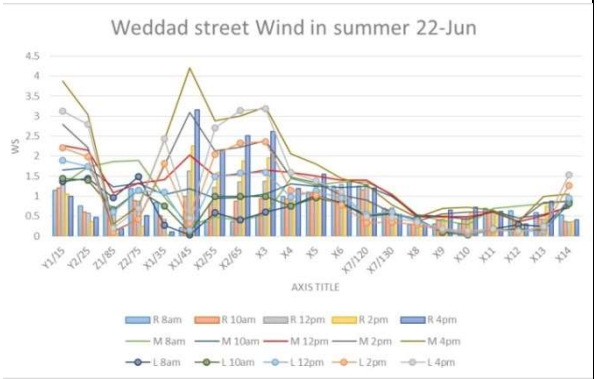	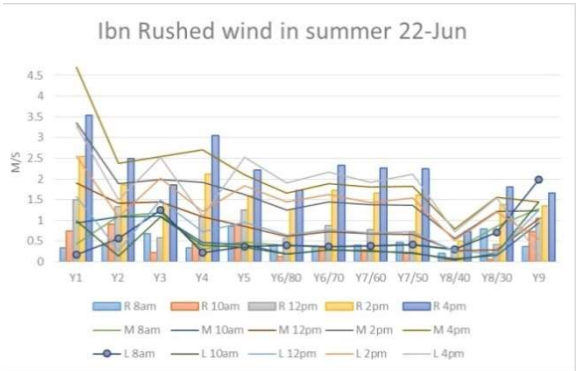
Figure D2-3 Weddad street wind speed for three sides in summer	Figure D2-4 Ibn rushed street wind speed for three sides

Weddad street and Himonies street Note:Y1/15 -Y2/25 - Z1/85 - Z2/75 are point for Himonies street	Ibn rushed street
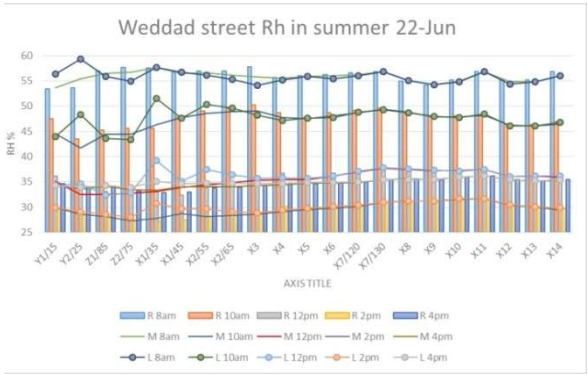	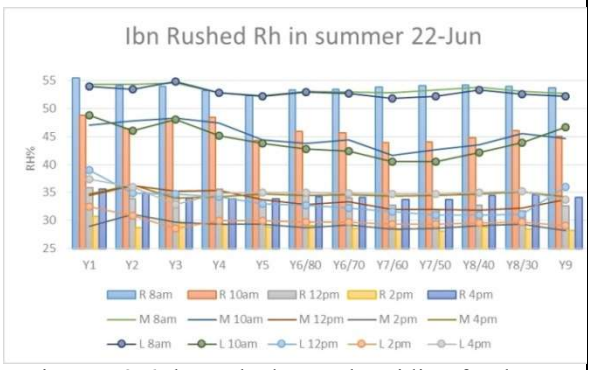
Figure D2-5 Weddad street relative humidity for three sides in summer	Figure D2-6 Ibn rushed street humidity for three sides
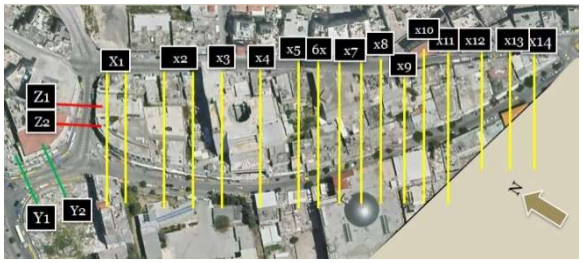	

Analysis of the climatic variables along the street revealed that temperatures remained relatively uniform across both sides and the middle , ranging from 25.5 to 25.7°C at 8:00 AM, gradually rising to approximately 28.8°C at 10:00 AM, peaking at midday (≈32.7°C) and 2:00 PM (≈34.3°C), before decreasing slightly at 4:00 PM. Relative humidity was highest in the morning (≈56%) and decreased significantly with the rising temperature, reaching approximately 36% at midday and around 30% at 2:00 PM, with a slight increase again at 4:00 PM, while dispersion remained low throughout. In contrast, wind speed showed greater variation. It started low in the morning (0.62–0.79 m/s) and gradually increased towards midday, recording its highest values at 4:00 pm (up to 1.65 m/s), with a relatively high standard deviation throughout the day, reflecting a clear difference in ventilation between sections and a direct effect on thermal perception as shown in TableD2-3.

TableD2-3 summary of Microclimatic Conditions of Weddad streets by time of day in Weddad street in summer

Weddad street 22/6									
Factors	**Air temperature (°C)**			**Relative humidity (%)**			**Wind speed (m/s)**		
Output	Max ,min ,mean ,SD			Max ,min ,mean ,SD			Max ,min ,mean ,SD		
time	Left	Right	Mid	Left	Right	Mid	Left	Right	Mid
8 A.M.	Min:24.92,max:26.11,mean:25.73,SD:0.35	Min:24.87,max:26.15,mean:25.49,SD:0.35	Min:24.9,max:26.21,mean:25.61,SD:0.33	Min:54.1,max:57.8,mean:56.22,SD:1.01	Min:54.18,max:57.8,mean:56.22,SD:1.01	Min:54.2,max:57.67,mean:55.88,SD:0.88	Min:0.03,max:1.49,mean:0.62,SD:0.45	Min:0.22,max:1.25,mean:0.64,SD:0.34	Min:0.26,max:1.45,mean:0.79,SD:0.39
10 A.M.	Min:28,max:29.88,mean:28.9,SD:0.51	Min:28.08,max:29.58,mean:28.73,SD:0.44	Min:28.04,max:30.14,mean:28.92,SD:0.57	Min: 45.57 max: 50.2,mean:48.15,SD:1.26	Min:45.57,max:50.2,mean:48.15,SD:1.26	Min:46.1,max:49.4,mean:47.85,SD:1.03	Min:0.03,max:1.45 mean:0.66,SD:0.43	Min:0.3,max:1.16,mean:0.70SD:0.3	Min:0.43,max:1.31,mean:0.88,SD:0.31
12 P.M.	Min:31.63,max:33.55,mean:32.58,SD:0.59	Min:31.72,max:34.3,mean:32.7,SD:0.77	Min:31.68,max:34.16,mean:32.8,SD:0.82	Min: 32.4,max:37.6,mean:35.93,SD:1.61	Min:32.4, max:37.6, mean:35.93,SD:1.6	Min:33.045,max:37.7,mean:35.92,SD:1.34	Min:0.05, max:1.9, mean:0.83,SD:0.6	Min:0.29, max:1.62,mean:0.85,SD:0.47	Min:0.36, max:2.03, mean:1.10,SD:0.53
2 P.M.	Min:33.29,max:34.89,mean:34.1,SD:0.50	Min:33.42,max:35.62,mean:34.35,SD:0.74	Min:33.36,max:35.36,mean:34.32,SD:0.66	Min:27.15,max:31.6,mean:29.7,SD:1.4	Min:27.15,max:31.6,mean:29.75,SD:1.41	Min:27.28max:31.6,mean:29.77,SD:1.24	Min:0.09, max:2.36,mean:0.93,SD:0.85	Min:0.034,max:2.25,mean:0.9,SD:0.65	Min:0.38, max:3.1, mean:1.24,SD:0.81
4 P.M.	Min:32.45,max:33.44,mean:33.07,SD:0.30	Min:32.5 max:34.18,mean:33.22,SD:0.5	Min:32.47,max:34.01,mean:33.1,SD:0.42	Min:33.82,max:36.2,mean:34.78,SD:0.96	Min:32.82max:36.2,mean:34.8,SD:0.96	Min:33.29,max:36.2,mean:34.85,SD:0.79	Min:0.12, max:3.18,mean:1.26,SD:1.16	Min:0.11 max:3.16,mean:1.19,SD:0.91	Min:0.37, max:4.21,mean:1.65,SD:1.13

As shown in Table D2-4 , air temperature exhibited a clear and consistent rise throughout the day, beginning with stable and closely aligned values at 8:00 AM (26.06–26.25°C) and increasing to about 28.9°C at 10:00 AM, before reaching higher and nearly identical levels at midday (≈33.4°C). Temperatures peaked at 2:00 PM (34.23–34.85°C) and then declined slightly by 4:00 PM. The low standard deviation across all periods indicates thermal uniformity along the street. Relative humidity displayed an inverse trend, starting higher in the morning (≈53–54%) and decreasing steadily toward midday (≈33%) and early afternoon (≈29%), with a slight increase at 4:00 PM; yet variability remained low, confirming stable humidity distribution. Wind speed showed the highest spatial and temporal variability, beginning with moderate turbulence at 8:00 AM (0.46–0.60 m/s), increasing slightly at 10:00 AM, and peaking between noon and 2:00 PM (0.70–1.70 m/s), before reaching its maximum at 4:00 PM (up to 2.30 m/s). Unlike temperature and humidity, wind conditions were marked by notable

fluctuations—particularly between 10:00 AM and 12:00 PM—reflecting unstable ventilation patterns that influence thermal comfort along the canyon.

Table D2-4 summary of Microclimatic Conditions by time of day in Ibn rushed street in summer

Ibn rushed street 22/6									
Factors	**Air temperature (°C)**			**Relative humidity (%)**			**Wind speed (m/s)**		
time	Left	Right	Mid	Left	Right	Mid	Left	Right	Mid
Output	Max ,min ,mean ,SD								
8 A.M.	Min:25.77,max:26.52 ,mean:26.25,SD:0.2	Min:25.32,max:26.61, mean:26.06,SD:0.3	Min:25.66,max:26.42,mean:26.15,SD:0.21	Min:51.76,max:54.78,mean:52.89,SD:0.85	Min:52.35,max:55.47,mean:53.79,SD:0.74	Min:52.28,max:54.55,mean:53.31,SD:0.72	Min:0.17, max:1.98, mean:0.59,SD:0.52	Min:0.21, max:0.86, mean:.46, SD:0.19	Min:0.28, max:1.28, mean:0.6, SD:0.36
10 A.M.	Min:28.68,max:30.77,mean:29.63,SD:0.69	Min:27.97,max:29.65,mean:28.9,SD:0.49	Min:28.04,max:30.29 ,mean:29.26,SD:0.64	Min:40.53,max:48.85 ,mean:44.23,SD:2.7	Min:43.95,max:48.76 ,mean:45.92,SD:01.67	Min:41.58,max:48.35,mean:45.11,SD:2.15	Min:0.04, max:1.44 mean:0.46,SD:0.44	Min:0.05 max:0.9 ,mean:0.4 SD:0.32	Min:0.08, max:1.1, mean:0.5, SD:0.93
12 P.M.	Min:31.29,max:34.61 ,mean:33.41,SD:0.95	Min:32.72,max:34.25,mean:33.49,SD:0.46	Min:31.85,max:34.27 ,mean:33.44,SD:0.68	Min:30.93,max:38.95,mean:33.44SD:2.41	Min:31.75,max:35.84 ,mean:33.56SD:1.31	Min:31.85,max:36.18 ,mean:33.57 SD:1.47	Min:0.2, max:1.58 ,mean:0.7 SD:0.45	Min:0.25, max:1.5 ,mean:0.8 SD:0.38	Min:0.27, max:2.03 ,mean:0.99SD:0.54
2 P.M.	Min:33.07,max:34.98,mean:34.23,SD:0.52	Min:33.92,max:35.28,mean:34.85,SD:0.38	Min:33.7, max:35.14,mean:34.64,SD:0.37	Min:28.61,max:32.51 mean:29.85 SD:1	Min:28.1, max:23.69,mean:28.87SD:0.7	Min:28.16,max:31.1,mean:29.15 SD:0.75	Min:0.52, max:2.56, mean:1.42SD:0.57	Min:0.5, max:2.54, mean:1.58SD:0.49	Min:0.56, max:3.51, mean:1.7 SD:0.8
4 P.M.	Min:32.36,max:34.23 ,mean:33.19,SD:0.46	Min:32.64max:33.83,mean:33.48,SD:0.36	Min:32.64,max:33.89 ,mean:33.34,SD:0.31	Min:32.82max:37.42,mean:34.95,SD:1.1	Min:33.75,max:35.67 ,mean:34.28,SD:0.56	Min:33.94,max:36.34,mean:34.67,SD:0.6	Min:0.17 max:3.28, mean:1.7, SD:0.84	Min:0.72 max:3.53 ,mean:2.15 SD:0.71	Min:0.79, max:4.88 ,mean:2.3 ,SD:1.16

Effect of H/W Ratio on Air Temperature (Ta), wind speed, and relative humidity:

This appendix presents a quantitative summary of the effect of the height-to-width ratio (H/W) on air temperature (Ta), wind speed (Ws), and relative humidity (RH) in Weddad and Ibn Rushed Streets during the summer season. For temperature and humidity, the critical time was mainly 12:00 p.m., while wind speed exhibited its largest variation at 4:00 p.m. (unless otherwise stated). Haymoni Street points were excluded from this subsection. The values reported below are extracted from the detailed analyses and tables presented below and are provided here to support comparative reference.

Note: The numerical ranges and differences reported in this appendix provide a concise quantitative reference to the detailed tables and figures presented for Weddad and Ibn Rushed Streets. These values are intended to support cross-comparison and validation of trends discussed in the main text without repeating interpretive analysis.

a) Weddad Street:

Temperature varied across the right side, left side, and street middle. On the right side, the maximum temperature was 34.3°C at M3f-W-C6 (H/W=1.1), while the minimum was 31.7°C at M3i-SW-C11 (H/W=1.8), producing the largest reported difference of 2.58°C for the same material (M3), explained by the combined effect of orientation and H/W. For M1, increasing H/W from 0.6 to 3.8 reduced Ta from 33.25°C to 31.97°C (Δ 1.28°C). Similarly, for M2 (U=2.504), increasing H/W from 0.6 to 3.8 reduced Ta from 33.87°C to 32.09°C (Δ 1.78°C). A notable case is M2d-SW-C0 (H/W=0) with 32.29°C, attributed to openness and ventilation despite limited shade; however, the best overall performance for M2 remained near H/W=3.8. For M3, Ta decreased with higher H/W and improved shading, with ratios of 1.5–2.0 generally outperforming H/W≈1.1. An exception was observed when a missing opposite façade increased ventilation: at M3g-W-C0 (H/W=0) the temperature was lower than the H/W=1.1 cases due to higher wind speed. For M7 (U=2.934), Ta decreased by about 0.5°C when H/W increased from 3 to 3.8, supporting the shading effect in deep canyons. On the left side, the trend also indicated lower temperature with higher H/W for conductive materials. For example, M3 recorded 33.55°C (m3d-E-C6) versus 31.63°C (m3e-NE-C12) (Δ 1.92°C). Under similar H/W, the E façade was ~1.35°C warmer than the NE façade, showing strong orientation influence. Additionally, increasing H/W in some E-oriented cases increased Ta (e.g., 32.72°C, at H/W=0.6 to 33.55°C, at H/W=1.1), indicating that shading was insufficient to offset reduced ventilation and heat accumulation under pre-noon solar exposure. For M6, the lowest values were reported around H/W=1.5–1.6 (~31.9°C), whereas H/W=0.8 showed higher temperature; in open regions, H/W=1.1 was 0.93°C lower than H/W=0.4. At the street center, Ta ranged from 34.16°C (X1/45) to 31.68°C (X11) (Δ 2.48°C). The lowest center temperature coincided with high H/W + NE orientation and coordinated shading from both sides (e.g., X11: center 31.68°C, right 31.68°C, left 31.63°C with M3). In contrast, low H/W and W/SW exposure increased solar penetration and raised center temperature (e.g., X1/45).

Wind speed was assessed mainly at the façade level (right and left) and at the street center. For M1, Ws dropped from 1.55 m/s (H/W=0.8) to 0.30 m/s (H/W=3.8), with an intermediate value around 0.88 m/s (H/W=2.1), confirming reduced ventilation in deeper canyons. For M2, the highest Ws occurred at H/W=0.6–0.8 (2.13–2.51 m/s), while it decreased at H/W=3.8 (0.65

m/s) and also remained low in fully open areas H/W=0 (0.41 m/s) due to possible flow separation. For M3, the range was wide (0.11–3.16 m/s), with a peak at H/W≈1.1 (M3f-W-C6) and also high values in open conditions (e.g., H/W=0 to 2.62 m/s), indicating local acceleration effects. On the left side, the highest Ws reached 3.14 m/s in M1b-NE-C4 (H/W≈0.6–0.8), while M3 ranged from 2.44 m/s (H/W=0.6) down to 0.18 m/s (H/W=1.9). Some cases (e.g., M5) showed ~1.0 m/s differences under identical H/W, indicating the role of local configuration. At the open region (no c, no d), the high H/W (1.1) recorded a wind speed 1.54m/s lower than the case with H/W = 0.4, supporting the general pattern. At the middle of street, Ws ranged from 4.21 m/s (X1/45) to 0.37 m/s (X12), reflecting the combined effects of H/W, orientation relative to prevailing winds, and street-network position. In the case of X1/45, the highest wind speeds were recorded in the center of the street and near the prevailing westward face, while they decreased sharply on the eastward face due to the blocking effect, with the central flow enhanced by air acceleration between the air masses. In the case of X12, the aerodynamic performance was poor at all locations due to the misalignment of the orientation with the prevailing wind and the location of the measurement point at the end of the street with limited permeability.

On the right side, RH for M1 (SW) increased from 35.6% (H/W=0.6) to 37.4% (H/W=3.8) (Δ 1.8%). M2 followed a similar pattern (e.g., up to ~37.1% at higher H/W). For M3, the trend depended on orientation: on W facades, RH decreased from 35.6% (H/W=0) to 32.4% (H/W=1.2), while on SW the relationship differed due to radiation and evaporation dynamics. On the left side, M3 decreased from 39.25% (H/W=0.6) to 35.1% (H/W=1.1), with NE around 36.1% at H/W=0.9. At the middle of street, RH ranged from 37.7% (X7/130, H/W>1) to 33.04% (X1/35, H/W<1).

Table D2-5 M1,M3,M5,M6,no M temperature ,wind apeed,relative humidity results in Weddad street for left side in summer

	Case	H/W	Façade orientation	Ta 12pm	Ws 4pm	Rh
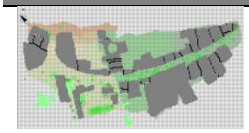	X2/55-M1a-NE-C4	0.8	NE	32.78	2.71	37.5%
	X2/65-M1b-NE-C4	0.8	NE	33.15	3.14	36.4%
	X5-M1c-NE-C3	0.6	NE	33.14	1.39	35.7%
	X1/35-M3c-E-C3	0.6	E	32.72	2.44	39.25%
	X1/45-M3d-E-C6	1.1	E	33.55	0.45	35.1%

	Case	H/W	Façade orientation	Ta 12pm	Ws 4pm	Rh
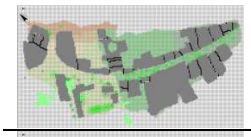	X11-M3e-NE-C12	1.9	NE	31.63	0.18	37.5%
	X13-M3f-NE-C5	0.9	NE	32.2	0.25	36.1%
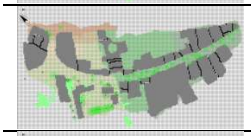	X6-M5a-NE-C6	1.1	NE	33.01	1.11	36.2%
	X12-M5b-NE-C6	1.1	NE	32.3	0.12	36%
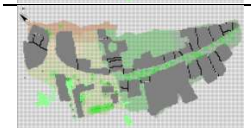	X7/120-M6a-NE-C8	1.3	NE	32.55	0.49	37.1%
	X7/130-M6b-NE-C10	1.6	NE	31.98	0.47	37.8%
	X8-M6c-NE-C9	1.5	NE	31.91	0.35	37.6%
	X9-M6d-NE-C4	0.8	NE	32.01	0.19	37.3%
	X10-M6e-NE-C5	0.9	NE	31.95	0.14	37.1%
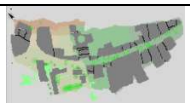	X3-noc-NE-C2	0.4	NE	33.3	3.18	35.7%
	X14-nod-NE-C6	1.1	NE	32.37	1.54	36.1%

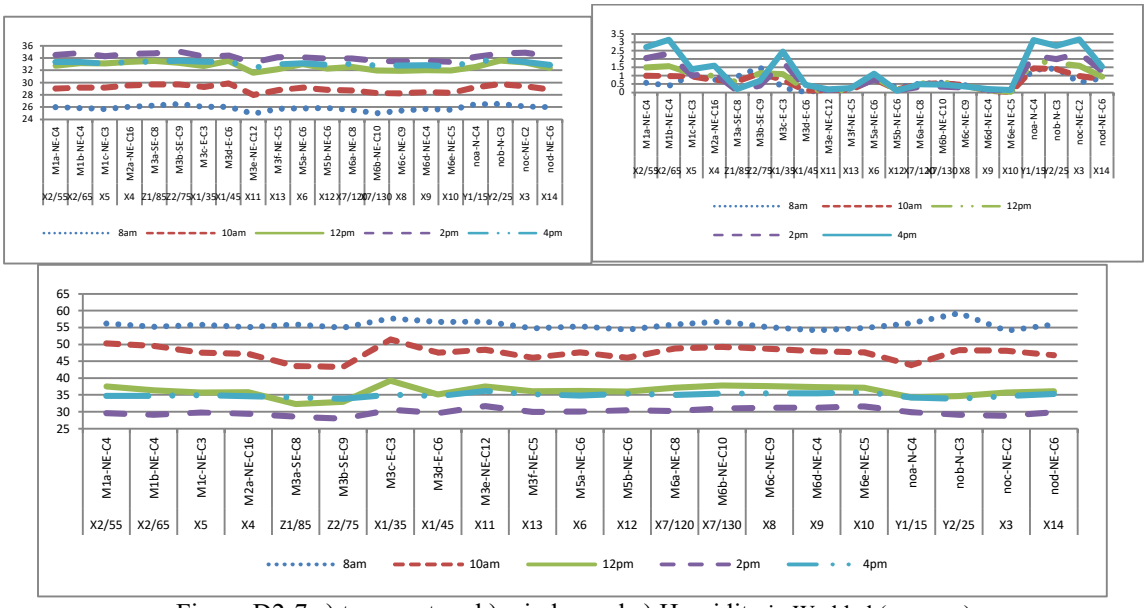

Figure D2-7 a) temperature b) wind speed c) Humidity in Weddad (summer)

Table D2-6 X1/45-X2/55 wind speed result in summer at 4pm

layout	Location	H/W	orientation	Wind speed 4pm
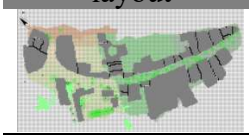	Right	1.1	W	3.16 m/s
	Middle	-	-	4.21 m/s
	Left	1.1	E	0.45 m/s
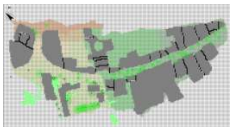	Right	0.6	W	2.13 m/s
	Middle	–	–	2.88 m/s
	Left	0.8	NE	2.71 m/s

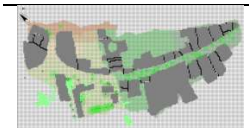	Right	0.4	SW	0.31 m/s
	Middle	–	–	0.37 m/s
	Left	1.1	NE	0.12 m/s

a) Ibn rushed:

On the right side (W orientation) for M3, Ta increased with H/W: 32.7°C (H/W=0.6) to 34.25°C (H/W=1.2) (Δ 1.55°C), with intermediate cases around 33.68–33.92°C (H/W=0.8) and 33.93–34.25°C (H/W=1.1–1.2). For M7 (W), the variation was minimal: 33.23°C (H/W=0.0) versus 33.12–33.16°C (H/W=0.9) (Δ <0.2°C). On the left side, Ta ranged from 34.61°C (M9a-E-C4, H/W=0.8) and 34.31°C (M3e-E-C3, H/W=0.6) down to 31.29°C (M6a-E-C7, H/W=1.2) (Δ 3.32°C). For M3, higher H/W reduced Ta (e.g., 33.23–33.47°C, at H/W=1.1 vs. 34.10–34.31°C, at H/W=0.6). For M7, Ta increased from 32.46°C (H/W=0.4) to 33.65°C (H/W=0.6) (Δ 1.19°C). For M9, Ta increased from 32.68°C (H/W=0.6) to 34.50–34.61°C (H/W=0.8) (Δ ~1.9°C). At the street center, Ta ranged from 34.27°C (Y8/30) to 31.85°C (Y2) (Δ 2.42°C), reflecting the combined influence of both sides.

On the right side, Wind speed ranged from 3.53 m/s (M6a-W-C6) to 0.72 m/s (M3d-W-C6) despite identical H/W (1.1), attributed to measurement location (entrance/intersection vs. end segment) and material differences. For M3, Ws decreased as H/W increased: 3.05 m/s (H/W=0.6) to ~2.2 m/s (H/W=0.8) to 0.72–1.80 m/s (H/W=1.1–1.2). For M7, Ws varied between 2.32 m/s and 1.73 m/s at H/W=0.9, while the open case H/W=0 recorded 1.86 m/s. On the left side, Ws ranged from 3.28 m/s down to 0.17 m/s, with higher values generally associated with lower H/W (e.g., ~1.92–2.12 m/s at H/W=0.6 for M3). For M7, Ws increased from 1.49 m/s (H/W=0.4) to 2.52 m/s (H/W=0.6). For M9, maximum values at H/W=0.8 reached 1.54 m/s. In the middle, Ws peaked at 4.7 m/s (Y1) in open configurations, while very low values (0.08–0.79 m/s) occurred in enclosed sections (e.g., Y8/40). The right side has a higher flow than the left, but the middle outperforms. The difference suggests a centripetal acceleration caused by the influence of wind channels within the urban valley, and the longitudinal configuration of the street may be the cause. There is also a green area (Ibn Rushed Square) in the center.

The largest RH variation occurred on the right side at 10:00 a.m. RH ranged from 48.76% (M6a-W-C6) to 43.95% (M3b-W-C4) (Δ 4.81%). For M3, RH was highest at H/W=0.6 (48.46%), decreased to 43.95–45.04% at H/W=0.8, then increased slightly to 44.79–46.00% at H/W=1.1–1.2. For M7, RH decreased from 47.78% (H/W=0.0) to 45.71–45.94% (H/W=0.9)

(Δ ~2%). On the left side, M9 showed a broad range (42.14–46.65%) despite similar H/W (0.6–0.8), indicating strong location/configuration effects. At the center, RH ranged from 48.35% (Y3) to 41.58% (Y7/60). For Y3, humidity is high on the sides, and the center reflects this with a slightly higher value. For Y7/60, the middle is affected by low humidity on the east side (40.56%). H/W is relatively high, especially in the east orientation, making the formation thermally trapped. M3 is a poorly insulating material; this leads to significant moisture loss in the middle.

Table D2-7 M3,M7,M9 temperature ,wind apeed,relative humidity results in Ibn rushed street for left side in summer

layout	case	H/W	Façade orientation	Ta 12pm	Ws 4pm	Rh
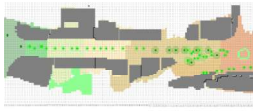	Y4-M3a-E-C6	1.1	E	33.23	1.11	45.2
	Y6/80-M3b-E-C6	1.1	E	33.39	1.91	42.79
	Y6/70-M3c-E-C6	1.1	E	33.47	2.16	42.41
	Y7/60-M3d-E-C3	0.6	E	34.1	1.92	40.56
	Y7/50M3e-E-C3	0.6	E	34.31	2.12	40.53
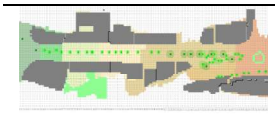	Y2-M7a-E-C2	0.4	E	32.46	1.49	45.99
	Y5-M7b-E-C3	0.6	E	33.65	2.52	43.73
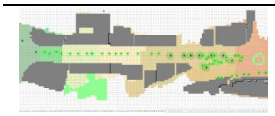	Y8/40-M9a-E-C4	0.8	E	34.5	0.72	42.14
	Y8/30-M9a-E-C4	0.8	E	34.61	1.54	43.91
	Y9-M9b-E-C3	0.6	E	32.68	0.17	46.65

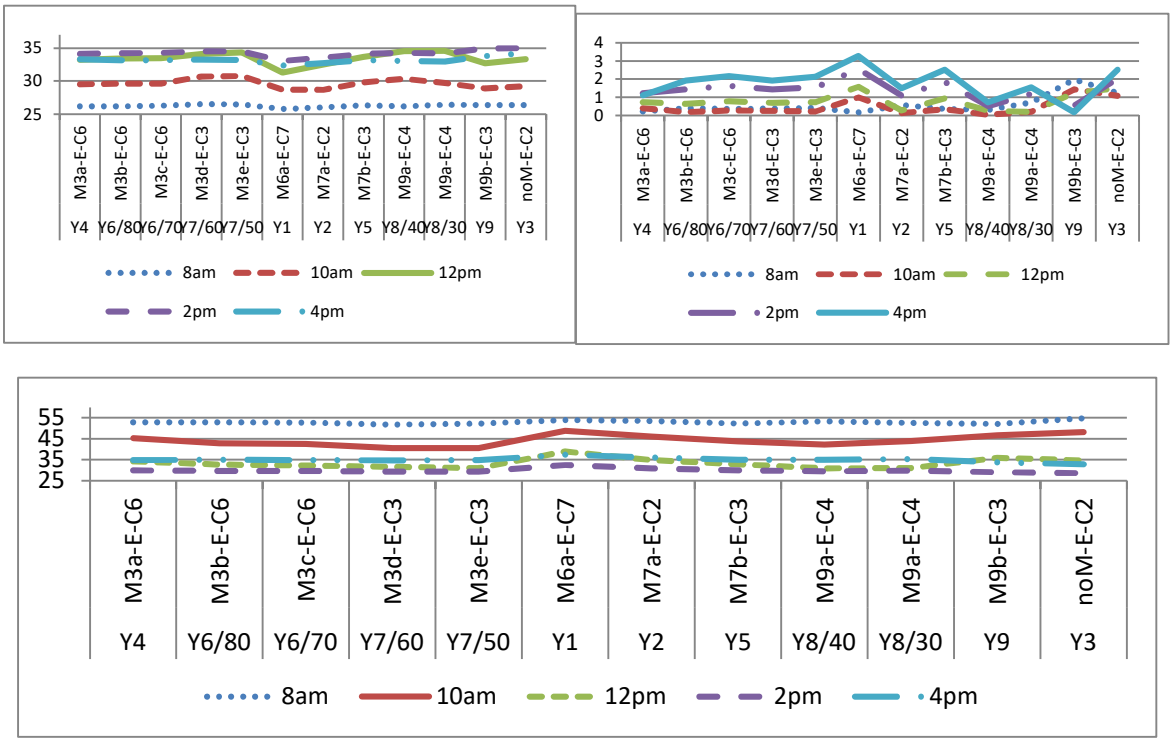

Figure D2-8 a) temperature b) wind speed c) Humidity in Ibn rushed (summer)

Table D2-8 Y8/30 temperature results in Ibn rushed street in summer

layout	location	H/W	orientation	Temperature 12pm
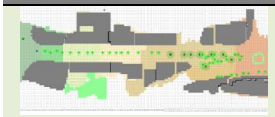	Right	1.2/1.1	W	34.25
	Middle	–	–	34.27
	Left	0.8	E	34.61

Table D2-9 Y1 wind speed result in Ibn rushed street in summer

	location	H/W	orientation	**Wind speed 4pm**
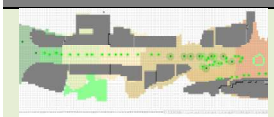	Right	1.1	W	3.53
	Middle	–	–	4.7
	Left	1.2	E	3.28

Table D2-10 Y3 relative humidity result in Ibn rushed street in summer

	location	H/W	material	orientation	**Relative humidity%**
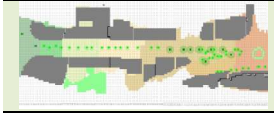	Right	0	M7	W	47.78%
	Middle	–	-	–	48.35%
	Left	0.4	No material	E	48.1%

Table D2-11 Y7/60 relative humidity result in Ibn rushed street in summer

	location	H/W	material	orientation	**Relative humidity%**
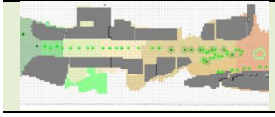	Right	0.8	M3	W	43.95%
	Middle	–	-	–	41.58%
	Left	0.6	M3	E	40.56%

Appendix D-3

Microclimatic Conditions (Temperature, Wind Speed, and Humidity)-winter:

This section presents the detailed winter air temperature, relative humidity, and wind speed statistics for Weddad and Ibn Rushed Streets. Mean values and standard deviations are reported for the right, middle, and left sides at different daytime hours. These data provide a quantitative basis for interpreting the seasonal thermal behavior discussed in Chapter 4.

Table D3-1 Two street result in winter 21-Dec

Weddad street	Ibn rushed street
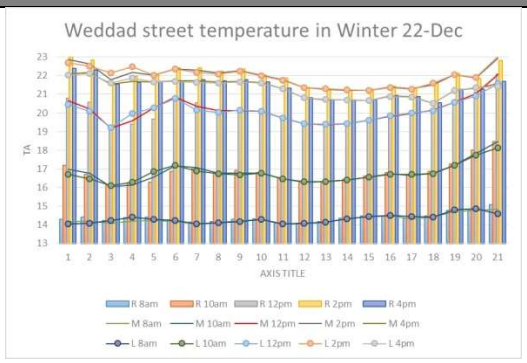 Figure D3-1 Weddad street temperature for three sides in Winter	 Figure D3-2 Ibn rushed street temperature for three sides in winter
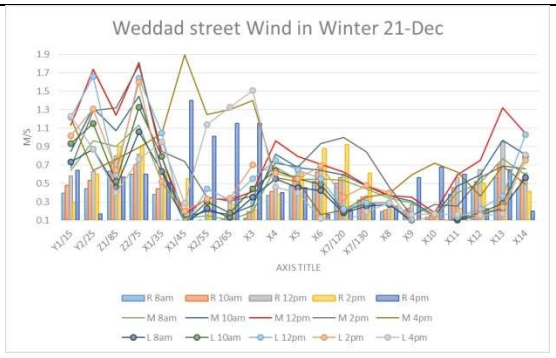 Figure D3-3 Weddad street wind speed for three sides in winter	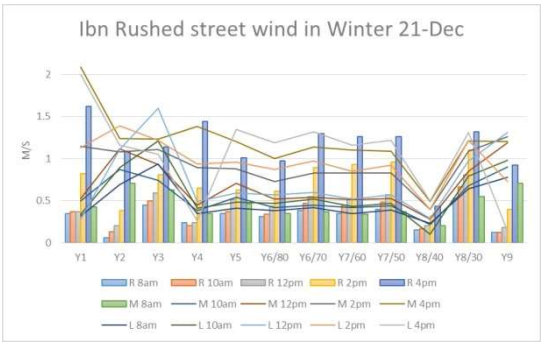 Figure D3-4 Ibn rushed street wind speed for three sides in winter
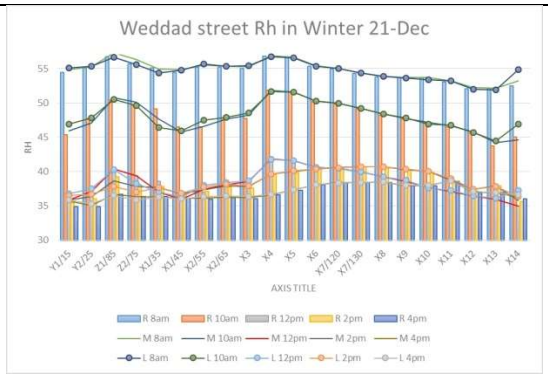 Figure D3-5 Weddad street relative humidity for three sides in Winter	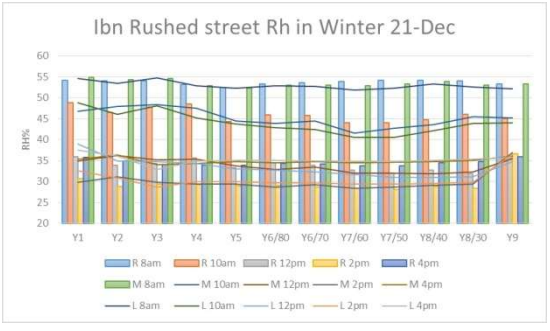 Figure D3-6 Ibn rushed street relative humidity for three sides in winter

As shown in Table D3-2, On Weddad Street on December 21 (winter), the results showed remarkable thermal stability throughout the day across the three sides of the street (left, right, and center). At 8 a.m., temperatures were very similar (around 14.3°C) with a low standard deviation (0.25–0.27), while high humidity prevailed, reaching around 54% with little variation. Wind speed remained very low (0.27–0.40 m/s). At 10 a.m., temperatures gradually rose to around 16.8°C, and humidity decreased to 47–48% with an increase in variation (SD≈2.2), indicating the beginning of clear surface heating due to solar radiation. Winds also began to move slightly, especially in the center of the street, recording an average of 0.48 m/s, which enhances ventilation during transitional periods. At noon, temperatures reached approximately 20°C across the board, with a standard deviation of less than 1°C, indicating good thermal stability. Humidity decreased to approximately 38% across the board, with slight variation. Wind speeds increased to between 0.4 and 0.6 m/s, contributing to improved ventilation in the street. At 2 p.m., temperatures reached their highest daily values (≈21.8°C) with significant stability (SD≈0.5), while humidity remained almost constant (≈38.8%), and winds were between 0.38 and 0.57 m/s, particularly in the center of the street, which exhibited better air movement. At 4 p.m., temperatures began to drop slightly to approximately 21.2°C, humidity dropped to approximately 37%, and winds reached their highest daily values (0.73 m/s in the center), indicating normal evening air activity before sunset.

Table D3-2 Summary of Microclimatic Conditions by time of day in Weddad street in winter

Weddad street 21/12									
Factors	**Air temperature (°C)**			**Relative humidity (%)**			**Wind speed (m/s)**		
Output	Max ,min ,mean ,SD			Max ,min ,mean ,SD			Max ,min ,mean ,SD		
time	Left	Right	Mid	Left	Right	Mid	Left	Right	Mid
8 A.M.	Min:14.04,max:14.87,mean:14.34,SD:0.25	Min:14.07,max:15.08,mean:14.39,SD:0.27	Min:14.05,max:14.84,mean:14.33,SD:0.25	Min:51.89,max:56.68,mean:54.47,SD:1.38	Min:52.05,max:56.83,mean:54.33,SD:1.41	Min:52.15,max:56.9,mean:54.48,SD:1.35	Min:0.06, max:0.63,mean:0.27,SD:0.18	Min:0.06,max:0.5, mean:0.31,SD:0.17	Min:0.1, max:0.77, mean:0.40,SD:0.20
10 A.M.	Min:16.3, max:18.13,mean:16.84,SD:0.48	Min:16.27,max:18.46,mean:16.8,SD:0.58	Min:16.29max:18.47,mean:16.8,SD:0.55	Min:44.46,max:51.68,mean:47.97,SD:2.02	Min:43.73,max:51.79,mean:47.87SD:2.22	Min:44.23,max:51.82,mean:47.82,SD:2.2	Min:0.06, max:0.79 mean:0.33,SD:0.23	Min:0.1, max:71, mean:0.37SD:0.20	Min:0.13, max:0.97,mean:0.48,SD:0.26
12 P.M.	Min:19.39max:21.58,mean:20.12,SD:0.58	Min:19.38,max:22.1,mean:20.1,SD:0.7	Min:19.38,max:22.05,mean:20.17,SD:0.67	Min:36.1 max:41.74,mean:38.53,SD:1.8	Min:34.95,max:42.2mean:38.34SD:2.1	Min:34.94,max:41.86,mean:38.31,SD:2.04	Min:0.03, max:1.05,mean:0.41,SD:0.31	Min:0.08, max:0.95,mean:0.45,SD:0.23	Min:0.16, max:1.32, mean:0.59,SD:0.31
2 P.M.	Min:21.21,max:23.03,mean:21.81,SD:0.50	Min:21.22,max:22.81,mean:21.85,SD:0.49	Min:21.21,max:22.93,mean:21.82,SD:0.50	Min:36.38,max:40.68,mean:38.9,SD:1.46	Min:35.62max:40.69,mean:38.71,SD:1.62	Min:35.76max:40.7,mean:38.8,SD:1.58	Min:0.06, max:0.75,mean:0.38,SD:0.22	Min:0.05, max:0.92,mean:0.43,SD:0.24	Min:0.15, max:1.0, mean:0.57,SD:0.26
4 P.M.	Min:20.52,max:21.7,mean:21.19 SD:0.42	Min:20.53max:21.78,mean:21.24,SD:0.45	Min:20.5 max:21.73,mean:21.21,SD:0.44	Min:36.07,max:38.63,mean:37.29,SD:0.9	Min:35.95max:38.58,mean:37.17,SD:0.99	Min:36.09,max:38.66,mean:37.23,SD:0.96	Min:0.08, max:1.51,mean:0.49,SD:0.46	Min:0.16 max:1.4, mean:0.58 SD:0.38	Min:0.16, max:1.9,mean:0.73,SD:0.47

As shown in Table D3-3 , In Ibn rushed street at 8 am, the average temperature in winter on the right side was 14.46°C, which is the most thermally stable. The left side was 14.49°C with a slight variation, indicating a stable morning and midday coolness of 14.33°C. At 10 am, the average rose to 16.78°C on the right side, 17.18°C on the left side, and 16.79°C in the middle. The deviation was low. At 12 pm, the average reached 20.36°C with a higher variation on the right side, 20.93°C on the left side, and 20.54°C in the middle. At 2 pm, it reached its highest value, reaching 22.32°C on the right side and 22.13°C on the left side with a low deviation and 22.22°C in the middle. At 4 pm, it decreased to 21.56°C on the right side and 21.49°C on the left side. The middle value was 21.46°C, and overall, the deviation was low, indicating that all values were close to the mean and that the variance was not high. All aspects showed high thermal stability in the morning and evening.

In winter at 8 am, the average relative humidity on the right side was 53.65%, while on the left side it was 52.9%. Relative humidity was high with moderate variability, and the middle was 53.51% with a lower deviation. At 10 o'clock, the average dropped to 45.92% on the right side and 44.0% on the left side with a standard deviation of 2.64, reflecting the beginning of warming weather, and 45.24% in the middle. At 12 pm, the average reached 33.81% on the right side and 33.34% on the left side, with medium variability and 33.84% in the middle. At 2 pm, it reached 30.46% on the right side, 29.85% on the left side, and 29.93% in the middle. At 4 pm, it rose to 35.11% on the right side, 34.95% on the left side, and 34.9% in the middle. This decrease in humidity is apparent in the afternoon. (12-2 PM), which indicates the impact of sun rays even during winter. The highest variation was at 12 and 10 AM on the left side of the humidity.

In winter, at 8 am, the average wind speed on the right side is 0.30 m/s. On the left side, the wind speed is moderate but relatively stable, at 0.49 m/s, and in the middle, it is 0.45 m/s. At 10 am, the average reached 0.35 m/s on the right side and 0.59 m/s on the left side, with noticeable fluctuations, and 0.54 m/s with relatively low fluctuations in the middle. At 12 p.m., the average reached 0.43 m/s on the right side and 0.7 m/s on the left side, with some fluctuations, and 0.66 m/s in the middle. At 2 pm, it reached 0.70 m/s on the right side, 0.9 m/s on the left, and 0.94 m/s in the middle. At 4 pm, it rose to 1.14 m/s on the right side, 1.0 m/s on the left, and 1.26 m/s in the middle. The variability is high. At all times and on all sides, the mean speed was highest at 8 am and 10 am.

Table D3-3 summary of Microclimatic Conditions by time of day in Ibn rushed street in winter

Ibn rushed street 21/12									
Factors	**Air temperature (°C)**			**Relative humidity (%)**			**Wind speed (m/s)**		
Output	Max ,min ,mean ,SD			Max ,min ,mean ,SD			Max ,min ,mean ,SD		
time	Left	Right	Mid	Left	Right	Mid	Left	Right	Mid
8 A.M.	Min:14.02,max:14.96 ,mean:14.49 ,SD:0.27	Min:14.14,max:14.75 ,mean:14.46 ,SD:0.18	Min:13.97max:14.64,mean:14.33,SD:0.2	Min:51.76,max:54.78,mean:52.9,SD:0.95	Min:52.35,max:54.2,mean:53.65,SD:0.54	Min:52.28,max:55.05,mean:53.51,SD:0.85	Min:0.23, max:0.94, mean:0.49SD:0.21	Min:0.06, max:0.53, mean:0.3, SD:0.13	Min:0.2, max:0.71, mean:0.45,SD:0.15
10 A.M.	Min:16.51,max:18.08mean:17.18,SD:0.41	Min:15.87,max:17.98mean:16.78SD:0.46	Min:15.95,max:17.68 ,mean:16.79,SD:0.4	Min:40.53,max:48.85 ,mean:44.0,SD:2.64	Min:43.95,max:48.76 ,mean:45.92,SD:01.67	Min:41.58,max:48.35,mean:45.24,SD:2.08	Min:0.1, max:1.21 mean:0.59,SD:0.31	Min:0.12, max:0.66, mean:0.35,SD:0.16	Min:0.22, max:0.9, mean:0.54,SD:0.19
12 P.M.	Min:20.1 max:21.58 ,mean:20.93,SD:0.42	Min:19.71,max:21.5,mean:20.36,SD:0.48	Min:19.88,max:21.31 ,mean:20.54,SD:0.39	Min:30.93,max:38.95,mean:33.34SD:2.32	Min:31.75,max:35.84 ,mean:33.81SD:1.39	Min:31.85,max:36.18 ,mean:33.84 SD:1.56	Min:0.28, max:1.6 ,mean:0.7 SD:0.41	Min:0.18, max:0.81 ,mean:0.43SD:0.19	Min:0.28, max:1.19 ,mean:0.66SD:0.27
2 P.M.	Min:21.4, max:22.83,mean:22.13,SD:0.32	Min:21.86,max:22.76,mean:22.32,SD:0.22	Min:21.98,max:22.64mean:22.22,SD:0.18	Min:28.61,max:32.51 mean:29.85 SD:1	Min:28.6, max:36.49,mean:30.46 SD:2.1	Min:28.41,max:36.87,mean:29.93 SD:2.21	Min:0.4, max:1.39, mean:0.9 SD:0.25	Min:0.32, max:1.1, mean:0.7 SD:0.25	Min:0.4, max:1.26, mean:0.94SD:0.23
4 P.M.	Min:21.24max:22, mean:21.49,SD:0.18	Min:21.35max:21.89,mean:21.56,SD:0.15	Min:21.27,max21.79,mean:21.46,SD:0.13	Min:32.82max:37.42,mean:34.95,SD:1.1	Min:32.82,max:37.42,mean:35.11,SD:1.05	Min:33.94,max:36.34,mean:34.9,SD:0.73	Min:0.14 max:2 ,mean:1.0 ,SD:0.51	Min:0.43, max:1.62 ,mean:1.14,SD:0.3	Min:0.49, max:2.15 ,mean:1.26,SD:0.42

Appendix D-4

PET & UTCI Detailed Results (summer & winter)

- **Summer:**

As shown in Table D4-1, PET values exhibited a pronounced diurnal increase across all street positions, with relatively moderate conditions in the early morning and progressively higher thermal stress toward midday and early afternoon. At 8:00 AM, PET values were lower and more stable on the right and middle sides, while the left side recorded higher and more variable values, reflecting limited shading conditions. By 10:00 AM, PET increased substantially at all positions, with the middle and left sides reaching similarly high and relatively stable levels, indicating sustained heat exposure. Midday and early afternoon (12:00–2:00 PM) represented the most thermally stressful period, as PET peaked across the canyon, particularly on the right side, which also showed the greatest variability, suggesting strong solar exposure and unstable thermal conditions. By 4:00 PM, PET values declined slightly but remained high, with

increased variability on the right side and comparatively more stable conditions in the middle and left positions.

UTCI followed a similar temporal pattern but displayed lower variability than PET throughout the day, indicating more stable perceived thermal conditions. Morning UTCI values were moderate, with higher and more variable conditions on the left side. Toward late morning and midday, UTCI increased steadily across all positions, peaking between 12:00 PM and 2:00 PM, particularly on the right and middle sides. In the late afternoon, UTCI values decreased slightly, with the left side showing the most stable conditions, while the right side remained the most exposed and thermally unstable. Overall, UTCI demonstrated smoother spatial and temporal transitions compared to PET, while the right side of the street consistently emerged as the most thermally stressed and variable zone, especially during peak afternoon hours.

Table D4-1 summary of thermal comfort result by time of day in Weddad street in summer

Weddad street 22/6						
Factors	**PET (°C)**			**UTCI (°C)**		
Output	Max ,min ,mean ,SD			Max ,min ,mean ,SD		
time	left	right	mid	left	right	mid
8 A.M.	Min:28.23,max:39.77,mean:33.56,SD:4.0	Min:26.96,max:37.55,mean:28.84,SD:2.24	Min:27.18,max:35.29,mean:29.74,SD:2.62	Min:25.7,max:33.52,mean:29.84,SD:2.82	Min:24.78,max:27.64,mean:25.98,SD:0.7	Min:25.46,max:31.78,mean:27.79,SD:2.27
10A.M.	Min:32.29,max:44.66 ,mean:38.18,SD:2.74	Min:31.6,max:42.1 ,mean:35.05,SD:2.89	Min:33.98,max:40.2,mean:38.2, SD:1.74	Min:28.33,max:35.63 ,mean:33.77,SD:2.15	Min:29.54,max:33.94 ,mean:31.77,SD:1.36	Min:30.5,max:34.48,mean:33.25SD:1.09
12 P.M.	Min:34.86,max:44.63 ,mean:39.36SD:3.328	Min:37.15,max:44.3 ,mean:41.34SD:1.79	Min:36.8,max:44.2 ,mean:41.34SD:2.31	Min:31.23,max:37.07 ,mean:34.4SD:1.88	Min:34.22,max:37.56 ,mean:36.14SD:1.00	Min:32.88,max:37.44 ,mean:35.91SD:1.47
2 P.M.	Min:35.14,max:46.6,mean:39.1SD:3.6	Min:35.74,max:52.5,mean:43.64SD:4.91	Min: 35.36, max: 47.6, mean:41.73SD:4. 38	Min:32.28,max:38.97,mean:34.86SD:2.13	Min:32.91,max:40.8,mean:37.66SD:2.79	Min:32.52,max:39.91,mean:36.91 SD:2.75
4 P.M.	Min:33.98,max:44.5,mean:36.37,SD:2.72	Min:33.58,max:51.14 ,mean:38.77,SD:4.54	Min:33.85,max:45.43,mean:38.21,SD:3.82	Min:31.19,max:36.28 ,mean:32.69,SD:1.22	Min:31.45,max:40.64,mean:35.25,SD:2.91	Min:31.4,max:37.25,mean:34.56,SD:2.54

As shown in Table D4-2, PET and UTCI values revealed a clear diurnal escalation in thermal stress across all street sections, with notable spatial contrasts in both intensity and variability. In the early morning (8:00 AM), thermal conditions were relatively moderate, particularly on the right and middle sides, which exhibited lower PET and UTCI values with limited variability, indicating more stable and comparatively comfortable conditions. In contrast, the left side already showed higher PET values and greater dispersion, reflecting heterogeneous thermal exposure and reduced comfort. By 10:00 AM, thermal stress intensified markedly, especially on the left and middle sides, where PET values increased sharply, indicating the

onset of severe heat stress. The right side, despite showing some variability, remained comparatively less stressful, particularly in terms of UTCI, suggesting a more favorable microclimatic response during late morning hours. Midday conditions (12:00 PM) were characterized by uniformly high PET and UTCI values across all sections, with minimal spatial differences, indicating widespread and sustained thermal discomfort throughout the canyon. The most extreme thermal conditions occurred at 2:00 PM, when PET and UTCI reached their daily maxima, particularly on the right and middle sides. The middle section exhibited the highest variability in PET, highlighting pronounced spatial fluctuations in perceived heat stress. Although the left side showed slightly lower average values at this time, thermal conditions remained severely uncomfortable. By 4:00 PM, PET and UTCI values declined modestly but remained elevated, confirming prolonged heat exposure into the late afternoon. The middle section displayed comparatively more balanced conditions, with lower variability, while the right side continued to experience unstable and intense thermal stress. Overall, the results indicate that while all sections were exposed to significant heat stress during peak hours, the right side was more stable in the morning, the middle side demonstrated more balanced conditions in the late afternoon, and the left side consistently exhibited lower UTCI variability despite high absolute temperatures.

Table D4-2 summary of thermal comfort result by time of day in Ibn rushed street

Ibn rushed street 22/6						
Factors	**PET (°C)**			**UTCI (°C)**		
Output	Max ,min ,mean ,SD			Max ,min ,mean ,SD		
time	left	right	mid	left	right	mid
8 A.M.	Min:28.69,max: 41.27,mean:33. 97 ,SD:4.77	Min:27.66,max: 35.94,mean:29. 65,SD:2.12	Min:28.39,max: 38.2,mean:30.3, SD:2.51	Min:25.92,max: 34.11,mean:31. 82,SD:2.3	Min:25.33,max: 30.95,mean:27. 48,SD:1.9	Min:25.57,max: 31.75,mean:28. 78,SD:2.35
10A.M.	Min:38.29,max: 50.88 ,mean:42.33,SD :3.26	Min:30.14,max: 40.56 ,mean:33.94,SD :2.46	Min:32.38,max: 43.32 ,mean:39.09,SD :3.13	Min:32.53,max: 36.26 ,mean:34.83,SD :1.07	Min:29.31,max: 33.98 ,mean:31.47,SD :1.57	Min:32.89,max: 36.18 ,mean:34.7 ,SD:0.89
12 P.M.	Min:36.54,max: 44.72 ,mean:42.4 SD:2.19	Min:39.74,max: 45.36 ,mean:42.86,SD :1.62	Min:40.23,max: 45.41 ,mean:42.73 SD:1.87	Min:32.66,max: 37.6 ,mean:36.4SD:1 .38	Min:35.68,max: 38.2 ,mean:37.09 SD:0.75	Min:34.85,max: 39.53 ,mean:37.49 SD:1.35
2 P.M.	Min:36.33,max: 46.44 ,mean:38.29,SD :3.64	Min:39.81,max: 49.49,mean:45. 64,SD:2.54	Min:36.33,max: 47.72 ,mean:42.87SD: 4.01	Min:33,max:39. 92,mean:35.33 SD:2.04	Min:37.59,max: 41.45,mean:39. 97 SD:1.2	Min:32.37 ,max:40.45 ,mean:38.36 SD:2.37
4 P.M.	Min:33.44,max: 45.66 ,mean:36.21,SD :3.93	Min:33.84,max: 45.09 ,mean:39.3,SD: 3.97	Min:33.95,max: 43.16 ,mean:36.75 ,SD:2.88	Min:31.34,max: 38.48 ,mean:33.34,SD :2.26	Min:31.88,max: 40.03 ,mean:36.53,SD :3.11	Min:30.55 ,max:38.14 ,mean:34.21 ,SD:2.55

Effect of Height-to-Width Ratio (H/W) on PET and UTCI – Summer Season

(Weddad Street & Ibn Rushed Street – Himonies Street excluded)

a) Weddad street:

At 2:00 PM, the effect of H/W on PET and UTCI exhibited strong spatial and material dependency. On the right side, the highest thermal stress was consistently recorded for M3 in west-facing configurations, with PET reaching up to 52.5°C and UTCI exceeding 40.8°C, at H/W = 0.6–1.1, indicating extreme heat stress. In contrast, the lowest PET and UTCI values were observed in southwest-oriented deep canyons, notably M3h-SW-C5 (PET = 35.74°C) and M7b-SW-C15, confirming the effectiveness of increased shading at higher H/W. For M1 and M2, PET and UTCI decreased systematically with increasing H/W. For M1, PET dropped from approximately 47°C (extreme heat stress) at H/W = 0.8 to 37.07°C, at H/W = 3.8 (Δ PET ≈ 9.9°C), while UTCI declined from 39.85°C to 33.58°C (ΔUTCI ≈ 6.27°C). Similar trends were observed for M2, with UTCI differences reaching 6.78°C, indicating high sensitivity to urban morphology despite constant material properties. M3 showed the highest sensitivity to H/W variation, with PET and UTCI peaking in narrow canyons (H/W = 0.6–0.8) due to heat accumulation and reflected radiation, particularly in west-facing orientations. Increasing H/W did not consistently improve comfort for M3 unless combined with a favorable orientation (SW or NE). M7 demonstrated stable and improved thermal performance with increasing H/W, where PET reductions of approximately 5°C and UTCI reductions of 6.8°C were recorded between medium and high H/W values, reflecting the combined effect of good insulation and extended shading.

On the left side, PET and UTCI generally decreased with increasing H/W, especially in NE- and E-facing configurations. The highest PET/UTCI was 45.8°C (M1b-NE-C4, H/W = 0.9) and 38.97°C, respectively, while the lowest UTCI was 32.28°C (M3e-NE-C12, H/W = 1.9) ΔUTCI = 6.69°C. For M2 and M3, higher H/W values (≥1.9) reduced UTCI by 1.6–2°C, whereas changes in H/W had limited impact in purely east-facing cases, confirming the dominant role of orientation. For M5, PET differences were <0.5°C around H/W=1.2. At H/W=1.1, the UTCI difference is ≈ 0.9°C. For M6 material (left side), both PET and UTCI recorded the best performance at H/W ≈ 1.5–1.6 due to improved shading, while open cases led to increased radiative load and higher thermal stress values.

The middle of Weddad Street recorded PET values up to 47.60°C and UTCI up to 39.91°C (X1/35), while the lowest values were observed at X8 (PET = 35.36°C; UTCI = 32.52°C). In most cases, middle values lie between the two sides; however, in low H/W configurations and

west-facing scenarios, reflected radiation caused the middle to exceed one or both sides by 2–3°C, emphasizing its role as a thermal transfer zone.

Table D4-3M1,M3,M5,no M PET and UTCI results for left side in weddad street in summer

layout	case	H/W	Façade orientation	PET 2pm	UTCI 2pm
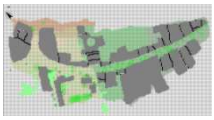	M1a-NE-C4	0.9	NE	37.8	35.18
	M1b-NE-C4	0.9	NE	45.8	38.97
	M1c-NE-C3	0.8	NE	39.7	37.23
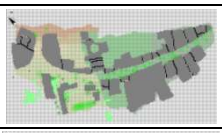	M3c-E-C3	0.8	E	37	34.37
	M3d-E-C6	1.2	E	38.26	34.58
	M3e-NE-C12	2.1	NE	35.58	32.28
	M3f-NE-C5	1.1	NE	36.72	33.92
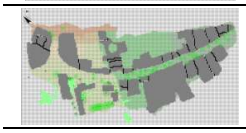	M5a-NE-C6	1.2	NE	38.03	35.08
	M5b-NE-C6	1.2	NE	37.68	34.18
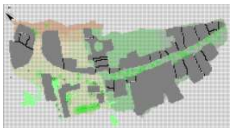	M6a-NE-C8	1.3	NE	38.32	34.86
	M6b-NE-C10	1.6	NE	35.4	32.84
	M6c-NE-C9	1.5	NE	35.14	32.39
	M6d-NE-C4	0.8	NE	35.72	32.72
	M6e-NE-C5	0.9	NE	35.5	32.37
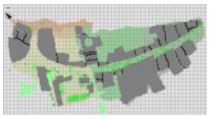	noc-NE-C2	0.4	NE	45.15	38.71
	nod-NE-C6	1.1	NE	40.43	37.03

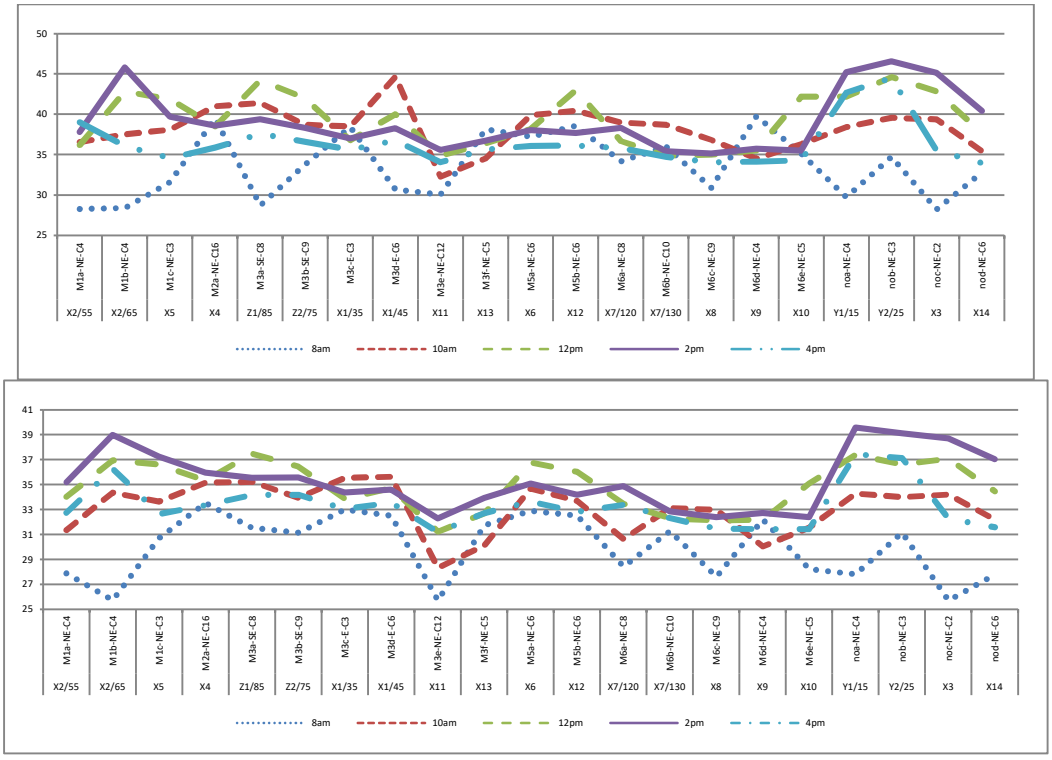

Figure D4-1 a) PET b) UTCI in Weddad (suumer)

Table D4-4 X1/35 PET results compared three sides

layout	Location	H/W	orientation	PET 2pm	UTCI 2pm
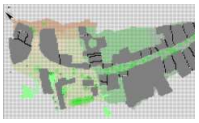	Right	0.6	W	52.5	40.8
	Middle	-	-	47.6	39.91
	Left	0.6	E	37.0	34.37

Table D4-5 X2/65 PET results compared three sides

layout	Location	H/W	orientation	PET 2pm
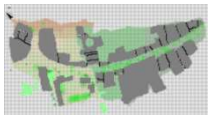	Right	0.6	W	46.1
	Middle	-	-	45.9
	Left	0.8	NE	45.8

Table D4-6X8 PET result compared three sides

layout	Location	H/W	orientation	PET 2pm	UTCI 2pm
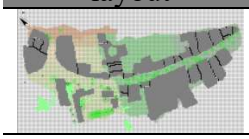	Right	3.8	SW	37.07	33.58
	Middle	-	-	35.36	32.52
	Left	1.5	NE	35.14	32.39

b) Ibn rushed street:

In Ibn Rushed Street, the combined effect of H/W ratio, street orientation, and façade material strongly influenced both PET and UTCI values. On the right (west-facing) side, PET ranged from 39.81 °C (M6a-W-C6) to 49.49 °C (M3d-W-C6), with a difference of 9.68 °C, while UTCI varied between 37.59 °C and 41.45 °C, with a difference of 3.86°C. For M3, both PET and UTCI increased as H/W rose from 0.6 to 0.8–1.1, reaching peak values due to enhanced heat retention and radiative trapping within the moderately narrow canyon, before slightly decreasing at H/W = 1.2 as self-shading improved. In contrast, M7 showed smaller variations in PET and nearly stable UTCI values across different H/W ratios, indicating that better insulating materials reduce sensitivity to geometric changes under west-facing exposure.

On the left (east-facing) side, the response was reversed. Increasing H/W generally reduced both PET and UTCI, with differences remaining relatively small (≈ 1 °C for PET and up to 2–3 °C for UTCI), highlighting the effectiveness of shading in limiting morning solar exposure. Even for less insulating materials, deeper canyons provided measurable thermal benefits under east-facing conditions.

In the middle of Ibn Rushed Street, PET varied between 47.21 °C and 37.71 °C (Δ = 9.5 °C), indicating strong sensitivity to the hotter canyon side; however, in some cases, a more closed west-facing geometry (H/W = 1.2) provided sufficient shading to reduce PET despite high

thermal stress on the west side. Similarly, UTCI in the middle ranged from 40.45 °C (Y3) to 34.87 °C (Y1) (Δ = 5.58 °C). Open west-facing configurations (H/W = 0.0) markedly increased UTCI due to direct solar exposure, whereas enclosed or shaded configurations on either side helped mitigate heat stress, confirming that the middle zone is predominantly governed by the hotter façade, particularly when it is west-facing.

Across both streets, higher H/W often reduces PET/UTCI by increasing shade, but the effect is orientation-dependent. In east/NE exposures, increasing H/W generally reduces thermal stress. In west-facing exposures, moderate narrowing (e.g., H/W 0.8–1.1) can increase PET/UTCI via heat retention and wall-to-wall radiative exchange, especially with high U-value materials (e.g., M3). Middle-street conditions reflect the combined influence of both sides and can exceed one side by ~2–3°C under exposed/low-shading conditions, highlighting the need for balanced design rather than optimizing one façade only.

Table D4-7 M3, M7 PET result in Ibn rushed street for right side in summer

layout	case	H/W	Façade orientation	PET 2pm	UTCI 2pm
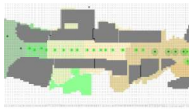	M3a-W-C3	0.6	W	44.64	38.82
	M3b-W-C4	0.8	W	47.21	41.44
	M3c-W-C4	0.8	W	46.43	41.45
	M3d-W-C6	1.1	W	49.49	40.81
	M3e-W-C7	1.2	W	46.25	40.52
	M3f-W-C4	0.8	W	47.01	40.83
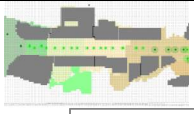	M7a-W-C0	0	W	42.7	40.18
	M7b-W-C5	0.9	W	47.77	40.3
	M7c-W-C5	0.9	W	45.34	40.21

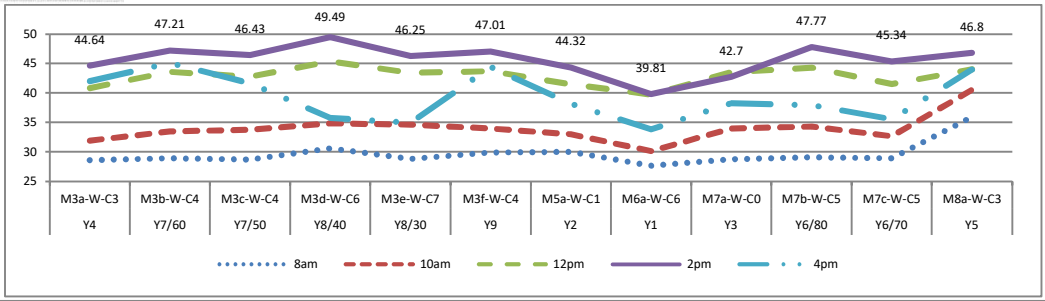

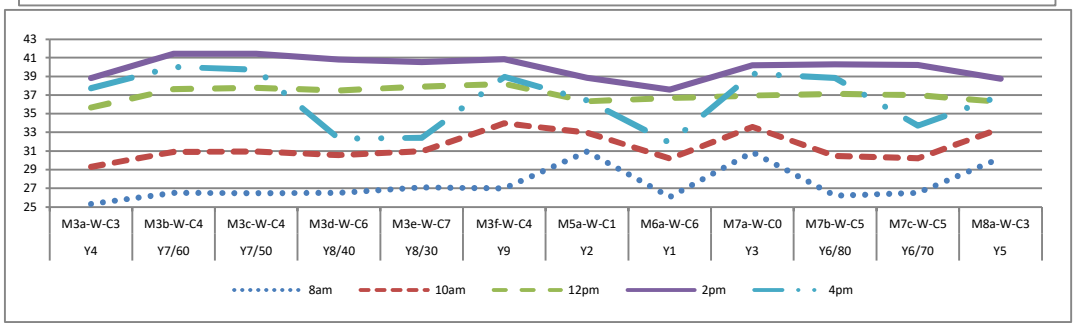

Figure D4-2 a) PET b) UTCI in Ibn rushed

Table D4-8 M3,M7,M9 PET result in Ibn rushed street for left side in summer

layout	case	H/W	Façade orientation	PET 2pm	UTCI 2pm
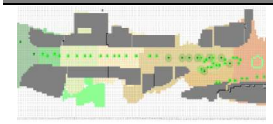	M3a-E-C6	1.1	E	36.38	34.61
	M3b-E-C6	1.1	E	36.59	33.96
	M3c-E-C6	1.1	E	36.6	34.29
	M3d-E-C3	0.6	E	37.63	34.8
	M3e-E-C3	0.6	E	37.38	34.71
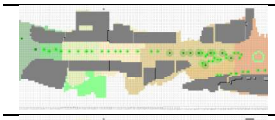	M7a-E-C2	0.4	E	36.81	37.51
	M7b-E-C3	0.6	E	36.6	34.78
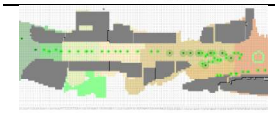	M9a-E-C4	0.8	E	36.68	34.16
	M9a-E-C4	0.8	E	36.42	34.2
	M9b-E-C3	0.6	E	46.44	39.92

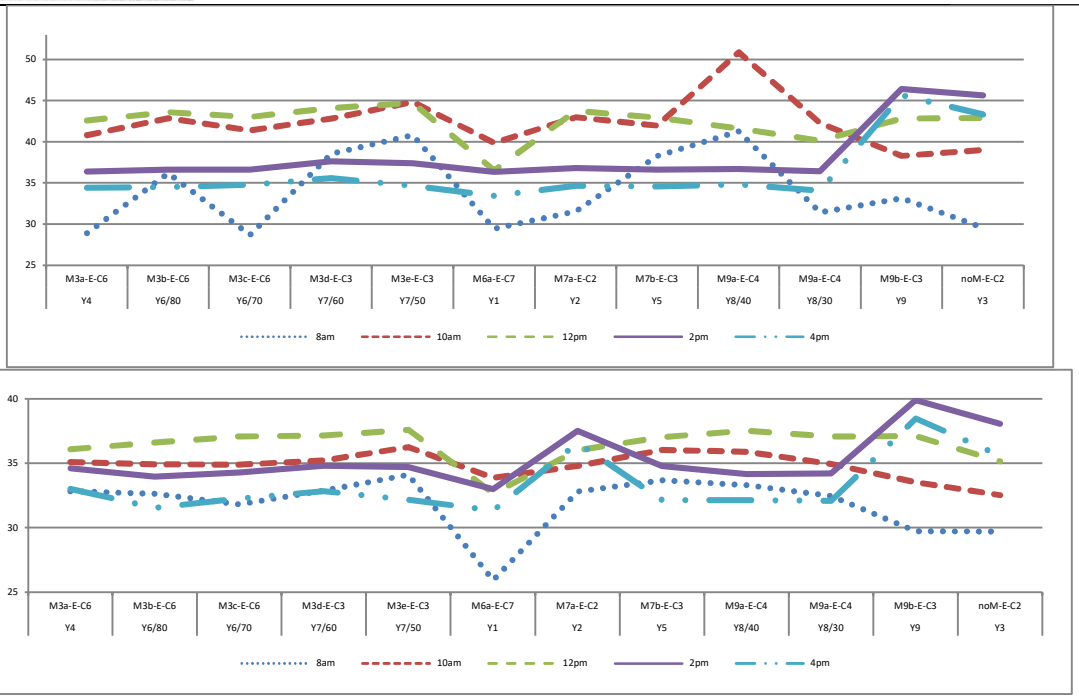

Figure D4-3 a) PET b) UTCI in Ibn rushed

Table D4-9 Y7/60 PET Result in Ibn rushed street in suumer

layout	Location	H/W	Material	orientation	PET 2pm
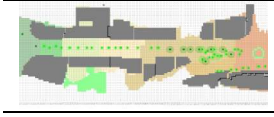	Right	0.8	M3	W	47.21
	Middle	-	-	-	47.72
	Left	0.6	M3	E	37.63

Table D4-10Y8/30 PET Result in Ibn rushed street in suumer

layout	Location	H/W	Material	orientation	PET 2pm
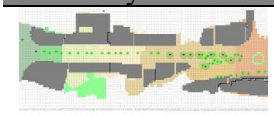	Right	1.2	M3	W	46.25°C
	Middle	-	-	-	37.71°C
	Left	0.8	M3	E	36.42°C

Table D4-11 Y3 UTCI result in Ibn rushed street in summer

layout	Location	H/W	Material	orientation	PET 2pm
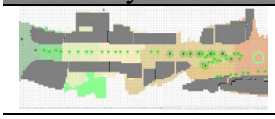	Right	0	M7	W	40.18°C
	Middle	-	-	-	40.45°C
	Left	0.4	No material	E	38.07°C

Table D4-12Y1 UTCI result in Ibn rushed street in summer

layout	Location	H/W	Material	orientation	PET 2pm
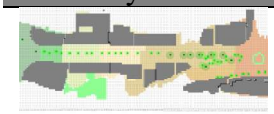	Right	1.1	M6	W	37.59°C
	Middle	-	-	-	34.87°C
	Left	1.2	M6	E	33°C

- **winter**

As shown in table D4-13, the results for Weddad Street on December 21 showed that the PET and UTCI indices reflected a moderate and stable thermal pattern throughout the day, with slight variations between the three sides of the street. In the early morning (8 a.m.), values were relatively low (PET ≈ 18–19°C, UTCI ≈ 15–19°C) with a small standard deviation. As the sun rose at 10 a.m. and 12 p.m., values gradually increased to around 26–28°C for PET and 21–23°C for UTCI, accompanied by an increase in variability. The indices peaked at midday (12–2 p.m.) and then began to decline again towards evening (4 p.m.), stabilizing at 22–23°C for PET and 19–20°C for UTCI, with the lowest standard deviation recorded throughout the day, reflecting a state of stability and optimal thermal comfort. Overall, these values show that winter is characterized by spatial homogeneity and clear thermal moderation within the street, in contrast to summer, which is characterized by high temperatures and large variations between sides, confirming improved climatic comfort and reduced thermal stress during winter.

Table D4-13 summary of thermal comfort result by time of day in Weddad street in winter

Weddad street 21/12						
Factors	**PET (°C)**			**UTCI (°C)**		
Output	Max ,min ,mean ,SD			Max ,min ,mean ,SD		
time	left	right	mid	left	right	mid
8 A.M.	Min: 16.28, max: 25.69 mean: 19. 31,SD:2.37	Min:16.97,max: 28.44,mean:19. 66SD:3.29	Min:15.87,max: 25.8,mean:18.2 4SD:2.24	Min:17.77,max: 25.02,mean:19. 3,SD:1.54	Min:14.37,max: 21.97,mean:15. 91,SD:2. 1	Min:13.29,max: 22.11,mean:15. 65,SD:2.55
10A.M.	Min:18.68,max: 35.91 ,mean:23.7,SD: 5.4	Min:18.7,max:3 8.1 ,mean:24.99,SD :7.1	Min:18.21,max: 36.55 ,mean:23.6,SD: 6.1	Min:13.29,max: 23.15 ,mean:19.84,SD :4.09	Min:16.08,max: 27.38 ,mean:20.35,SD :4.42	Min:15.93,max: 27.44,mean:19. 77 SD:4.11
12 P.M.	Min:21.67,max: 41.14,mean:26. 22SD:5.6	Min:21.05,max: 42.19 ,mean:27.98SD: 7.53	Min:21.13,max: 39.99 ,mean:26.7SD:6 .5	Min:17.53,max: 29.96 ,mean:21.42SD: 3.46	Min:16.61,max: 30.71 ,mean:23.36 SD:5.14	Min:16.73,max: 30.13 ,mean:22.6 SD:4.66

2 P.M.	Min:23.31,max: 36.21,mean:26. 63 SD:3.6	Min:22.09,max: 41.31,mean:28. 39 SD:5.83	Min:21.97,max: 38.77,mean:25. 79SD:3.89	Min:19.85,max: 29.35,mean:22. 25 SD:2.52	Min:19.5,max:3 1.18,mean:24.8 3 SD:4.8	Min:19.47,max: 30.13,mean:223 .94 SD:3.68
4 P.M.	Min:21.05,max: 25.03 ,mean:23.19 ,SD:1.08	Min:22,max:24. 48,mean:23.02, SD:0.87	Min:20.85,max: 23.69,mean:22. 28,SD:0.68	Min: 17.77 max: 24. 4,mean:20.4,SD :1.4	Min:18.77,max: 21.79,mean:19. 62,SD:0.84	Min:17.77,max: 25.02,mean:19. 37 ,SD:1.54

As shown in Table D4-14, in winter, at 8 am, the average PET on the right side was 17.86°C, and the average UTCI was 14.14°C. The deviation is low. The left side had an average PET of 17.56°C, with moderate variation, and the average UTCI of 16.7°C fluctuated significantly. Thermal perception varied across various locations. The middle, with an average PET of 17.92°C and an average UTCI of 14.35°C, showed relatively cold and more stable conditions compared to the left side. At 10 am, the average PET reached 21.8°C and the average UTCI was 18.29°C. On the right side, the average PET rose suddenly to 30.87. The average UTCI of 26.66°C on the left side indicated an atypically warm winter sensation. The PET average was 24.98°C, and the UTCI average was 23.77°C in the middle. At 12 pm, the PET average reached 31.9°C, and the UTCI average was 27.07°C on the right side. The highest PET average of the day was 35.67°C, while the UTCI average was 27.25°C on the left side, which contributed to a relatively uncomfortable temperature during winter. The average PET was 30.63°C, and the average UTCI was 27.53°C, both with moderate fluctuations, indicating a warm and stable environment in the middle. At 2 pm, the average PET reached 34.52°C, and the average UTCI was 29.09°C on the right side, with relatively low variability. The average PET dropped to 24.6°C, but the variability was high. The average UTCI was 21.9°C, reflecting a relatively pleasant feeling on the left side. The average PET was 25.93°C, and the average UTCI was 25.05°C in the middle, with significant variability. At 4 PM, the average PET was 23.05°C, and the average UTCI was 19.91°C on the right side. The average PET decreased to 22.37°C, while the average UTCI was 18.88°C on the left side. The middle side recorded a mean UTCI of 18.68°C, with an average PET of 22.52°C. The highest variation for the PET mean was at 10:00 a.m. on the right and middle sides, and the lowest variation was on the left side at noon, indicating stable temperatures despite the rise. For the mean UTCI, the right side at 10:00 a.m. had the highest fluctuation, indicating clear differences in thermal sensation across sites. Therefore, 10:00 a.m. was the period with the greatest fluctuation in thermal sensation, whether PET or UTCI. At 2:00 and 4:00 a.m., all sites were stable in terms of thermal comfort distribution. The center side showed a balanced performance most of the time, while the right side was characterized by significant fluctuations.

Table D4-14 summary of thermal comfort result by time of day in Ibn rushed street in winter

Ibn rushed street 21/12						
Factors	**PET (°C)**			**UTCI (°C)**		
Output data	Max ,min ,mean ,SD			Max ,min ,mean ,SD		
time	left	right	mid	left	right	mid
8 A.M.	Min:14.22,max: 25.49,mean:17. 56,SD:2.7	Min:16.23,max: 20.39,mean:17. 86,SD:1.23	Min:14.62,max: 24.96,mean:17. 92,SD:2.4	Min:11.03,max: 23.3,mean:16.7, SD:4.1	Min:12.78,max: 15.38,mean:14. 14,SD:0.8	Min:11.65,max: 21.97,mean:14. 35SD:2.47
10A.M.	Min:16.35,max: 35.49 ,mean:30.87,SD :5.8	Min:18.67,max: 37.61 ,mean:21.8,SD: 5.12	Min:17.38,max: 34.68 ,mean:24.98,SD :5.4	Min:20.37,max: 29.22 ,mean:26.66,SD :2.5	Min:14.95,max: 27.35 ,mean:18.29,SD :3.96	Min:14.28,max: 27.12 ,mean:23.77 ,SD:3.8
12 P.M.	Min:29.44,max: 41.71 ,mean:35.67 SD:2.89	Min:22.61,max: 40.48 ,mean:31.9,SD: 6.4	Min:24.27,max: 35.91 ,mean:30.63 SD:4.32	Min:21.73,max: 29.83 ,mean:27.25,SD :2.6	Min:19.91,max: 29.73 ,mean:27.07 SD:2.38	Min:24.93,max: 28.58 ,mean:27.53 SD:1.1
2 P.M.	Min:22.17 ,max:37.41 ,mean:24.6 ,SD:4.1	Min:25.38 ,max:40.04, mean:34.52 ,SD:4.57	Min:23.36 ,max:34.34 ,mean:25.93 SD:3.55	Min:19.42 ,max:30.64 ,mean:21.9 SD:3.2	Min:28.1 ,max:30.23 ,mean:29.09 SD:0.64	Min:20.17 ,max:28.62 ,mean:25.05 SD:3.6
4 P.M.	Min:20,max:34. 77,mean:22.37, SD:3.96	Min:20.76,max: 30.92 ,mean:23.05,SD :3.5	Min:20.15,max: 28.88 ,mean:22.52,SD :2.79	Min:16.79,max: 26.78 ,mean:18.88,SD :2.5	Min:17.21,max: 26.56 ,mean:19.91,SD :3.53	Min:16.68 ,max:24.66 ,mean:18.53,SD :2.03

Winter UTCI results show that Waded Street maintains relatively uniform thermal conditions. At 8:00, values are within the comfort range to slightly cool, gradually rising between 10:00 and 12:00, especially on exposed sides, without exceeding moderate heat stress. The highest values are recorded at 14:00 before returning to the comfort range at 16:00. In contrast, Ibn Rushed Street exhibits more pronounced variations. The eastern side is warmest between 8:00 and 10:00, values converge at 12:00, and the western side becomes the hottest at 14:00. All sides then return to comfortable or slightly cooler conditions at 16:00, reflecting a higher sensitivity to solar exposure and orientation.as shown in Table E-19 and Table E-20.

Effect of Height-to-Width Ratio (H/W) on PET and UTCI – winter Season

The 2:00 p.m. time was selected for both summer and winter analysis, as it represents the peak daily thermal condition, recording the highest average air temperature and thermal comfort indices. Although winter results showed higher variability at 12:00 p.m., the highest average PET and UTCI values occurred at 2:00 p.m., making it suitable for seasonal comparison.

a) Weddad street:

As shown in Table D4-15, For M1, the highest PET value (28.09°C) occurred at H/W = 0.8, while values decreased at H/W = 2.1 and 3.8 due to increased shading. M2 showed a clear

inverse relationship between H/W and PET; the open case (H/W = 0) recorded 34.87°C, while PET decreased to 25.79°C, at higher ratios. Intermediate conditions (H/W = 0.8) recorded moderate values between 27.8 and 28.3°C. M3 recorded very high PET values (41.3°C) at low ratios (H/W = 0–0.4), decreasing gradually to approximately 25°C, at H/W = 1.8. M7 showed stable thermal conditions at high H/W ratios, with PET values ranging between 22 and 23°C, indicating limited sensitivity beyond H/W ≈ 3. Overall, increasing H/W on the right side resulted in lower PET values due to increased shading, while open conditions produced higher thermal sensation in winter.

M1 recorded the highest UTCI value (29.81°C) at H/W = 0.6, decreasing to approximately 20°C, at higher ratios due to excessive shading. M2 showed increased UTCI values (≈30°C) at H/W = 0–0.6, decreasing to 20.39°C, at H/W = 3.8. M3 showed UTCI values of approximately 31°C at low H/W (0–1.1) on western facades, decreasing to about 21°C, at higher H/W on southwest facades. M7 exhibited stable UTCI values at high H/W (3.0–3.8), ranging between 19.5 and 19.96°C.

Table D4-15 M1,M2,M3,M7 PET and UTCI result for right side in weddad street in winter

layout	case	H/W	Façade orientation	PET 2pm	UTCI 2pm
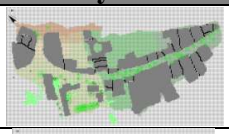	M1a-SW-C15	3.8	SW	24.33	20.25
	M1b-SW-C3	0.8	SW	28.09	29.81
	M1c-SW-C13	2.1	SW	23.78	20.33
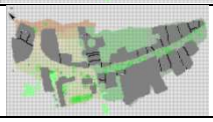	M2a-W-C3	0.8	W	27.82	25.74
	M2b-W-C3	0.8	W	28.31	30.55
	M2c-SW-C15	3.8	SW	25.79	20.39
	M2d-SW-C0	0	SW	34.87	28.85
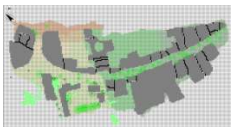	M3e-W-C3	0.6	W	27.1	30.27
	M3f-W-C6	1.1	W	37.02	29.63
	M3g-W-C0	0	W	41.31	31.18
	M3h-SW-C5	0.9	SW	26.4	21.81
	M3i-SW-C11	1.8	SW	25.28	21
	M3j-SW-C2	0.4	SW	38.22	30.6
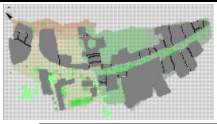	M7a-SW-C14	3.0	SW	22.09	19.5
	M7b-SW-C15	3.8	SW	23.11	19.96

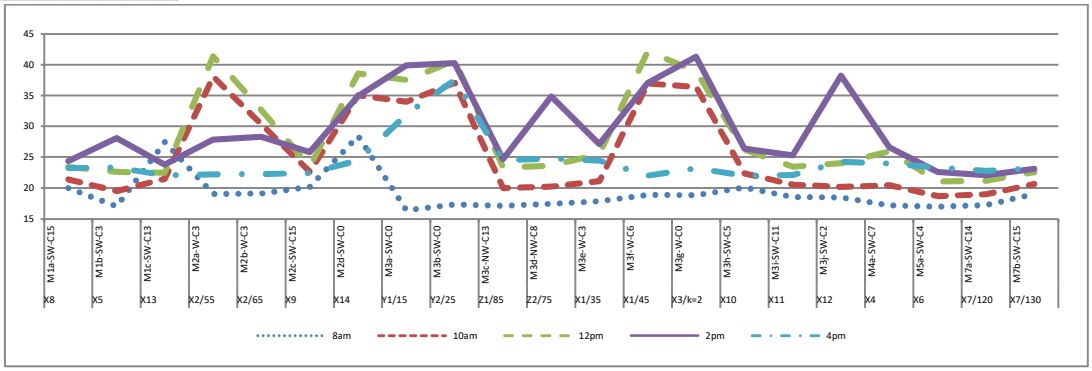

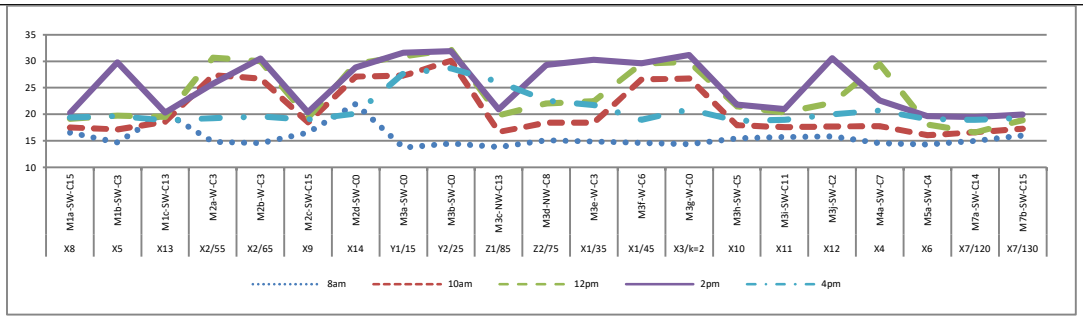

Figure D4-4 a)PET b) UTCI in Weddad (winter)

As shown in Table D4-16, the highest PET value was recorded at X3 (H/W = 0.4), while the lowest value (23.31°C) occurred at M6 (H/W = 1.5). Increasing H/W from 0.8 to 0.9 increased PET by approximately 2–3°C, indicating enhanced heat retention in deeper canyons. The M3d case (H/W = 1.2) recorded the highest PET value (28.65°C), reflecting greater heat trapping. The eastern facades were also warmer than the northeastern facades, reflecting the effect of direct solar radiation on east-oriented streets during winter afternoons. Despite constant H/W and orientation, a difference of ≈2.45°C was recorded between the two cases, with M5b showing higher PET due to increased heat reflection or trapping. For M6 material, the highest PET values were recorded at low H/W ratios (0.8–0.9) at a maximum of 25.77°C, and decreased with increasing depth (1.3–1.6), indicating that wider streets receive more solar radiation in winter compared to deeper ones. Open areas (H/W = 0.4) were approximately 1.2°C warmer than deeper sections (H/W = 1.1), confirming the effect of openness on winter PET.

Left and middle sections showed that the highest UTCI values were recorded at low H/W (0.4–0.9), reaching up to 29.35°C, while values decreased with increasing depth (H/W > 1.3). In deep sections such as X7/130, UTCI values were stable due to reduced lateral radiation influence. Despite the constant H/W, the UTCI in case M5b increased by about 1.5°C.

Table D4-16 M1,M3,M5,M6 PET and UTCI result for the left side in weddad street in winter

layout	case	H/W	Façade orientation	PET 2pm	UTCI 2pm
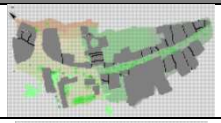	M1a-NE-C4	0.9	NE	26.72	22.3
	M1b-NE-C4	0.9	NE	27.53	23
	M1c-NE-C3	0.8	NE	24.3	21.32
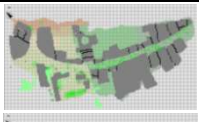	M3c-E-C3	0.8	E	24.96	21.04
	M3d-E-C6	1.2	E	28.65	23.14
	M3e-NE-C12	2.1	NE	26.81	21.3
	M3f-NE-C5	1.1	NE	25.58	21.64
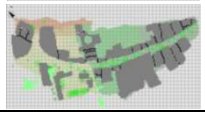	M5a-NE-C6	1.2	NE	24.2	20.87
	M5b-NE-C6	1.2	NE	26.65	22.37

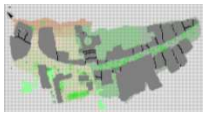	M6a-NE-C8	1.3	NE	23.31	20.73
	M6b-NE-C10	1.6	NE	23.39	20.17
	M6c-NE-C9	1.5	NE	23.37	19.85
	M6d-NE-C4	0.8	NE	25.21	20.18
	M6e-NE-C5	0.9	NE	25.77	20.89
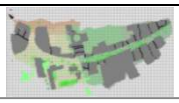	noc-NE-C2	0.4	NE	36.21	29.35
	nod-NE-C6	1.1	NE	34.99	27.31

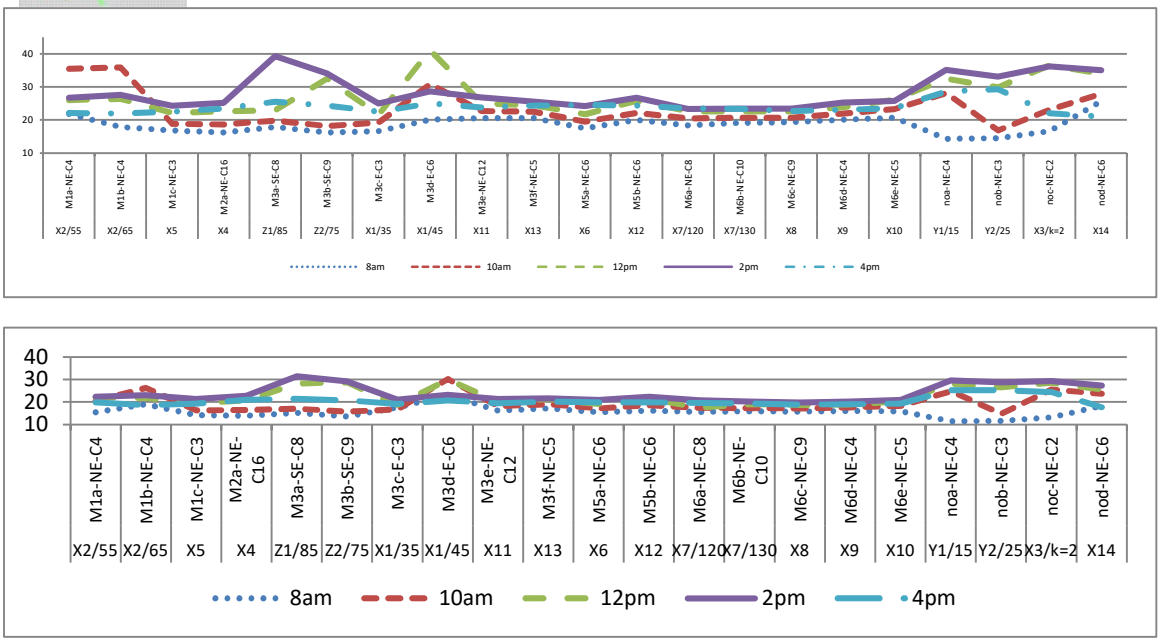

Figure D4-5 a)PET b) UTCI in Weddad (winter)

In X7/120, lateral effects were weak due to balanced orientation, while X3 showed strong heating from westerly exposure affecting the canyon center.

Table D4-17 X7/120 PET results compared three sides

layout	Location	H/W	orientation	PET 2pm
	Right	0.6	SW	22.09
	Middle	-	-	21.97
	Left	0.6	NE	23.31

Table D4-18 X3 PET results compared three sides

layout	Location	H/W	orientation	PET 2pm
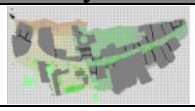	Right	0.6	W	41.31
	Middle	-	-	38.77
	Left	0.8	NE	36.21

As shown in Table D4-19 and Table D4-20,In narrow, open sections such as X2/65, the center is strongly influenced by the sunny west side, while in deep sections such as X7/130 the influence of the sides is reduced and the microclimate within the groove is stable.

Table D4-19X2/65 UTCI results compared for three sides

layout	Location	H/W	Material	orientation	UTCI 2pm

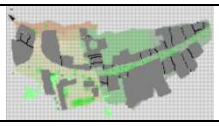	Right	0.6	M2	W	30.55
	Middle	-	-	-	30.13
	Left	0.6	M1	E	23

Table D4-20X7/130 UTCI results compared for three sides

layout	Location	H/W	Material	orientation	UTCI 2pm
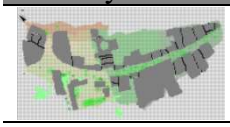	Right	3.8	M7	SW	19.96
	Middle	-	-	-	19.47
	Left	1.5	M6	NE	20.17

b) Ibn rushed street:

As shown in Table D4-21, the highest PET value was recorded at H/W = 1.1, while the lowest value (25.38°C) occurred at H/W = 0. M3 recorded its highest PET value (40.04°C) at H/W = 1.1, with other cases ranging between 34 and 38.5°C without a clear linear pattern. M7 showed an increase in PET to above 36°C, at H/W = 0.9, compared to 25.38°C in the open condition, indicating strong afternoon solar exposure on western facades.

UTCI values generally ranged between 28.6 and 30.2°C for M3, showing near-thermal stability with slight increases at low H/W. M7 recorded values between 28.3 and 29.3°C, indicating limited sensitivity to H/W under strong western solar exposure.

Table D4-21 M3,M7 PET and UTCI result in Ibn rushed street for right side in winter

	case	H/W	Façade orientation	PET 2pm	UTCI 2pm
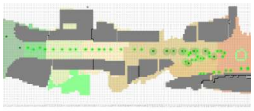	M3a-W-C3	0.6	W	35.17	28.6
	M3b-W-C4	0.8	W	35.33	30.01
	M3c-W-C4	0.8	W	34.02	29.36
	M3d-W-C6	1.1	W	40.04	29.46
	M3e-W-C7	1.2	W	34.37	29.07
	M3f-W-C4	0.8	W	38.52	30.23
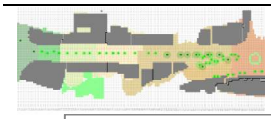	M7a-W-C0	0	W	25.38	28.35
	M7b-W-C5	0.9	W	36.18	29.26
	M7c-W-C5	0.9	W	34.33	29.3

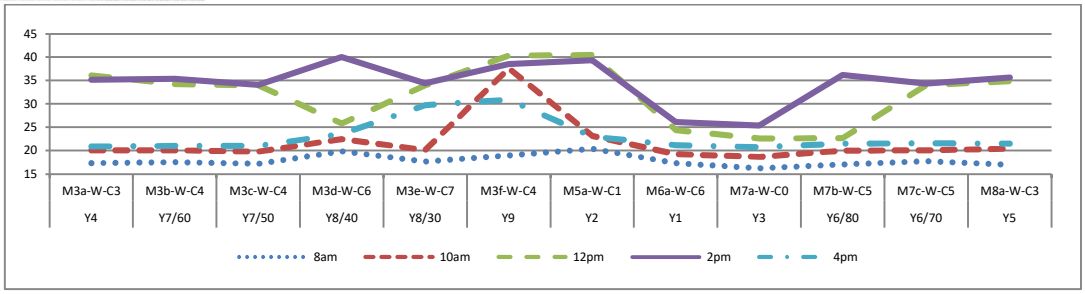

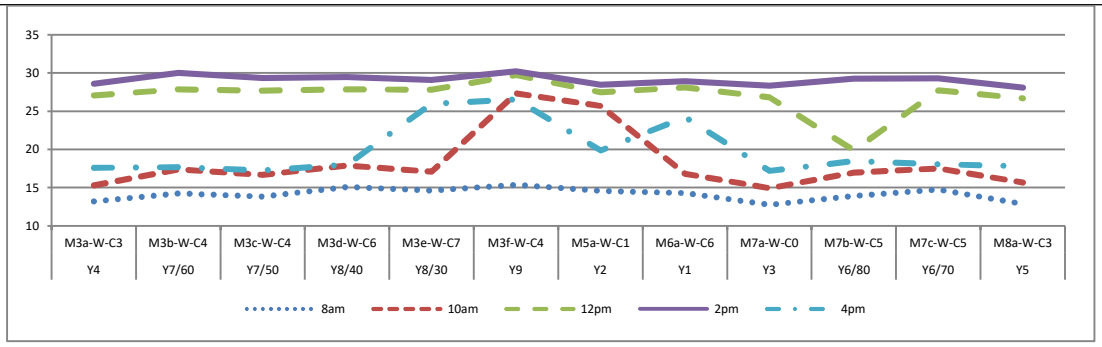

Figure D4-6 a)PET b) UTCI in Ibn rushed

Wider streets (H/W = 0.6) recorded higher PET values, while deeper gullies (H/W = 1.1) were cooler due to shading.M7 Increasing H/W from 0.4 to 0.6 resulted in a slight PET increase of approximately 0.36°C. M9b (H/W = 0.6) recorded the highest PET value (37.41°C), while M9a (H/W = 0.8) showed lower values due to increased shading.

Wider streets (H/W = 0.6) recorded UTCI values up to 21.69°C, while deeper gullies (H/W = 1.1) showed lower values. Open conditions (H/W = 0.4) increased UTCI to 26.6°C, while deeper configurations reduced it to 20.6°C. M9b (H/W = 0.6) recorded the highest UTCI value (30.64°C.

Table D4-22 M3,M7,M9 PET and UTCI result in Ibn rushed street for the left side in winter

layout	case	H/W	Façade orientation	PET 2pm	UTCI 2pm
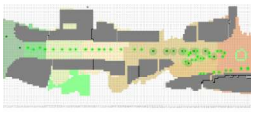	M3a-E-C6	1.1	E	23.07	20.19
	M3b-E-C6	1.1	E	23.36	20.34
	M3c-E-C6	1.1	E	23.62	20.74
	M3d-E-C3	0.6	E	24.33	21.69
	M3e-E-C3	0.6	E	22.98	20.42
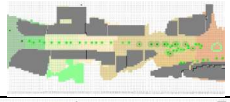	M7a-E-C2	0.4	E	22.94	26.64
	M7b-E-C3	0.6	E	23.3	20.56
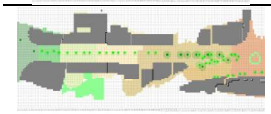	M9a-E-C4	0.8	E	25.26	21.37
	M9a-E-C4	0.8	E	23.95	20.69
	M9b-E-C3	0.6	E	37.41	30.64

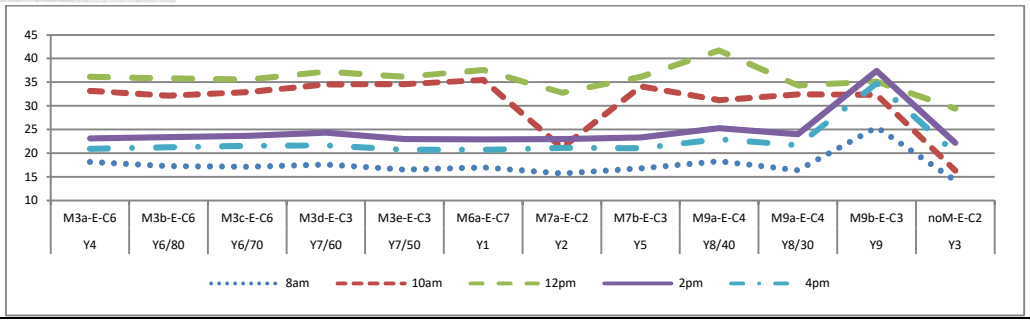

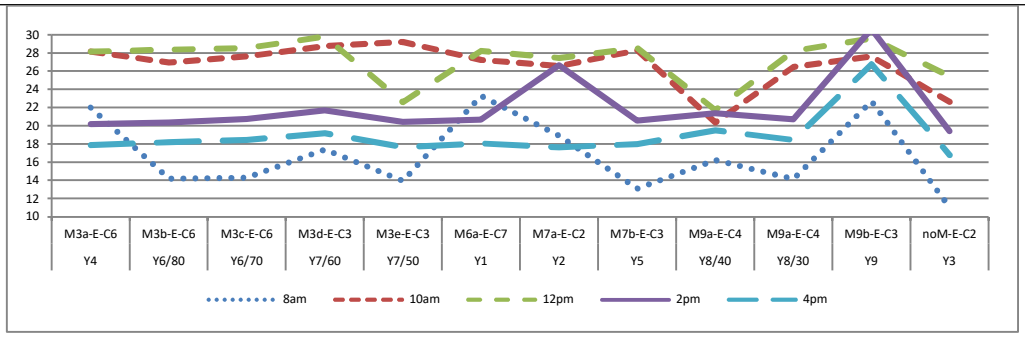

Figure D4-7 a)PET b) UTCI in Ibn rushed

In section Y3, lateral contrast contributed to cooling, while in Y9, combined heating from both sides increased PET and winter heat stress.

Table D4-23 Y3 PET Result in Ibn rushed street in winter

layout	Location	H/W	Material	orientation	PET 2pm
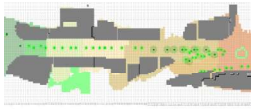	Right	0.8	M7	W	25.38
	Middle	-	-	-	23.47
	Left	0.6	noM	E	22.17

In shaded sections such as Y7/50 the medium remains cooler due to limited radiation, while in more open sections such as Y9 the medium is directly affected by reflected radiation from the sides, so the UTCI rises and the thermal sensation increases.

Table D4-24Y9 PET Result in Ibn rushed street in winter

layout	Location	H/W	Material	orientation	PET 2pm	UTCI 2pm
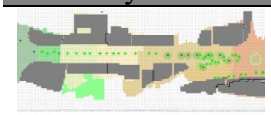	Right	1.2	M3	W	38.52	30.23
	Middle	-	-	-	33.02	28.42
	Left	0.8	M9	E	37.41	30.64

Table D4-25 Y7/50 UTCI result in Ibn rushed street in winter

layout	Location	H/W	Material	orientation	UTCI 2pm
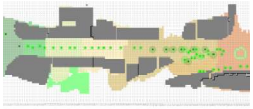	Right	0.8	M3	W	29.36
	Middle	-	-	-	20.28
	Left	0.4	M3	E	20.42

The left and middle side analyses for both streets are presented to support the detailed interpretation provided in the main text, while maintaining numerical completeness for reference and comparison.

APPENDIXD-5:

ENVI-met full maps

Table D5-1 (heat maps and ENVI-met images) provides a spatial reference for Weddad, Ibn Rushed, and Haymoni Streets on the summer day (June 22), supporting interpretation of thermal and ventilation patterns across sections.

Table D5-1 Thermal map for wedad street , Ibn rushed ,and example in street (section 1) in summer

Weddad street, himonies and Ibn rushed 22/6						
Factors		8	10	12	2	4
General street	Ta					
	W	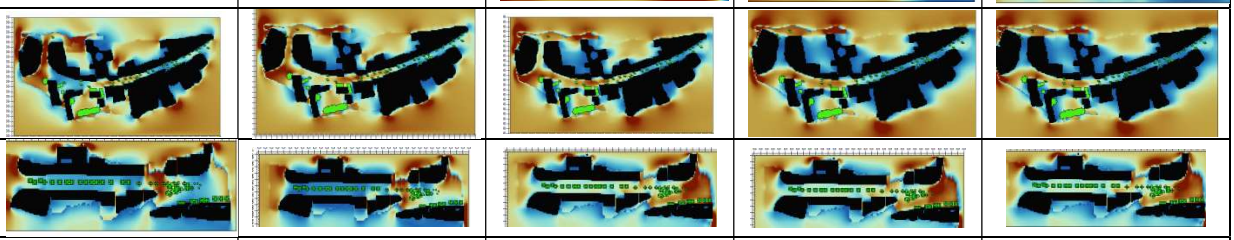				
	Rh	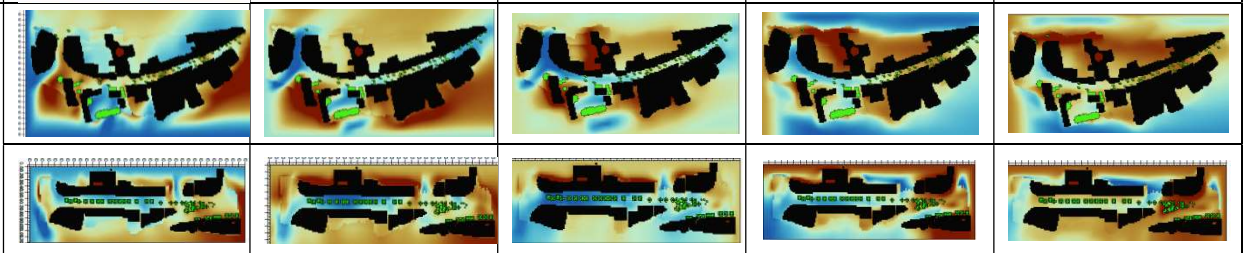				
	PET	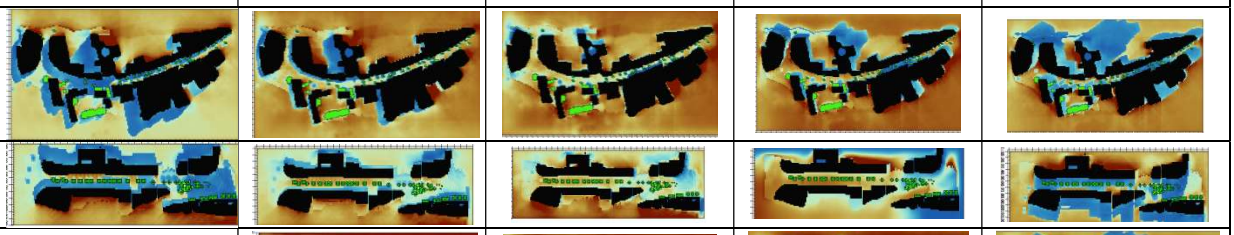				
	UTCI	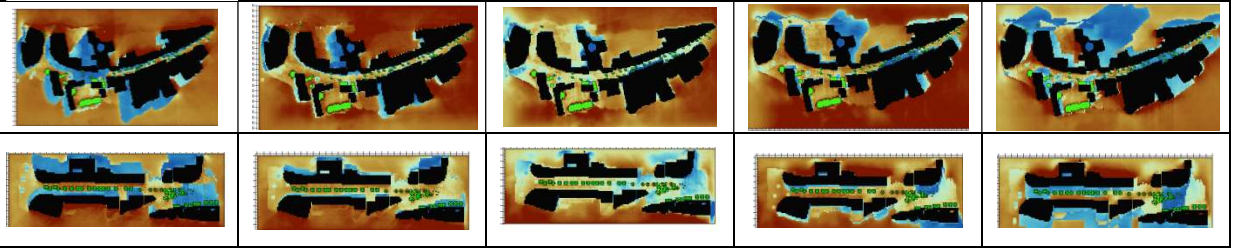				

Example of section in weddad street in summer(data extract from three sides right,left,middle)						
X7/130	Ta	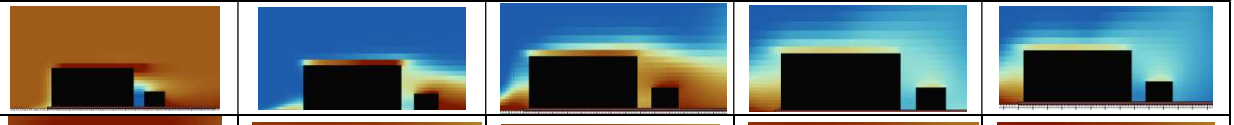				
	W	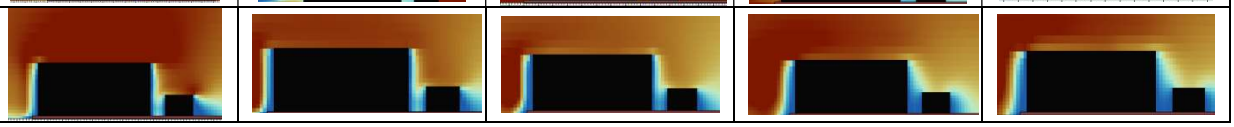				

	Rh	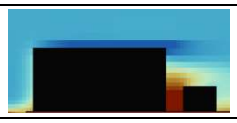	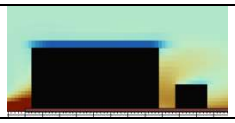	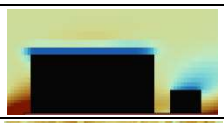	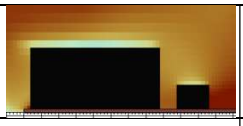	
	PET	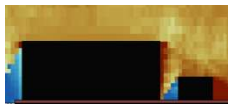		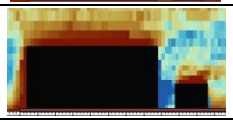		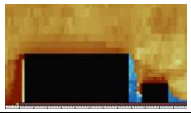
	UTCI	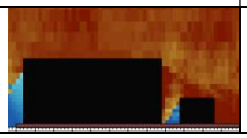	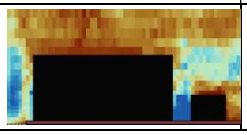	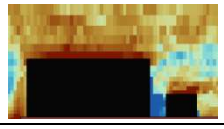	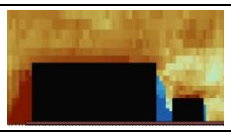	

Appendix D - 6

Statistical Outputs:

- **Inferential statistics MLR (summer):**

Table D6-1 Tukey HSD test results in summer

Tukey HSD test results						
case	**Materials**	**Notes**				
time		8	10	12	2	4
Case 1	M1a-SW-C15(X8) M2c-SW-C15(X9) M7b-SW-C15(X7/130)	Ta				
		-	-	-	-	-
		Wind speed				
		M1a-M7b M2c-M7b	M1a-M7b M2c-M7b	-	-	M1a-M2c M1a-M7b
		Relative humidity				
		-	-	-	-	-
		UTCI				
		M1a-M2c M2c-M7b	M1a-M2c M1a-M7b M2c-M7b	-	-	-
		PET				
		M1a-M2c M1a-M7b M2c-M7b	M1a-M2c M1a-M7b M2c-M7b	-	-	-
Case 2	M2d-SW-C0(X14) M3a-SW-C0(Y1/15) M3b-SW-C0(Y2/25)	Ta				
		-	-	-	-	-
		Wind speed				
		-	-	M2d-M3a M3a-M3b	M2d-M3a M3a-M3b	M2d-M3a M3a-M3b
		Relative humidity				
		-	-	-	-	-
		UTCI				
		M2d-M3b M3a-M3b	M2d-M3b M3a-M3b	-	-	M2d-M3a
		PET				
		M2d-M3b M3a-M3b	M2d-M3b M3a-M3b	M2d-M3b	M2d-M3a M3a-M3b	M2d-M3a M3a-M3b
Case 3	M2a-W-C3(X2/55) M2b-W-C3(X2/65) M3e-W-C3(X1/35) M3a-W-C3(Y4) M8a-W-C3((Y5)	Ta				
		-	-	-	-	-
		Wind speed				
		M2a-M3a M2a-M8a M2b-M3a M2b-M8a	M2a-M3a M3a-M3e	M2a-M3a M2b-M3a M3a-M3e	M2a-M3a M2a-M3e M2b-M3a M2b-M3e M3a-M3e M3e-M8a M3a-M8a	Al groups except M2a-M2b M2a-M8a M2b-M8a

Tukey HSD test results						
case	**Materials**	**Notes**				
time		8	10	12	2	4
		Relative humidity				
		-	-	-	-	-
		UTCI				
		M3e- M8a M2a-M8a M2b-M3a M3a-M8a	M2a-M3a M2b-M3a M3a-M8a	-	-	M3e-M8a
		PET				
		M2a-M8a M2b-M8a M3a-M8a M3e-M8a	M2a-M8a M2b-M8a M3a-M8a M3e-M8a	-	M3a-M3e M3e-M8a	M2a-M3e M3a-M3e M3e-M8a
Case 4	M3f-W-C6(X1/45) M3d-W-C6(Y8/40) M6a-W-C6(Y1)	Ta				
		-	-	-	-	-
		Wind speed				
		M6a-M3d	M3f-M6a M6a-M3d	M3f-M6a M6a-M3d	M3f-M6a M3f-M3d M6a-M3d	M3f-M6a M3f-M3d M6a-M3d
		Relative humidity				
		-	-	-	M3f-M6a	M3f-M6a M3f-M3d
		UTCI				
		-	-	-	-	M3f-M6a M3f-M3d
		PET				
		M6a-M3d	M3f-M6a M6a-M3d	-	M3f-M6a M6a-M3d	M3f-M6a M3f-M3d
Case 5	M7a-W-C0(Y3) M3g-W0C0(X3)	Ta				
		-	-	-	-	-
		Wind speed				
		M3-M7	-	-	-	-
		Relative humidity				
		-	-	-	-	-
		UTCI				
		M3-M7	M3-M7	-	-	-
		PET				
		-	-	-	-	-
Case 6	M3c-E-C3(X1/35) M3d-E-C3(Y7/60) M3e-E-C3Y7/50) M7b-E-C3(Y5) M9b-E-C3(Y9)	Ta				
		-	-	-	-	-
		Wind speed				
		-	-	M3c-M3d M3c-M3e M3c-M7b M3e-M9b M7b-M9b	All groups except M3d-M3e M3e-M7b	M3c-M9b M3d-M9b M3e-M9b M7b-M9b
		Relative humidity				
		-	-	M3c-M3d M3c-M3e M3c-M7b	-	-
		UTCI				
		-	-	-	-	-
		PET				
		M3c-M3e M3e-M9b	-	M3c-M3e M3c-M7b M3c-M9b	M3c-M9b M3d-M9b M3e-M9b M7b-M9b	M3c-M0b M3d-M9b M3e-M9b M7b-M9b
Case 7	M1a-NE-C4(X2/55) M1b-NE-C4(X2/65) M6d-NE-C4(X9)	Ta				
		-	-	-	-	-
		Wind speed				

Tukey HSD test results						
case	**Materials**	**Notes**				
time		8	10	12	2	4
	noa-NE-C4(Y1/15)	M1a-noa M1b-noa M6d-noa	M6d-noa	M1a-M6d M1b-M6d M6d-noa	M1a-M6d M1b-M6d M6d-noa	All group except M1a-M1b M1b-noa
		Relative humidity				
		-	-	-	-	-
		UTCI				
		All groups except M6d-noa	All groups except M1b-noa	M1b-M6d M6d-noa	M1b-M6d M6d-noa	M1b-M6d M6d-noa
		PET				
		All groups except M1a-M1b	M1a-M6d M1b-M6d M6d-n0a	All groups except M1a-M6d M1b-noa	All groups except M1a-M6d M1b-noa	M1a-M6d M1b-noa M6d-noa
Case 8	M3f-NE-C5(X13) M6e-NE-C5(X10)	Ta				
		-	-	-	-	-
		Wind speed				
		-	M3f-M6e	M3f-M6e	-	-
		Relative humidity				
		-	-	-	-	-
		UTCI				
		M3f-M6e	M3f-M6e	M3f-M6e	-	-
		PET				
		M3f-M6e	M3f-M6e	M3f-M6e	-	-

Table D6-2 Adjusted R^2 and regression model for MLR in summer

SUMMER results/U (U-value)/C (canyon H/W)					
Independent	orientation	time	Regression model	R^2 adjusted	P-value(model)
temperature	SW	2	Ta2pm=35.14−0.28*U−0.22*C (H/W)	0.53	0.0066
	NE	8	Ta 8pm=26.29−0.25*U+0.03*C (H/W)	0.48	0.0042
		10	Ta 10pm=29.33−0.26*U+0.10*C	0.36	0.017
		2	Ta 2pm=34.6−0.27*U+0.08*C(H/W)	0.33	0.025
		4	Ta 4pm=33.41−0.17*U+0.04*C(H/W)	0.32	0.027
Wind speed	NE	8	Ws 8am=1.058−0.242*U+0.052*C	0.46	0.0049
		10	Ws 10am=1.217−0.278*U+0.031*C	0.53	0.0018
		12	Ws 12pm=1.658−0.394*U+0.029*C	0.53	0.0019
		2	Ws 2pm=2.124−0.542*U+0.022*C	0.54	0.0015
		4	Ws 4pm=2.878−0.742*U+0.039*C	0.54	0.0017
Relative humidity	SW	12	RH = 35.804 + 0.000 × U + 0.449 × C	0.28	0.064
		2	RH = 29.135 + 0.218 × U + 0.392 × C	0.31	0.0503
	NE	12	RH = 35.280 + 0.587 × U – 0.104 × C	0.42	0.008589
		2	RH = 29.331 + 0.467 × U – 0.111 × C	0.32	0.024119
		4	RH = 34.488 + 0.304 × U – 0.067 × C	0.33	0.023542
PET	SW	2	PET= 50.399 -2.339 × U + -1.770 × C	0.41	0.020205
	NE	2	PET=44.682−2.298×U−0.150×C	054	0.00159
UTCI	E	2	UTCI=45.030−2.328×U−3.597×C	0.37	0.0289
	W	10	UTCI=39.99-2.61*U-0.85*C	0.22	0.068
		4	UTCI=37.97+0.701*U-4.16*C	0.15	0.122
	SW	2	UTCI=42.0−1.3×U−1.06×C	0.31	0.049

SUMMER results/U (U-value)/C (canyon H/W)					
Independent	orientation	time	Regression model	R^2 adjusted	P-value(model)
	NE	12	UTCI=33.55-0.73*U+0.48*C	0.13	0.13
		2	UTCI= 38.939−1.679×U+0.067×C	0.61	0.0004

- **Inferential statistics MLR (winter):**

"Table D6-3 MLR P-VALUE results for independent variables (u-value, H/W) in winter

WINTER P-value (P-value <0.05 green, P-value >0.05 pink)									
Independent	time	E		W		SW		NE	
		u-value	canyon	u-value	canyon	u-value	canyon	u-value	canyon
temp	8	0.76	0.91	0.12	0.28	0.91	0.72	0.2	0.97
	10	0.45	0.6	0.67	0.88	0.57	0.21	0.46	0.93
	12	0.73	0.68	0.31	0.17	0.65	0.042	0.07	0.84
	2	0.8	0.43	0.52	0.65	0.66	0.0023	6.6E-05	0.45
	4	0.84	0.65	0.73	0.98	0.36	0.005	0.00046	0.47
wind	8	0.19	0.03	0.71	0.57	0.88	0.17	0.0001	0.07
	10	0.39	0.03	0.68	0.63	0.9	0.13	7.2E-05	0.1
	12	0.26	0.017	0.97	0.93	0.92	0.11	5.3E-05	0.19
	2	0.56	0.55	0.46	0.2	0.67	0.71	0.00011	0.32
	4	0.89	0.95	0.94	0.7	0.89	0.94	0.0005	0.81
humid	8	0.64	0.51	0.7	0.46	0.13	0.57	0.03	0.12
	10	0.31	0.54	0.71	0.2	0.17	0.68	0.82	0.09
	12	0.98	0.56	0.7	0.13	0.1	0.29	0.58	0.11
	2	0.78	0.91	0.78	0.41	0.51	0.007	0.002	0.7
	4	0.97	0.25	0.91	0.89	0.52	0.0049	0.00046	0.61
PET	8	0.503	0.45	0.74	0.91	0.68	0.95	0.27	0.509
	10	0.96	0.057	0.83	0.61	0.56	0.07	0.63	0.38
	12	0.37	0.06	0.94	0.78	0.76	0.02	8.6E-06	0.31
	2	0.38	0.88	0.12	0.92	0.43	0.006	1.8E-07	0.56
	4	0.33	0.91	0.29	0.44	0.49	0.09	0.28	0.98
UTCI	8	0.95	0.21	0.34	0.14	0.66	0.85	0.044	0.44
	10	0.56	0.45	0.83	0.51	0.59	0.057	0.06	0.44
	12	0.67	0.23	0.72	0.87	0.26	0.007	7E-07	0.82
	2	0.49	0.5	0.04	072	0.73	0.0023	6.8E-09	0.55
	4	0.404	0.83	0.47	0.34	0.61	0.08	0.005	0.72

Table D6-4 Adjusted R^2 for MLR in winter

SUMMER results/U (U-value)/C (canyon H/W)					
Independent	orientation	time	Regression model	R^2 adjusted	P-value
temperature	SW	12	Ta12pm=21−0.11*U−0.29*C(H/W)	0.2	0.115
		2	Ta2pm=22.57−0.07*U−0.33*C(H/W)	0.51	0.008
		4	Ta4pm=22.1−0.15*U−0.29*C(H/W)	0.43	0.02
	NE	2	Ta2pm=22.59−0.37*U+0.05*C(H/W)	0.65	0.0002
		4	Ta4pm=21.8−0.3*U+0.05*C(H/W)	0.53	0.0017
Wind speed	E	8	Ws8am=1.78−0.31*U-0.45*C	0.44	0.015
		10	Ws 10am=1.99−0.3*U-0.65*C	0.36	0.03
		12	Ws 12pm=2.91−0.48*U-0.93*C	0.47	0.011
	NE	8	Ws8am=0.57−0.15*U+0.062*C	0.59	0.00069
		10	Ws 10am=0.76−0.21*U+0.07*C	0.64	0.00028
		12	Ws 12pm=1.05−0.29*U+0.075*C	0.65	0.0002
		2	Ws 2pm=0.9−0.22*U+0.04*C	0.61	0.0004
		4	Ws 4pm=1.2−0.29*U+0.017*C	0.55	0.0013
Relative humidity	SW	2	RH = 38.28 - 0.37 × U + 0. 92 × C	0.43	0.016
		4	RH = 35.63 + 0.22 × U + 0.62 × C	0.44	0.016

SUMMER results/U (U-value)/C (canyon H/W)					
Independent	orientation	time	Regression model	R^2 adjusted	P-value
PET	NE	8	RH = 55.22 - 0.58 × U + 0.447 × C	0.22	0.068
		2	RH = 36.87 + 0.85 × U + 0.09 × C	0.44	0.0064
		4	RH = 35.97 + 0.63 × U – 0.07 × C	0.54	0.0016
	SW	12	PET= 29.29 +0.68 × U + -2.79 × C	0.26	0.07
		2	PET= 29.63 +1.48 × U + -3.09 × C	0.44	0.014
	NE	12	PET=33.26−3.004×U−0. 50×C	0.76	1.53E-05
		2	PET=34.62−3.2×U−0. 21×C	0.85	4.57E-07
UTCI	W	2	UTCI=22.95+2.15×U−0.29×C	0.14	0.12
	SW	12	UTCI=31.5-1.8*U-2.54*C	0.41	0.21
		2	UTCI=27.1+0.45*U-2.61*C	0.59	0.0068
	NE	8	UTCI=14.05+0.83×U−0.31×C	0.15	0.12
		12	UTCI=27.08-2.43*U- 0.07*C	0.82	1.96E-06
		2	UTCI= 28.44−2.58×U+0.13×C	0.9	2.42E-08
		4	UTCI= 22.86−1.22×U+0.14×C	0.35	0.017

Appendix D-7

- **LR In summer:**

Linear regression for NE, SW, E, W orientations:

All equations are statistically significant ($p < 0.05$).

The adjusted R^2 is good, ranging from 0.2 to 0.50, which is very close to the binary model (with canyon).The u-value alone reliably explains the thermal pattern in the NE direction, and the canyon does not add any significant explanation.

*Note: all P-value for the variables (H/W, U-value) in liner regression is new for one variable only.

Table D7-1 LR for temperature in summer for NE

NE orientation/Temperature all times in summer				
time	Simple Equation	adjusted R^2	P-value (model)	P-value (u-value)
8am	8am: Temp = 26.315 + (-0.247)*u-value	0.532856878	0.0009	0.000879
10am	10am: Temp = 29.420 + (-0.243)*u-value	0.382669818	0.0081	0.008
12pm	12pm: Temp = 33.087 + (-0.238)*u-value	0.252385372	0.0399	0.040
2pm	2pm: Temp = 34.676 + (-0.257)*u-value	0.374040379	0.0091	0.009
4pm	4pm: Temp = 33.448 + (-0.166)*u-value	0.382670469	0.0081	0.008

Table D7-2 LR for wind speed in summer for NE

NE orientation/wind speed all times in summer				
time	Simple Equation	adjusted R^2	P-value (model)	P-value (u-value)
8am	8am: wind = 1.099−0.230·u_value	0.478	0.00126	0.00126
10am	10am: wind = 1.242−0.270·u_value	0.561	0.000329	0.000329
12pm	12pm: wind = 1.680−0.387·u_value	0.562	0.000319	0.000319
2pm	2pm: wind = 2.142−0.537·u_value	0.577	0.000244	0.000244
4pm	4pm: wind = 2.908−0.734·u_value	0.569	0.000281	0.000281

Table D7-3 LR for SW and NE orientation for relative humidity in summer

SW orientation/relative humidity at 10/12/2pm in summer				
time	Simple Equation	adjusted R^2	P-value (model)	P-value (u-value)
10am	10am: RH = 46.737 + 0.590 × canyon	0.25	0.0383	0.0383
12pm	12pm: RH = 35.804 + 0.449 × canyon	0.34	0.01648	0.01648
2pm	2pm: RH = 29.737 + 0.376 × canyon	0.33	0.01769	0.01769
NE orientation/relative humidity at 10/12/2pm in summer				
12pm	12pm: RH = 35.19 + 0.56 × canyon	0.44	0.0021	0.0021
2pm	2pm: RH = 29.24 + 0.449 × canyon	0.35	0.0071	0.0071
4pm	4pm: RH = 34.43 + 0.29 × canyon	0.35	0.0067	0.0067

Table D7-4 LR eq for SW,NE orientation for PET in summer

SW orientation/PET at 2pm in summer				
time	Simple Equation	adjusted R^2	P-value (model)	P-value (canyon)
2pm	2pm: PET = 43.943−1.600×canyon	0.27	0.032	0.032
NE orientation/PET at 2pm in summer				
2pm	2pm: PET =44.563−2.333×u-value	0.57	0.000264	0.000264

Table D7-5 LR eq for E,W,SW,NE orientation for UTCI in summer

E orientation/UTCI at 2pm in summer				
time	Simple Equation	adjusted R^2	P-value (model)	P-value (u-value)
2pm	2pm: UTCI = 38.601−4.313×canyon	0.36	0.0137	0.0137
4pm	4pm: UTCI = 36.59−4. 13×canyon	0.255	0.037	0.037
W orientation/UTCI at 2pm in summer				
10am	10am: UTCI =39.91−2.79×u-value	0.23	0.0285	0.0285
time	Simple Equation	adjusted R^2	P-value (model)	P-value (canyon)
4pm	4pm: UTCI =40−4.06×canyon	0.20	0.039	0.039
SW orientation/UTCI at 2pm in summer				
2pm	2pm: UTCI = 38.39−0.96×canyon	0.22	0.048	0.048
NE orientation/UTCI at 12,and 2pm in summer				
time	Simple Equation	adjusted R^2	P-value (model)	P-value (u-value)
12pm	12pm: UTCI = 36.66−0.9×u-value	0.26	0.021	0.021
2pm	2pm: UTCI = 38.99−1.66×u-value	0.64	6.51E-05	6.51E-05

- **LR in winter:**

A linear regression analysis was not performed for the winter season only. Multiple linear regression analysis was used, as the results for the winter season are limited.

Appendix E
General result (By section)

Summer:

Table E-1 Temperature wedad street result(summer) in three point for 5 times by sections

+	WEDAD/Temperature 22/6/2021														
	At 1m from right building					At 5m middle distance					At 1m from left building				
Simulation	8am	10am	12pm	2pm	4pm	8am	10am	12pm	2pm	4pm	8am	10am	12pm	2pm	4pm
Y1/15	26.18	28.15	32.01	34.21	33.32	26.54	29.26	32.52	34.22	33.37	26.49	29.26	32.54	34.22	33.49
Y2/25	26.77	29.64	32.97	34.81	33.55	26.98	30.58	33.75	34.85	33.81	26.52	29.79	33.61	34.82	33.77
Z1/85	26.11	29.16	33.11	35.12	33.48	26.21	29.42	33.43	35.08	33.45	26.27	29.73	33.52	34.77	33.41
Z2/75	26.04	29.33	33.12	35.5	33.95	26.37	29.65	33.37	35.49	33.76	26.52	29.72	33.25	35.09	33.6
X1/35	26.15	29.58	33.37	35.62	34.18	26.21	30.14	34.13	35.36	34.01	26.06	29.29	32.72	34.27	33.44
X1/45	26.03	29.52	34.3	35.57	34.16	26.09	29.9	34.16	34.91	33.71	26.06	29.88	33.55	34.41	33.43
X2/55	25.68	29.16	33.87	35.21	33.77	25.85	29.4	33.75	35.01	33.64	26.03	29.06	32.78	34.53	33.36
X2/65	25.39	28.96	33.62	35.15	33.69	25.62	29.23	33.62	35.15	33.66	25.84	29.18	33.15	34.86	33.4
X3/k=2	24.87	28.59	33.1	34.86	33.51	25.52	29.05	33.33	34.95	33.5	26.11	29.41	33.3	34.89	33.36
X4	25.66	28.91	33.03	34.63	33.44	25.8	29.3	33.46	34.94	33.51	26.08	29.57	33.38	34.71	33.4
X5	25.6	29.1	33.25	34.6	33.32	25.64	29.21	33.28	34.56	33.25	25.68	29.18	33.14	34.31	33.14
X6	25.51	28.78	32.8	34.12	33.16	25.63	29.02	33.01	34.35	33.23	25.81	29.19	33.01	34.13	33.17
X7/120	25.28	28.55	32.56	34.03	33.07	25.41	28.74	32.58	34.11	33.09	25.52	28.74	32.55	33.98	33.06
X7/130	25	28.18	32.06	33.55	32.83	24.98	28.25	32.04	33.55	32.83	25.01	28.3	31.98	33.55	32.83
X8	25.39	28.26	31.97	33.51	32.79	25.4	28.25	31.93	33.49	32.79	25.44	28.27	31.91	33.49	32.79
X9	25.73	28.47	32.09	33.61	32.85	25.71	28.49	32.06	33.59	32.85	25.71	28.46	32.01	33.57	32.84
X10	25.44	28.23	31.88	33.42	32.65	25.52	28.33	31.95	33.43	32.67	25.6	28.37	31.95	33.39	32.66
X11	24.89	28.08	31.72	33.42	32.5	24.9	28.04	31.68	33.36	32.47	24.92	28	31.63	33.29	32.45
X12	25.54	28.64	32.2	34.08	32.94	25.69	28.76	32.27	34.06	32.94	25.86	28.82	32.3	33.96	32.92
X13	25.59	28.7	32.19	34.2	33.01	25.68	28.78	32.23	34.2	33.03	25.74	28.78	32.2	34.15	33.02
X14	25.52	28.71	32.29	34.34	32.91	25.82	28.9	32.42	34.5	33.01	26.02	28.9	32.37	34.32	32.93

Table E-2 Temperature Ibn rushed street result (summer) in three point for 5 times by sections

+	IBN rushed/Temperature 22/6/2021														
	At 1m from right building					At 5m middle distance					At 1m from left building				
Simulation	8am	10am	12pm	2pm	4pm	8am	10am	12pm	2pm	4pm	8am	10am	12pm	2pm	4pm
Y1	25.32	27.97	33.03	33.92	32.96	25.66	28.58	33.72	35.02	33.47	25.77	28.7	31.29	33.07	32.36
Y2	25.97	28.53	33.31	35.08	32.64	25.87	28.04	31.85	33.7	32.64	26.03	28.68	32.46	33.56	32.72
Y3	26.15	29.03	33.23	34.57	33.74	26.29	29.08	33.09	34.57	33.89	26.36	29.24	33.32	34.98	34.23
Y4	26.07	28.34	32.7	34.63	33.81	26.19	28.77	32.95	34.68	33.65	26.17	29.51	33.23	34.15	33.3
Y5	26.32	29.65	33.7	34.91	33.83	26.35	29.61	33.43	34.63	33.34	26.35	29.8	33.65	34.12	33.14
Y6/80	26.05	28.74	33.16	34.62	33.53	26.14	29.28	33.27	34.57	33.36	26.19	29.6	33.39	34.22	33.14
Y6/70	26.02	28.72	33.12	34.78	33.5	26.16	29.17	33.3	34.55	33.28	26.27	29.64	33.47	34.26	33.16
Y7/60	25.95	29.34	33.68	35.2	33.77	26.26	30.29	34.03	35.14	33.45	26.52	30.69	34.1	34.53	33.26
Y7/50	25.96	29.38	33.9	35.28	33.76	26.19	29.95	33.87	34.96	33.37	26.49	30.77	34.31	34.48	33.2
Y8/40	26.05	29.27	33.93	35	33.41	26.14	29.8	34.13	34.69	33.25	26.19	30.33	34.5	34.29	33.08
Y8/30	26.3	28.91	34.25	35.08	33.27	26.42	29.3	34.27	34.56	33.12	26.4	29.71	34.61	34.2	32.98
Y9	26.61	29.35	33.92	35.2	33.56	26.75	29.69	33.6	35.25	33.51	26.37	28.92	32.68	34.96	33.78

Table E-3wind speed wedad street result(summer) in three point for 5 times by sections

+	WEDAD/Wind speed 22/6/2021														
	At 1m from right building					At 5m					At 1m from left building				
Simulation	8am	10am	12pm	2pm	4pm	8am	10am	12pm	2pm	4pm	8am	10am	12pm	2pm	4pm
Y1/15	1.14	1.21	1.28	1.05	1	1.3	1.66	2.27	2.8	3.87	1.37	1.45	1.9	2.21	3.13
Y2/25	0.76	0.6	0.57	0.37	0.47	1.73	1.71	2.15	2.21	3.04	1.45	1.4	1.75	1.99	2.79
Z1/85	0.97	0.76	0.69	0.07	0.19	1.86	1.24	1.09	0.13	0.3	0.97	0.67	0.61	0.09	0.2
Z2/75	1.19	0.89	0.87	0.25	0.51	1.89	1.33	1.32	0.42	0.76	1.49	1.15	1.15	0.43	0.69
X1/35	0.84	0.52	0.43	0.034	0.11	0.98	1.04	1.41	1.78	2.41	0.28	0.76	1.1	1.82	2.44
X1/45	0.22	0.99	1.62	2.25	3.16	0.26	1.19	2.03	3.1	4.21	0.03	0.1	0.16	0.32	0.45
X2/55	0.35	0.8	1.22	1.59	2.13	0.48	0.95	1.51	2.14	2.88	0.59	1	1.49	2.05	2.71
X2/65	0.36	0.88	1.35	1.88	2.51	0.4	0.97	1.55	2.23	3.01	0.41	0.99	1.58	2.33	3.14
X3	0.52	0.93	1.37	1.95	2.62	0.55	1.05	1.66	2.39	3.23	0.6	0.99	1.6	2.36	3.18
X4	1	0.93	1.09	0.87	1.19	1.45	1.31	1.59	1.48	2.06	0.75	0.76	0.98	1.14	1.59
X5	1.1	1.09	1.3	1.16	1.55	1.28	1.25	1.5	1.34	1.81	1.03	0.97	1.13	1.03	1.39
X6	1.25	1.13	1.3	0.95	1.36	1.35	1.22	1.4	1.02	1.45	0.83	0.81	0.95	0.78	1.11
X7/120	1.25	1.16	1.29	0.85	1.21	1.36	1.25	1.4	0.9	1.28	0.53	0.5	0.55	0.34	0.49
X7/130	0.69	0.67	0.71	0.42	0.55	1.05	0.99	1.03	0.59	0.78	0.59	0.56	0.6	0.35	0.47
X8	0.29	0.3	0.29	0.24	0.3	0.53	0.53	0.49	0.38	0.47	0.43	0.42	0.39	0.29	0.35
X9	0.3	0.4	0.43	0.52	0.65	0.4	0.5	0.48	0.56	0.69	0.12	0.1	0.14	0.15	0.19
X10	0.3	0.43	0.48	0.61	0.72	0.29	0.43	0.48	0.61	0.73	0.04	0.03	0.05	0.1	0.14
X11	0.69	0.62	0.59	0.58	0.62	0.7	0.63	0.61	0.61	0.65	0.18	0.16	0.16	0.16	0.18
X12	0.63	0.37	0.29	0.31	0.31	0.75	0.46	0.36	0.38	0.37	0.29	0.18	0.14	0.13	0.12
X13	0.59	0.43	0.43	0.75	0.88	0.82	0.54	0.51	0.85	0.99	0.24	0.15	0.13	0.22	0.25
X14	0.53	0.36	0.35	0.36	0.41	0.88	0.71	0.76	0.88	1.06	0.87	0.81	0.95	1.27	1.54

Table E-4 Wind speed Ibn rushed street result (summer) in three point for 5 times by sections

+	IBN rushed/Wind speed 22/6/2021														
	At 1m from right building					At 5m					At 1m from left building				
Simulation	8am	10am	12pm	2pm	4pm	8am	10am	12pm	2pm	4pm	8am	10am	12pm	2pm	4pm
Y1	0.33	0.75	1.5	2.54	3.53	0.44	0.95	1.91	3.36	4.7	0.17	0.99	1.58	2.56	3.28
Y2	0.4	0.9	1.33	1.85	2.49	1.11	1.08	1.41	1.88	2.38	0.57	0.14	0.27	1.09	1.49
Y3	0.68	0.22	0.58	1.4	1.86	1.18	1.1	1.44	1.98	2.54	1.25	1.08	1.49	2.02	2.52
Y4	0.33	0.43	1.09	2.12	3.05	0.31	0.47	1.08	1.92	2.71	0.22	0.4	0.73	1.22	1.11
Y5	0.86	0.9	1.25	1.59	2.22	0.48	0.42	0.86	1.62	2.1	0.36	0.35	0.95	1.84	2.52
Y6/80	0.41	0.12	0.57	1.26	1.73	0.38	0.19	0.61	1.25	1.66	0.4	0.19	0.64	1.44	1.91
Y6/70	0.37	0.34	0.88	1.72	2.32	0.36	0.28	0.73	1.44	1.89	0.37	0.28	0.78	1.63	2.16
Y7/60	0.4	0.28	0.78	1.66	2.26	0.38	0.27	0.68	1.38	1.8	0.38	0.25	0.7	1.43	1.92
Y7/50	0.46	0.2	0.73	1.61	2.24	0.4	0.21	0.66	1.36	1.82	0.41	0.22	0.73	1.55	2.12
Y8/40	0.21	0.06	0.25	0.5	0.72	0.28	0.08	0.27	0.56	0.79	0.31	0.04	0.25	0.52	0.72
Y8/30	0.79	0.05	0.42	1.38	1.8	0.85	0.16	0.29	1.22	1.56	0.71	0.2	0.2	1.2	1.54

Y9	0.37	0.72	1.06	1.35	1.65	1.28	0.94	1.03	1.24	1.45	1.98	1.44	1.25	0.54	0.17

Table E-5 relative humidity wedad street result(summer) in three point for 5 times by sections

+	WEDAD/Humidity% 22/6/2021														
	At 1m from right building					At 5m					At 1m from left building				
Simulation	8am	10am	12pm	2pm	4pm	8am	10am	12pm	2pm	4pm	8am	10am	12pm	2pm	4pm
Y1/15	53.38	47.48	36.2	29.82	34.63	53.7	44.55	35.07	29.84	34.48	56.38	43.91	34.27	29.86	34.27
Y2/25	53.71	43.43	33.53	28.45	34	55.38	41.77	32.45	28.6	33.58	59.34	48.35	34.64	29.1	33.92
Z1/85	57	45.27	33.08	28.03	34.13	56.46	44.47	32.5	28.08	34.19	55.92	43.55	32.34	28.55	34.25
Z2/75	57.71	45.66	33.27	27.31	33.22	56.77	44.41	32.75	27.28	33.46	54.98	43.38	32.89	27.95	33.88
X1/35	57.59	45.57	32.93	27.15	32.82	57.67	46.34	33.04	27.8	33.29	57.73	51.52	39.25	30.69	35.11
X1/45	56.7	47.9	32.4	27.4	33	56.5	47.7	33.9	28.7	34	56.7	47.6	35.1	29.6	34.6
X2/55	57	49	33.8	28.1	33.8	56.6	48.6	34.4	28.1	34	56.2	50.3	37.5	29.6	34.7
X2/65	57	49.5	34.6	28.2	33.9	56.2	48.9	34.9	28.3	34	55.3	49.6	36.4	29.1	34.7
X3	57.8	50.2	35.6	28.6	34.2	55.8	49	35.3	28.6	34.2	54.1	48.2	35.7	28.8	34.6
X4	55.7	48.7	36.8	30.1	34.7	55.5	47.7	35.5	29	34.4	55.2	47.2	35.8	29.4	34.6
X5	56	47.8	35.6	29.4	34.6	55.9	47.5	35.5	29.5	34.7	55.9	47.6	35.7	29.8	34.9
X6	56.3	48.7	36.8	30.2	34.8	56	48.1	36.2	29.8	34.7	55.4	47.7	36.2	30.1	34.8
X7/120	56.6	49.2	37.1	30.3	35	56.3	48.7	37	30.1	34.9	56	48.8	37.1	30.3	35
X7/130	56.8	49.6	37.6	31	35.4	56.8	49.4	37.7	31	35.4	56.8	49.3	37.8	31	35.4
X8	55	48.7	37.4	31.2	35.6	55.1	48.8	37.5	31.2	35.6	55.1	48.7	37.6	31.2	35.5
X9	54.1	47.9	37.1	31.2	35.5	54.2	47.9	37.2	31.2	35.5	54.2	48	37.3	31.2	35.5
X10	55.2	48.1	37.4	31.6	35.9	55	47.9	37.2	31.5	35.9	54.9	47.7	37.1	31.6	35.9
X11	56.9	48.1	37.3	31.5	36.2	56.8	48.2	37.4	31.6	36.2	56.8	48.4	37.5	31.7	36.2
X12	55.2	46.5	36.2	30.3	35.4	54.8	46.2	36	30.4	35.4	54.4	46.1	36	30.5	35.4
X13	55.2	46.3	36.1	30	35.2	54.9	46.1	36.1	30	35.2	54.8	46.1	36.1	30	35.2
X14	56.8	46.9	36.1	29.6	35.4	56	46.5	35.9	29.4	35.2	56	46.8	36.1	29.9	35.3

Table E-6 Relative humidity Ibn rushed street result (summer) in three point for 5 times by sections

+	**IBN rushed/Humidity% 22/6/2021**														
	At 1m from right building					At 5m					At 1m from left building				
Simulation	8am	10am	12pm	2pm	4pm	8am	10am	12pm	2pm	4pm	8am	10am	12pm	2pm	4pm
Y1	55.47	48.76	35.84	30.69	35.67	54.27	47.08	34.54	28.96	34.74	53.93	48.85	38.95	32.51	37.42
Y2	54.02	46.41	33.85	28.73	34.89	54.26	47.84	36.18	31.1	36.34	53.44	45.99	34.88	30.87	36.01
Y3	53.96	47.78	34.34	29.4	34	54.55	48.35	35.22	29.75	33.94	54.78	48.1	34.7	28.61	32.82
Y4	53.16	48.46	35.56	29.26	33.85	52.79	47.47	35.31	29.31	34.25	52.86	45.2	34.23	29.94	34.8
Y5	52.35	44.26	33.21	28.89	33.82	52.28	44.42	33.69	29.31	34.77	52.24	43.73	32.95	29.9	35.01
Y6/80	53.31	45.94	34.37	29.09	34.26	53.01	43.83	32.86	28.68	34.45	52.88	42.79	32.67	29.67	34.95
Y6/70	53.5	45.71	33.92	28.57	34.13	52.93	44.43	33.39	29.17	34.67	52.65	42.41	32.28	29.71	34.92
Y7/60	53.86	43.95	32.75	28.3	33.77	52.84	41.58	31.96	28.41	34.39	51.76	40.56	31.65	29.32	34.72
Y7/50	54.11	43.99	31.91	28.1	33.75	53.33	42.66	32.01	28.63	34.51	52.21	40.53	31.01	29.29	34.79

Y8/40	54.2	44.79	32.72	28.83	34.49	53.8	43.58	31.85	29.04	34.75	53.32	42.14	30.93	29.55	35
Y8/30	53.98	46	31.75	28.41	34.67	53.01	45.47	32.23	29.35	35.07	52.52	43.91	31.11	29.77	35.25
Y9	53.64	45.04	32.59	28.21	34.1	52.72	44.62	33.71	28.16	34.18	52.14	46.65	35.94	29.07	33.77

Table E-7 PET Weddad street result (summer) in three point for 5 times by sections

+ Section #	WEDAD/PET 22/6/2021																
	At 1m from right building						At middle						At 1m from left building					
Simulation	**case**	8am	10am	12pm	2pm	4pm	8am	10am	12pm	2pm	4pm	case	8am	10am	12pm	2pm	4pm
Y1/15	M3a-SW-C0	27.36	35.71	41.2	45.6	44.1	34.48	38.49	41.7	44.77	42	noa-NE-C4	29.73	38.42	42.2	45.2	42.7
Y2/25	M3b-SW-C0	37.55	42.1	44.3	40	37.8	34.7	39.7	43.2	45.3	43.13	nob-NE-C3	34.74	39.6	44.63	46.6	44.5
Z1/85	M3c-NW-C13	29	33.57	41.6	52	38.2	27.8	37.9	43.4	48.4	38	M3a-SE-C8	28.7	41.4	44.24	39.4	37.6
Z2/75	M3d-NW-C8	28.1	32.6	41	48.2	46.7	27.6	37.7	43	48.4	38.12	M3b-SE-C9	33.8	38.7	42	38.3	36.6
X1/35	M3e-W-C3	28.4	33.4	42.7	52.5	51.14	28.6	39.3	44.2	47.6	45.43	M3c-E-C3	38.44	38.5	36.8	37	35.6
X1/45	M3f-W-C6	30.35	32.9	42.8	46	37.34	29.83	39.38	42.6	37.38	35.53	M3d-E-C6	30.7	44.66	40	38.26	36.75
X2/55	M2a-W-C3	28.8	32.6	43.12	46.9	40	28.6	39.3	42.82	41.3	42.8	M1a-NE-C4	28.29	36.57	36.2	37.8	39.02
X2/65	M2b-W-C3	28.1	32.2	42.5	46.1	43.5	28.3	38.6	43	45.9	43	M1b-NE-C4	28.4	37.5	42.82	45.8	36.1
X3	M3g-W-C0	27.63	31.6	41.42	45.14	37.25	27.8	38.4	42.4	45.24	38.24	noc-NE-C2	28.23	39.38	42.82	45.15	35.5
X4	M4a-SW-C7	27.9	31.9	41.7	46.2	37.6	28	37.9	42.24	46.1	37.1	M2a-NE-C16	39.5	41	38.5	38.6	35.9
X5	M1b-SW-C3	27.6	38.2	43.3	47	37.1	27.87	39.01	43.35	46.23	36.47	M1c-NE-C3	31.6	38.1	41.9	39.7	34.6
X6	M5a-SW-C4	26.96	36.9	39.2	39.5	37.4	27.18	37.5	39.3	45.1	39.03	M5a-NE-C6	37.25	39.9	38.2	38.03	36.1
X7/120	M7a-SW-C14	27	36	41.3	40.8	35.6	27.2	37.3	40.3	45.04	38.7	M6a-NE-C8	34.2	39	36.7	38.32	35.8
X7/130	M7b-SW-C15	28.41	32.35	41.13	35.85	34.73	27.67	37.6	40	35.76	34.75	M6b-NE-C10	36	38.7	34.86	35.4	34.73
X8	M1a-SW-C15	29.9	38.5	41.12	37.07	34.37	29.03	33.98	36.8	35.36	33.85	M6c-NE-C9	30.9	36.84	35.01	35.14	34.07
X9	M2c-SW-C15	31.04	39.78	42.93	37.08	34.61	31.04	40.2	37.82	36.6	34.46	M6d-NE-C4	39.77	34.5	35.53	35.72	34.14
X10	M3h-SW-C5	28.69	34.9	37.15	35.74	33.58	29.55	37.33	42	35.9	34.05	M6e-NE-C5	35.12	36.31	42.2	35.5	34.3
X11	M3i-SW-C11	27.6	35.79	38.2	40.97	34.86	33.74	34.59	37.27	38.54	34.15	M3e-NE-C12	30.06	32.29	34.89	35.58	34.05
X12	M3j-SW-C2	28.26	33.74	42.51	46.77	39.56	35.29	39.79	43.23	39.44	36.38	M5b-NE-C6	38.59	40.44	43	37.68	36.13
X13	M1c-SW-C13	28.54	33.87	39.42	44.71	43.04	30.94	39.47	42.2	44.26	43.06	M3f-NE-C5	38.14	34.55	36.42	36.72	35.67
X14	M2d-SW-C0	28.59	37.64	39.55	42.4	35.87	35.02	39.84	43.27	43.74	42.61	nod-NE-C6	32.8	35.46	37.69	40.43	33.98

Table E-8 Ibn rushed PET result in summer for three sides

+	IBN rushed/PET 22/6/2021																
section	At 1m from right building						At 5m middle distance					At 1m from left building					
Simulation	case	8am	10am	12pm	2pm	4pm	8am	10am	12pm	2pm	4pm	case	8am	10am	12pm	2pm	4pm
Y1	M6a-W-C6	27.66	30.14	39.74	39.81	33.84	27.935	38.455	42.795	46.165	36.785	M6a-E-C7	29.43	39.88	36.54	36.33	33.44
Y2	M5a-W-C1	30.03	32.98	41.5	44.32	38.17	30.33	36.01	43.6	42.37	35.03	M7a-E-C2	31.55	43	43.77	36.81	34.67
Y3	M7a-W-C0	28.75	33.98	43.54	42.7	38.27	30.55	35.67	40.23	43	42.61	noM-E-C2	29.57	39.02	42.92	45.62	43.33
Y4	M3a-W-C3	28.58	31.89	40.84	44.64	42.04	29.8	39.33	43.17	46.17	36.57	M3a-E-C6	28.89	40.8	42.61	36.38	34.44
Y5	M8a-W-C3	35.94	40.56	44.01	46.8	43.95	38.2	42.48	44.26	46.12	35.92	M7b-E-C3	38.27	41.96	42.96	36.6	34.57

Y6/80	M7b-W-C5	29.07	34.29	44.29	47.77	37.92	30.14	42.94	45.22	47.49	37.44	M3b-E-C6	36.17	42.88	43.6	36.59	34.51
Y6/70	M7c-W-C5	28.93	32.68	41.52	45.34	35.55	29.61	38.48	40.71	39.27	35.43	M3c-E-C6	28.69	41.39	43.01	36.6	34.76
Y7/60	M3b-W-C4	28.91	33.48	43.62	47.21	45.09	30.66	43.32	45.41	47.72	36.93	M3d-E-C3	38.56	42.82	44.11	37.63	35.58
Y7/50	M3c-W-C4	28.72	33.78	42.78	46.43	41.66	30.16	39.19	40.26	41.62	35.73	M3e-E-C3	40.79	44.84	44.72	37.38	34.66
Y8/40	M3d-W-C6	30.62	34.86	45.36	49.49	35.79	30.25	39.59	41.79	37.93	35.44	M9a-E-C4	41.27	50.88	41.61	36.68	34.82
Y8/30	M3e-W-C7	28.8	34.64	43.43	46.25	34.96	28.79	40.81	43.31	37.71	34.46	M9a-E-C4	31.43	42.29	40.13	36.42	34.07
Y9	M3f-W-C4	**29.89**	34	43.71	47.01	44.41	28.69	40.38	44.02	46.45	43.16	M9b-E-C3	33.13	38.29	42.82	46.44	45.66

Table E-9 UTCI Weddad street result (summer) in three point for 5 times by sections

+		**WEDAD /UTCI 22/6/2021**															
Section #		At 1m from right building					At 5m						At 1m from left building				
Simulation		8am	10am	12pm	2pm	4pm	8am	10am	12pm	2pm	4pm		8am	10am	12pm	2pm	4pm
Y1/15	M3a-SW-C0	26.15	32.47	35.68	39.35	38.69	30.66	32.86	34.87	37.58	35.64	noa-NE-C4	27.8	34.29	37.38	39.57	37.44
Y2/25	M3b-SW-C0	32.61	35.21	37.25	36.26	34.72	30.97	33.72	36.19	37.09	36.91	nob-NE-C3	31.16	33.99	36.61	39.11	37.12
Z1/85	M3c-NW-C13	27.2	30.8	36.44	39.78	39.3	26.43	33.79	37.21	39.48	34.4	M3a-SE-C8	31.53	35.24	37.49	35.53	34.17
Z2/75	M3d-NW-C8	27.01	30.91	36.59	40.55	40.33	25.8	33.36	36.86	40.17	34.85	M3b-SE-C9	31.16	33.96	36.44	35.56	34.18
X1/35	M3e-W-C3	26.78	31.18	36.96	40.8	40.64	28.07	33.9	37.38	39.91	37.75	M3c-E-C3	32.99	35.55	33.87	34.37	33.06
X1/45	M3f-W-C6	27.04	31.28	37.26	39.66	37.75	26.65	34.23	36.59	34.38	31.96	M3d-E-C6	32.51	35.63	34.72	34.58	33.56
X2/55	M2a-W-C3	26.05	33.42	37.56	40.54	38.83	26.3	34.21	37.39	38.22	35.9	M1a-NE-C4	27.89	31.36	34.02	35.18	32.73
X2/65	M2b-W-C3	25.38	33.01	36.93	39.61	37.82	25.65	33.82	37.25	39.52	37.14	M1b-NE-C4	25.73	34.35	36.96	38.97	36.28
X3	M3g-W-C0	24.78	29.54	36.33	39.28	37.54	25.46	33.56	36.9	38.82	36.52	noc-NE-C2	25.71	34.2	37.07	38.71	32.27
X4	M4a-SW-C7	26.05	30.01	37.01	40.16	35.48	26.11	33.35	36.99	39.81	34.03	M2a-NE-C16	33.52	35.15	35.3	35.94	33.36
X5	M1b-SW-C3	26.16	33.8	37.45	39.85	34.24	27.24	33.72	37.02	38.87	32.79	M1c-NE-C3	30.71	33.63	36.61	37.23	32.64
X6	M5a-SW-C4	25.19	31.48	35.18	36.76	33.97	25.56	32.03	35.47	37.87	36.31	M5a-NE-C6	32.89	34.68	36.78	35.08	33.64
X7/120	M7a-SW-C14	25.49	32.87	36.62	39.72	34.59	29.75	32.87	33.74	38.92	37.74	M6a-NE-C8	28.43	30.63	33.46	34.86	33.38
X7/130	M7b-SW-C15	26.29	29.83	35.5	32.91	32.36	26.05	32.91	35.06	33.14	32.49	M6b-NE-C10	31.28	33.13	32.31	32.84	32.31
X8	M1a-SW-C15	26.52	32.57	35.44	33.58	31.45	26.3	30.5	32.88	32.52	31.43	M6c-NE-C9	27.66	32.96	32.13	32.39	31.49
X9	M2c-SW-C15	27.64	33.94	36.22	33.76	32.15	31.78	33.77	33.74	33.59	32.07	M6d-NE-C4	32.2	30.05	32.19	32.72	31.44
X10	M3h-SW-C5	25.08	31.01	34.22	33.14	31.45	26.37	33.26	35.81	32.91	31.74	M6e-NE-C5	28.23	31.57	35.1	32.37	31.42
X11	M3i-SW-C11	25.02	31.34	34.68	36.11	32.13	27.84	31.13	34.25	35.51	31.4	M3e-NE-C12	25.7	28.33	31.23	32.28	31.19
X12	M3j-SW-C2	26.04	31.17	36.25	39.38	37.9	31.01	33.6	36.47	35.17	33.25	M5b-NE-C6	32.5	33.7	36.04	34.18	32.81
X13	M1c-SW-C13	26.41	31.14	35.05	37.5	37.62	31.38	34.02	36.28	38.67	37.65	M3f-NE-C5	31.75	30.11	32.68	33.92	32.72
X14	M2d-SW-C0	25.81	32.58	35.86	37.54	33.39	31.05	34.48	37.44	39.71	37.48	nod-NE-C6	27.78	32.21	34.47	37.03	31.59

Table E-10 Ibn rushed UTCI result in summer for three sides

+		**IBN rushed/ UTCI 22/6/2021**															
		At 1m from right building					At 5m middle distance						At 1m from left building				
Simulation		8am	10am	12pm	2pm	4pm	8am	10am	12pm	2pm	4pm		8am	10am	12pm	2pm	4pm

Y1	M6a-W-C6	26.06	30.2	36.68	37.59	31.88	25.57 25.96	32.89 33.83	36 34.85	37.37 32.37	31.04 30.55	M6a-E-C7	25.92	33.88	32.66	33	31.34
Y2	M5a-W-C1	30.95	32.99	36.33	38.84	36.46	29.92	33.97	37.07	39.16	36.86	M7a-E-C2	32.82	34.8	36.02	37.51	36.59
Y3	M7a-W-C0	30.87	33.6	36.97	40.18	39.3	31.25	34.74	37.92	40.45	37.12	noM-E-C2	29.71	32.53	35.16	38.07	35.59
Y4	M3a-W-C3	25.33	29.31	35.68	38.82	37.74	26.33	34.24	36.47	39.52	37.44	M3a-E-C6	32.83	35.1	36.09	34.61	33
Y5	M8a-W-C3	30.25	33.43	36.26	38.74	36.94	31.37	34.02	36.14	38.11	35.7	M7b-E-C3	33.69	36.05	37.05	34.78	32.13
Y6/80	M7b-W-C5	26.22	30.48	37.14	40.3	38.84	28.31	35.13	37.25	39.3	33.78	M3b-E-C6	32.63	34.92	36.62	33.96	31.54
Y6/70	M7c-W-C5	26.52	30.24	36.99	40.21	33.75	26.73	35.36	38.68	39.91	32.68	M3c-E-C6	31.81	34.89	37.1	34.29	32.27
Y7/60	M3b-W-C4	26.52	30.93	37.64	41.44	40.03	31.75	34.96	37.76	40.02	33.8	M3d-E-C3	32.88	35.23	37.17	34.8	32.84
Y7/50	M3c-W-C4	26.48	30.95	37.78	41.45	39.74	31.37	35.83	39.03	40.1	32.65	M3e-E-C3	34.11	36.26	37.6	34.71	32.16
Y8/40	M3d-W-C6	26.53	30.59	37.51	40.81	32.34	27.24	36.18	39.53	36.31	32.33	M9a-E-C4	33.31	35.89	37.53	34.16	32.14
Y8/30	M3e-W-C7	27.1	30.97	37.92	40.52	32.44	27.52	35.06	38.54	35.69	32.65	M9a-E-C4	32.47	34.94	37.1	34.2	32.08
Y9	M3f-W-C4	27.01	33.98	38.2	40.83	38.95	30.82	34.97	38.16	40.42	38.14	M9b-E-C3	29.72	33.54	37.12	39.92	38.48

Winter:

Table E-11 Temperature wedad street result(winter) in three point for 5 times by sections

Weddad/Temperature 21/12/2021															
	At 1m from right building					At 5m					At 1m from left building				
	8am	10am	12pm	2pm	4pm	8am	10am	12pm	2pm	4pm	8am	10am	12pm	2pm	4pm
Y1/15	14.28	17.19	20.8	23.01	22.39	14.16	16.99	20.68	22.87	22.1	14.06	16.71	20.45	22.68	22.02
Y/25	14.41	16.72	20.56	22.83	22.3	14.19	16.78	20.22	22.62	22.19	14.09	16.47	20.09	22.51	22.12
Z1/85	14.24	16.14	19.2	21.52	21.53	14.09	16.05	19.18	21.79	21.54	14.22	16.1	19.22	22.14	21.6
Z2/75	14.37	16.24	19.41	21.97	21.64	14.2	16.13	19.58	22.17	21.69	14.41	16.28	19.98	22.48	21.86
X1/35	14.4	16.27	19.68	22.01	21.65	14.23	16.55	20.26	22.02	21.66	14.28	16.87	20.27	22.01	21.65
X1/45	14.26	16.87	20.89	22.41	21.73	14.16	17.15	20.86	22.37	21.71	14.23	17.18	20.79	22.36	21.7
X2/55	14.13	17.07	20.54	22.43	21.78	14.06	17.07	20.37	22.31	21.73	14.04	16.9	20.14	22.17	21.64
X2/65	14.18	16.8	20.17	22.24	21.71	14.12	16.78	20.13	22.16	21.67	14.12	16.73	20.02	22.08	21.61
X3	14.29	16.91	20.17	22.36	21.78	14.22	16.78	20.13	22.27	21.69	14.18	16.69	20.16	22.23	21.65
X4	14.32	16.81	20.18	22.04	21.65	14.27	16.77	20.1	22.01	21.62	14.3	16.77	20.08	22	21.6
X5	14.07	16.5	19.73	21.86	21.34	14.05	16.47	19.72	21.78	21.31	14.05	16.47	19.73	21.75	21.29
X6	14.07	16.3	19.43	21.36	20.83	14.06	16.29	19.42	21.36	20.82	14.07	16.3	19.43	21.37	20.82
X7/120	14.17	16.32	19.38	21.25	20.7	14.14	16.3	19.38	21.26	20.69	14.14	16.31	19.39	21.29	20.72
X7/130	14.35	16.43	19.45	21.22	20.7	14.33	16.41	19.44	21.22	20.69	14.33	16.41	19.43	21.23	20.7
X8	14.48	16.61	19.64	21.26	20.71	14.44	16.57	19.61	21.21	20.67	14.45	16.57	19.6	21.21	20.66
X9	14.48	16.79	19.84	21.41	20.95	14.48	16.73	19.81	21.39	20.91	14.51	16.72	19.84	21.36	20.89
X10	14.34	16.67	20.01	21.35	20.89	14.33	16.66	19.98	21.31	20.88	14.44	16.72	19.99	21.28	20.84
X11	14.48	16.85	20.23	21.6	20.53	14.42	16.78	20.16	21.51	20.5	14.41	16.75	20.11	21.6	20.52

X12	14.77	17.26	20.59	22.12	21.26	14.72	17.2	20.58	22.07	21.21	14.81	17.2	20.57	22.07	21.21
X13	14.76	18	21.11	21.83	21.27	14.77	17.82	21.03	21.86	21.32	14.87	17.72	20.91	21.89	21.36
X14	15.08	18.46	22.1	22.81	21.69	14.84	18.47	22.05	22.93	21.58	14.6	18.13	21.58	23.03	21.43

Table E-12 Temperature Ibn rushed street result (winter) in three point for 5 times by sections

IBN rushed/Temperature 21/12/2021															
	At 1m from right building					At 5m middle distance					At 1m from left building				
	8am	10am	12pm	2pm	4pm	8am	10am	12pm	2pm	4pm	8am	10am	12pm	2pm	4pm
Y1	14.14	15.87	19.71	21.86	21.35	13.97	15.95	20.23	22.46	21.45	14.02	17.08	20.59	21.4	21.24
Y2	14.18	16.64	20.27	22.38	21.68	14.02	16.59	20.06	22.05	21.27	14.19	16.7	20.44	22.06	21.4
Y3	14.3	16.7	19.87	22.08	21.36	14.1	16.56	19.88	21.98	21.28	14.07	16.51	20.1	21.99	21.35
Y4	14.56	16.68	20.08	22.19	21.46	14.35	16.82	20.33	22.06	21.37	14.48	17.05	20.64	22	21.37
Y5	14.42	16.68	19.94	22.24	21.5	14.36	16.66	20.48	22.17	21.41	14.52	17.02	20.88	22.07	21.42
Y6/80	14.51	16.65	20.12	22.29	21.54	14.42	16.65	20.44	22.12	21.45	14.59	16.89	20.89	22.1	21.46
Y6/70	14.61	16.73	20.44	22.43	21.61	14.47	16.78	20.6	22.16	21.46	14.65	17.19	21.09	22.16	21.49
Y7/60	14.59	16.82	20.6	22.5	21.58	14.46	16.95	20.88	22.31	21.52	14.64	17.48	21.4	22.27	21.55
Y7/50	14.47	16.79	20.52	22.39	21.52	14.31	16.85	20.72	22.18	21.46	14.52	17.38	21.24	22.18	21.5
Y8/40	14.48	16.85	20.53	22.3	21.53	14.39	16.91	20.74	22.16	21.45	14.58	17.28	21.12	22.15	21.49
Y8/30	14.61	17.02	20.79	22.47	21.76	14.47	17.11	20.85	22.35	21.61	14.71	17.56	21.24	22.37	21.62
Y9	14.75	17.98	21.5	22.76	21.89	14.64	17.68	21.31	22.64	21.79	14.96	18.08	21.58	22.83	22

Table E-13 Wind speed wedad street result(winter) in three point for 5 times by sections

+	Weddad/Wind speed 21/12/2024														
	At 1m from right building					At 5m					At 1m from left building				
Simulation	8am	10am	12pm	2pm	4pm	8am	10am	12pm	2pm	4pm	8am	10am	12pm	2pm	4pm
Y1/15	0.39	0.48	0.58	0.29	0.64	0.64	0.85	1.13	0.67	1.21	0.73	0.93	1.22	1.02	1.23
Y2/25	0.44	0.53	0.63	0.6	0.17	0.96	1.32	1.74	1.29	0.64	0.87	1.15	1.66	1.31	0.87
Z1/85	0.63	0.72	0.8	0.9	0.57	0.9	1.07	1.24	1.32	0.76	0.46	0.52	0.59	0.64	0.4
Z2/75	0.6	0.7	0.82	0.91	0.6	1.13	1.45	1.81	1.78	0.89	1.06	1.33	1.64	1.6	0.76
X1/35	0.38	0.44	0.5	0.62	0.51	0.52	0.66	0.78	0.85	1.04	0.63	0.79	1.05	0.52	0.95
X1/45	0.09	0.1	0.08	0.55	1.4	0.12	0.13	0.16	0.74	1.9	0.07	0.07	0.03	0.2	0.28
X2/55	0.06	0.1	0.23	0.27	1.01	0.15	0.2	0.34	0.35	1.25	0.23	0.3	0.44	0.33	1.14
X2/65	0.08	0.14	0.29	0.27	1.15	0.1	0.16	0.32	0.31	1.3	0.13	0.18	0.32	0.34	1.33
X3	0.12	0.19	0.34	0.21	1.15	0.19	0.26	0.41	0.36	1.4	0.35	0.44	0.55	0.7	1.51
X4	0.37	0.41	0.46	0.38	0.4	0.68	0.82	0.96	0.72	0.56	0.55	0.64	0.75	0.61	0.46
X5	0.47	0.58	0.69	0.61	0.45	0.54	0.67	0.79	0.68	0.52	0.45	0.55	0.65	0.55	0.4
X6	0.52	0.62	0.69	0.88	0.16	0.55	0.64	0.71	0.93	0.16	0.42	0.49	0.55	0.69	0.12
X7/120	0.5	0.56	0.6	0.92	0.21	0.53	0.59	0.62	1	0.21	0.18	0.2	0.22	0.35	0.08
X7/130	0.32	0.35	0.36	0.61	0.27	0.44	0.47	0.48	0.84	0.35	0.25	0.28	0.29	0.48	0.19
X8	0.19	0.21	0.22	0.24	0.25	0.34	0.36	0.37	0.46	0.39	0.27	0.29	0.29	0.4	0.29
X9	0.21	0.23	0.27	0.05	0.56	0.29	0.31	0.35	0.15	0.59	0.09	0.1	0.11	0.08	0.16
X10	0.13	0.15	0.2	0.19	0.68	0.13	0.15	0.18	0.27	0.72	0.06	0.06	0.04	0.15	0.17
X11	0.38	0.45	0.56	0.23	0.6	0.4	0.47	0.59	0.25	0.62	0.1	0.12	0.14	0.06	0.16

X12	0.45	0.52	0.65	0.5	0.22	0.51	0.59	0.75	0.56	0.36	0.16	0.18	0.22	0.17	0.15
X13	0.56	0.71	0.95	0.47	0.65	0.77	0.97	1.32	0.69	0.69	0.23	0.28	0.36	0.24	0.17
X14	0.44	0.54	0.61	0.41	0.2	0.59	0.81	1.04	0.66	0.49	0.56	0.79	1.03	0.75	0.81

Table E-14 Wind speed Ibn rushed street result (winter) in three point for 5 times by sections

+	IBN rushed/WIND SPEED 21/12/2021														
	At 1m from right building					At 5m middle distance					At 1m from left building				
Simulation	8am	10am	12pm	2pm	4pm	8am	10am	12pm	2pm	4pm	8am	10am	12pm	2pm	4pm
Y1	0.35	0.37	0.37	0.82	1.62	0.42	0.48	0.51	1.13	2.02	0.32	0.34	0.28	1.13	2
Y2	0.06	0.13	0.2	0.38	1.09	0.71	0.87	1.12	1.08	1.24	0.69	0.89	1.11	1.39	1.16
Y3	0.45	0.5	0.59	0.81	1.14	0.63	0.74	0.93	1.11	1.23	0.94	1.21	1.6	1.22	1.05
Y4	0.24	0.2	0.24	0.65	1.44	0.35	0.38	0.45	0.89	1.38	0.35	0.41	0.49	0.94	0.26
Y5	0.35	0.37	0.51	0.63	1.01	0.46	0.54	0.71	0.88	1.2	0.41	0.48	0.59	0.96	1.35
Y6/80	0.31	0.34	0.43	0.61	0.97	0.35	0.42	0.52	0.73	1	0.38	0.47	0.57	0.87	1.19
Y6/70	0.38	0.47	0.55	0.89	1.3	0.37	0.45	0.54	0.83	1.14	0.42	0.52	0.6	0.97	1.32
Y7/60	0.35	0.45	0.53	0.93	1.26	0.34	0.42	0.51	0.83	1.1	0.35	0.43	0.52	0.85	1.16
Y7/50	0.4	0.48	0.57	0.96	1.26	0.37	0.44	0.53	0.83	1.09	0.39	0.47	0.57	0.92	1.22
Y8/40	0.15	0.17	0.2	0.32	0.43	0.2	0.22	0.28	0.4	0.49	0.23	0.1	0.29	0.4	0.5
Y8/30	0.53	0.66	0.81	1.1	1.32	0.55	0.68	0.85	1.09	1.21	0.64	0.79	0.97	1.22	1.31
Y9	0.12	0.12	0.18	0.4	0.92	0.71	0.9	1.19	1.26	1.2	0.78	0.98	1.31	0.73	0.14

Table E-15 Relative humidity wedad street result(winter) in three point for 5 times by sections

	Weddad/Humidity/21/12/2024														
	At 1m from right building					At 5m middle distance					At 1m from left building				
	8am	10am	12pm	2pm	4pm	8am	10am	12pm	2pm	4pm	8am	10am	12pm	2pm	4pm
Y1/15	54.43	45.36	35.56	35.47	34.9	54.81	45.91	35.83	35.83	35.67	55.07	46.89	36.77	36.55	35.89
Y2/25	55.06	47.76	36.57	36.01	34.88	55.26	47.07	37.07	36.32	35.09	55.32	47.77	37.48	36.71	35.32
Z1/85	56.74	50.42	40.13	39.2	36.7	57.25	50.72	40.34	38.65	36.67	56.61	50.5	40.31	37.86	36.49
Z2/75	55.65	49.62	39.37	38.04	36.39	56.34	50.07	39.35	37.85	36.35	55.54	49.57	38.21	36.98	35.89
X1/35	55.12	49.15	38.55	37.85	36.32	54.94	47.62	37	37.67	36.25	54.36	46.4	36.98	37.63	36.28
X1/45	54.45	46.47	35.78	36.7	36.08	54.85	45.73	35.93	36.79	36.12	54.74	45.89	36.31	36.88	36.07
X2/55	55.17	46.49	36.98	37.07	35.95	55.48	46.6	37.39	37.38	36.09	55.69	47.47	38	37.78	36.37
X2/65	55.19	47.52	37.99	37.78	36.17	55.31	47.61	38.1	37.95	36.25	55.34	47.85	38.38	38.17	36.43
X3/k=2	54.98	47.75	38.45	37.6	36.03	55.28	48.2	38.6	37.82	36.22	55.43	48.57	38.61	37.93	36.35
X4	56.83	51.79	42.2	39.63	36.62	56.9	51.82	41.86	39.6	36.64	56.68	51.68	41.74	39.59	36.68
X5	56.67	51.66	41.68	39.9	37.25	56.64	51.6	41.6	40.04	37.31	56.56	51.55	41.55	40.08	37.34
X6	55.33	50.2	40.59	40.41	38.06	55.37	50.23	40.6	40.39	38.08	55.33	50.22	40.61	40.37	38.08
X7/120	54.9	49.82	40.37	40.65	38.35	54.99	49.89	40.41	40.64	38.37	55	49.91	40.42	40.56	38.3
X7/130	54.27	49.11	39.89	40.69	38.39	54.34	49.17	39.92	40.7	38.4	54.31	49.18	39.95	40.68	38.38
X8	53.74	48.22	39.13	40.57	38.4	53.88	48.36	39.22	40.67	38.47	53.85	48.39	39.26	40.68	38.49
X9	53.7	47.65	38.53	40.29	37.88	53.71	47.73	38.59	40.3	37.95	53.6	47.79	38.69	40.36	38

X10	53.72	47.11	37.64	39.87	37.93	53.72	47.14	37.69	40.02	37.96	53.33	46.93	37.62	40.02	38.03
X11	53	46.51	37	38.47	38.58	53.2	46.67	37.13	38.7	38.66	53.22	46.74	37.24	38.94	38.63
X12	52.05	45.57	36.48	37.14	36.94	52.23	45.72	36.45	37.41	37.05	51.94	45.71	36.44	37.44	37.06
X13	52.14	43.73	35.71	37.93	36.95	52.15	44.23	35.95	37.9	36.95	51.89	44.46	36.1	37.86	36.95
X14	52.48	45.04	34.95	35.62	36.01	53.21	44.65	34.94	35.76	36.25	54.8	46.87	37.27	36.38	36.59

Table E-16 Relative humidity Ibn rushed street result(winter) in three point for 5 times by sections

+	IBN rushed/RELATIVE HUMIDITY 21/12/2021														
	At 1m from right building					At 5m middle distance					At 1m from left building				
Simulation	8am	10am	12pm	2pm	4pm	8am	10am	12pm	2pm	4pm	8am	10am	12pm	2pm	4pm
Y1	54.09	48.76	35.84	30.69	35.67	54.61	47.08	34.54	28.96	34.74	54.64	48.85	38.95	32.51	37.42
Y2	54.02	46.41	33.85	28.73	34.89	54.26	47.84	36.18	31.1	36.34	53.44	45.99	34.88	30.87	36.01
Y3	53.96	47.78	34.34	29.4	34	54.55	48.35	35.22	29.75	33.94	54.78	48.1	34.7	28.61	32.82
Y4	53.16	48.46	35.56	29.26	33.85	52.79	47.47	35.31	29.31	34.25	52.86	45.2	34.23	29.94	34.8
Y5	52.35	44.26	33.21	28.89	33.82	52.28	44.42	33.69	29.31	34.77	52.24	43.73	32.95	29.9	35.01
Y6/80	53.31	45.94	34.37	29.09	34.26	53.01	43.83	32.86	28.68	34.45	52.88	42.79	32.67	29.67	34.95
Y6/70	53.5	45.71	33.92	28.57	34.13	52.93	44.43	33.39	29.17	34.67	52.65	42.41	32.28	29.71	34.92
Y7/60	53.86	43.95	32.75	28.3	33.77	52.84	41.58	31.96	28.41	34.39	51.76	40.56	31.65	29.32	34.72
Y7/50	54.11	43.99	31.91	28.1	33.75	53.33	42.66	32.01	28.63	34.51	52.21	40.53	31.01	29.29	34.79
Y8/40	54.2	44.79	32.72	28.83	34.49	53.8	43.58	31.85	29.04	34.75	53.32	42.14	30.93	29.55	35
Y8/30	53.98	46	31.75	28.41	34.67	53.01	45.47	32.23	29.35	35.07	52.52	43.91	31.11	29.77	35.25
Y9	53.32	45.08	35.53	36.66	35.88	53.25	45.13	35.38	36.87	36.07	52.13	43.97	34.73	36.49	35.68

Table E-17 PET wedad street result(winter) in three point for 5 times by sections

+		WEDAD/PET 21/12/2021															
section		At 1m from right building					At 5m					At 1m from left building					
Simulation		8am	10am	12pm	2pm	4pm	8am	10am	12pm	2pm	4pm		8am	10am	12pm	2pm	4pm
Y1/15	M3a-SW-C0	16.4	34.02	37.53	39.85	31.92	14.95	29.43	33.4	35.07	29.02	noa-NE-C4	14.34	28.11	32.54	35.07	28.61
Y2/25	M3b-SW-C0	17.35	37.05	40.66	40.23	37.57	14.75	18.89	26.83	33.91	31.04	nob-NE-C3	14.56	16.89	29.93	33.09	29.3
Z1/85	M3c-NW-C13	17.14	20	23.31	24.66	24.49	16.1	18.94	21.98	33.42	30.81	M3a-SE-C8	17.89	19.84	22.88	39.3	25.52
Z2/75	M3d-NW-C8	17.44	20.23	23.61	34.83	24.83	15.16	17.77	30.21	31.43	29.88	M3b-SE-C9	16.25	18.15	32.46	34.03	24.41
X1/35	M3e-W-C3	17.85	21.11	25.52	27.1	24.43	16.02	28	28.9	24.95	22.16	M3c-E-C3	16.64	19.28	21.67	24.96	22.57
X1/45	M3f-W-C6	18.91	36.97	42.19	37.02	22.03	17.7	36.15	39.9	26.27	20.85	M3d-E-C6	20.08	30.89	41.14	28.65	25.03
X2/55	M2a-W-C3	19.03	38.1	41.36	27.82	22.22	18.24	36.55	39.86	28.19	22.07	M1a-NE-C4	21.83	35.47	26.01	26.72	22.11
X2/65	M2b-W-C3	19.08	30.32	32.68	28.31	22.27	18.26	27.27	33.04	27.77	21.99	M1b-NE-C4	17.93	35.91	26.39	27.53	21.94
X3	M3g-W-C0	18.83	36.4	38.95	41.31	23.22	17.39	22.7	33.03	38.77	22.48	noc-NE-C2	16.6	23.16	36.6	36.21	22.01
X4	M4a-SW-C7	17.16	20.47	25.97	26.59	24.01	15.87	18.21	22.31	25.17	23.69	M2a-NE-C16	16.28	18.68	22.63	25.12	23.15
X5	M1b-SW-C3	17.04	19.53	22.61	28.09	23.31	16.57	18.83	22.08	24.63	22.33	M1c-NE-C3	16.8	18.91	22.16	24.3	22.55
X6	M5a-SW-C4	16.97	18.7	21.05	22.57	23.29	16.9	18.9	21.18	22.68	23.52	M5a-NE-C6	17.53	19.5	21.81	24.2	24.54
X7/120	M7a-SW-C14	17.22	18.98	21.18	22.09	22.79	17.04	18.91	21.13	21.97	22.89	M6a-NE-C8	18.35	20.49	22.59	23.31	23.51
X7/130	M7b-SW-C15	19.03	20.64	22.6	23.11	23.19	18.04	19.65	21.67	22.23	22.44	M6b-NE-C10	19.19	20.72	22.6	23.39	23.42

X8	M1a-SW-C15	19.97	21.39	23.39	24.33	23.28	18.76	20.34	22.29	23.17	22.42	M6c-NE-C9	19.31	20.71	22.63	23.37	22.71
X9	M2c-SW-C15	20.22	22.64	23.46	25.79	22.42	18.43	20.84	22.77	24.62	21.72	M6d-NE-C4	20.09	21.96	23.87	25.21	23.1
X10	M3h-SW-C5	20.07	22.39	26.23	26.4	22	19.18	22.11	25.38	25.21	21.45	M6e-NE-C5	20.72	23.27	26.23	25.77	23.65
X11	M3i-SW-C11	18.52	20.58	23.45	25.28	22.11	18.39	20.61	23.38	25.38	21.98	M3e-NE-C12	20.61	22.72	25.08	26.81	23.82
X12	M3j-SW-C2	18.46	20.19	24.06	38.22	24.22	17.28	20.17	23.52	25.02	22.71	M5b-NE-C6	19.98	22.19	25.78	26.65	24.41
X13	M1c-SW-C13	27.49	21.47	22.46	23.78	22.09	20.21	19.91	21.82	23.44	21.9	M3f-NE-C5	20.64	22.51	24.47	25.58	24.37
X14	M2d-SW-C0	28.44	35.02	38.59	34.87	24.48	25.8	32.13	32.7	29.06	22.22	nod-NE-C6	25.69	27.99	34.09	34.99	21.05

Table E-18 PET Ibn reshed street result(winter)

+		**IBN rushed/PET 21/12/2021**															
		At 1m from right building					At 5m middle distance					At 1m from left building					
Simulation		8am	10am	12pm	2pm	4pm	8am	10am	12pm	2pm	4pm		8am	10am	12pm	2pm	4pm
Y1	M6a-W-C6	17.31	19.26	24.41	26.07	21.16	16.19	19.18	35.69	26.37	20.72	M6a-E-C7	17.03	35.49	37.55	22.91	20.72
Y2	M5a-W-C1	20.39	23.13	40.48	39.32	23.04	18.77	23.16	33.1	23.74	20.99	M7a-E-C2	15.73	21.11	32.78	22.94	21.17
Y3	M7a-W-C0	16.23	18.67	22.61	25.38	20.76	14.62	17.38	26.81	23.47	20.15	no M-E-C2	14.22	16.35	29.44	22.17	20
Y4	M3a-W-C3	17.33	20.05	36.12	35.17	20.87	17.57	34.68	30.78	24.98	21.59	M3a-E-C6	18.19	33.18	36.17	23.07	20.94
Y5	M8a-W-C3	17.02	20.44	34.89	35.61	21.52	16.65	20.58	35.91	24.7	21.49	M7b-E-C3	16.81	34.12	36.17	23.3	21.09
Y6/80	M7b-W-C5	17.03	19.99	22.66	36.18	21.52	17.79	21.18	24.27	24.27	21.99	M3b-E-C6	17.29	32.14	35.83	23.36	21.3
Y6/70	M7c-W-C5	17.74	20.05	34.04	34.33	21.55	17.66	27.31	25.92	24.4	21.97	M3c-E-C6	17.14	32.94	35.56	23.62	21.51
Y7/60	M3b-W-C4	17.56	20.08	34.26	35.33	21.02	18.34	26.83	25.75	24.8	21.28	M3d-E-C3	17.61	34.52	37.25	24.33	21.65
Y7/50	M3c-W-C4	17.22	19.77	34.01	34.02	21.04	17.44	21.19	28.21	23.95	21.49	M3e-E-C3	16.53	34.63	36.14	22.98	20.72
Y8/40	M3d-W-C6	19.84	22.45	25.85	40.04	23.59	19.56	22.31	27.9	25.71	23.75	M9a-E-C4	18.32	31.22	41.71	25.26	22.99
Y8/30	M3e-W-C7	17.69	20.14	33.98	34.37	29.72	16.89	32.78	35.31	34.34	28.88	M9a-E-C4	16.42	32.43	34.36	23.95	21.68
Y9	M3f-W-C4	18.96	37.61	40.38	38.52	30.92	24.96	31	33.35	33.02	28.06	M9b-E-C3	25.49	32.39	35.13	37.41	34.77

Table E-19 UTCI wedad street result(winter) in three point for 5 times by sections

+		**WEDAD / UTCI 21/12/2021**															
section		At 1m from right building					At 5m					At 1m from left building					
Simulation	**case**	8AM	10AM	12pm	2pm	4pm	8AM	10AM	12pm	2pm	4pm	case	8AM	10AM	12pm	2pm	4pm
Y1/15	M3a-SW-C0	13.75	27.34	30.92	31.6	27.72	12.23	25.35	28.48	30.07	25.38	noa-NE-C4	11.52	24.83	28.13	29.61	25.28

Y2/25	M3b-SW-C0	14.53	30.11	32.24	31.95	28.7	11.94	24.54	26.76	28.6	25.69	nob-NE-C3	11.7	14.83	26.62	28.71	25.34
Z1/85	M3c-NW-C13	13.85	16.72	19.83	20.91	26.11	12.92	15.41	18.62	27.16	25.69	M3a-SE-C8	15.22	17.1	28.32	31.52	21.54
Z2/75	M3d-NW-C8	15.13	18.47	22.09	29.32	22.59	12.36	15.67	25.96	26.82	25.67	M3b-SE-C9	13.72	15.78	28.76	29.13	20.74
X1/35	M3e-W-C3	14.86	18.43	22.52	30.27	21.79	13.31	23.67	24.34	22.05	19.24	M3c-E-C3	17.67	16.77	18.84	21.04	19.25
X1/45	M3f-W-C6	14.64	26.57	29.62	29.63	18.97	14.18	26.23	28.9	25.84	17.77	M3d-E-C6	23.15	30.26	29.96	23.14	20.75
X2/55	M2a-W-C3	14.8	27.38	30.71	25.74	19.27	14.72	27.44	30.13	24.01	19.59	M1a-NE-C4	15.55	20.53	22.13	22.3	19.9
X2/65	M2b-W-C3	14.58	26.79	30.02	30.55	19.57	14.35	23.91	27.51	30.13	19.68	M1b-NE-C4	19.12	26.26	21.84	23	18.65
X3	M3g-W-C0	14.41	26.75	29.83	31.18	20.92	22	21.39	28.98	29.93	25.02	noc-NE-C2	13.29	25.61	28.52	29.35	24.4
X4	M4a-SW-C7	14.61	17.76	29.47	22.61	20.75	13.29	16.22	20.48	21.89	20.12	M2a-NE-C16	13.97	16.56	20.8	22.82	21.07
X5	M1b-SW-C3	14.71	17.2	19.76	29.81	19.7	14.26	16.47	19.54	28.1	19.13	M1c-NE-C3	14.25	16.36	19.61	21.32	19.3
X6	M5a-SW-C4	14.37	16.08	18.06	19.63	19.1	14.23	15.93	17.99	19.64	19.15	M5a-NE-C6	15.45	17.25	19.15	20.87	19.88
X7/120	M7a-SW-C14	15	16.61	16.61	19.5	18.98	15.05	16.73	16.73	19.5	19.26	M6a-NE-C8	15.65	17.53	17.53	20.73	19.57
X7/130	M7b-SW-C15	16.01	17.27	18.95	19.96	19.37	15.45	16.85	18.64	19.47	18.98	M6b-NE-C10	16.01	17.32	19.01	20.17	19.37
X8	M1a-SW-C15	16.55	17.56	19.19	20.25	19.41	15.65	16.91	18.66	19.7	18.89	M6c-NE-C9	15.75	17.15	18.83	19.85	18.94
X9	M2c-SW-C15	16.58	18.51	19.35	20.39	19.04	15.28	17.51	19.1	20.02	18.58	M6d-NE-C4	16.04	17.71	19.1	20.18	19.12
X10	M3h-SW-C5	15.46	17.96	21.5	21.81	18.77	15.56	17.8	20.3	20.8	18.54	M6e-NE-C5	15.97	18.33	20.33	20.89	19.28
X11	M3i-SW-C11	15.71	17.6	20.39	21	19.01	15.44	17.39	19.62	20.84	18.62	M3e-NE-C12	16.24	18.22	20.19	21.3	19.46
X12	M3j-SW-C2	15.85	17.72	22.21	30.6	20	14.62	17.41	27.54	21.43	19.12	M5b-NE-C6	16.17	18.57	21.6	22.37	19.96
X13	M1c-SW-C13	20.36	18.65	19.51	20.33	18.86	16.67	17.73	19.34	20.74	18.81	M3f-NE-C5	17.15	19.09	21.29	21.64	20.13
X14	M2d-SW-C0	21.97	27.15	29.58	28.85	20.16	22.11	26.6	27.22	25.92	18.84	nod-NE-C6	18.35	23.77	25.57	27.31	17.77

Table E-20 UTCI Ibn reshed street result(winter)

+		**IBN rushed/ UTCI 21/12/2021**															
		At 1m from right building					At 5m middle distance						At 1m from left building				
Simulation		8am	10am	12pm	2pm	4pm	8am	10am	12pm	2pm	4pm		8am	10am	12pm	2pm	4pm
Y1	M6a-W-C6	14.32	16.82	28.14	28.93	24.23	12.99	25.23	28.16	27.33	16.87	M6a-E-C7	23.3	27.24	28.25	20.66	18.06
							13.38	25.24	27.1	20.17	16.68						
Y2	M5a-W-C1	14.62	25.7	27.5	28.48	19.89	12.27	22.59	27.63	27.66	17.49	M7a-E-C2	18.92	26.58	27.47	26.64	17.64
Y3	M7a-W-C0	12.78	14.95	26.84	28.35	17.21	11.65	14.28	28.1	26.54	17.49	no M-E-C2	11.03	22.63	25.47	19.42	16.79
Y4	M3a-W-C3	13.22	15.32	27.1	28.6	17.63	13.98	26.01	28.42	28.62	18.21	M3a-E-C6	22.01	28.17	28.17	20.19	17.9
Y5	M8a-W-C3	12.87	15.69	26.7	28.1	17.81	13.86	25.33	27.38	27.8	17.57	M7b-E-C3	13.12	28.31	28.55	20.56	17.99
Y6/80	M7b-W-C5	13.93	17	19.91	29.26	18.5	14.22	17.85	26.3	20.9	18.49	M3b-E-C6	14.2	26.98	28.39	20.34	18.22
Y6/70	M7c-W-C5	14.79	17.54	27.75	29.3	18.09	14.34	26.72	28.58	27.64	18.48	M3c-E-C6	14.31	27.65	28.54	20.74	18.44
Y7/60	M3b-W-C4	14.28	17.41	27.88	30.01	17.72	14.8	26.33	28.26	28.23	17.78	M3d-E-C3	17.4	28.78	29.82	21.69	19.2
Y7/50	M3c-W-C4	13.83	16.68	27.7	29.36	17.27	14.06	23.35	26.31	20.28	17.81	M3e-E-C3	13.93	29.22	22.6	20.42	17.67

Y8/40	M3d-W-C6	15.09	17.92	27.86	29.46	18.05	14.59	27.12	28.55	20.62	17.56	M9a-E-C4	16.24	20.37	21.73	21.37	19.51
Y8/30	M3e-W-C7	14.63	17.1	27.82	29.07	25.99	14.44	22.51	24.93	21.54	19.48	M9a-E-C4	14.17	26.47	28.22	20.69	18.45
Y9	M3f-W-C4	15.38	27.35	29.73	30.23	26.56	21.97	26.47	28.27	28.42	24.66	M9b-E-C3	22.71	27.63	29.62	30.64	26.78

Appendix F
ANOVA test cases samples result (summer):

Table F-1 Anova test 8 cases in summer (22/6-23/6-24/6-276)

Case 1

factor			Ta					Wind speed					Relative humidity					UTCI					PET				
date	section	material	8am	10am	12pm	2pm	4pm	8am	10am	12pm	2pm	4pm	8am	10am	12pm	2pm	4pm	8am	10am	12pm	2pm	4pm	8am	10am	12pm	2pm	4pm
22/6			25.43	28.26	31.97	33.51	32.79	0.29	0.3	0.29	0.24	0.3	55	48.7	37.4	31.2	35.6	26.52	32.57	35.44	33.58	31.45	29.9	38.5	41.12	37.07	34.37
23/6	**X8**	**M1a(noor)-SW-C15**	26.34	29.6	33.47	35.77	36.27	0.23	0.37	0.31	0.27	0.34	58.21	49.53	40.14	34.59	33.72	26.73	33.39	37.1	36.28	34.93	29.75	38.39	42.09	38.69	36.65
24/6			27.39	30.5	35.1	37.93	37.57	0.27	0.21	0.31	0.087	0.22	46.73	41.45	34.99	28.71	27.45	26.71	33.61	38.24	37.66	35.03	29.9	39.56	43.14	39.74	37.12
27/6			26.11	29.7	33.82	36.64	36.95	0.11	0.24	0.23	0.21	0.25	55.1	45.17	35.62	27.64	28.58	26.23	33.05	36.83	36.39	34.04	30.03	38.68	42.3	38.92	36.41
22/6			25.73	28.47	32.09	33.61	32.85	0.3	0.4	0.43	0.52	0.65	54.1	47.9	37.1	31.2	35.5	27.64	33.94	36.22	33.76	32.15	31.04	39.78	42.93	37.08	34.61
23/6	**X9**	**M2c-SW-C15**	26.66	29.9	33.7	36.83	36.34	0.14	0.57	0.7	0.56	0.75	57.63	48.49	40.16	33.26	33.68	27.58	34.62	37.93	37.27	35.89	30.96	39.32	43.69	39.53	37.37
24/6			27.74	31.1	35.85	38.01	37.6	0.26	0.16	0.39	0.21	0.5	45.95	39.9	33.75	28.52	27.46	27.58	35.11	39.17	37.86	36.57	30.8	41.56	45.31	40.12	38
27/6			26.41	30.1	34.2	36.7	36.8	0.12	0.11	0.29	0.39	0.52	54.48	44.88	34.95	27.48	28.52	27.09	34.44	37.76	36.53	35.32	30.84	41.05	44.46	39.18	37.11
22/6			25	28.18	32.06	33.55	32.83	0.69	0.67	0.71	0.42	0.55	56.8	49.6	37.6	31	35.4	26.29	29.83	35.5	32.91	32.36	28.41	32.35	41.13	35.85	34.73
23/6	**X7/130**	**M7b-SW-C15**	25.98	29.44	33.43	35.33	36.38	0.55	0.63	0.35	0.25	0.54	59.09	50.82	39.79	34.92	33.41	26.56	30.67	37.04	34.98	36.11	28.65	32.79	43.19	37.29	37.51
24/6			26.93	30.1	34.95	37.95	37.66	0.55	0.41	0.58	0.21	0.43	47.94	43.8	36.82	28.76	27.25	26.58	30.75	38.3	36.95	36.84	29.08	33.48	43.72	38.54	38.13
27/6			25.73	29.27	33.72	36.83	36.9	0.41	0.67	0.61	0.51	0.59	55.9	46.49	36.88	27.61	28.42	26.14	30.12	37.03	35.95	35.79	28.77	32.44	42.61	37.89	37.41

Case 2

factor			Ta					Wind speed					Relative humidity					UTCI					PET				
date	section	material	8am	10am	12pm	2pm	4pm	8am	10am	12pm	2pm	4pm	8am	10am	12pm	2pm	4pm	8am	10am	12pm	2pm	4pm	8am	10am	12pm	2pm	4pm
22/6			25.52	28.71	32.29	34.34	32.91	0.53	0.36	0.35	0.36	0.41	56.8	46.9	36.1	29.6	35.4	25.81	32.58	35.86	37.54	33.39	28.59	37.64	39.55	42.4	35.87
23/6	**X14**	**M2d-SW-C0**	26.7	30.08	34	37.3	36.73	0.48	0.33	0.28	0.18	0.42	60.22	47.9	38.87	30.02	32.58	26.58	33.3	37.45	40.62	37.84	28.94	37.63	40.44	45.32	39.24
24/6			27.5	31.33	36.32	38.63	37.75	0.45	0.3	0.35	0.23	0.34	47.38	43.15	33.75	26.83	27.21	26.1	33.96	39.34	41.91	38.34	28.94	38.33	41.49	45.87	39.67
27/6			26.44	30.53	34.53	37.24	36.4	0.42	0.55	0.57	0.42	0.44	57.15	49.34	35.37	26.28	28.32	26.04	33.64	37.62	40.68	37.11	28.76	37.29	40.07	44.87	38.79
22/6			26.18	28.15	32.01	34.21	33.32	1.14	1.21	1.28	1.05	1	53.38	47.48	36.2	29.82	34.63	26.15	32.47	35.68	39.35	38.69	27.36	35.71	41.2	45.6	44.1
23/6	**Y1/15**	**M3a-SW-C0**	27.97	30.29	34.07	38.62	37.54	0.5	1.02	0.81	0.65	0.88	55.96	46.24	37.55	28.43	31.51	27.85	33.75	38.09	44.44	45.43	29.31	36.69	43.49	49.73	49.96
24/6			29.32	33	39.19	40.08	38.37	0.7	0.36	1.02	1.02	1.04	42.64	38.43	27.15	25.61	26.35	27.72	35.79	41.64	45.24	45.87	29.19	39.39	47.01	49.91	50.02

27/6			27.83	31.44	36.97	37.71	36.75	0.16	0.61	1.56	1.51	1.58	52.82	46.68	29.97	25.84	27.95	27.35	35.05	38.95	42.55	43.81	29.79	38.15	44.88	49.47	49.67
22/6			26.77	29.64	32.97	34.81	33.55	0.76	0.6	0.57	0.37	0.47	53.71	43.43	33.53	28.45	34	32.61	35.21	37.25	36.26	34.72	37.55	42.1	44.3	40	37.8
23/6	**Y2/25**	**M3b-SW-C0**	27.87	31.62	35.64	37.97	37.7	0.67	0.36	0.41	0.15	0.35	55.71	43.03	33.94	29.18	31.04	31.49	36.24	39.29	39.54	39.56	34.92	42.99	51.79	42.58	41.79
24/6			29.16	33.64	39.12	40.98	38.57	0.6	0.41	0.53	0.33	0.39	43.93	39.83	29.65	23.18	25.87	32	38	42.57	42.02	40	36.17	44.25	48.39	44.07	42.27
27/6			27.72	31.95	36.85	38	36.9	0.67	0.36	0.41	0.15	0.35	55.7	43.03	33.94	29.18	31.04	31.16	36.61	40.37	39.31	38.4	34.65	41.87	46.25	42.38	40.98

Case 3

factor			Ta					Wind speed					Relative humidity					UTCI					PET				
date	section	material	8am	10am	12pm	2pm	4pm	8am	10am	12pm	2pm	4pm	8am	10am	12pm	2pm	4pm	8am	10am	12pm	2pm	4pm	8am	10am	12pm	2pm	4pm
22/6			25.68	29.16	33.87	35.21	33.77	0.35	0.8	1.22	1.59	2.13	57	49	33.8	28.1	33.8	26.05	33.42	37.56	40.54	38.83	28.8	32.6	43.12	46.9	40
23/6			27.04	30.65	34.99	38.31	38.01	0.2	0.99	1.36	0.88	1.95	56.69	50.36	35.28	28.69	30.61	26.88	34.14	38.75	45.18	46.23	29.67	32.56	43.92	49.92	47.15
24/6	**X2/55**	**M2a-W-C3**	27.95	31.93	37.85	40.6	38.85	0.12	0.04	0.56	1.11	1.83	46.77	42.88	32.98	24.46	25.69	26.52	34.74	41.45	47.04	46.88	29.75	34.2	46.6	50.19	47.74
27/6			26.8	31.11	35.84	39.09	37.57	0.54	0.3	0.59	1.22	1.86	53.65	43.26	34.59	24.94	27	26.3	34.18	39.5	45.31	45.26	28.44	33.58	45.13	49.95	46.47
22/6			25.39	28.96	33.62	35.15	33.69	0.36	0.88	1.35	1.88	2.51	57	49.5	34.6	28.2	33.9	25.38	33.01	36.93	39.61	37.82	28.1	32.2	42.5	46.1	43.5
23/6			26.49	30.43	34.96	38.28	37.96	0.15	1.09	1.64	0.98	2.32	58.25	50.78	35.44	28.95	30.67	26.14	33.73	38.13	44.38	45.12	29.25	32.23	43.4	49.82	50.01
24/6	**X2/65**	**M2b-W-C3**	27.3	31.5	37.94	40.4	38.76	0.07	0.39	0.6	1.35	2.17	48.03	42.52	32.15	24.73	25.8	25.83	34.21	41.07	46.03	45.81	29.3	33.95	46.31	50.07	50.12
27/6			26.15	30.75	36.37	38.86	37.47	0.54	0.27	0.66	1.39	2.12	55.37	43.7	32.73	25.18	27.09	25.5	33.63	39.43	44.33	44.46	27.69	33.34	45.04	49.82	49.78
22/6			26.15	29.58	33.37	35.62	34.18	0.84	0.52	0.43	0.034	0.11	57.59	45.57	32.93	27.15	32.82	26.78	31.18	36.96	40.8	40.64	28.4	33.4	42.7	52.5	51.14
23/6	**X1/35**	**M3e-W-C3**	27.45	31.2	34.72	37.85	37.96	0.73	0.05	0.51	0.51	0.15	55.89	47.21	35.95	29.47	30.67	27.4	31.9	38.54	44.52	47.3	29.03	34.38	43.15	49.85	53.36
24/6			28.72	32.33	37.98	41.62	39.37	0.62	0.45	0.45	0.034	0.3	45.65	43.69	33.23	22.3	24.76	27.53	32.78	41.42	46.96	47.98	29.56	33.99	45.12	53.36	54.1
27/6			27.28	30.7	35.79	39.45	37.9	0.73	0.93	1.03	0.73	0.8	52.74	45.23	35.83	23.36	26.14	26.9	31.67	39.2	45.26	47.72	28.73	32.68	43.24	49.92	50.36
22/6			26.07	28.34	32.7	34.63	33.81	0.33	0.43	1.09	2.12	3.05	53.16	48.46	35.56	29.26	33.85	25.33	29.31	35.68	38.82	37.74	28.58	31.89	40.84	44.64	42.04
23/6	**Y4**	**M3a-W-C3**	25.88	29.17	33.07	34.67	33.71	0.8	1.68	2.5	3.14	3.47	58.91	46.64	34.4	30.78	33.87	25.78	29.08	35.14	38.2	37.46	27.97	30.57	39.9	44.1	41.81
24/6			27.68	29.29	34.32	36.52	35.84	1.18	2.27	2.72	2.86	3.26	52.69	43.44	32.81	29.23	33.01	23.94	26.38	34.06	37.85	37.62	27.17	28.91	40.27	45.4	43.5
27/6			30.52	32.94	37.72	39.2	38.2	0.97	2.39	2.89	3.41	3.79	40.67	37.23	27.43	28.56	31.6	28.75	31.82	39.77	43.14	42.48	30.79	33.6	44.97	49.47	47.43
22/6			26.32	29.65	33.7	34.91	33.83	0.86	0.9	1.25	1.59	2.22	52.35	44.26	33.21	28.89	33.82	30.25	33.43	36.26	38.74	36.94	35.94	40.56	44.01	46.8	43.95
23/6	**Y5**	**M8a-W-C3**	26.14	29.71	33.46	34.91	33.82	0.7	1.31	1.71	2.03	2.04	56.4	45.05	33.68	30.46	33.7	31.26	33.91	36.37	38.79	37.52	37.5	40.66	43.18	46.48	44.25
24/6			27.81	29.71	34.67	36.83	35.99	1.05	1.53	1.77	1.79	2.1	51.85	42.06	32.34	28.96	32.8	29.82	31.67	35	38.01	37.12	36.52	39.25	43.31	47.62	45.48
27/6			30.79	33.5	38.17	39.49	38.33	1.04	1.65	1.92	2.13	2.18	39.3	36	26.79	28.2	31.41	34.03	36.67	40.85	43.6	42.42	39.84	43.48	47.7	49.78	49.07

Case 4

factor			Ta					Wind speed					Relative humidity					UTCI					PET				
date	section	material	8am	10am	12pm	2pm	4pm	8am	10am	12pm	2pm	4pm	8am	10am	12pm	2pm	4pm	8am	10am	12pm	2pm	4pm	8am	10am	12pm	2pm	4pm
22/6			26.03	29.52	34.3	35.57	34.16	0.22	0.99	1.62	2.25	3.16	56.7	47.9	32.4	27.4	33	27.04	31.28	37.26	39.66	37.75	30.35	32.9	42.8	46	37.34
23/6	**X1/45**	**M3f-W-C6**	27.3	31.02	35.16	38.23	38.5	0.48	1.3	1.88	1.22	2.78	56.11	49.79	34.89	28.72	29.79	27.48	31.92	38.35	44.36	45.39	29.59	32.81	43.29	49.72	43.68
24/6			28.39	32.13	38.24	41.23	39.4	0.1	0.19	0.63	1.53	2.67	45.96	42.78	33.14	23.32	24.85	27.3	32.53	41.45	46.76	46.19	30.61	34.29	46.44	50.11	44.41

27/6			27.09	30.74	35.92	40.02	38.22	0.912	0.66	0.48	1.7	2.75	53.06	44.52	34.7	23.56	26	26.76	31.65	39.56	44.82	44.58	28.45	33.2	45.04	49.9	43.004
22/6			26.05	29.27	33.93	35	33.41	0.21	0.06	0.25	0.5	0.72	54.2	44.79	32.72	28.83	34.49	26.55	30.48	37.85	41	32.44	30.62	34.86	45.36	49.49	35.79
23/6	**Y8/40**	**M3d-W-C6**	25.95	29.77	33.74	35.01	33.69	0.13	0.27	0.37	0.48	0.54	55.9	44.84	33.38	30.4	33.81	26.96	30.42	37.13	40.46	32.52	31.21	34.13	44.85	49.37	35.98
24/6			27.63	29.79	34.73	36.88	35.79	0.18	0.36	0.43	0.42	0.52	51.43	41.9	32.25	28.8	32.98	25.26	27.68	35.54	39.72	32.4	30.15	32.54	44.58	49.61	36.33
27/6			30.31	33.36	38.21	39.45	38.09	0.15	0.36	0.42	0.49	0.61	39.96	36.21	26.96	28.29	31.7	29.6	32.92	41.46	45.18	37.56	32.8	35.68	47.77	51.6	39.24
22/6			25.32	27.97	33.03	33.92	32.96	0.33	0.75	1.5	2.54	3.53	55.47	48.76	35.84	30.69	35.67	26.06	30.2	36.68	37.59	31.88	27.66	30.14	39.74	39.81	33.84
23/6	**Y1**	**M6a-W-C6**	25.2	27.58	32.13	33.95	33.08	1.03	1.94	2.94	3.71	4.11	60.74	50.15	36.19	32.21	35.37	26.29	28.4	34.08	36.71	31.86	26.63	28.5	37.84	39.38	33.92
24/6			27.2	27.7	33.36	35.98	35.17	1.5	2.6	3.13	2.93	3.9	54.29	46.54	34.55	29.94	34.48	24.64	25.87	33.78	37.55	32.9	26.37	27.22	38.38	41.19	35.71
27/6			30.01	31.69	36.94	38.56	37.55	1.4	2.76	3.4	3.83	4.56	41.8	39.53	28.7	29.68	32.98	29.39	31.36	39.39	42.44	38.44	29.88	32.18	46.65	45.55	40.2

Case 5

factor			Ta					Wind speed					Relative humidity					UTCI					PET				
date	section	material	8am	10am	12pm	2pm	4pm	8am	10am	12pm	2pm	4pm	8am	10am	12pm	2pm	4pm	8am	10am	12pm	2pm	4pm	8am	10am	12pm	2pm	4pm
22/6			26.15	29.03	33.23	34.57	33.74	0.68	0.22	0.58	1.4	1.86	53.96	47.78	34.34	29.4	34	30.87	33.6	36.97	40.18	39.3	28.75	34.21	43.57	42.7	44.3
23/6	**Y3**	**M7a-W-C0**	26.06	29.52	33.3	34.6	33.62	0.6	1.25	1.8	2.28	2.3	58.04	46.03	34.04	30.97	34.13	31.73	33.9	36.62	39.78	38.93	29.46	32.39	41.93	43.65	37.52
24/6			27.76	29.64	34.56	36.46	35.69	0.84	1.72	2.06	2.05	2.34	51.78	42.94	32.46	29.3	33.36	30.17	31.4	35.01	38.79	38.23	28.5	30.66	42.08	44.7	38.74
27/6			30.8	33.27	37.98	39.17	38.17	0.61	1.71	1.98	2.35	2.51	40.03	36.63	27.13	28.67	31.7	34.61	36.63	41.09	44.62	43.72	32.25	35.11	46.52	48.54	42.66
22/6			24.87	28.59	33.1	34.86	33.51	0.52	0.93	1.37	1.95	2.62	57.8	50.2	35.6	28.6	34.2	24.78	29.54	36.33	39.28	37.54	27.63	31.6	41.42	45.14	37.25
23/6	**X3**	**M3g-W-C0**	27.07	29.93	34.62	37.92	37.73	0.09	1.13	1.66	0.98	2.41	56.88	51.66	36.1	29.76	30.97	26.43	30.17	37.6	44.03	44.78	30	31.64	42.51	49.63	43.62
24/6			26.6	31.7	37.79	39.9	38.53	0.27	0.07	0.68	1.42	2.26	49.46	40.83	31.44	25.35	26.02	25.26	30.81	40.7	45.56	45.48	28.62	33.68	45.53	49.86	44.22
27/6			26.85	30.99	36.18	38.41	37.21	0.5	0.23	0.74	1.44	2.18	53.7	43.62	32.33	25.6	27.37	25.92	30.6	39.09	43.9	44.17	28.49	33.3	44.26	49.62	42.86

Case 6

factor			Ta					Wind speed					Relative humidity					UTCI					PET				
date	section	material	8am	10am	12pm	2pm	4pm	8am	10am	12pm	2pm	4pm	8am	10am	12pm	2pm	4pm	8am	10am	12pm	2pm	4pm	8am	10am	12pm	2pm	4pm
22/6			26.06	29.29	32.72	34.27	33.44	0.28	0.76	1.1	1.82	2.44	57.73	51.52	39.25	30.69	35.11	32.99	35.55	33.87	34.37	33.06	38.44	38.5	36.8	37	35.6
23/6	**X1/35**	**M3c-E-C3**	27.53	30.94	34.5	37.9	37.8	0.15	1.08	1.5	0.84	2.24	55.8	52.47	36.8	29.29	31.47	31.41	36.52	35.12	38.71	38.59	36.03	38.48	37.6	40.24	41.2
24/6			28.73	32.37	36.92	40.06	38.5	0.24	0.31	0.69	1.37	2.13	45.5	44.42	37.9	26.44	27	32	37.5	38.03	40.69	39.17	36.48	41.05	39.96	42.2	41.76
27/6			27.36	30.88	34.85	37.98	37.3	0.07	0.15	0.42	1.05	1.82	52.64	45.3	38.82	28.81	28.61	31.05	36.03	35.81	38.45	37.89	36.44	40.39	38.39	40.27	40.37
22/6			26.52	30.69	34.1	34.53	33.26	0.38	0.25	0.7	1.43	1.92	51.76	40.56	31.65	29.32	34.72	32.88	35.23	37.17	34.8	32.84	38.9	42.82	44.11	37.63	35.58
23/6	**Y7/60**	**M3d-E-C3**	26.71	30.49	34.05	34.6	33.59	0.64	1.27	1.74	2.17	2.19	53.29	43.11	32.38	30.71	33.95	33.54	35.86	37.02	34.75	33.14	38.88	41.41	43.03	37.79	36.02
24/6			27.97	30.47	35.05	36.44	35.65	0.88	1.67	1.97	1.91	2.23	50.48	40.3	31.3	29.17	33.19	32.21	33.43	35.39	34.09	32.78	38.18	39.8	42.98	38.5	37.12
27/6			30.77	34.08	38.6	39.09	38.11	0.69	1.67	1.93	2.2	2.37	38.82	34.9	26.06	28.55	31.76	36.17	38.52	41.43	39.7	38.13	41.39	44.05	47.47	42.47	40.9
22/6	**Y7/50**	**M3e-E-C3**	26.42	30.6	34.08	34.31	33.12	0.41	0.22	0.73	1.55	2.12	52.38	40.92	31.4	29.55	34.93	34.11	36.26	37.6	34.71	32.16	40.79	44.84	44.72	37.38	34.66

23/6			27.14	30.48	34.04	34.6	33.54	0.63	1.35	1.95	2.45	2.57	51.88	43.06	32.32	30.69	34.03	35.03	36.96	37.17	34.59	32.36	41.36	42.99	43.25	37.56	35.12
24/6			28.14	30.48	35.02	36.45	35.59	0.92	1.87	2.21	2.24	2.53	49.82	40.28	32.43	29.12	33.27	33.58	34.45	35.57	34.05	32.24	40.33	41.18	43.15	38.32	36.33
27/6			30.84	33.4	38.58	39.07	37.96	0.71	1.87	2.18	2.55	2.82	38.64	34.73	26.01	28.56	31.88	37.57	39.53	41.6	39.58	37.48	43.64	45.59	47.87	42.46	40.31
22/6			26.35	29.8	33.65	34.12	33.14	0.36	0.35	0.95	1.84	2.52	52.24	43.73	32.95	29.9	35.01	33.69	36.05	37.05	34.78	32.13	38.27	41.96	42.96	36.6	34.57
23/6	**Y5**	**M7b-E-C3**	26.14	30.07	33.54	34.39	33.45	0.74	1.54	2.211	2.72	2.88	56.05	43.83	33.2	31.11	34.26	34.34	36.58	36.55	34.64	32.3	37.69	40.5	41.56	36.82	34.96
24/6			27.83	30.09	34.7	36.27	35.57	1.06	2.07	2.44	2.48	2.81	51.62	41.03	31.93	29.49	33.38	33.1	34.2	35.28	34.27	32.42	36.96	38.76	41.69	37.68	36.34
27/6			30.75	33.79	38.23	38.95	37.99	0.86	2.11	2.48	2.86	3.42	39.28	35.26	26.49	28.8	31.89	37.18	39.21	41.17	39.8	37.65	40.45	43.33	46.45	41.97	40.45
22/6			26.37	28.92	32.68	34.96	33.78	1.98	1.44	1.25	0.54	0.17	52.14	46.65	35.94	29.07	33.77	29.72	33.54	37.12	39.92	38.48	33.13	38.29	42.82	46.44	45.66
23/6	**Y9**	**M9b-E-C3**	25.97	30.07	33.77	35.09	33.93	0.5	0.59	0.25	0.24	0.35	55.81	45.07	33.6	30.04	33.32	32.29	35.72	38.3	40.14	38.77	37.88	42.16	45.79	47.12	45.86
24/6			27.85	30.27	34.9	37.09	36.11	0.67	0.17	0.22	0.14	0.23	50.8	41.24	31.91	28.2	32.37	30.98	32.64	35.42	37.58	36.71	37.3	42.76	45.07	47.4	45.82
27/6			30.84	33.87	38.4	39.65	38.41	1	0.21	0.21	0.17	0.23	38.7	35.63	26.73	27.79	31.15	35.04	38.49	42.32	44.47	43.28	39.76	45.84	48.45	51.4	49.68

case 7

factor			Ta					Wind speed					Relative humidity					UTCI					PET				
date	section	material	8am	10am	12pm	2pm	4pm	8am	10am	12pm	2pm	4pm	8am	10am	12pm	2pm	4pm	8am	10am	12pm	2pm	4pm	8am	10am	12pm	2pm	4pm
22/6			26.03	29.06	32.78	34.53	33.36	0.59	1	1.49	2.05	2.71	56.2	50.3	37.5	29.6	34.7	27.89	31.36	34.02	35.18	32.73	28.29	36.57	36.2	37.8	39.02
23/6	**X2/55**	**M1a-NE-C4**	27.4	30.64	34.66	37.84	37.54	0.26	1.16	1.73	0.98	2.5	55.74	51.23	36.41	29.74	31.53	28.38	32.75	35.92	39.68	38.26	29.67	37.06	37.5	41.51	46.46
24/6			28.58	32.19	36.82	39.74	38.33	0.3	0.19	0.73	1.49	2.36	45.3	43.3	35.75	26.2	26.35	28.65	33.64	38.45	41.52	38.7	29.93	40.7	39.53	43.23	47.15
27/6			27.18	31.35	34.66	37.74	36.87	0.47	0.36	0.92	1.55	2.3	52.69	43.68	37.85	27.35	28.15	27.9	32.92	36.23	39.25	37.31	28.86	38.84	37.83	41.34	45.57
22/6			25.84	29.18	33.15	34.86	33.4	0.41	0.99	1.58	2.33	3.14	55.3	49.6	36.4	29.1	34.7	25.73	34.35	36.96	38.97	36.28	28.4	37.5	42.82	45.8	36.1
23/6			27.31	30.78	34.86	38.14	37.62	0.18	1.26	1.99	1.13	2.91	55.86	50.53	36.1	29.32	31.4	26.83	35.05	37.82	44.28	43.5	29.69	37.44	43.96	49.83	42.3
24/6	**X2/65**	**M1b-NE-C4**	28.13	32.69	37.82	40.13	38.4	0.14	0.07	0.6	1.65	2.71	45.88	41.39	33.13	25.37	26.47	26.49	36.31	41.57	45.81	44.26	29.52	41.11	47.39	50.08	42.92
27/6			27.09	31.61	36.09	38.3	36.98	0.57	0.3	0.72	1.64	2.57	52.77	42.15	34.06	26.22	27.94	26.23	35.47	39.65	43.79	43.82	28.37	39.58	45.93	49.7	41.34
22/6			25.71	28.46	32.01	33.57	32.84	0.12	0.1	0.14	0.15	0.19	54.2	48	37.3	31.2	35.5	32.2	30.05	32.19	32.72	31.44	39.77	34.5	35.53	35.72	34.14
23/6	**X9**	**M6d-NE-C4**	26.61	29.86	33.55	36.39	36.32	0.08	0.18	0.2	0.16	0.22	57.66	48.64	40.28	33.74	33.69	30.65	30.8	33.61	35.79	34.96	36.4	34.27	35.7	37.26	36.3
24/6			27.66	31.04	35.35	38.01	37.6	0.11	0.08	0.14	0.05	0.14	46.1	40.05	34.23	28.59	27.45	31.02	31.01	34.7	36.77	35.56	37.06	34.95	36.43	37.75	36.65
27/6			26.37	30.13	33.99	36.68	36.36	0.03	0.08	0.1	0.12	0.15	54.47	44.69	35.16	27.54	28.53	30.29	30.57	33.38	35.33	34.36	37.05	34.54	35.75	37.03	35.96
22/6			26.49	29.26	32.54	34.22	33.49	1.37	1.45	1.9	2.21	3.13	56.38	43.91	34.27	29.86	34.27	30.65	34.28	35.43	37.64	37.44	30.96	37.88	41.51	44.61	42.34
23/6	**Y1/15**	**noa-NE-C4**	28.08	31.36	33.97	38.36	37.85	0.93	1.31	1.88	1.12	2.93	56.32	43.35	37.95	28.96	30.74	30.73	34.29	37.4	44.48	43.13	31.17	38.33	42.27	49.75	49.92
24/6			29.55	32.79	38.24	41.2	38.69	0.87	0.6	1.12	1.7	2.78	43.49	43.82	31.45	23.21	25.66	31.16	36.5	41.48	45.31	44.18	31.72	40.32	46.36	50.11	50.04
27/6			27.94	31.08	35.74	38.24	37.13	1.05	1.19	1.8	2.2	3.15	53.16	49.85	35.11	24.45	27.03	30.28	34.98	38.54	42.07	41.98	30.84	38.4	43.82	49.6	49.72

case 8

factor			Ta					Wind speed					Relative humidity					UTCI					PET				
date	section	material	8am	10am	12pm	2pm	4pm	8am	10am	12pm	2pm	4pm	8am	10am	12pm	2pm	4pm	8am	10am	12pm	2pm	4pm	8am	10am	12pm	2pm	4pm

22/6			25.74	28.78	32.2	34.15	33.02	0.24	0.15	0.13	0.22	0.25	54.8	46.1	36.1	30	35.2	31.75	30.11	32.68	33.92	32.72	38.14	34.55	36.42	36.72	35.67
23/6	**X13**	**M3f-NE-C5**	26.94	30.17	34.2	38	36.8	0.19	0.17	0.24	0.15	0.31	58.11	46.88	38.82	29.04	32.73	30.64	30.87	34.51	37.51	36.8	35.53	34.43	36.79	38.7	38.49
24/6			27.6	31.4	36.15	38.5	37.8	0.2	0.14	0.15	0.07	0.18	46.65	40.8	32.99	26.98	27.19	30.71	31.4	35.85	37.8	37.16	36.15	34.98	37.7	38.85	38.8
27/6			26.6	30.6	34.4	37	36	0.13	0.22	0.23	0.2	0.22	55.06	45.67	34.42	26.44	28.28	30.25	31.2	34.32	36.52	35.94	35.84	34.5	36.76	38.18	38.07
22/6			25.6	28.37	31.95	33.39	32.66	0.04	0.03	0.05	0.1	0.14	54.9	47.7	37.1	31.6	35.9	28.23	31.57	35.1	32.37	31.42	35.12	36.31	42.2	35.5	34.3
23/6	**X10**	**M6e-NE-C5**	26.7	29.7	33.5	36.15	36.1	0.2	0.1	0.17	0.15	0.72	58.22	48.43	40.56	34.17	34.17	28.08	32.38	37.04	35.45	34.95	33.39	35.79	42.86	37.03	36.35
24/6			27.5	31	35.7	37.8	37.4	0.02	0.015	0.03	0.042	0.1	46.84	41.42	33.83	28.58	27.78	27.92	32.95	38.4	36.54	35.57	33.68	36.79	49.66	37.59	36.74
27/6			26.5	30.1	34.1	36.4	36.8	0.4	0.02	0.03	0..04	0.09	55.04	46.62	35.16	27.75	28.87	27.64	32.48	36.95	34.93	34.29	33.03	36.28	43.68	36.81	36.03